



NTNU – Trondheim
Norwegian University of
Science and Technology

Synthesis and Mechanistic Studies of Optically Active Tartaric Acid Based Surfactants

Thomas Aleksander Bakka

Chemistry

Submission date: May 2013

Supervisor: Odd Reidar Gautun, IKJ

Co-supervisor: Susana Gonzalez, IKJ

Norwegian University of Science and Technology
Department of Chemistry

"K, som i potet"
-Per Carlsen

Acknowledgements

I would like to thank my supervisor, associate professor Odd Reidar Gautun, for his guidance throughout this study. Thank you for always being available and for showing genuine interest in my project. I am also grateful for you taking me on as a master student after the retirement of professor Per Carlsen. Furthermore, I would like to thank my friend and mentor, dr. Susana Villa Gonzalez, for all her support and assistance throughout this work and for giving helpful advice and encouragement. Thank you for sharing high fives with me when things went well, and for teaching me Spanish anger management when things did not go well.

Working with this project would not have been the same without the social atmosphere created by my lab colleagues, the research group and fellow students. I would like to thank Ph.D. candidate Rajesh Raju for all the advice and assistance in the lab. I would also like to thank professor Per Carlsen for sparking my interest in physical-organic chemistry and for creating a challenging project for me to embark on.

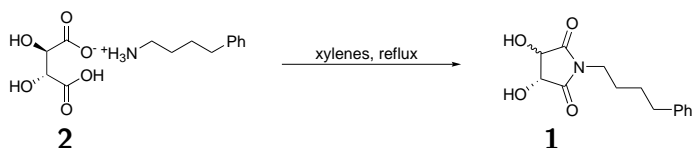
I would like to express my genuine gratitude and thanks to all of my friends at the university and everyone on the rugby team for making these two years truly memorable. I would especially like to thank the "Tuesday night supper crew" for support, encouragement and for supplying waffles when I was down with the blues. I would also like to thank my friends Knut Andreas and Anders for being top notch housemates and loyal members of "The EJ6 breakfast club". Special thanks also go to my good friends Karsten Kirste and Ragni Mikalsen for all the laughs, discussions and pats on the back.

And last, but not least, I would like to thank my family for their unconditional love and support. Thank you for always believing in me, I could not have done this without you.

Thomas Aleksander Bakka
Trondheim, May 2013

Sammendrag

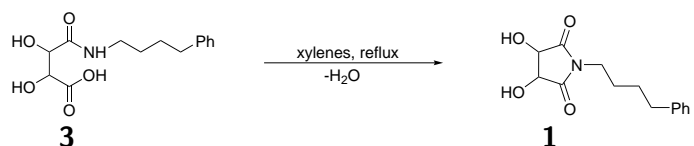
I denne studien ble kinetikk og reaksjonsmekanisme for synteseveier til vinsyre-baserte surfaktanter undersøkt. Stereokjemien til de ulike synteseveiene har i særlig grad vært et av hovedfokusene, da spesielt mekanismen for delvis isomerisering av stereosenterene i **1** syntetisert fra **2**.



Det å tilegne seg kunnskap om isomeriseringsmekanismene er sentralt for stereokjemisk ren syntese. Optisk rene vinsyrebaserte surfaktanter er viktige potensielle kandidater for optisk aktive liposomer, som videre kan brukes til målbasert medisintransport i menneskekroppen.

Et sett med stereokjemisk rene referansematerialer har blitt syntetisert, i tillegg har flere analysemetoder blitt utforsket.

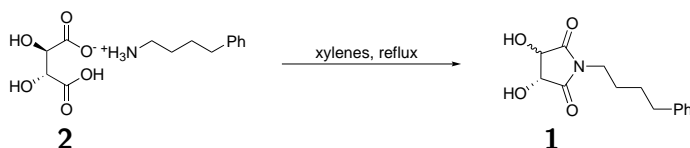
En reaksjonsmekanisme for dannelse av **1** fra **3** i upolart miljø har blitt foreslått på bakgrunn av mekanistiske data.



Tilgang på ureagert "fritt" amin i reaksjonsblandingen ble funnet å være viktig for dannelse av amider og for at isomerisering skal finne sted. Det ble også funnet at stereokjemien i større grad dikterer oppførselen av de ulike stoffene i høyere grad enn først antatt. Dette ble særlig observert for "imid-diamide"-likevekten, der forandring av stereokjemi for utgangsstoffet førte til endringer i isomeriseringstendenser og produktsammensetning.

Abstract

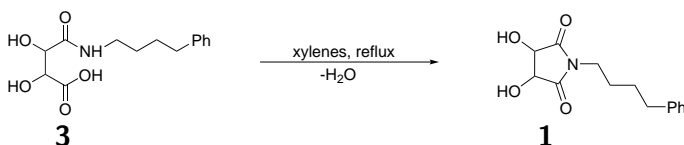
The reaction mechanism and kinetics in synthesis of surfactants derived from tartaric acid have been investigated. Stereochemical aspects of the different synthetic pathways have been of interest, especially the partial isomerization mechanism taking place in synthesis of **1** from **2**.



Gaining knowledge of the isomerization mechanisms are of pivotal importance for stereochemically pure synthesis. Optically pure tartaric acid based surfactants are seen as important precursors for optically active superstructures. From these superstructures, liposomes are known candidates for drug delivery nanovessels in the human body.

A number of optically pure reference compounds were synthesized and several analysis methods were outlined.

A mechanistic route for formation of **1** from **3** in nonpolar solvents have been proposed on the background of various mechanistic assessment techniques.



The presence of free amine in the reaction mixtures were found to be of importance for initial amide formation and for isomerization of stereocenters to take place. It was also discovered that stereochemistry dictates chemical behaviour of some compounds in question to a higher degree than expected. This was particularly apparent for the imide-diamide equilibrium, where both product ratios and isomerization tendencies changed with different initial stereochemistry.

Contents

Acknowledgements	iii
Sammendrag	v
Abstract	vii
Abbreviations and symbols	xv
List of Tables	xviii
List of Figures	xxi
1 Introduction and objective	1
1.1 Background	1
1.1.1 Surfactants	1
1.1.2 Aggregates and self-assembly properties ²	3
1.1.3 Importance and application of optically pure surfactants	4
1.2 Objective	5
1.2.1 The problem	6
1.2.2 Objective of this project	8
2 Theory	9
2.1 Kinetics ^{17,22}	9
2.1.1 Introduction	9
2.1.2 Reaction rate orders	10
2.1.3 Reaction rate constants	11
2.1.4 Kinetic isotope effect ¹⁷	11
2.2 Microwave assisted synthesis ^{23,24}	13
2.3 Modelling ²⁷	14
2.3.1 Introduction	14
2.3.2 Force field calculations ²⁷	15

2.3.3	Density function theory ²⁷	16
2.4	Mechanistic considerations	17
2.4.1	Hard-soft-acid-base theory ¹⁷	17
2.4.2	Bürgi-Dunitz trajectory ^{30,31}	18
2.5	Suggested isomerization mechanisms	19
2.5.1	Ketene intermediates	19
2.5.2	Isomerization through an ion-pair intermediate ^{41,42}	21
3	Thermolysis of the ammonium tartrate salt 2	23
3.1	Deuterium experiments	24
3.2	Isomerization mechanisms	26
4	Cyclization condensation of the monoacid 3	27
4.1	Kinetics	28
4.1.1	Initial experiments	28
4.1.2	The effect of water present in the system	30
4.1.3	Determination of kinetic parameters	32
4.2	DFT modelling	35
4.2.1	Determination of possible intermediates	36
4.2.2	Calculation of potential energy for the listed candidates	37
4.2.3	Determination of lowest energy pathway	38
4.3	Reaction mechanism	39
4.3.1	Initial activation of 3	39
4.3.2	Proton transfer and condensation of water in order to form the cyclized tartramide 1	42
4.3.3	Proposed reaction mechanism	43
5	Opening of tartramide 1 with an amine	45
5.1	Initial experiments	46
5.1.1	Formation of an equilibrium	47
5.1.2	Outlier data points	47
5.2	Stereochemical aspects regarding 1	48
5.3	Stereochemical aspects of formed diamides 27	50
5.3.1	Stereochemical preferences	53
5.4	Suggested isomerization mechanisms	55
6	Reactions of the monoacid (<i>R,R</i>)-3 with free amine	59
6.1	Isomerization of the formed cyclic imides 1	60
6.2	Isomerization of diamides 27	62
6.3	Possible explanations for the observed changes in stereochemistry	63

7	Studying the initial amide formation from 2	65
8	Conclusion and further work	67
8.1	Further work	70
8.1.1	Synthesis of deuterated tartaric acid (32)	70
8.1.2	Deuterium experiments	70
8.1.3	Initial amide formation	70
9	Synthesis results	73
9.1	Synthesis of 2d,3d-(<i>DL</i>)-tartaric acid (13)	73
9.1.1	α -H activation in 6 with ionic barium in basic media	73
9.1.2	Acid induced α -H activation in 6	77
9.1.3	α -H activation in 6 using microwave radiation	79
9.2	Introduction to synthesis of stereochemically pure compounds	82
9.3	Synthesis of 36 , a starting block for 3	82
9.4	Synthesis of octyl monoamido (<i>R,R</i>)-tartaric acid 16	83
9.5	Synthesis of 4-phenylbutyl monoamido tartaric acids 3	85
9.6	Synthesis of 4-phenylbutyl tartrimidides 1	86
9.7	Synthesis of 4-phenylbutyl tartradiamides 27	87
9.8	Synthesis of 4-phenylbutyl ammonium (<i>R,R</i>)-tartrate 2	88
9.9	Synthesis of diethyl monoamido (<i>R,R</i>)-tartaric acid 29	88
10	Compound analysis	91
10.1	Spectroscopy of new compounds	91
10.1.1	4-Phenylbutyl monoamido tartaric acids 3	91
10.1.2	4-Phenylbutyl tartaric diamides 27	94
10.1.3	4-Phenylbutyl tartrimidides 1	96
10.1.4	4-Phenylbutyl monoamido methyl (<i>R,R</i>)-tartrate 42	99
10.1.5	4-Phenylbutyl ammonium (<i>R,R</i>)-tartrate 2	101
10.2	Quantification of deuterium in tartaric acid	102
10.2.1	MS quantification of deuterium in tartaric acid	102
10.3	Chromatography	103
10.3.1	Detection and quantification of the monoamido tartaric acids 16 and 44	103
10.3.2	Quantification of compounds 1 and 27	107
11	Experimental section	111
11.1	General methods	111
11.1.1	Chemicals and solvents	111
11.1.2	Spectroscopic analyses	111
11.1.3	Chromatography	112

11.1.4	Other equipment	112
11.2	Preparation of α -deutero tartaric acid (13)	113
11.2.1	α -Deuteration with Barium compounds	113
11.2.2	α -Deuteration with acid catalysis	114
11.2.3	α -Deuteration in a basic environment	115
11.2.4	α -Deuteration using microwave irradiation	115
11.3	Diacetyltartaric anhydrides (36) ^{73–75}	116
11.4	Octylammonium tartaric acid system	117
11.4.1	Synthesis of 16	117
11.5	4-Phenyl butyl ammonium tartaric acid system	118
11.5.1	Synthesis of (<i>R,R</i>)- 3	118
11.5.2	Synthesis of (<i>S,S</i>)- 3	119
11.5.3	Synthesis of (<i>R*,S*</i>)- 3	120
11.5.4	Synthesis of 42	121
11.5.5	Synthesis of (<i>R,R</i>)- 27	122
11.5.6	Synthesis of (<i>S,S</i>)- 3	123
11.5.7	Synthesis of (<i>R*,S*</i>)- 3	123
11.5.8	Synthesis of (<i>R,R</i>)- 1	124
11.5.9	Synthesis of (<i>S,S</i>)- 1	125
11.5.10	Synthesis of (<i>R*,S*</i>)- 1	126
11.5.11	Synthesis of 2	127
11.5.12	Synthesis of 52	127
11.5.13	Attempted synthesis of 29	128
11.6	Molecular modelling parameters and data	128
11.6.1	DFT ^{85,86}	128
11.6.2	Force field optimizations (MM2) ²⁸	129
11.7	Kinetic experiments	129
11.7.1	Cyclization of 3 to form 1	129
11.7.2	Ringopening of 1 with an amine	130
11.7.3	Refluxing 3 with an amine	130
11.7.4	Attempted monitoring of the monoacid formation	130
11.7.5	Monitoring of the entire reaction	131
11.8	Various mechanistic experiments	131
11.8.1	Cyclization of 2d,3d-tartaric acid with an amine	131
11.8.2	Cyclization of 52	131
11.8.3	Possible ringopening of 1 in aqueous reflux	131
11.8.4	isomerization of 1 with a hindered base	132
11.8.5	Isomerization of dimethyltartrate with NaOH	132
11.9	Test of possible internal standards	132
11.10	Derivatization of 53 with diazomethane	132

Appendixes	141
A Spectroscopic data for 3	141
B Spectroscopic data for 27	153
C Spectroscopic data for 1	167
D Spectroscopic data for 42	181
E Spectroscopic data for 2	187
F Spectroscopic data for 36	191
G Spectroscopic data for 16	193
H Spectroscopic data from 2d,3d-tartaric acid synthesis	195
I Spectroscopic data from attempted synthesis of 29	197
J General procedure for kinetic experiments	199
K Supplementary data for Chapter 3	203
L Supplementary data for Chapter 4	207
M Supplementary data for Chapter 5	215
N Supplementary data for Chapter 6	223
O Supplementary data for Chapter 7	229

Abbreviations and symbols

A	Pre-exponential factor in Arrhenius' equation
c	Speed of light in vacuum
c	g/100mL
h	The Planck constant
J	Coupling constant in ^1H NMR spectroscopy
k_b	The Boltzmann constant
m/z	mass over charge ratio
δ	Chemical shift in NMR spectroscopy
λ	Wavelength
η	Chemical hardness
σ	Chemical softness
Ψ	Sign for a wavefunction
ΔG	Gibbs free energy
ΔG^\ddagger	Activation energy
$\rho(\vec{r})$	Electron density
$[\alpha]_D^{20}$	Optical rotation at 20 °C at the Na D-line
$E[\rho(\vec{r})]$	Energy as a functional of electron density
$E_H[\rho(\vec{r})]$	Electron-electron coulomb energy
$E_{KE}[\rho(\vec{r})]$	Kinetic energy for an ideal electron gas
$E_{XC}[\rho(\vec{r})]$	Energy contribution from exchange-correlation interactions
$F[\rho(\vec{r})]$	Unknown functional in the DFT equation
V_{ext}	External potential
1D	1-Dimensional
2D	2-Dimensional
Ac	Acetyl group
AcCl	Acetyl chloride
AcOH	Acetic acid
Avg.	Average
Cat.	Catalytic amounts

CMC	Critical Micelle Concentration
Conc.	Concentration
Conv.	Conversion
DFT	Density Function Theory
DMF	Dimethyl formamide
E	Energy
E₁cb	Unimolecular-Elimination-conjugate-base mechanism
E_a	Activation energy
EA	Electron affinity
eq.	Equivalents
ESI	Electron Spray Ionization
Et₂O	Diethylether
EtOH	Ethanol
eV	Electron volt
HOMO	Highest Occupied Molecular Orbital
HPLC	High performance liquid chromatography
HSAB	Hard-Soft-Acid-Base theory
HSQC	Heteronuclear Single Quantum Coherence
IP	Ionization potential
IPA	Isopropanol
IR	InfraRed radiation
IS	Internal Standard
k	Rate constant
KIE	Kinetic Isotope Effect
LUMO	Lowest Unoccupied Molecular Orbital
Me	Methyl group
MeOH	Methanol
Methyltruncated	Substituent chain truncated with a methyl group
MM2	A universal molecular mechanics force field
Monoacids	Alkyl monoamido tartaric acids
MS	Mass spectroscopy
MW	Microwave radiation
NMR	Nuclear magnetic resonance
NOE	Nuclear Overhauser Enhancement
Ph	Phenyl group
ppm	Parts per million
R	The universal gas constant, 8.314 JK ⁻¹ mol ⁻¹
R²	Statistical measure of how well a regression line fits the data points (1 = perfect fit)
r_t	Retention time

S_N1	Unimolecular nucleophilic substitution
S_N2	Bimolecular nucleophilic substitution
std.	Standard deviance
T	Temperature
TFA	TriFluoro Acetic acid
THF	Tetrahydrofuran
UV	Ultraviolet
ZPVE	Zero Point Vibrational Energy

List of Tables

3.1	H/D ratios and amount of <i>meso</i> at reaction end point. . . .	25
4.1	Cyclization of monoamido tartaric acids to form cyclic tartrimidates in refluxing xylenes (134 – 140 °C).	29
4.2	Calculated reaction orders for the first 1-1.5 hours, for conversion of (<i>R,R</i>)- 3 and (<i>R*,S*</i>)- 3	35
6.1	Different amounts of amine added to (<i>R,R</i>)- 3 (56.9×10^{-3} mol/L) in refluxing xylenes (12.5 mL).	60
6.2	Observed difference in rate of isomerization for 27	62
9.1	Yields and conditions for attempts to synthesize 13 from (<i>R,R</i>)- 6 , where deuteration with BaO, BaCl and NaOD was attempted.	76
9.2	Yields and conditions for attempts to synthesize 13 from (<i>R,R</i>)- 6 with strong acids.	79
9.3	Yields and conditions for attempts to synthesize 13 from (<i>R,R</i>)- 6	80
9.4	Yields for the synthesis of 3 from 36	85
9.5	Yields for the synthesis of 1 from 3	86
10.1	Mass spectrometry (ESI) of 3	91
10.2	Infrared spectroscopy of 3 for the C=O stretching frequencies.	92
10.3	Optical rotation of 3 in methanol.	92
10.4	Assigned shifts for 3	93
10.5	Mass spectrometry (ESI) of 27	94
10.6	Optical rotation of 27 in DMF.	94
10.7	Assigned shifts for 27	95
10.8	Mass spectrometry (ESI) of 1	96
10.9	Infrared spectroscopy of 1 for the C=O stretching frequencies.	96
10.10	Optical rotation of 1 in DMF.	97

10.11	Assigned shifts for 1	98
10.12	Mass spectrometry (ESI) of 42	99
10.13	Assigned shifts for 43	100
10.14	Assigned shifts for 2	101
10.15	Different elution systems and conditions tried for quantifi- cation of 16 and 3 with HPLC.	104
10.16	Elution order and retention time extremas for 1 and 27 . . .	109
11.1	Incorporation of deuterium and conditions for experiments with assisted microwave irradiation in basic environment. . .	116
J.1	Data deduced from ^1H NMR analysis of reaction mixtures for the cyclization of 3	202

List of Figures

1.1	Simplified graphic of a surfactant molecule.	1
1.2	Non-ionic monorhamnolipid.	2
1.3	Examples of surfactant secondary structures.	3
1.4	Changes of surface tension due to aggregate formation.	4
1.5	N-octylgluconamide.	5
1.6	<i>L</i> -, <i>D</i> - and <i>meso</i> -tartaric acid.	5
1.7	1) Shows the wanted results for synthesis of these compounds. 2) Shows the actual observations.	6
1.8	The two suggested pathways for explaining the observed partial racemization of 7 prepared from 11	7
1.9	1) Example of functionalization possibilities for 1 . 2) Main reaction to be studied in this thesis.	8
2.1	Energetic differences between a protium- and a deuterium substituted moiety.	12
2.2	Space filling representation of benzene.	14
2.3	Example contributions to the potential energy surface in force fields.	16
2.4	Graphic representation of polarization of the valence electron distribution in an atom or ion.	17
2.5	The Bürgi-Dunitz trajectory for nucleophilic addition to a carbonyl group.	18
2.6	Partial isomerization of the polar headgroups in refluxing xylenes.	19
2.7	Formation of ketene intermediates from tertiary amines and acid chlorides.	19
2.8	The frontier molecular orbitals for ketene.	20
2.9	The different mechanisms for reactions with ketenes.	21
2.10	Basic isomerization of saturated carbon centers through ion-pair intermediates.	21

3.1	Formation of partially isomerized 1 and minor amounts of diamide from the ammonium tartrate salt 2	23
3.2	Observed trends in the cyclic imide formation from the ammonium tartrate monosalt.	24
3.3	Results from synthesis of 1 from deuterated ammonium tartrate salt (14).	25
3.4	Results from synthesis of 1 from heteroatom deuterated ammonium tartrate salt (15).	25
3.5	The two suggested pathways for explaining the observed partial isomerization of 1 prepared from 2	26
4.1	Partial racemization when starting from 2 to make 1	27
4.2	Cyclization of 3 to form 1	27
4.3	Monoacid conversion over time at different concentrations.	29
4.4	Thermal condensation of (<i>R,R</i>)- 3 to form (<i>R,R</i>)- 1 with and without azeotropic removal of water.	31
4.5	Aqueous reflux of (<i>R,R</i>)- 1 to test the ability of water to induce the reverse reaction (ring opening of cyclic tartramide).	31
4.6	Breakage of carboxylic acid cyclic dimers.	32
4.7	Typical rate plot for conversion of 3 into 1	33
4.8	A log-log plot of rate vs concentration for the first 1 to 1.5 hours of the conversion of 3 into 1	34
4.9	Cyclization condensation to form 1 from 3	35
4.10	Possible intermediates chosen for modelling.	36
4.11	Obtained relative potential energy surface for the intermediates.	37
4.12	Lowest energy pathway determined by DFT modelling.	38
4.13	Proposed mechanism for direct amide formation by Charville <i>et al.</i>	39
4.14	Suggested dimer-form of 3 in nonpolar solvent.	40
4.15	Difference in reaction order and rate constant on basis of the stereochemistry of the monoacid 3	40
4.16	Intramolecular reorganization of 3	41
4.17	Aqueous reflux of (<i>R,R</i>)- 1 to test the ability of water to induce the reverse reaction (the ring opening of cyclic tartramide).	42
4.18	The two proposed mechanistic pathways for the cyclic tartramide 1 formation from 3	43
5.1	1) Partial isomerization when starting from 2 to make 1 . 2) Ringopening of 1 with an amine to form the diamide 27	45
5.2	Conversion of (<i>R,R</i>)- 1 into 27	46
5.3	Equilibrium between 1 and 27	47

5.4	Difference in conversion plots was observed when starting from different stereochemistry of 1	48
5.5	Ring opening equilibrium of 1 with different stereochemistry into diamides.	48
5.6	Possible explanation to the observed differences between using (<i>R,R</i>)- 1 and (<i>R*,S*</i>)- 1	49
5.7	(<i>R*,S*</i>)- 1 reacted with 4-phenylbutylamine (1 eq.).	50
5.8	Changes of stereochemistry for the formed diamides 27 when starting from (<i>R,R</i>)- 1 and adding one equivalent of amine.	51
5.9	Changes of stereochemistry for formed 27 when starting from (<i>R,R</i>)- 1 and adding two equivalents of amine.	52
5.10	Comparison of the conversion plots for (<i>R*,S*</i>)- 27 when starting from (<i>R,R</i>)- 1 and adding one or two equivalents of amine.	52
5.11	Observed isomerization trends for the formed diamides 27	53
5.12	Isomerization of the formed diamides 27 is different depending on the stereochemistry of the starting tartramide 1	54
5.13	Possible explanations for the observed trends.	54
5.14	Grade of isomerization in different substrates under different reaction conditions.	55
5.15	Possible explanation for isomerization from optically active diamides to <i>meso</i> -diamide being slower than the opposite reaction.	56
5.16	Suggested isomerization mechanism with the cyclic imide 1 as an intermediate.	57
6.1	Formation of partially isomerized cyclic tartramide from ammonium tartrate monosalt.	59
6.2	Thermolytic reaction of (<i>R,R</i>)- 3 with varying amounts of 4-phenylbutylamine in refluxing xylenes.	59
6.3	The observed composition of 1 (from HPLC) after 9 hours of refluxing time with 1 equivalent of amine added.	61
6.4	Suggested explanation to the observed doubly inverted (<i>S,S</i>)- 1	61
6.5	Formation and stereochemical isomerization of 27	62
6.6	Reaching a stereoisomeric equilibrium between the different forms of 27 was observed to be faster from 3 + 2 eq. amine than for 1 + 2 eq. amine.	63

6.7	1) Direct diamide formation with isomerization through an carboxylic acid dimer assisted mechanism (4.3). 2) Initial cy- clization condensation followed by imide-diamide equilibrium and rapid ringopening of formed (R^*,S^*)- 1 due to higher steric energy.	64
7.1	Formation of partially isomerized 1 from 2 , with 3 as a stable intermediate.	65
7.2	Strategy laid out in order to separately study the initial amide formation.	66
8.1	Proposed mechanisms for cyclic imide formation.	68
8.2	Suggested isomerization mechanism for 1 and 27	69
8.3	Suggested deuterium experiment for further studies.	71
9.1	2d,3d-tartaric acid	73
9.2	Barium <i>L</i> -tartrate crystal structure.	74
9.3	Deuterium incorporation in mandelic acid with barium(II)oxide and heavy water.	75
9.4	Synthesis of 13 with Ba(II) in basic media.	75
9.5	Formation of monomethyl- and dimethyltartrate with deuter- ated methanol in the NMR tube. Esterification was a lot higher for sample containing residual barium(II).	77
9.6	Possible enolformation of tartaric acid in acidic environment.	78
9.7	Synthesis of 13 from R,R - 6 with strong acids.	78
9.8	Synthesis of 13	80
9.9	Partial isomerization when starting from 2 to make 1	82
9.10	Extrapolation of the reaction system.	82
9.11	Synthesis of 36	83
9.12	Synthesis of 16	83
9.13	Observed product 38 with AcCl as deacetylation reagent.	84
9.14	Synthesis of 3	85
9.15	Synthesis of 1	86
9.16	Synthesis of 27	87
9.17	Synthesis of 2	88
9.18	Synthesis of 42	88
10.1	Numbering of carbon atoms in 3	91
10.2	Numbering of carbon atoms in 27	94
10.3	Numbering of carbon atoms in 1	96
10.4	Numbering of carbon atoms in 42	99

10.5	Numbering of carbon atoms in 2	101
10.6	Main fragment elucidated for quantification of deuterium in tartaric acid.	102
10.7	Chromatogram of compound (<i>R,R</i>)- 3	105
10.8	2-Quinoxaloyl chloride for alpha hydroxy derivatization.	106
10.9	Possible products from 2-quinoxaloyl derivatization, there might also be possibility of forming the anhydride product.	106
10.10	Derivatization with diazomethane.	107
10.11	Reference mixture of all 27 and 1	108
A.1	¹ H NMR spectra of (<i>R,R</i>)- 3	141
A.2	¹³ C NMR spectra of (<i>R,R</i>)- 3	142
A.3	HSQC spectra of (<i>R,R</i>)- 3	143
A.4	IR spectra of (<i>R,R</i>)- 3	144
A.5	¹ H NMR spectra of (<i>S,S</i>)- 3	145
A.6	¹³ C NMR spectra of (<i>S,S</i>)- 3	146
A.7	HSQC spectra of (<i>S,S</i>)- 3	147
A.8	IR spectra of (<i>S,S</i>)- 3	148
A.9	¹ H NMR spectra of (<i>R*,S*</i>)- 3	149
A.10	¹³ C NMR spectra of (<i>R*,S*</i>)- 3	150
A.11	HSQC spectra of (<i>R*,S*</i>)- 3	151
A.12	IR spectra of (<i>R*,S*</i>)- 3	152
B.1	¹ H NMR spectra of (<i>R,R</i>)- 27	153
B.2	¹³ C NMR spectra of (<i>R,R</i>)- 27	154
B.3	HSQC spectra of (<i>R,R</i>)- 27	155
B.4	IR spectra of (<i>R,R</i>)- 27	156
B.5	¹ H NMR spectra of (<i>S,S</i>)- 27	157
B.6	¹³ C NMR spectra of (<i>S,S</i>)- 27	158
B.7	HSQC spectra of (<i>S,S</i>)- 27	159
B.8	IR spectra of (<i>S,S</i>)- 27	160
B.9	¹ H NMR spectra of (<i>R*,S*</i>)- 27	161
B.10	¹³ C NMR spectra of (<i>R*,S*</i>)- 27	162
B.11	HSQC spectra of (<i>R*,S*</i>)- 27	163
B.12	IR spectra of (<i>R*,S*</i>)- 27	164
B.13	HPLC chromatogram of the three diamides 27 . 1) (<i>R,R</i>) 2) (<i>S,S</i>) 3) (<i>R*,S*</i>).	165
C.1	¹ H NMR spectra of (<i>R,R</i>)- 1	167
C.2	¹³ C NMR spectra of (<i>R,R</i>)- 1	168
C.3	HSQC spectra of (<i>R,R</i>)- 1	169

C.4	IR spectra of (<i>R,R</i>)- 1	170
C.5	¹ H NMR spectra of (<i>S,S</i>)- 1	171
C.6	¹³ C NMR spectra of (<i>S,S</i>)- 1	172
C.7	HSQC spectra of (<i>S,S</i>)- 1	173
C.8	IR spectra of (<i>S,S</i>)- 1	174
C.9	¹ H NMR spectra of (<i>R*,S*</i>)- 1	175
C.10	¹³ C NMR spectra of (<i>R*,S*</i>)- 1	176
C.11	HSQC spectra of (<i>R*,S*</i>)- 1	177
C.12	IR spectra of (<i>R*,S*</i>)- 1	178
C.13	HPLC chromatogram of the three imides 1 . 1) (<i>R,R</i>) 2) (<i>S,S</i>) 3) (<i>R*,S*</i>).	179
D.1	¹ H NMR spectra of 42	181
D.2	¹³ C NMR spectra of 42	182
D.3	HSQC spectra of 42	183
D.4	IR spectra of 42	184
D.5	HPLC chromatogram of 42	185
E.1	¹ H NMR spectra of 2	187
E.2	¹³ C NMR spectra of 2	188
E.3	HSQC spectra of 2	189
E.4	IR spectra of 2	190
F.1	¹ H NMR spectra of 36	191
G.1	¹ H NMR spectra of 16	193
H.1	Mass spectra of 13	195
H.2	¹ H NMR spectra of esterification in NMR tube.	196
I.1	¹ H NMR spectra of impure 29	197
J.1	Typical ¹ H NMR spectra from the cyclization of 3	199
J.2	α-H region of the spectra shown in Figure J.1.	200
J.3	α-H region of all the spectra in a typical experiment (cycliza- tion of 3).	201
J.4	Plot of the results from Table J.1 with fitted curves.	202
K.1	¹ H NMR spectra from formation of 1 from 2	203
K.2	¹ H NMR spectra from formation of 1 from 2	204
K.3	HPLC chromatogram from formation of 1 from 2	205

K.4	HPLC chromatogram from: 1) Experiment conducted with 13 . 2) Experiment conducted with 15	206
L.1	^1H NMR spectra from formation of 1 from 3 with a Dean-Stark apparatus.	207
L.2	^1H NMR spectra from aqueous reflux of 1	208
L.3	^1H NMR spectra from formation of 1 from 3	209
L.4	^1H NMR spectra from formation of 1 from 3	210
L.5	^1H NMR spectra from formation of 1 from 3	211
L.6	^1H NMR spectra from formation of 1 from 3	212
L.7	^1H NMR spectra from formation of 1 from 3	213
M.1	^1H NMR spectra from opening of (<i>R,R</i>)- 1 with 1 eq. 4-phenylbutylamine.	215
M.2	^1H NMR spectra from opening of (<i>R,R</i>)- 1 with 0.1 eq. 4-phenylbutylamine.	216
M.3	^1H NMR spectra from opening of (<i>R,R</i>)- 1 with 2 eq. 4-phenylbutylamine.	217
M.4	^1H NMR spectra from opening of (<i>R</i> [*] , <i>S</i> [*])- 1 with 1 eq. 4-phenylbutylamine.	218
M.5	^1H NMR spectra from opening of (<i>R</i> [*] , <i>S</i> [*])- 1 with 2 eq. 4-phenylbutylamine.	219
M.6	^1H NMR spectra from reflux of 1 and 2,2,6,6-tetramethylpiperidine in xylenes.	220
M.7	^1H NMR spectra from reflux of 54 and NaOD in xylenes.	221
M.8	HPLC chromatogram from formation opening of (<i>R</i> [*] , <i>S</i> [*])- 1 with 2 eq 4-phenylbutylamine.	222
N.1	^1H NMR spectra from reaction of (<i>R,R</i>)- 3 with 0.1 eq. 4-phenylbutylamine.	223
N.2	^1H NMR spectra from reaction of (<i>R,R</i>)- 3 with 1.0 eq. 4-phenylbutylamine.	224
N.3	^1H NMR spectra from reaction of (<i>R,R</i>)- 3 with 1.1 eq. 4-phenylbutylamine.	225
N.4	^1H NMR spectra from reaction of (<i>R,R</i>)- 3 with 2.0 eq. 4-phenylbutylamine.	226
N.5	HPLC chromatogram from from reaction of (<i>R,R</i>)- 3 with 1.0 eq. 4-phenylbutylamine.	227
O.1	^1H NMR spectra from attempted amidation of 29 with 4-phenylbutylamine.	229

1. Introduction and objective

1.1 Background

1.1.1 Surfactants¹

Surface active agents or "surfactants" are most commonly known for creating the desired "fat-dissolving" properties of soap. However, their function as a part of biological membranes are far more important, by rendering it possible for vital biological reactions to take place in an aqueous media.² As stated by their name, these compounds are active at a surface, and are characterized by their tendency to adsorb at surfaces and interfaces. An interface denotes the boundary between two immiscible phases where the term surface indicates that one of the phases is a gas (usually air). A surfactant adsorbs to these interfaces in order to lower the total free energy of the boundary, the free energy of an interface is the amount of work needed to expand the interface. One well known example of this phenomenon is commercial detergent in water, the surfactant molecules adsorb to the water surface in order to obtain a more preferred low-energy state for the interface. For the water-air system the free energy per unit is the equivalent of the surface tension, so lowering of the free energy will cause a reduction in the surface tension of the water phase.

Surfactants are amphiphilic molecules, where amphi is derived from Greek, meaning both, and in this case refers to the double nature of these molecules, hydrophobic and hydrophilic based on their tail and head respectively (Figure 1.1).

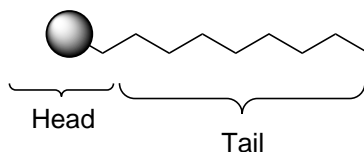


Figure 1.1 Simplified graphic of a surfactant molecule.

In addition to being able to alter the boundaries between immiscible phases, surfactants also have the ability to self-assemble into a vast number of aggregates. The size and properties of the aggregates alter with the characteristics for each amphiphile, the concentration ratios and the environment the surfactant is dissolved in.²

Surfactants are classified by their hydrophilic head group:

1. Anionic surfactants have a negatively charged head group, most often a sulfate, carboxylate, sulfonate or phosphate group, and is the most widely produced category of surfactants. Approximately 60% of the surfactants produced annually are anionic surfactants. The most common counter ion to these compounds are sodium, potassium, calcium and various ammonium groups.
2. Cationic surfactants have a positively charged head group and the vast majority of these compounds rely on nitrogen to carry the positive charge. Alkyl ammonium salts are common.
3. Non-ionic surfactants have no charged head group so the hydrophilic properties arise from the polarity of the head group. The head group in these compounds often consists of polyhydroxyl or polyether groups to render the head group polar enough to achieve the wanted characteristic of the surfactants. This is a group of surfactants in expansion, one particular interesting field of research is the use of lipids with rhamnose as the polar head group (4) as non-toxic oil dispersants in the oil industry.³

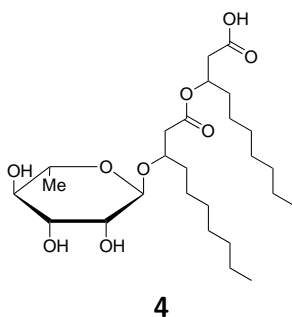


Figure 1.2 Non-ionic monorhamnolipid.

4. Zwitter-ionic surfactants have two charged moieties in the head group with opposite charge, where the positive group almost indiscriminately

is a nitrogen group and the negative group is often a carboxylate group. Due to these surfactants having multiple groups with different pK_a values they have amphoteric properties, which enables these compounds to switch between positive, neutral and negative net charge with change in pH, i.e. these surfactants are only zwitter-ionic over a certain pH range.

In addition to this coarse classification, surfactants are also classified based on the raw material used to prepare them. Furthermore, in recent days classification into green and brown surfactants have risen due to the increased focus on green chemistry. Green surfactants are generally surfactants made by microbial fermentation and are often more expensive to prepare, and thus are not as universal as petroleum based surfactants.⁴

1.1.2 Aggregates and self-assembly properties²

The concept of self-assembly for surfactants are based on the fact that surfactants form intermolecular aggregates in solution, in order to lower the total free energy of the system. This effect comes in addition and in most cases after the free energy is lowered in the interface. There is a wide range of aggregates that a surfactant can assemble to in solution; micelles, reversed micelles, vesicles, bilayers, etc (Figure 1.3). To what degree the surfactant inherits these secondary structures are dependent on a wide range of parameters where surfactant concentration plays the most important role.

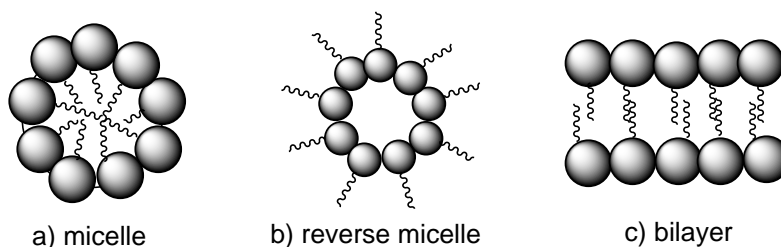


Figure 1.3 Examples of surfactant secondary structures.

The critical micelle concentration (CMC) for a surface active amphiphile in solution is defined as the concentration where the previously mentioned aggregate formation starts. As the name states, the first aggregates to be formed are usually spherical micelles. However, a vast number of superstructures are known to be formed, where a couple of simple examples are shown in Figure 1.3. The concentration at which aggregation occurs are

dependent on a range of surfactant structural properties as; chain length, ionic/nonionic head group, counter-ion valency and alkyl chain perfluorination. The CMC of a surfactant can be determined by plotting the physical properties of the surfactant system towards surfactant concentration, and the break points of the curves indicate the narrow concentration range where significant aggregation starts (Figure 1.4).

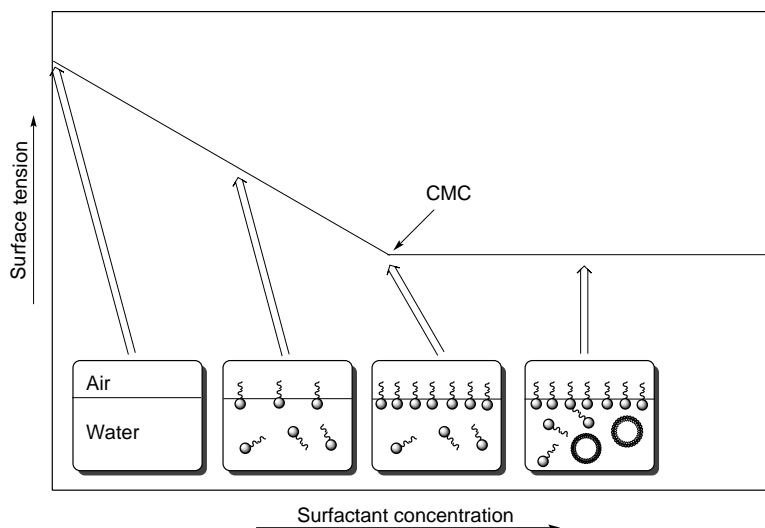
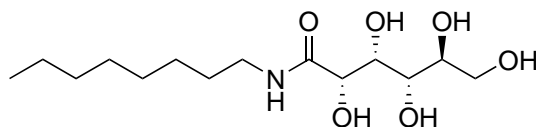


Figure 1.4 Changes of surface tension due to aggregate formation. (Inspired by original schematic).²

1.1.3 Importance and application of optically pure surfactants

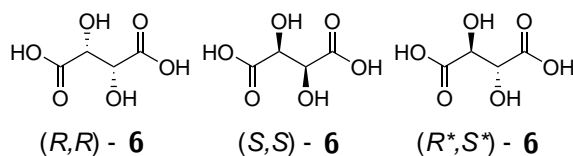
The self-assembly properties of surfactants are heavily dependent on chirality.⁵ Superstructures formed from one enantiomer of an amphiphile will most often differ from the aggregate formed from the other enantiomer and the racemate. Studies have shown that chiral N-octylgluconamide (**5**) form a quadruple helix, with right hand or left hand rotation depending on the enantiomer (*D* or *L*).⁵ However, as it turns out; when the two enantiomers are mixed together into a racemix mixture, the amphiphiles assemble into platelets without curvature.

The chirality is most often built into the head group of the amphiphile, and these compounds have been deemed useful in a wide range of fields. They are used as possible drug delivery vessels and transport of genetic

**5****Figure 1.5** N-octylgluconamide.⁵

material,⁶⁻⁸ chiral separation methods,⁹ ultrasound diagnosis,^{10,11} chiral induction in conventional organic synthesis¹² and several other fields of science.

1.2 Objective

**Figure 1.6** *L*-, *D*- and *meso*-tartaric acid.

In this project tartaric acid was chosen as the source of chirality for the synthesis of optically active surfactants. Tartaric acid is a diprotic aldaric acid with high natural occurrence.¹³ It is, as an example, one of the main acids in wine, the directly translated name for tartaric acid from Norwegian is "wine acid". Tartaric acid contains two stereocenters, and was among the first compounds to be found that rotates polarized light (by Biot in 1815).¹⁴

All the isomers of tartaric acid (**6**) are readily available and inexpensive compounds. In addition to the availability and price factor, tartaric acid contains two hydroxy groups, two carboxylic acid groups and two chiral centers. This makes it possible to create a wide variety of compounds from this scaffold, due to its versatility in functionalization possibilities. All of the above mentioned properties of tartaric acid explains why it was chosen as a starting block for surfactant synthesis.

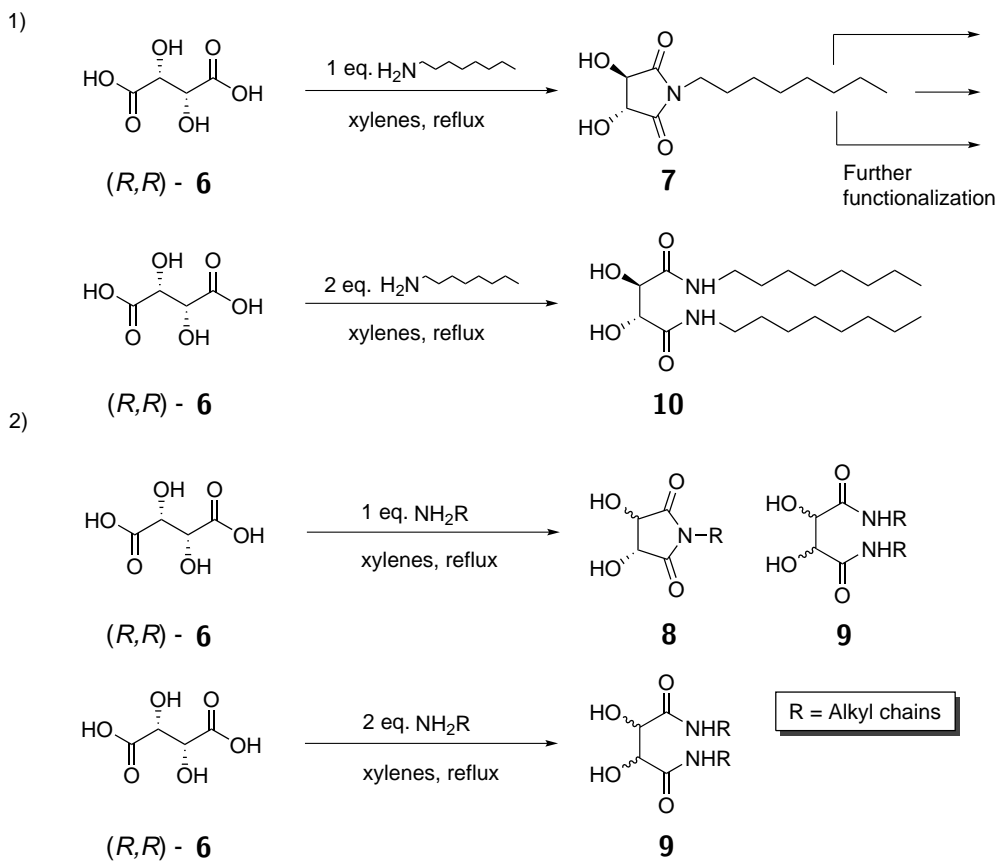


Figure 1.7 1) Shows the wanted results for synthesis of these compounds. 2) Shows the actual observations.

1.2.1 The problem

Considering the fact that tartaric acid contains two carboxylic acid groups, a practical functionalization method would be creation of the cyclic tatrime or tartaric diamides. Coupling tartaric acid with a long chained primary amine will create a cyclic imide **7** (from 1 eq. amine) or a diamide **10** (from 2 eq. amine) which can readily be further functionalized.¹⁵ However, it turns out that these thermolytic reactions causes partial isomerization of the stereochemistry in tartaric acid along with formation of some minor byproducts (minor amount of diamides from 1 eq. amine).^{2,15,16} The major concern is the partial isomerization which makes this into an unfavorable reaction since optical purity is obviously one of the main requirements in

this project. In order to make the optically pure cyclic imides **7** a longer synthetic route with lower yields is required. In any of the mentioned reactions the general tendency is the increasing challenge of purification when the length of the aliphatic chain increases (Section 9).

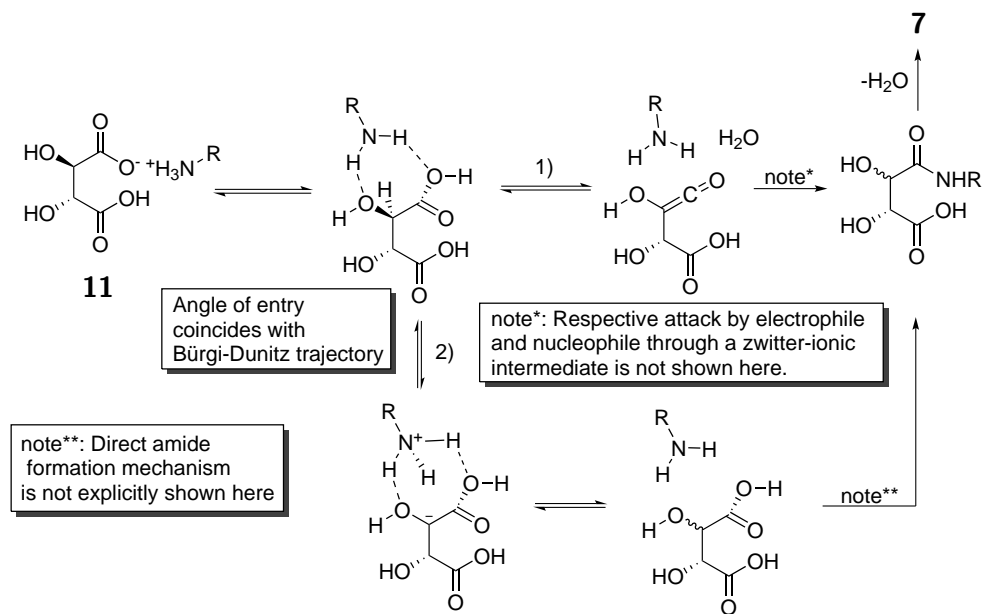


Figure 1.8 The two suggested pathways for explaining the observed partial racemization of **7** prepared from **11**.

The mechanism for direct formation of amide bonds^{13,17–19} do not explain the partial isomerization that takes place during the reaction. However, the Per Carlsen research group at NTNU have postulated possible mechanisms that explains the phenomenon.^{2,20,21} These mechanisms explains the partial isomerization through the formation of a ketene transition state or an asymmetric ion-pair induced by the presence of amine, causing partial racemization at the α -carbon (C2 and C3) (Figure 1.8).

All previous experiments have been conducted with aliphatic octyl chains as substituents on the amine. However, due to difficulties encountered with these compounds, as further elaborated in Section 10.3, the octyl chain was substituted for a 4-phenylbutyl moiety.

1.2.2 Objective of this project

The objective of this master study was to provide further evidence towards the isomerization mechanism proposed by the research group. The partial isomerization taking place in the reaction for preparing the cyclic imides **1** was of particular interest, as the cyclic imides can be precursors for monoacids **3** and diamides with two different substituents (**12**). Thus the main focus in this study was chosen to be the reaction for creating **1** from its corresponding ammonium tartrate salt **2** (reaction 2 in Figure 1.9).

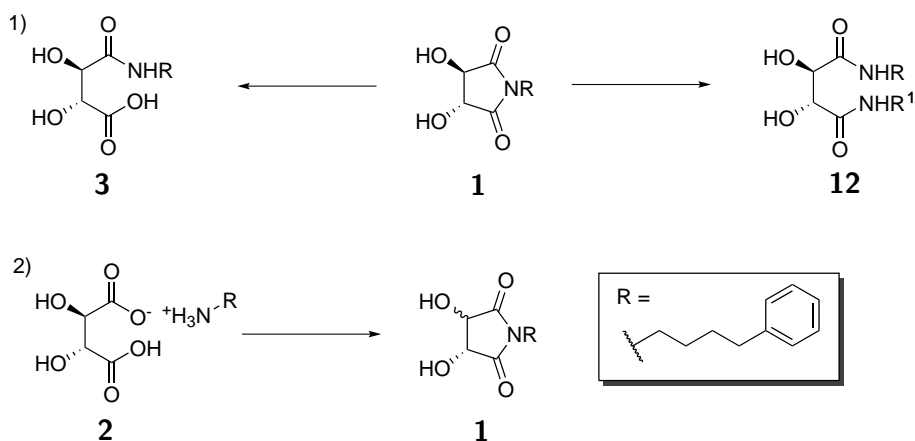


Figure 1.9 1) Example of functionalization possibilities for **1**. 2) Main reaction to be studied in this thesis.

The plan was to study kinetics and make mechanistic assessments for the partial reactions taking place in the chosen reaction system in order to provide further evidence towards the proposed mechanisms. In addition to kinetics, various methods as molecular modelling and deuterium tagging were also assumed to be of importance for elucidation of mechanisms. The objectives also encompassed outlining of different stereochemical analysis methods and synthesis of reference- and starting materials. This, in order to create a platform for further studies on similar reactions and other stereochemical challenges.

2. Theory

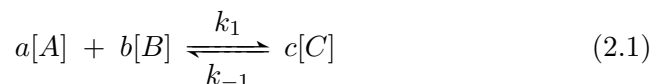
This chapter will introduce most of the theoretical principles applied in this work. This includes a general introduction to chemical kinetics, microwave synthesis and molecular modelling. In addition various physical-organic principles as HSAB and the Bürgi-Dunitz trajectory is presented, along with theoretical background for the two possible isomerization mechanisms.

2.1 Kinetics^{17,22}

2.1.1 Introduction

Chemical kinetics is used as a mean to quantitatively relate structure to reactivity,¹⁷ and also relate the reaction rate to macroscopic constants as concentration and temperature. To understand what reaction rate and kinetics encompass, one must start with looking at the most fundamental examples of chemical reactions.

A reaction takes place between molecules A and B to form the product C in a reaction vessel according to the following equation 2.1:



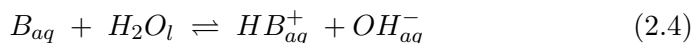
The bracketed form of the components is used to describe concentration in solution, as [A] is the concentration of substrate A in a given solvent. This is the most widely applied form for describing amounts of compounds in kinetics for organic reactions, whereas in other areas different units are applied. The forward and backward constants (k) in equation 2.1 describe the relative size of the forward and backward reaction rate. The reaction rate is described from the formation of products or the disappearance of reactants,²² which can be seen from equation 2.2:

$$\text{rate} \equiv -\frac{1}{a} \frac{d[A]}{dt} = -\frac{1}{b} \frac{d[B]}{dt} = \frac{1}{c} \frac{d[C]}{dt} \quad (2.2)$$

An elementary reaction is a reaction which proceeds through one step, meaning it cannot be divided into subsequent steps and that it proceeds as equation 2.1. A reaction mechanism is considered to be a sequence of elementary steps. If a reaction is elementary the rate law can be expressed in the following way by equation 2.3:

$$\frac{1}{c} \frac{d[C]}{dt} = k_1[A]^a[B]^b - k_{-1}[C]^c \quad (2.3)$$

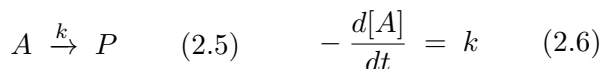
Equation 2.3 is written with possibility of the reverse reaction taking place, hence the reaction dictated by k_{-1} may take place in addition to the formation of product C . The size of the rate constants (k) determine whether the reaction in question is considered to be a reversible equilibrium or an "irreversible" reaction. One example of the latter is the isomerization of cyclopropane to propene, where the reverse reaction barely takes place and is neglected in the rate law describing the kinetics of the reaction. An example of an equilibrium is the protonation of a weak base, which will, due to its reversibility, assume equilibrium concentrations after some time (equation 2.4). When working with kinetics regarding chemical equilibria it is often practical to do measurements far away from equilibrium conditions in order to simplify the rate equations.



2.1.2 Reaction rate orders

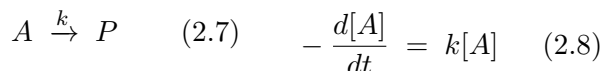
The order of a reaction is the sum of all the exponents to the concentrations in the rate law, for equation 2.3 the overall reaction order would be $a + b + c$. Elementary one-step reactions have integer overall reaction orders while multistep reactions often have non-integer overall reaction orders. The most common reaction orders for elementary reactions are:

- **Zero order kinetics:** When a reaction (equation 2.5) proceed with zero order kinetics the rate (equation 2.6) is constant throughout the reaction. This type of reactions are not common, but some heterogeneous reactions and some photochemical reactions are known to proceed with this overall reaction order.

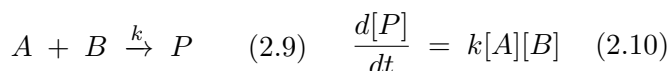


- **First order kinetics:** When the rate of the reaction is first order, it depends on one reactant molecule. Unimolecular nucleophilic substitutions (S_N1) are examples of chemical reactions that undergoes first

order kinetics, however, all radioactive decay also undergo first order kinetics.



- **Second order kinetics:** The most known organic reactions that undergo second order kinetics are the bimolecular nucleophilic substitutions (S_N2). These reactions depend on one stoichiometric unit of each reactant (equation 2.9), which makes the overall reaction order two (equation 2.10).



2.1.3 Reaction rate constants

As mentioned above, the reaction rate constant dictates the speed of a chemical reaction. The rate constant (k) can be described in several ways, and the Arrhenius equation (equation 2.12) undoubtedly being one of the most known.

$$\Delta G = -RT \ln K \quad (2.11) \quad k = A e^{\frac{-E_a}{k_b T}} \quad (2.12)$$

However, regardless of the way to describe it, temperature is a governing factor for determination of the rate constant. Most chemists have experienced the importance of temperature for a particular reaction to take place, this is easily explained from the Arrhenius equation (equation 2.12). As the activation energy increases the rate constant is lowered, which is countered by increasing the temperature. The activation energy can be translated to transition state energy, so the higher the transition state energy is, the higher temperature is required for the reaction to take place. A relevant example describing this phenomenon can be seen in Section 9.6, in the original synthesis toluene was used as solvent for refluxing of the monoamido tartaric acids **3** in order to form the cyclic tartrimidides **1**. However, due to slow conversion rate, toluene was swapped for xylene which has a higher boiling point. The increase in temperature from 111 °C to 130 °C increased the conversion rate by tenfolds.²

2.1.4 Kinetic isotope effect¹⁷

Isotope tagging of molecules have been proven valuable in mechanistic assessments, a typical example being providing evidence for hydrogen trans-

fers in reaction mechanisms by NMR or mass spectrometry. There is also a kinetic factor involved for isotope substitutions called the kinetic isotope effect. Kinetic isotope effect is most commonly associated with hydrogen isotopes, as they give the biggest quantitative differences between the different isotopes.

The arisal of rate differences on background of isotope comes from zero point energy contributions. As any C-H bond have characteristic vibrations which contribute energy to the entirety of the molecule, this energy is known as zero point energy. The frequency, hence the energy, associated with these vibrations are closely related to the reduced mass of the atoms involved in the vibration. Considering a C-D bond versus a C-H bond, the carbon and deuterium have a higher reduced mass than the corresponding carbon-protium bond. The vibrational frequency will then be lower for C-D than for C-H and less energy is contributed to the zero point energy. Hence, a C-H bond is considered to be weaker than a corresponding C-D bond, which gives arisal to rate differences as shown in Figure 2.1.

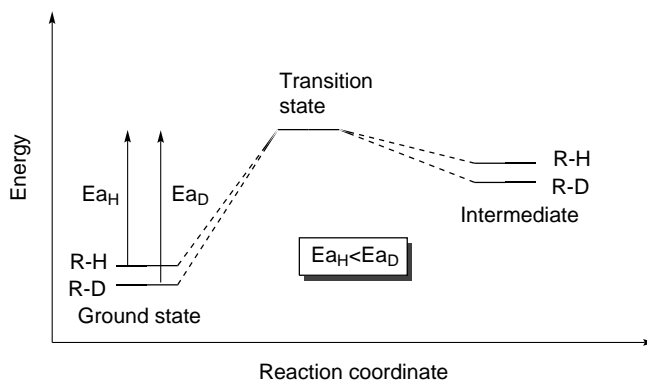


Figure 2.1 Energetic differences between a protium- and a deuterium substituted moiety.¹⁷

If removal of the hydrogen specie from the molecule in question is the rate determining step, this will give rise to primary kinetic isotope effects. Due to the higher activation energy for removal of hydrogen in order to create the cationic deprotonated specie, the rate is slowed down for deuterium substituted compounds. Due to the hydrogen being removed, the zero energy difference between the two species disappear in the transition state, hence the difference in activation energy is observed.

The above mentioned concept is known as primary kinetic isotope effects and involve breakage of the R-isotope bond in the rate determining step. The other forms for KIE¹⁷ are not discussed in this thesis.

2.2 Microwave assisted synthesis^{23,24}

The first use of microwave radiation as a substitution for conventional heating methods were reported by the groups Gedye and Giguere/Majetich^{25,26} in 1986. After this initial breakthrough over 3500 articles in which microwave radiation are utilized have been published worldwide. The development of specialized vessels and reactors over the last decades in order to improve safety and reproducibility, have helped to make microwave assisted synthesis into a established method in both academia and chemical industry.

One of the main advantages of microwave irradiation is the often dramatic reduction in reaction time. This enables the chemist to more easily do reaction scouting and process optimization. If a failure takes merely minutes compared to days, one can optimize a process in the course of one day. Instead of using weeks in order to do achieve the same results. Not surprisingly, this is one of the main reasons to microwave chemistry being a rapidly growing field.

$$E = \frac{hc}{\lambda} \quad (2.13)$$

The microwave region of the electromagnetic spectrum lies between the infrared and radio regions, and is considered to be low energy radiation. Microwaves have traditionally been used for telecommunication or energy transmission. Due to its relatively long wavelengths, the waves are able to travel over relatively long distances which makes them favorable for telecommunication not unlike radiowaves. However, as can be seen from equation 2.13, the longer wavelength (λ) of the radiation corresponds to lower energy (E). h is the Planck constant and c is the speed of light in vacuum. From the Planck relation (equation 2.13) it is evident that due to its relatively long wavelength between 1 mm and 1 m, microwave photons do not contain sufficient energy to directly induce chemical reactions by energy absorption like, for example, ultraviolet radiation. Microwave chemistry is based on the ability of materials to absorb microwave energy and convert it into heat, this is called "*microwave dielectric heating*". Dielectric heating can be divided into two main mechanisms; dipolar polarization and ionic conduction. Heat generated from dipolar polarization will, in short, arise from molecular friction and collisions from dipoles trying to realign to a fluctuating electric field. Ionic conduction creates heat more or less the same way, except that in this case it is dissolved charged particles that oscillate and creates molecular friction.

When looking into the mechanisms for heating with microwave irradiation one comes to understand why the reaction times are lower than for conventional heating equipment. When using an oil bath or a heating jacket the heat is applied from the outside of the system, thus the transfer of energy is by far less efficient and external heating might cause the arisal of local "hotspots" and heating gradients. When using microwaves, the system itself generates the heat and in this way more rapid and efficient energy transfer to the reaction site is obtained, in addition to having a uniform heat distribution.²⁴

2.3 Modelling²⁷

2.3.1 Introduction

In the early years of molecular modelling, the term was most commonly associated with physical models such as Dreidings stick model or the space filling model of Corey, Pauling and Koltun. The first space filling models were made out of hardwood spheres with accurate representations of the atom's Van der Waal radius.

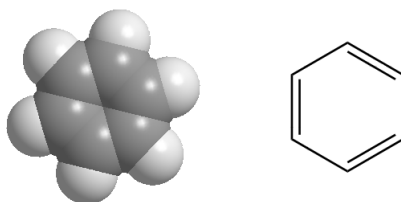


Figure 2.2 Space filling representation of benzene.

Molecular modelling is today almost solely based on computer modelling, due to the rapid development of more powerful hardware the last 20 years. Chemists nowadays are able to run quantum mechanical models on his or hers home computer and get the results within a reasonable time-frame. The development of faster and more powerful supercomputers makes it possible to do accurate modelling on big molecular systems like proteins and protein folding. The hardware used in molecular modelling today are only recently developed, the fundamental theories that the models are based

on however, were established years before the first computers were born. A prime example is quantum mechanics, which is used in a big percentage of all computational models today, but preceded the first computers by decades.

2.3.2 Force field calculations²⁷

Force fields are used to calculate the *potential energy surface* of molecules, which is the molecular energy as a function of the nuclear coordinates. Force field calculations, or molecular mechanics, ignore the electronic motion in the system and does only require a fraction of the time to compute compared to quantum mechanical methods. However, in order to work, molecular mechanics is dependent on the validity of several assumptions. The most important one being the Born-Oppenheimer approximation, which states that due to the vast mass difference between an electron and a nuclei, an electron may rapidly adjust to any positional changes in the nuclei. Thus, the total wavefunction for the molecule may be divided so that the total energy is the sum of the nuclear energy and the electronic energy (equations 2.14 and 2.15).

$$\Psi_{tot}(nuclei, electrons) = \Psi(electrons)\Psi(nuclei) \quad (2.14)$$

$$E_{tot} = E(electrons) + E(nuclei) \quad (2.15)$$

Being able to separate the nuclear and electronic energies makes it possible to write the energy as a function of the nuclear coordinates. Which is the basis for molecular mechanics, writing the energy as functions based upon simple processes dependent on nuclear positions within the system, like bond stretching and bond angles as seen in Figure 2.3.

There exists parameters for non-bonded and bonded interactions alongside intra- and intermolecular interactions. Force fields exists by the dozens, where the included parameters define the force field. Some are extremely simple and only include a few parameters while others are extremely detailed including a vast number of contributions to the potential energy surface. The keyword for molecular mechanics is transferability, some force fields are only applicable to certain types of molecules while others are very versatile and may be applied to most systems. Where the MM2 force field is one of the latter, and is widely used by organic chemists.²⁸

Force field calculations are often a useful tool for "quick and dirty" calculations, an example may be finding a local minima for a structure in order to better predict compound behaviour. Molecular mechanics may be applied

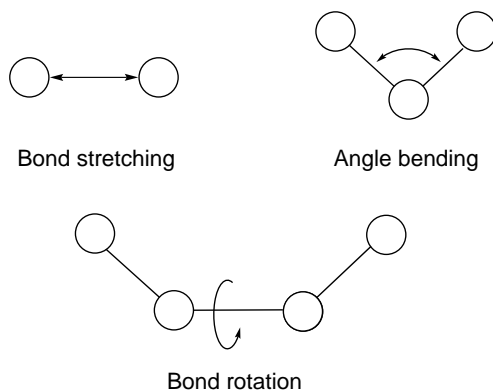


Figure 2.3 Example contributions to the potential energy surface in force fields.

to calculate most properties, as long as they are not connected to electron distribution and electronic effects.

2.3.3 Density function theory²⁷

Density function theory, or DFT, is the current workhorse of quantum mechanical calculations and is widely used for a huge variety of calculations. The central dogma in DFT is that there is a relation between the total electronic energy and the overall electronic density. Equation 2.16 shows this formulated as an energy functional of the electron density, where $V_{ext}(\vec{r})$ is the external potential and $F[\rho(\vec{r})]$ is an unknown functional containing the rest of the terms. The remaining terms expressed in the unknown functional may be electron-electron correlations and electron kinetic energy.

$$E[\rho(\vec{r})] = \int V_{ext}(\vec{r})\rho(\vec{r})d\vec{r} + F[\rho(\vec{r})] \quad (2.16)$$

The problem with solving equation 2.16 for a set of interacting electrons is that $F[\rho(\vec{r})]$ is not known. Kohn and Sham postulated a possible solution for this problem in 1965, this is called the Kohn-Sham approach and this approach suggests that $F[\rho(\vec{r})]$ should be approximated as the sum of three terms:

$$F[\rho(\vec{r})] = E_{KE}[\rho(\vec{r})] + E_H[\rho(\vec{r})] + E_{XC}[\rho(\vec{r})] \quad (2.17)$$

Where $E_{KE}[\rho(\vec{r})]$ is the kinetic energy for an ideal electron gas, $E_H[\rho(\vec{r})]$ is the electron-electron coulomb energy (similar to the coulomb term in

Hartree-Fock theory) and $E_{XC}[\rho(\vec{r})]$ is the contributions from exchange and correlation interactions. The reason for the huge success of DFT is the exchange-correlation functional. Due to the fact that even relatively simple approximations to the exchange-correlation functional may yield accurate results is part of what makes DFT such a valuable method for molecular modelling. The "choice" of exchange-correlation functional is important for the validity of the calculation, and there are literally hundreds of different functionals to choose from.

2.4 Mechanistic considerations

2.4.1 Hard-soft-acid-base theory¹⁷

Polarizability describes the strength of the interaction between an atoms nucleus and the corresponding valence electrons. If an atom is easily polarizable, the electrons in the valence shell are easily distorted by an external charge, where the uneven electron distribution is defined as being polarized. This is often the case for relatively large atoms or ions with low effective nuclear charge, for example iodine is considered to be an easily polarizable ion.

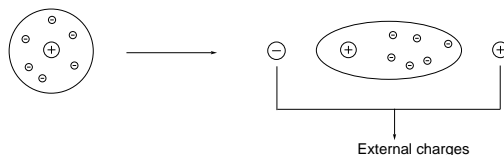


Figure 2.4 Graphic representation of polarization of the valence electron distribution in an atom or ion.

The concept of hard-soft interactions were first introduced by Pearson in 1967,²⁹ and relates stability and reactivity to the polarizability of atoms. A hard reaction partner is considered to be an atom or ion that is less prone to polarization, often due to high ion charge and high effective nuclear charge. A soft reaction partner on the other hand is considered to be an easily polarizable atom or ion, like iodine mentioned above. The hard-soft-acid-base theory presented by Pearson states that hard-hard and soft-soft interactions give more favorable orbital overlaps than hard-soft interactions. This has been widely applied to qualitative reactivity trends.

In order to get a numerical or quantitative scope of these interactions, electron affinity (EA) and ionization potential (IP) is utilized, as seen from equations 2.18 and 2.19.

$$\text{Hardness} = \eta = \frac{1}{2}(IP - EA) \quad (2.18)$$

$$\text{Softness} = \sigma = \frac{1}{\eta} \sim 2(IP - EA) \quad (2.19)$$

2.4.2 Bürgi-Dunitz trajectory^{30,31}

The Bürgi-Dunitz trajectory was presented by Bürgi and Dunitz in 1973, and describes the orientation of a nucleophile before attacking the electrophilic carbon in a carbonyl group.³⁰ The discovery of the trajectory was due to structural similarities in compounds containing both electrophilic and nucleophilic centers. The crystal structures of these compounds showed nucleophilic addition to the carbonyl groups with differing grade of completion, this was deduced from the distance in angstrom between the carbonyl carbon and the nucleophile. The reason for the different compounds showing addition to greater or lesser extent comes from intra- or intermolecular steric constraints imposed on the nucleophile, freezing it in the observed position. From these studies they came up with a generalized rule known today as the Bürgi-Dunitz trajectory, which predicts the position of entry of a nucleophile as shown in Figure 2.5.

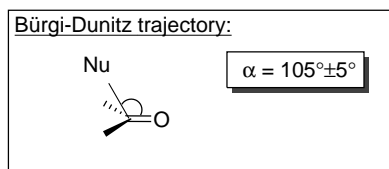


Figure 2.5 The Bürgi-Dunitz trajectory for nucleophilic addition to a carbonyl group.

One of the explanations to why this trajectory occurs, are the lowering of the molecular orbital energy in the tetrahedral intermediate. The angle of the trajectory is similar to the tetrahedral angle, and as the nucleophile approaches the substituents on the carbonyl bend away and there is an elongation of the C-O bond. When planarity of the carbonyl is lost, the π and π^* develop into a oxygen lone-pair and an empty sp^n orbital on the carbon.³⁰

2.5 Suggested isomerization mechanisms

As mentioned in the objective of this study, partial isomerization of stereocenters in the polar head groups of the imide **1** synthesized through thermal condensation from the ammonium tartrate salt **2** was of particular interest (Figure 2.6). Two particular isomerization mechanisms have been looked into, as they have been assumed to be probable for the conditions imposed on the compounds.

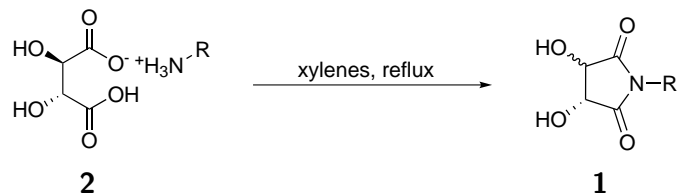


Figure 2.6 Partial isomerization of the polar headgroups in refluxing xylenes.

2.5.1 Ketene intermediates

Ketene intermediates are well known from reactions of acid chlorides with tertiary amines, and are utilized in various synthetic pathways (Figure 2.7).^{32–34} Ketenes are formed from a $\text{E}_{1\text{cb}}$ -mechanism (Unimolecular-Elimination-conjugate-base mechanism).

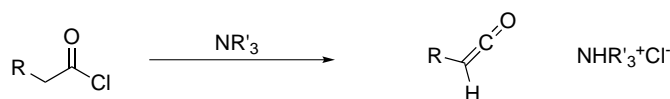


Figure 2.7 Formation of ketene intermediates from tertiary amines and acid chlorides.

One important aspect with ketenes are their tendency to react both with electrophilic and nucleophilic species, explaining their ability to undergo [2+2] cycloaddition reactions.³⁵ This ability can be explained by looking at the frontier molecular orbitals of a ketene specie, as depicted in Figure 2.8.

The HOMO and LUMO for a ketene is perpendicular to each other, and hence dictates that the entry trajectory of a nucleophile will be different from that of an electrophile. A nucleophile is expected to attack in the plane at the first carbon, seeing from Figure 2.8 that the LUMO coefficient is largest on this carbon. Where an electrophile will interact with the second carbon perpendicular to the plane for the same reasons.

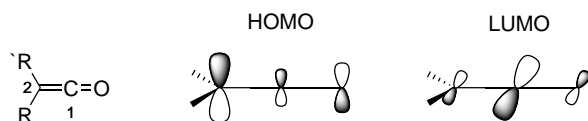


Figure 2.8 The frontier molecular orbitals for ketene (relative size on orbital lobes).³⁵

Aspects determining the probability of ketene intermediate formation:

- **Base/nucleophile properties** are important, as can be seen from the literature,^{32–34} the less nucleophilic the base is, the higher possibility for a ketene intermediate. As a tertiary amine will be basic (triethylamine $pK_a = 8.6$) and not very nucleophilic, it will be more likely to induce a ketene compared to a primary amine.
- **The leaving group** is important, considering that the better the leaving group, the higher the probability for a ketene intermediate. If a poor leaving group is present, the reaction will be more likely to proceed through a nucleophilic addition/elimination mechanism instead of a ketene formation. As seen in literature where acid anhydrides prepared from dehydrating reagents form ketenes in presence of tertiary amines.^{36–38}
- **α -Proton acidity**, as the formation of ketene is induced by removal of the α -proton in the molecule. In order for this to happen, the relative acidity of the proton must be sufficient for removal with a base present under the given reaction conditions. The acidity requirements are closely related to which nucleophile/base being utilized in the reaction.
- **Steric factors** are not vital for formation of ketenes, but rather important for their relative reactivity. Tidwell *et al.* conducted a study on ketenes of various steric hindrance, and found more sterically hindered ketenes to have a lower relative reactivity.^{35,39} As can be seen from Figure 2.8, the steric bulk of the substituents is expected to have a bigger impact on interactions with electrophiles, as they interact closer to the substituents.

Reaction mechanisms^{35,40}

Ketenes can react through two main types of reaction mechanisms, one with initial electrophilic attack and one with nucleophilic. The steric bulk and

the nature of the species reacting with the ketenes dictates which mechanism to be more likely (Figure 2.9).

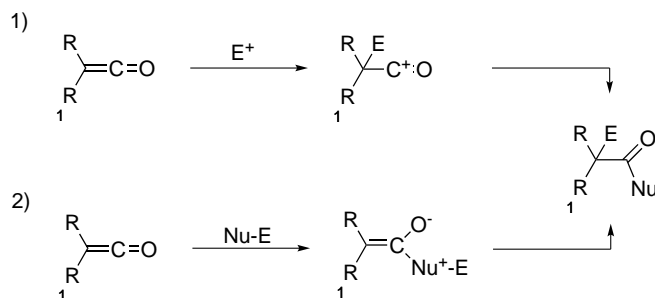


Figure 2.9 The different mechanisms for reactions with ketenes, species like EtOH are assumed to go through the zwitterionic intermediate in pathway 2.

2.5.2 Isomerization through an ion-pair intermediate^{41,42}

Cram *et al.* have presented several articles on isomerization of saturated carbon centers.^{41,42} The isomerization takes place in basic media and through an ion-pair intermediate (Figure 2.10). The ion-pair mechanism is dependent on the base strength, same as with the ketene mechanism presented above, the base properties must outweigh the nucleophilic properties in order for the isomerization to take place. The reaction order for the base in this mechanism was found to be slightly above one, as the rate determining step is the removal of proton to form the ion-pair.

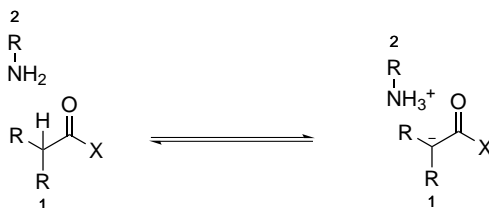


Figure 2.10 Basic isomerization of saturated carbon centers through ion-pair intermediates.

3. Thermolysis of the ammonium tartrate salt **2**

In order to provide a better understanding of how to outline the further work in this study, experiments were performed under various conditions to look into different aspects of the reaction shown in Figure 3.1. As where the partial isomerization takes place, and what compounds are present at different times in the reaction mixture. All detailed experimental descriptions can be found in Sections 11.7.5, 11.8.1, 11.5.12 and 11.8.2. Spectra and chromatograms can be found in Appendix K.

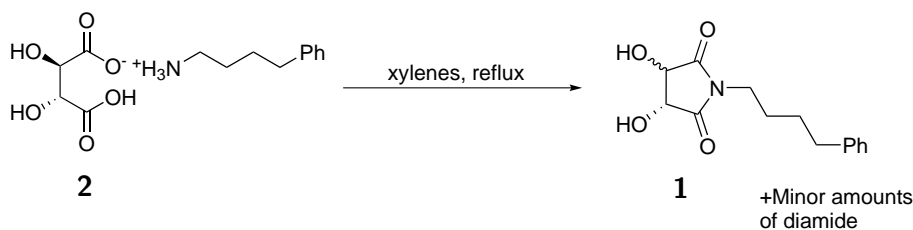


Figure 3.1 Formation of partially isomerized **1** and minor amounts of diamide from the ammonium tartrate salt **2**.

Experiments monitoring the entirety of the reaction, points towards the initial amide formation being the bottleneck of the reaction. As there was only minor amounts of **3** present in the reaction mixture at any given time (Figure 3.2). This can be explained by the need for the reactants to not be in ionic salt-form to be reactive in the initial amide coupling. This is shown in a study performed by Charville *et al.*,^{18,19} which states that the ammonium carboxylate salts are inactive in amide formation reactions. The study showed that the more susceptible the compounds were for forming ammonium salts (acid-base interactions), the less reactive were they found to be in amide couplings. This is supported by observations made while preparing the salt **2**, the initial formation of **2** was found to be highly

exothermic. Hence, it makes sense that the reverse reaction, in order to form the neutral species, is the rate determining step of the mechanism for forming **1**. The direct amide formation is elaborated in the following chapter concerning the cyclization mechanism for **3** to form **1**.

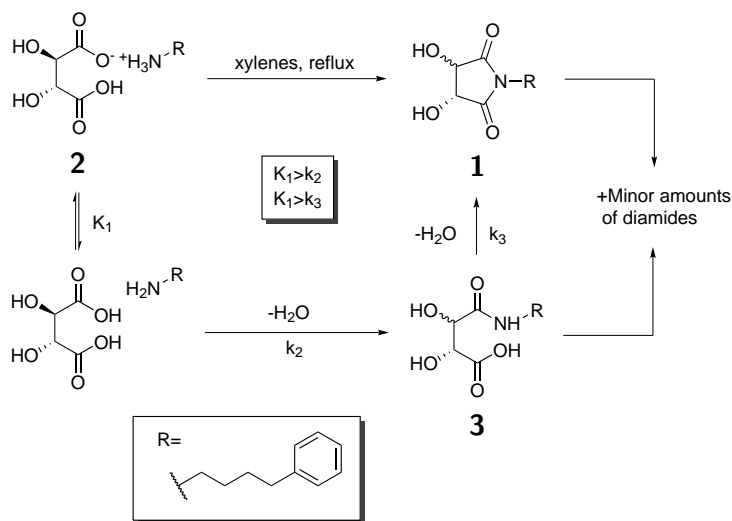


Figure 3.2 Observed trends in the cyclic imide formation from the ammonium tartrate monosalt.

3.1 Deuterium experiments

The partial isomerization for the formed cyclic tartramide most likely arises from loss of stereochemistry due to proton exchange. Experiments with deuterium exchanged molecules were then conducted to verify the proton exchange.

2d,3d-Tartaric acid (**13**) had been previously prepared by Rajesh Raju following a literature procedure,⁴³ this tartaric acid was added together with 1 eq. of amine and refluxed for a given amount of time before analysis was performed (Figure 3.4).

The degree of H-D exchange was found to be higher than the observed inversion in one stereocenter (found from ESI MS). This can be explained by one side of the racemization intermediate being more sterically hindered than the other, hence reattachment of hydrogen will favor one side over the other. This is supported by DFT calculations performed by Vegard Lien on both the ketene and the ion-pair intermediates, which shows that one face

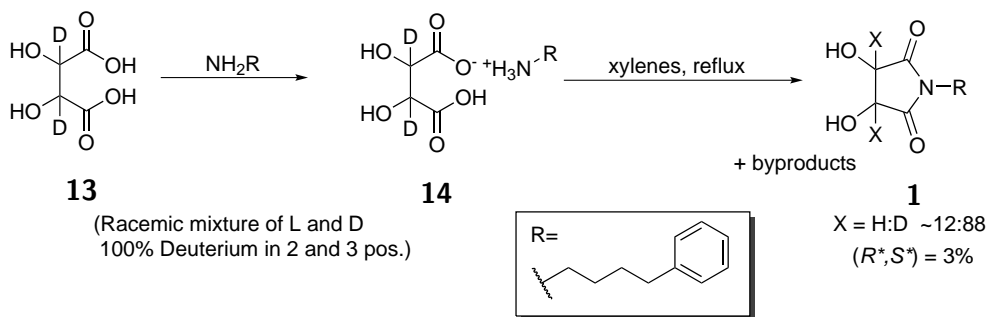


Figure 3.3 Results from synthesis of **1** from deuterated ammonium tartrate salt (**14**).

of the intermediate is more hindered than the other, due to steric clash with the non-reacting carboxylic acid group.⁴⁴ The degree of proton exchange is expected to be lower for this reaction than for the non-deuterated species, due to kinetic isotope effects, as presented in the theory chapter.

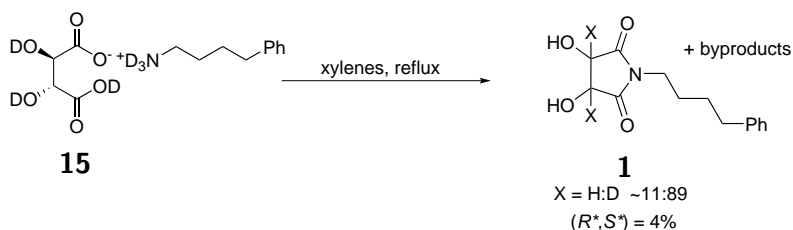


Figure 3.4 Results from synthesis of **1** from heteroatom deuterated ammonium tartrate salt (**15**).

To confirm presence of kinetic isotope effects, the ammonium tartrate monosalt **2** was deuterated on all hetero-atoms and subjected to the same treatment as the 2d,3d-salt (deuterium content was not successfully measured from the starting salt). This experiment showed slightly lower degree of H-D exchange in the 2 and 3 position, but 1% higher content of (R^*, S^*)-**1** (Table 3.1).

Table 3.1 H/D ratios and amount of *meso* at reaction end point.

Compound	(R^*, S^*) (%)	H:D
14	3	12:88
15	4	89:11

As heteroatoms are prone to exchange protons relatively easy, the lower than expected content of deuterium might come from not 100% heteroatom deuterated starting material. The increased amount of (*R**,*S**)-1 however, coincides with the expected results. All in all, the experiments with deuterated species provided evidence of proton exchange taking place in the 2 and 3 position on tartaric acid, and this proton exchange is most likely the reason for partial isomerization taking place.

3.2 Isomerization mechanisms

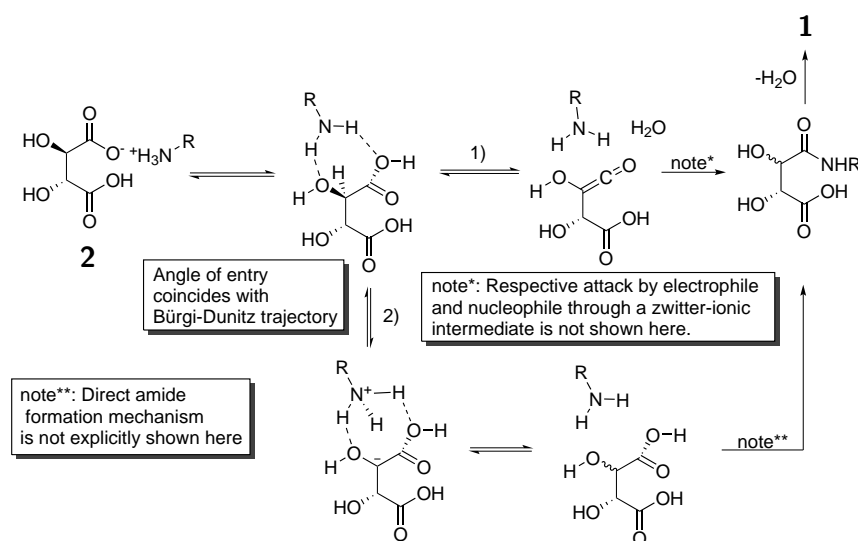


Figure 3.5 The two suggested pathways for explaining the observed partial isomerization of **1** prepared from **2**.

The proposed mechanisms for the partial racemization observed when starting from the ammonium tartrate salt (**2**). The ketene mechanism (pathway 1) is assumed to be the main isomerization route, due to making a highly reactive intermediate which will react with a nucleophile. The ion-pair mechanism (pathway 2) will deactivate the tartaric acid for nucleophilic interactions and deactivate the amine as a nucleophile, and needs to go back to the neutral species in order to react by direct amide formation. However, as there is no data available for distinguishing between the two pathways, both of them are included as viable explanations for partial isomerization.

4. Cyclization condensation of the monoacid **3**

As stated in previous chapters, one of the main goals of this study was to further elaborate the different reaction steps in the synthesis of cyclic tartramide **1** from the ammonium tartrate salt **2** and to present data supporting the proposed reaction pathways for partial isomerization and byproducts.

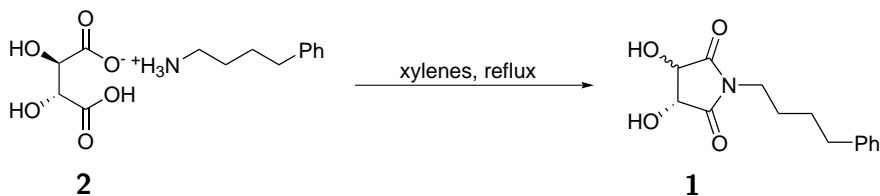


Figure 4.1 Partial racemization when starting from **2** to make **1**.

The cyclization condensation reaction of monoamido tartaric acid **3** to form the cyclic tartramide **1** was chosen as the first partial reaction to be evaluated. This reaction proceeds with no partial isomerization,⁴⁵ and was assumed to be easier to elucidate when there was one compound going in and one coming out.

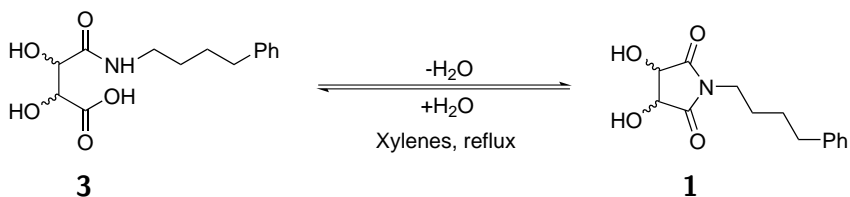


Figure 4.2 Cyclization of **3** to form **1**.

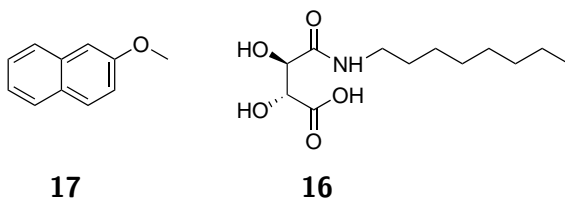
The analysis of this reaction relies on 1H NMR data, mostly due to the issues regarding quantification of **3** (Section 10.3). However, due to no

partial isomerization and no overlapping of proton signals in the area of interest, ^1H NMR was considered to be sufficient for obtaining reasonably accurate and reliable data. Detailed experimental description and parameters for molecular modelling for this chapter can be found in Section 11.7.1, 11.8.3 and 11.6. All supporting spectra can be found in Appendix L. A general procedure for treatment of the obtained raw data from ^1H NMR is outlined in Appendix J.

4.1 Kinetics

4.1.1 Initial experiments

The initial experiments were done to find a suitable concentration for the reactant **3**. Finding a concentration where the reaction goes within a reasonable timeframe but still does not proceed too fast in order to minimize measuring errors. Due to the change of tailgroup, as further elaborated in Section 10.3, one of the initial experiments was a reference experiment with the n-octyl monoamido tartaric acid **16** in order to validate the extrapolation and make sure that there were no big differences in conversion rate between the two different tail groups. In addition to these reactions, some experiments were done to verify that reactions with the same concentration but in different vessel size exhibited the same reaction rate. The series of different concentrations can be seen from Table 4.1 and their corresponding conversion (% vs time) graphs from Figure 4.3. The internal standard (IS) added to the reaction mixtures was 2-methoxynaphthalene (**17**). Initially it was added as an IS for HPLC. However, when HPLC analysis of the samples was discarded for this system, as further elaborated in Section 10.3, the amount of **17** was increased in order to use it as an IS for ^1H NMR spectroscopy. The problem with using **17** as IS was fluctuations of the methoxy peak integral which was used for concentration calculations. The cause of these fluctuations was not determined, hence calculations were performed without IS correction.



The conversion rate at the concentration exhibited in experiment number 5 (Figure 4.3) was found to be fitting for the experiments conducted on

Table 4.1 Cyclization of monoamido tartaric acids to form cyclic tartrimides in refluxing xylenes (134 – 140 °C).

Ex. No.	Substrate	Mass (g)	Solvent (mL)	Conc. (10^{-3} mol/L)	IS (mg)
1	(<i>R,R</i>)- 3	0.200	100	7.1	1
2	16	0.200	100	7.6	1
3	(<i>R,R</i>)- 3	0.800	100	28.5	4
4	(<i>R,R</i>)- 3	0.400	50	28.5	2
5	(<i>R,R</i>)- 3	0.400	25	56.9	25

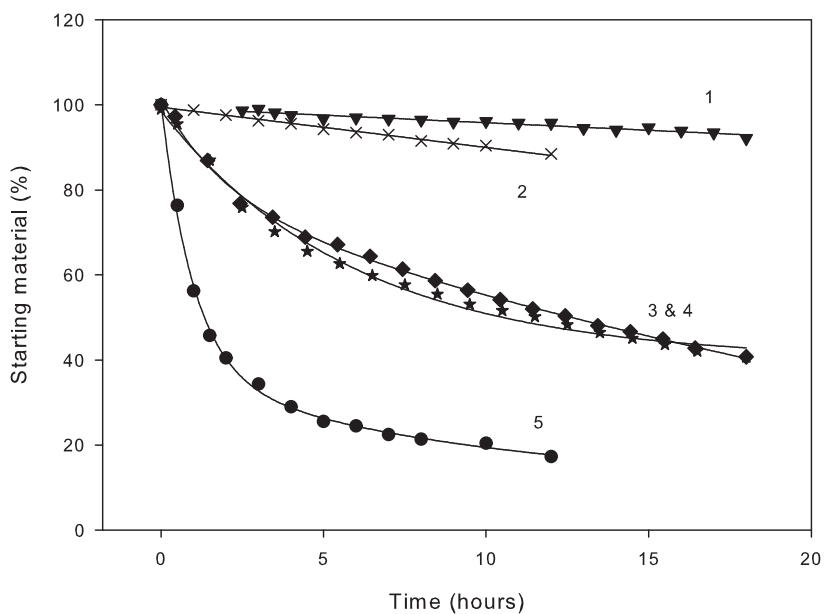


Figure 4.3 Starting material ((*R,R*)-**3** and **16** in entry 2) conversion over time at different concentration and vessel size, as dictated in table Table 4.1. Conversions were measured by $^1\text{H-NMR}$ (400 MHz).

this reaction. The amount of **3** and solvent was again halved in order to minimize the usage of starting materials, but keeping the same concentration.

The initial experiments conducted on this reaction (Figure 4.3) also shows a rapid decrease in the reaction rate after 1.5 hours for the chosen conditions. The reaction rate towards the end of the experiment was really low compared to the initial rates. The concentration range where rate decrease was observed, differed slightly with vessel size. In addition, as can be seen from the next section, active removal of water also changed this concentration range.

4.1.2 The effect of water present in the system

The above mentioned flattening of the conversion rate before completion, might be due to the effect of water in the system. Considering that the reaction is a condensation cyclization, there will be water present in addition to residual water in the solvent. Even though most of the water formed was thought to stick to the reflux condenser during the reaction. In order to verify the effect of water inducing the "equilibrium" concentration, an experiment with continuous water removal was conducted (Dean-Stark apparatus) and compared to a reference reaction. The resulting plots can be seen in Figure 4.4 and it shows that the conversion goes more towards completion with continuous removal of water.

This is in accordance with the literature, which shows that usage of molecular sieves⁴⁶⁻⁴⁸ and azeotropic water removal (as seen in Section 9.6^{2,49}) enhances amide formation reactions and makes it possible to do direct amide coupling with good conversion.

Amide formation equilibrium

The water effect can be explained by amide formation being a chemical equilibrium,⁴⁷ and presence of water will induce equilibrium conditions. At one point during the cyclization, water concentration in the reaction mixture will be high enough for the reverse reaction to effectively compete with the amide formation (equation 4.1) and an equilibrium will form.

$$rate = k_1[\mathbf{3}]^n - k_{-1}[\mathbf{1}]^o[\text{H}_2\text{O}]^p \quad (4.1)$$

To test this theory, (*R,R*)-**1** was refluxed in water for 4 hours with only minor formation of (*R,R*)-**3**. If there was a reverse reaction taking place in the cyclization, there should be higher conversion of tartramide **1** to

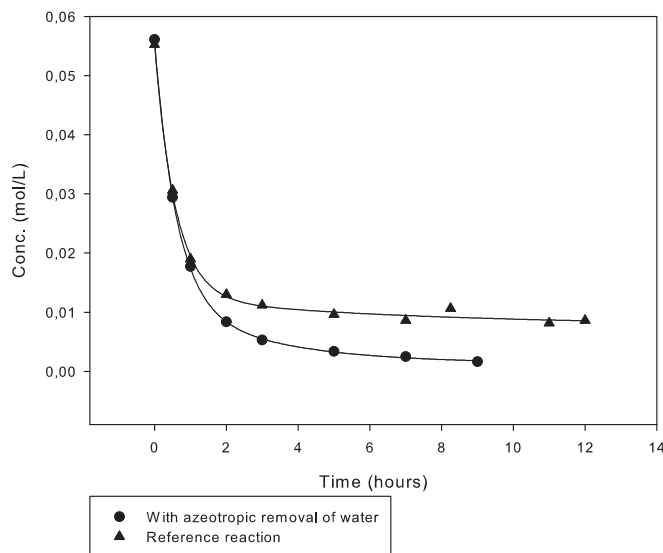


Figure 4.4 Thermal condensation of (*R,R*)-**3** to form (*R,R*)-**1** with and without azeotropic removal of water.

monoacid **3** regardless of the lower temperature. Due to one of the reagents being in large excess, in that case water. It was then considered unlikely that an equilibrium was responsible for the rate lowering effect observed in the experiments.

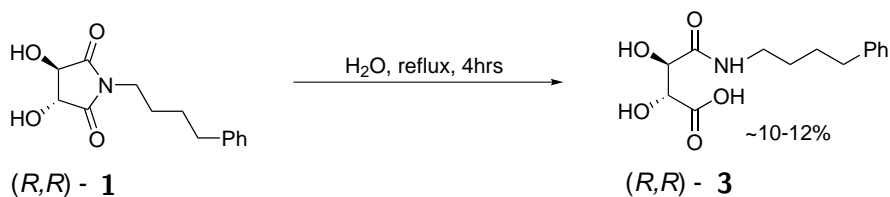


Figure 4.5 Aqueous reflux of (*R,R*)-**1** to test the ability of water to induce the reverse reaction (ring opening of cyclic tartramide).

Breakage of carboxylic acid dimers

Mechanistic studies conducted on the stability of carboxylic acid dimers⁵⁰ alongside the mechanistic aspects discussed in later sections, suggest that the rate inhibiting effect can be ascribed to water breaking up the carboxylic acid dimers formed before the initial nucleophilic attack by nitrogen. Chocholousova *et al.*⁵⁰ have shown through various modelling techniques

that even small amounts of water will break up the cyclic dimers that carboxylic acids form in non-polar solvents (Figure 4.6). These intermolecular coordinations have been shown to be of importance for direct amide formations.^{18,19} In addition, there are many literature examples of carboxylic acids forming dimers in nonpolar solvents.^{50–55}

Cleavage of carboxylic acid dimers was found to be the most probable mechanism for inhibition of the cyclization step, as the data discussed in later sections makes this more probable than the possible equilibrium effect discussed in the previous section. Formation of carboxylic acid dimers also turns out to be of importance for the postulated reaction mechanism in the concluding remarks regarding this reaction (Section 4.3).

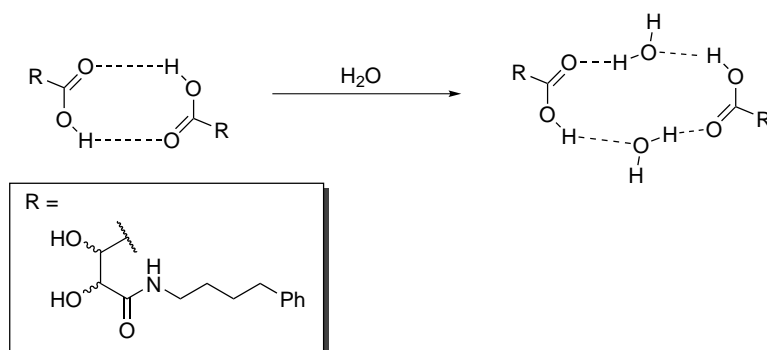


Figure 4.6 Breakage of carboxylic acid cyclic dimers.⁵⁰

4.1.3 Determination of kinetic parameters

In order to determine the reaction order for conversion of **3** to **1**, the data used in the calculations had to be recorded before the water concentrations in the reaction mixture became sufficient for inhibiting the amide coupling. The plot in Figure 4.7 shows the chosen interval for where the effect of water was assumed to be sufficiently low for reaction order determination. The chosen interval was supported by the rate plot for the comparison of with and without water removal (Figure 4.4), which showed little difference in rate for the first 1.5 hours.

When assuming the competing reaction of carboxylic acid dimer breaking is negligible compared to the wanted amide coupling reaction, the rate equation for the reaction can be written in the following way:

$$\ln(\text{rate}) = \ln(k) + n \ln([\mathbf{3}]) \quad (4.2)$$

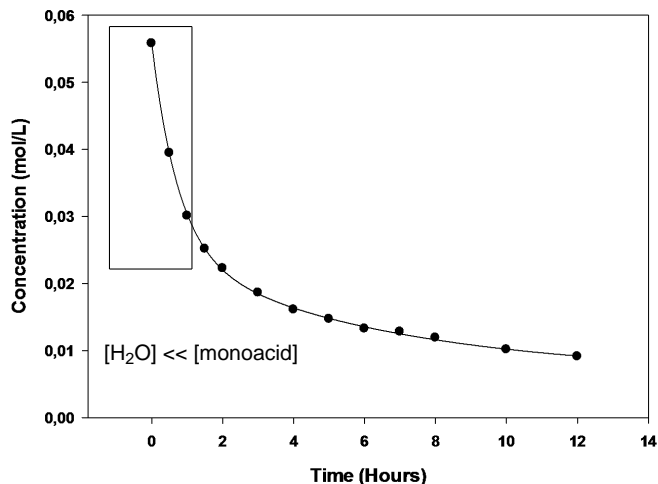


Figure 4.7 Typical rate plot for conversion of **3** into **1**. The box shows the timeframe where the water concentration was assumed to be sufficiently low compared to the concentration of **3** in order to determine the reaction order.

By plotting the natural logarithm of the rate versus the natural logarithm of the concentration of **3**, the reaction rate order was found as the constant a in a linear ($y = a \cdot x + b$) function. The partial order for the monoamido tartaric acid **3** is the same as the total reaction order, due to it being an intramolecular cyclization reaction.

Several experiments were conducted in order to determine the reaction order of the cyclization condensation equilibrium. The reactions order determined from these experiments can be found in Table 4.2 and a graphic representation of the linear \ln - \ln graphs can be seen from Figure 4.8.

After determining the reaction order, it was rather simple to find the reaction rate constant from equation 4.3. The reaction rate constant was determined at the half hour mark.

$$rate = k[Monoacid]^n \quad (4.3)$$

The reaction rate constant was found to be lower for (R^*,S^*)-**3** than the optically active forms of **3**. This might indicate that formation of (R^*,S^*)-**1** is less favored than ($R,R/S,S$)-**1**, this might come from difference in steric interactions of the hydroxyl groups in the cyclic imide. The reaction order was also found to be lower for (R^*,S^*)-**3** than the optically active species,

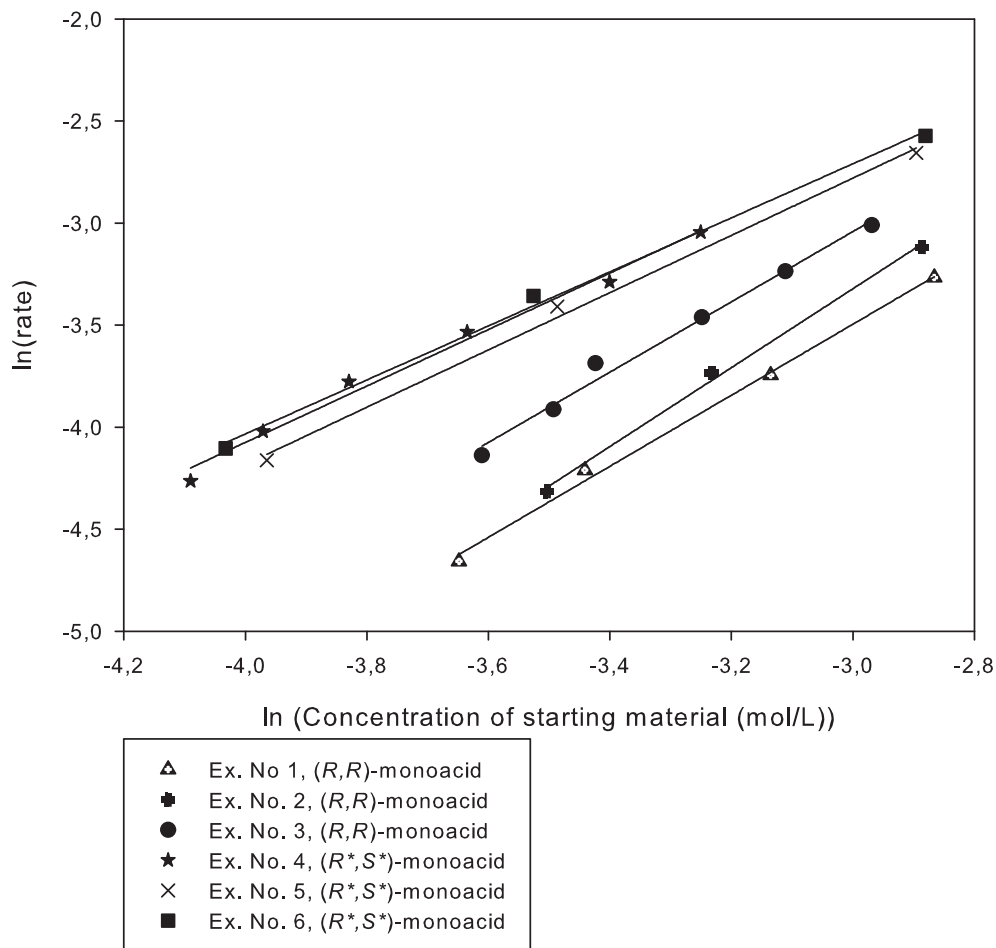


Figure 4.8 A log-log plot of rate vs concentration for the first 1 to 1.5 hours of the conversion of (*R,R*)-**3** and (*R*,S**)-**3** into their respective cyclic imides **1**. Results and reaction conditions are depicted in Table 4.2.

Table 4.2 Calculated reaction orders for the first 1-1.5 hours, for conversion of (*R,R*)-**3** and (*R*,S**)-**3** into their respective cyclic tartrimidides **1** in refluxing xylenes (134 – 140 °C). Starting concentration of **3** was $57 \times 10^{-3} \text{M}$ (12.5 mL solvent) for all experiments (1-6). R^2 values shown for the linear "ln(concentration) vs ln(rate) plot" and the conversion curve.

Ex.	Compound	Order (n)	k_{obs} (30 min) $10^{-3} \text{M}^{-n} \text{s}^{-n}$	R^2 ln-vs-ln	R^2 Conv.
1	(<i>R,R</i>)- 3	1.74	3.07	0.9961	0.9981
2	(<i>R,R</i>)- 3	1.93	6.79	0.9971	0.9998
3	(<i>R,R</i>)- 3	1.72	4.65	0.9886	0.9976
4	(<i>R*,S*</i>)- 3	1.38	2.45	0.9889	0.9939
5	(<i>R*,S*</i>)- 3	1.40	2.30	0.9962	0.9995
6	(<i>R*,S*</i>)- 3	1.32	2.06	0.9969	0.9981

Compound	Avg. order (n)	Avg. k_{obs} $10^{-3} \text{M}^{-n} \text{s}^{-n}$	std. order	std. k_{obs}
(<i>R,R</i>)- 3	1.80	4.83	0.09	0.0015
(<i>R*,S*</i>)- 3	1.37	2.27	0.03	0.00016

this concept along with the difference in rate is further discussed in the upcoming sections.

4.2 DFT modelling

In an attempt to provide a broader understanding of this reaction, a series of calculations were performed on possible intermediates in the cyclization condensation reaction (Figure 4.9).



Figure 4.9 Cyclization condensation to form **1** from **3**.

4.2.1 Determination of possible intermediates

In order to model the lowest energy pathway for the reaction, a set of possible intermediates had to be found. Wu *et al.*⁵⁶ have performed a computational study on a similar system. They looked into the imide formation of an *N*-(*o*-carboxybenzoyl)-*L*-amino acid. Furthermore, a study done by Charville *et al.*¹⁸ on direct amide formations in nonpolar media was also used in order to find suitable candidates. By extrapolating the reasonable intermediates from the different studies to the monoamido tartaric acid system, the structures depicted in Figure 4.10 were chosen as candidates for energy minimization. The calculations were performed on the methyl-truncated intermediates, as the full molecules would impose long calculation times with assumed little difference in relative energy.

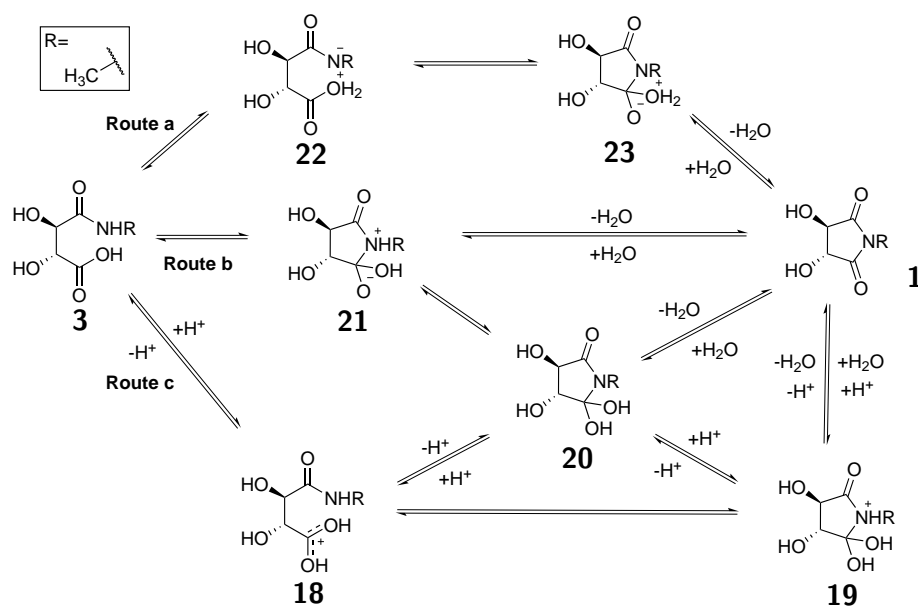


Figure 4.10 Possible intermediates chosen for modelling, on the background of studies on similar reactions.^{18,56}

Some of the candidates from the study performed by Wu *et al.* were not included on the background of being found as high-energy intermediates. They were neither included in the study performed by Charville *et al.* There was also made room for the possibility of intermolecular hydrogen transfer in order to form some of the intermediates (**18** and to some degree **20**). This based on the studies mentioned above, and the prevalence of dimer-formation of carboxylic acids in nonpolar solvents.^{50–55} Also, when looking

back on the previous section, the reaction order with an average at 1.8 for the optically active monoacid (*R,R*)-**3** might point towards some kind of intermolecular interactions. Consequently, one of the reaction steps should include two species of the monoacid.

4.2.2 Calculation of potential energy for the listed candidates

The different intermediates were subjected to geometry optimizations and zero point vibrational energy calculations according to the detailed method in Section 11.6.1. The reaction coordinate diagram of the obtained energies with ZPVE-correction can be seen from Figure 4.11.

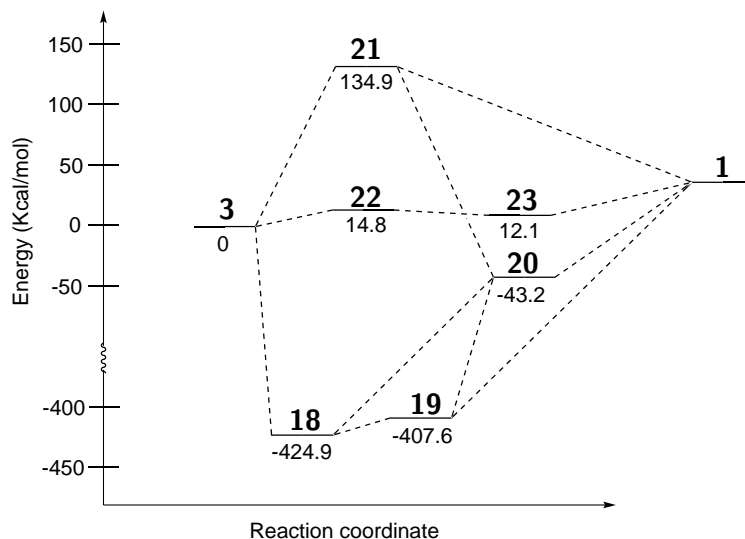


Figure 4.11 Obtained relative potential energy surface with zero point vibrational energy correction for the intermediates chosen for DFT modelling. Energies were obtained with the method described in Section 11.6.1.

The energies of the intermediates will not be compared to **3** and **1** in this thesis as the calculations were performed without a solvation model. The relative energy is only used for clearer data presentation. The plan was to run the intermediate calculations again with a solvent model, but due to a narrow timeframe and the relative energies between the intermediates seems to be in correlation with reported data,^{18,56} the plan was discarded. Furthermore, as discussed in previous sections, carboxylic acids in nonpolar solvents has a tendency towards creating hydrogen-bonding dimers^{50–55}

which will most likely lower the energy of the monoacid.

As can be seen from figure Figure 4.11, the energy for the cyclic tartramide **1** is not included in the reaction coordinate diagram, this is due to the calculated energy for this compound being far off the expected energy-range from literature.⁵⁶ The reason for why this calculation went awry is not known, and was not further elaborated. It is however placed qualitatively above the monoacid, due to the higher steric energy found with an MM2 force field optimization.

4.2.3 Determination of lowest energy pathway

By comparing the energies of the intermediates to each other, the three structures in pathway **c** were found to have the lowest energies (Figure 4.12).

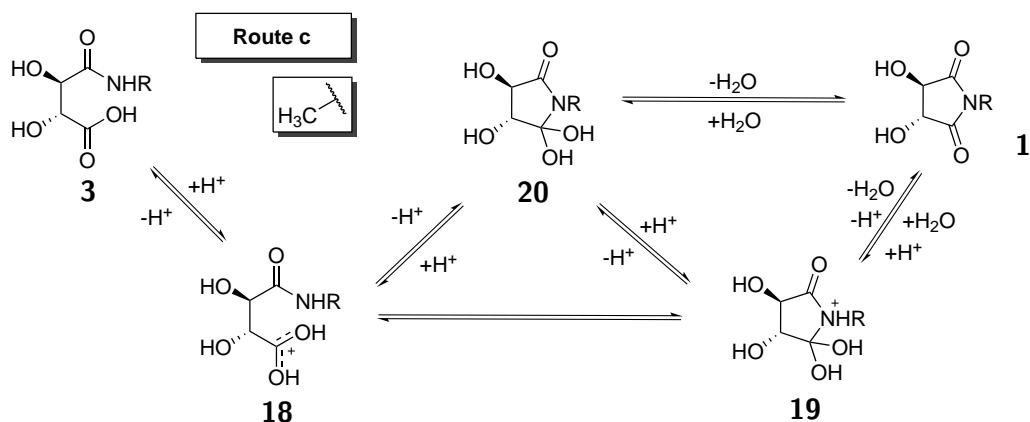


Figure 4.12 Lowest energy pathway determined by DFT modelling.

The energy difference between **18** and **19** is relatively small (17.3 kcal/mol), according to Figure 4.11. The two structures might then simultaneously exist with a slight excess of structure **18**. The pathway found in this experiment is in accordance with the study on direct amide formations described by Charville *et al.*^{18,19} The study proposed several possible mechanistic pathways for the direct amide formation between a primary amine and a carboxylic acid. They were able to exclude several pathways with experiments and calculations, and ended up with a carboxylic dimer assisted nucleophilic attack with intermolecular proton transfer as the favorable reaction pathway (Figure 4.13)

In the mechanism proposed by Charville *et al.* both the proton transfers and the nucleophilic attack happens in a one-step transition state **25**, resulting in the compound equivalent of **20** and a regained carboxylic acid.

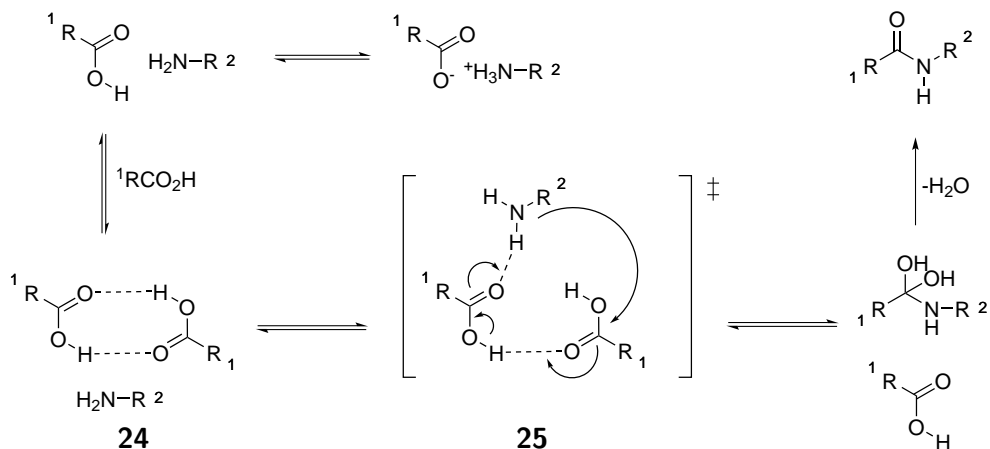


Figure 4.13 Proposed mechanism for direct amide formation by Charville *et al.*^{18,19}

This corresponds to the pathway **3-18-20-1**, where the proton transfer and nucleophilic attack is shown in two steps instead of one. However, due to these compounds being considered as unstable intermediates, none of them are expected to have a very long life span.

4.3 Reaction mechanism

On the background of the experimental and computational data in addition to studies conducted by other research groups,^{18,19,50,56} a reaction mechanism for the cyclization of the monoacid, **3**, to form the cyclic tartramide, **1**, have been outlined.

4.3.1 Initial activation of **3**

The reaction rate orders found in Section 4.1.3 and the intermolecular proton-transfer from calculations correlates with the study conducted by Charville *et al.*, which suggests that dimerization of the carboxylic acids in the non-polar solvent are required for the amide bond formation to take place (Figure 4.14). Dimerization of carboxylic acids in nonpolar environments have already been shown in several studies, computational as well as experimental.⁵⁰⁻⁵⁵ This also explains the results found in Section 4.1.2, considering how the study conducted by Chocholousova *et al.*⁵⁰ show that even small amounts of water will break the dimers as shown in Figure 4.6

and in this way inhibit the reaction. This way, by not having continuous removal of water, the reaction will stop, as seen in the kinetic experiments in Section 4.1.1.

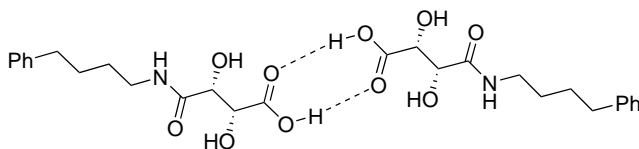


Figure 4.14 Suggested dimer-form of **3** in nonpolar solvent.

Reaction order versus stereochemistry

The average determined reaction orders from Section 4.1.3 suggests that there is a difference in rate order depending on whether the monoacid is optically active ($R,R/S,S$) or not (R^*,S^*). As seen from Figure 4.15 the reaction order for the R^*,S^* -monoacid (1.37) is lower than the one observed from the (R,R)-monoacid (1.80).

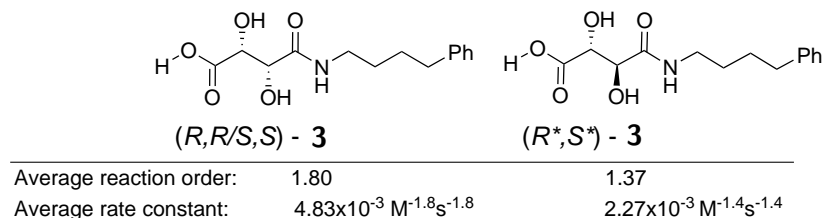


Figure 4.15 Difference in reaction order and rate constant on basis of the stereochemistry of the monoacid **3**.

In the mechanism outlined by Charville *et al.*, the rate determining step could be considered to be the transition state consisting of two carboxylic acids and one amine **25** (Figure 4.13). The expected reaction order for this mechanism would be a 2nd order dependence on the carboxylic and a 1st order dependence on the amine. However, for the intramolecular tartramide formation, the amide group and the carboxylic acid is not allowed to move independently of each other, as they are connected within the same molecule. One possible explanation for the observed reaction order not being 2nd order, but somewhat below is that there might be a steric hindrance for the initial orientation of the nitrogen before the nucleophilic-attack/proton-transfer reaction.

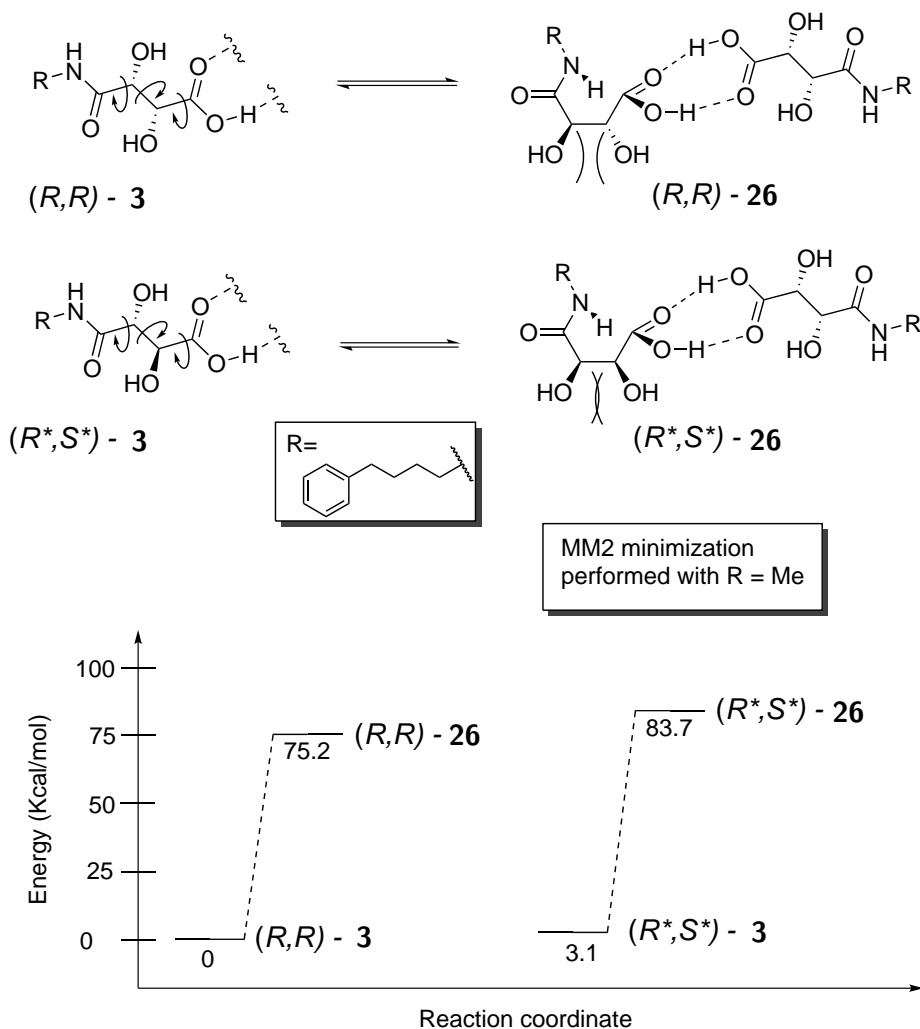


Figure 4.16 Intramolecular reorganization of **3** in order to make the nucleophilic attack by the nitrogen possible. Reorganization imposes bigger steric strain on (R^*,S^*) -**3** than on (R,R) -**3** (calculated by MM2 force field optimization on the methyltruncated molecules). The part of the dimer not reorganizing were set to (R,R) -stereochemistry in both optimizations, for easier energy correlations.

The suggestion for initial reorganization prior to the attack of the amide nitrogen is unimolecular, only dependent on the substrate which is reorganizing. This phenomenon might also explain why the observed rate orders and rate constants for the monoacids (*R,R/S,S*)-**3** is different from the ones observed for (*R*,S**)-**3**. An MM2 force field calculation showed that (*R*,S**)-**3** had an energy difference 5.38 kcal/mol higher between initial and reorganized structures than (*R,R*)-**3** (Figure 4.16). The extra energy needed to reorganize will lower the reaction rate, thus explaining the lower rate constant, for this step and the reaction will be less concentration dependent due to the step with increased steric energy is a mono-molecular reorganization.

However, as there is no further proof other than the difference in kinetic parameters and the need for the monoacid to reorganize before the nucleophilic attack, these are merely suggested explanations for the observed data.

4.3.2 Proton transfer and condensation of water in order to form the cyclized tartrimide **1**

The steric effects mentioned in the previous section might have an effect on whether both the proton transfers happen in one step (**25** in Figure 4.18) or if it is a two step transfer through charged intermediates (Figure 4.12). In order to determine this, more calculations must be performed, especially on the transitions between the intermediates, this will hopefully give enough data to exclude one of the possibilities.

The last step in the mechanism where water is removed from the intermediate and creating the cyclic tartrimide **1**, was calculated by Charville *et al.* to be a one-way reaction.^{18,19} This coincides with the experiment described in Section 4.1.2, which showed that the reverse reaction from **1** to **3** with refluxing water yielded low conversion (Figure 4.17).

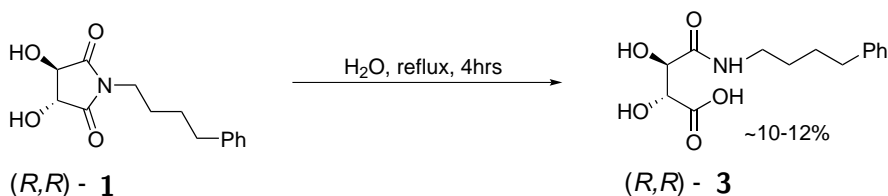


Figure 4.17 Aqueous reflux of (*R,R*)-**1** to test the ability of water to induce the reverse reaction (the ring opening of cyclic tartrimide).

4.3.3 Proposed reaction mechanism

The mechanism for the cyclic tartramide formation is suggested to be one of the two pathways shown in Figure 4.18. The current results cannot differentiate between the two pathways.

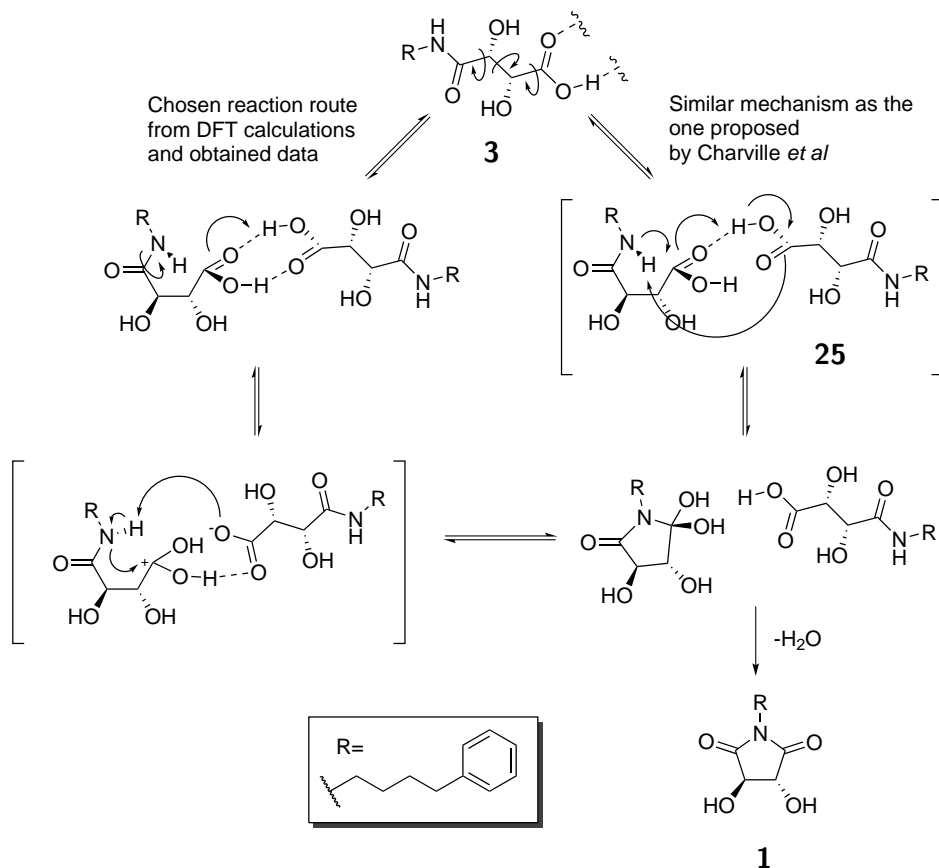


Figure 4.18 The two proposed mechanistic pathways for the cyclic tartramide **1** formation from **3**. The mechanism to the right is extrapolated from the mechanism for direct amide formation proposed by Charville *et al.*^{18,19} while mechanism to the left is based on data obtained in this study alongside the data presented by Charville *et al.*^{18,19}

5. Opening of tartramide **1** with an amine

The effects of free amine on the stereochemistry of the cyclic imide **1** was looked into, in an attempt to provide more data regarding the partial isomerization reaction taking place in reaction 1 in Figure 5.1. The presence of free amine in the system was found to be important for formation of amide bonds from ammonium salts (reaction 1 in Figure 5.1), as literature states that the ammonium salts are inactive in amide formation reactions.^{18,19} One of the observed byproducts from reaction 1 in Figure 5.1 is the diamide **27**, which further points towards presence of free amine in the reaction mixture during the course of the reaction. Detailed experimental description and parameters for MM2 minization can be found in Sections 11.7.2, 11.6.2 and 11.8. Spectra and chromatograms can be found in Appendix M. A general procedure for treatment of the obtained raw data from ¹H NMR is outlined in Appendix J.

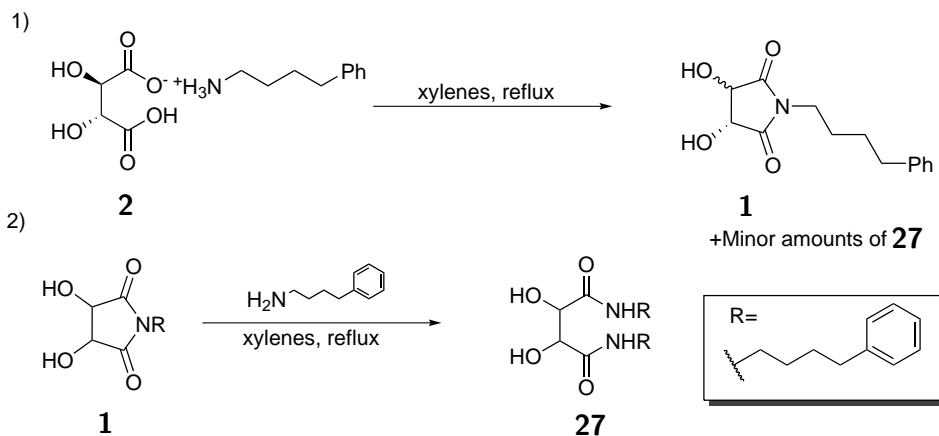


Figure 5.1 1) Partial isomerization when starting from **2** to make **1**. 2) Ringopening of **1** with an amine to form the diamide **27**.

5.1 Initial experiments

The initial experiments conducted in this part of the study encompassed exposing (*R,R*)-**1** to varying concentrations of 4-phenylbutyl amine (**28**) in refluxing xylenes. As can be seen from Figure 5.2, the conversion of cyclic tartramide **1** into diamide **27** looks rather different for the three different scenarios.

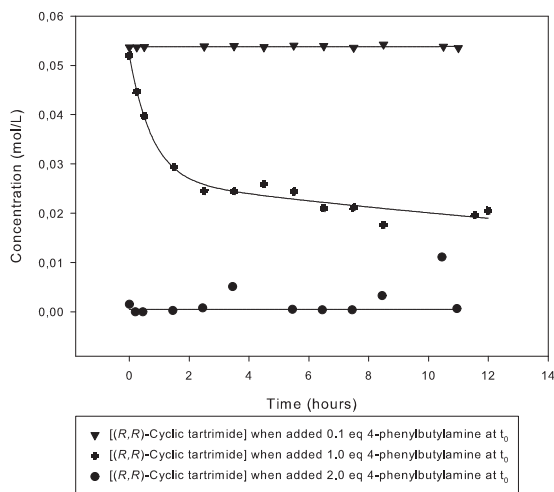


Figure 5.2 Conversion of tartramide (*R,R*)-**1** (shown decline) into **27** in refluxing xylenes (decline corresponds directly to formation of diamide). Parameters kept constant for all reactions: 0.373 g of **1** and 25 mL of xylenes giving a starting concentration of 56.7×10^{-3} mol/L.

When (*R,R*)-**1** was heated to reflux and added 0.1 equivalents of 4-phenylbutyl amine, there was a rapid conversion of 5% tartramide to diamide **27**. After this initial conversion, the concentration ratios were consistent throughout the reaction (Figure 5.2). This phenomenon was also observed for the reaction when the added amount of amine was 2 equivalents (Figure 5.2). There was an initial rapid conversion of nearly all of the cyclic imide **1** into diamide **27**, after the amine was added to the refluxing mixture. In this reaction, as well as the first one, the concentration ratios were consistent after the initial conversion, except from a couple of outliers which are discussed later in this chapter. As seen from the plot in Figure 5.2 the conversion for obtaining equilibrium-like conditions for the reaction where **1** was added 1 equivalent of 4-phenylbutyl amine, was slower than the other two experiments (0.1 and 2.0 eq). However, also this reaction reached an equilibrium-like state between **1** and **27** after some time.

5.1.1 Formation of an equilibrium

As there are no carboxylic acid groups capable of forming dimers and no free water present in the mixture, the flattening of the conversion curve cannot be explained like the cyclic imide formation mechanism in Section 4.1.2. In this case, the most likely explanation is the formation of an equilibrium between the two structures, as seen in Figure 5.3.

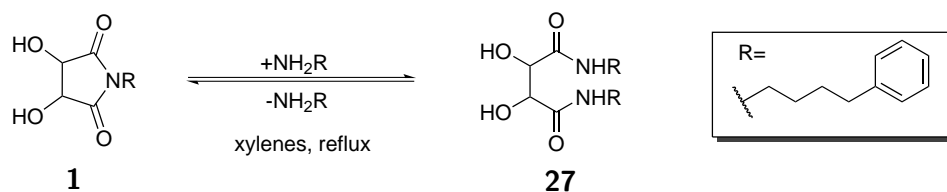


Figure 5.3 Equilibrium between 1 and 27.

A study on the sidereactions in synthesis of cyclic imide polymers conducted by Hermans and Street,⁵⁷ also suggests that the two species will lie in an equilibrium depending on the amount of free amine added to the solution. The diamide reaction was seen as an unwanted sidereaction in that study, and it was suggested to use a slight excess of acid in order to minimize the formation of diamides. As seen from the plots for the initial experiments (Figure 5.2), this correlates with the results obtained for this study, as when there was only small amounts of amine present (0.1 eq) there was only minor conversion to the corresponding diamide.

5.1.2 Outlier data points

In several experiments throughout this study outlier data points were observed, as the apparent deviances from the general tendency for the plots in Figure 5.2. One theory was presented; the fact that the reaction mixture samples were dried on a high vacuum line might affect the concentration ratios for the mixture. Any attempt to prove this however failed, as there was observed no correlation between drying time and the occurrence of the outlier data points. These data points are shown in some of the plots, but were not included in curve fits.

5.2 Stereochemical aspects regarding **1** in formation of diamides

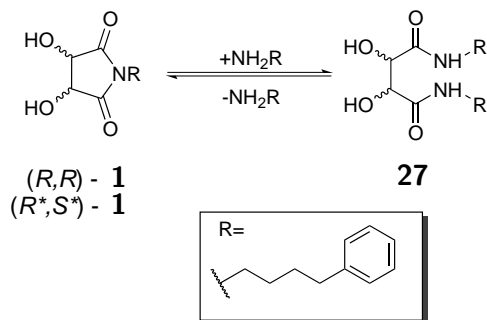


Figure 5.4 Difference in conversion plots was observed when starting from different stereochemistry of **1** ((R,R) vs (R^*,S^*)). Stereochemistry of formed **27** is not addressed in this section.

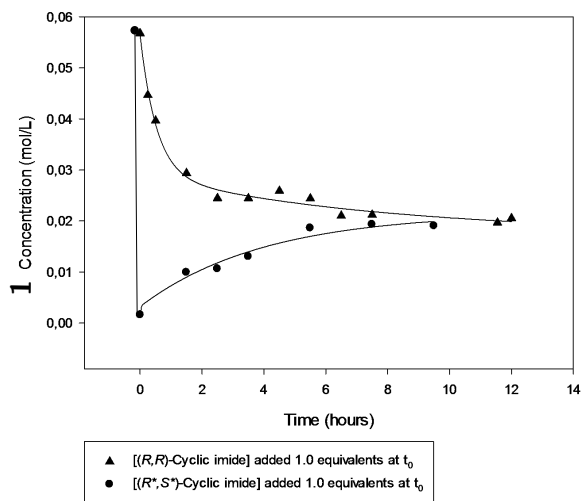


Figure 5.5 Ring opening equilibrium of **1** (shown decline) with different stereochemistry into diamides. Reaction takes place in refluxing xylenes with added 4-phenylbutylamine, with a 56.7×10^{-3} mol/L starting concentration of **1**.

A difference in conversion was observed for the cyclic imide-diamide equilibrium when using (R^*,S^*) -1 instead of the optically active (R,R) -1. The change in conversion is evident from the plots in Figure 5.5.

The different behaviour may arise from difference in steric energy for the two imides (R^*,S^*) -1 and (R,R) -1. This is supported by an MM2 minimization performed on the methyltruncated cyclic imide, stating that the difference in steric energy between the (R^*,S^*) -species are higher than for the corresponding (R,R) -compounds (as seen in Figure 5.6).

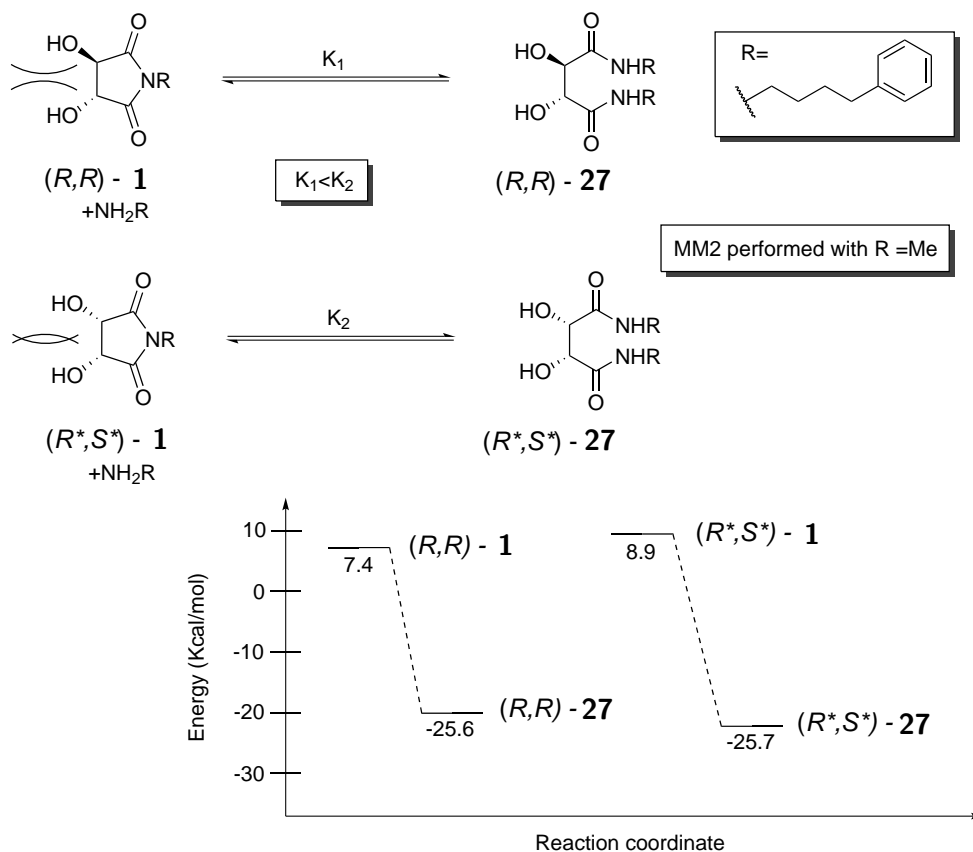


Figure 5.6 Possible explanation to the observed differences between using (R,R) -1 and (R^*,S^*) -1 as starting materials for diamide formation.

As the amine is added to (R^*,S^*) -1, there is a full conversion of 1 into 27 followed by the reverse reaction over time until equilibrium conditions are obtained. HPLC analysis on selected samples (one of these depicted in Figure M.8), showed racemic cyclic imide (R^*,R^*) -1 as the major product formed after the initial diamide formation. The minor amounts of (R^*,S^*) -

1 formed from the reverse reaction (cyclization from diamide) strengthens the assumption of (R^*,S^*)-**1** being less sterically favoured than the corresponding (R^*,R^*) configuration.

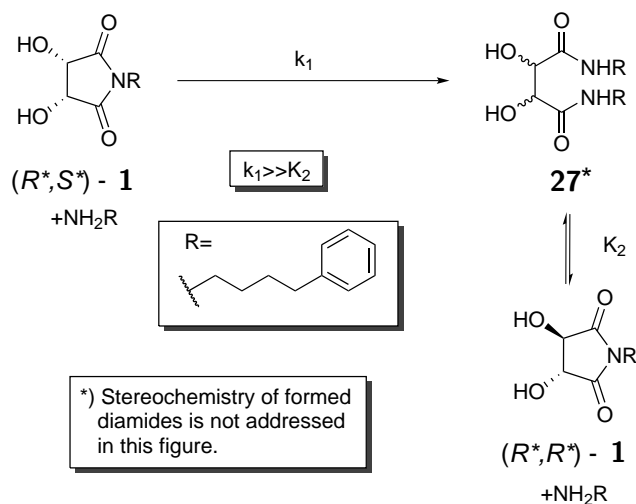
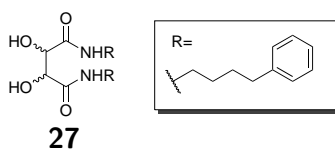


Figure 5.7 (R^*,S^*)-**1** reacted with 4-phenylbutylamine (1 eq.) resulting in formation of (R^*,R^*)-**1** as the imide part of the imide-diamide equilibrium.

As seen from Figure 5.7, the suggested explanation for the observed results is a full conversion into diamide followed by the reverse reaction back to a cyclic tartrimide. However the reverse reaction favors the racemic (R^*,R^*)-**1** above the (R^*,S^*)-tartrimide. This because of the increased steric energy for the (R^*,S^*)-tartrimide (Figure 5.6), which makes it less likely to be found in the reaction mixture.

5.3 Stereochemical aspects of formed diamides **27**



Previous in this chapter, only the stereochemistry of the cyclic tartrimide have been addressed. However, there is also evident changes in stereochemistry for the formed diamide throughout the reaction. The stereochemical

changes for the formed diamide during the scope of the reaction is depicted in Figure 5.8 and Figure 5.9. The reaction with 0.1 equivalents of amine did not show any formation of (R^*,S^*), thus is not further discussed in this section.

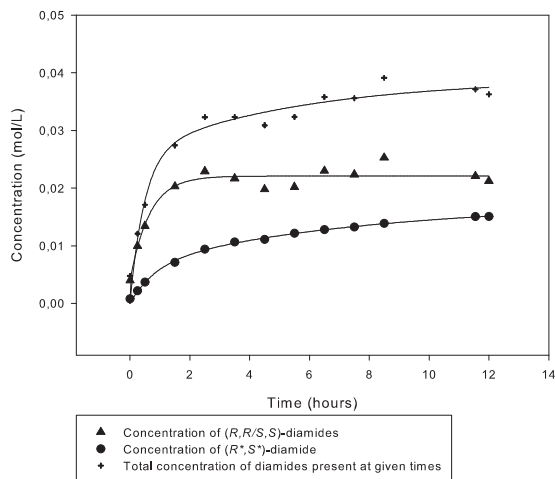


Figure 5.8 Changes of stereochemistry for the formed diamides **27** when starting from (R,R)-**1** and adding one equivalent of amine.

There is an inversion of one of the stereocenters, causing formation of (R^*,S^*)-**27** throughout the observed timeframe. It is fair to assume from the data so far that free amine in solution is the culprit responsible for isomerizing the stereocenters in the reaction system.

One interesting observation made during the analysis of the reaction data, was the rate of stereochemical inversion for **27** showed little dependence on free amine concentration, as seen from Figure 5.10. As mentioned above, the experiment when 0.1 equivalents of amine was added to cyclic tartramide did not show any measurable isomerization (by ^1H NMR). However, there seems to be little dependence on the concentration of free amine above a certain concentration. The plots of formation of (R^*,S^*)-diamide looks fairly alike for the experiments when one and two equivalents of amine was added (Figure 5.10). The same tendency is observed when starting from (R^*,S^*)-**27**, it should be noted that the isomerized diamides is a racemic mixture of (R,R)- and (S,S)-diamides (deduced from HPLC chromatograms).

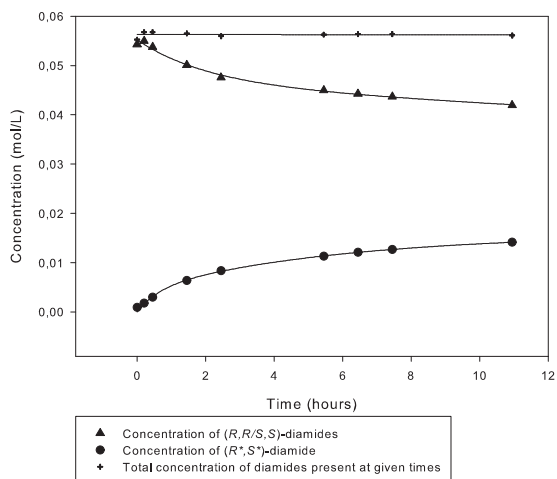


Figure 5.9 Changes of stereochemistry for formed **27** when starting from (R,R) -**1** and adding two equivalents of amine.

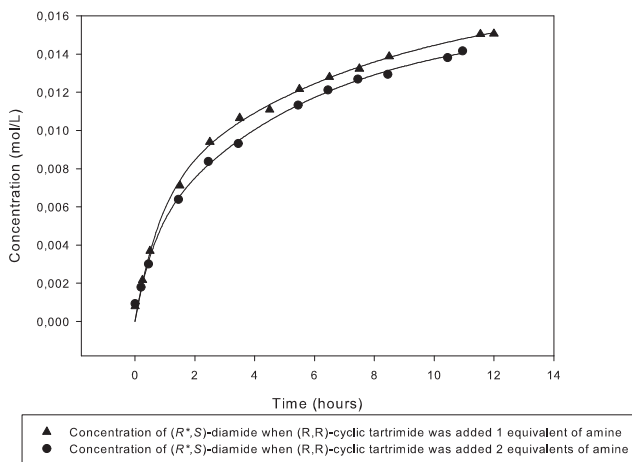


Figure 5.10 Comparison of the conversion plots for (R^*,S^*) -**27** when starting from (R,R) -**1** and adding one or two equivalents of amine.

5.3.1 Stereochemical preferences

When starting from (*R,R*)-**1** the isomerization to form (*R*,S**)-**27** is observed to be slower than the opposite reaction (isomerizing (*R*,S**)-**27** to form (*R*,R**)-**27**), depicted in Figure 5.11. This can be seen from the plots in Figure 5.12, which shows the comparison of isomerization from (*R,R*)-**27** to (*R*,S**)-**27** and from (*R*,S**)-**27** to (*R*,R**)-**27**.

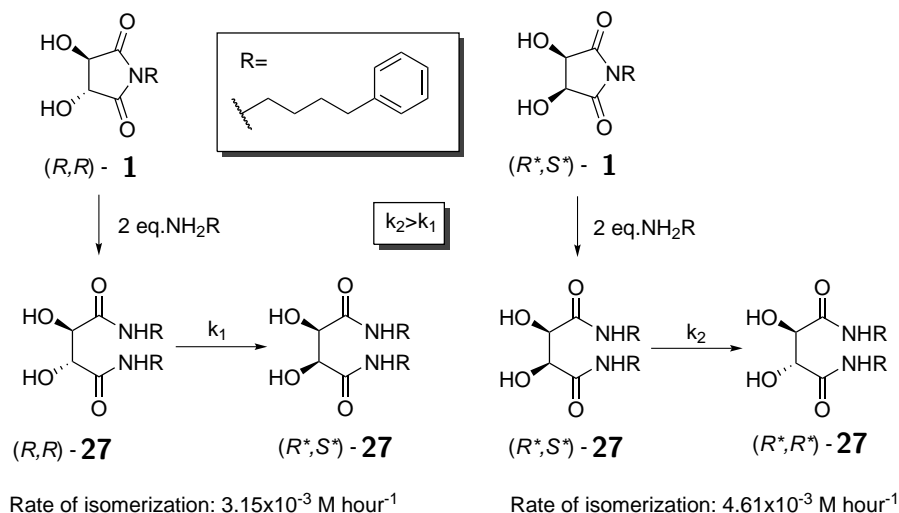


Figure 5.11 Observed isomerization trends for the formed diamides **27**. The rate of isomerization was determined at the one hour mark.

The slower isomerization of (*R,R*)-**27** to (*R*,S**)-**27** cannot be explained by difference in relative steric energy, as their energy difference was calculated by molecular mechanics to be 0.1 kcal/mol in the previous section. The observed trend might be explained either from having different intermediate energies for isomerization or there is a steric prevalence for the racemic (*R*,R**)-**27** from the same intermediate (Figure 5.13).

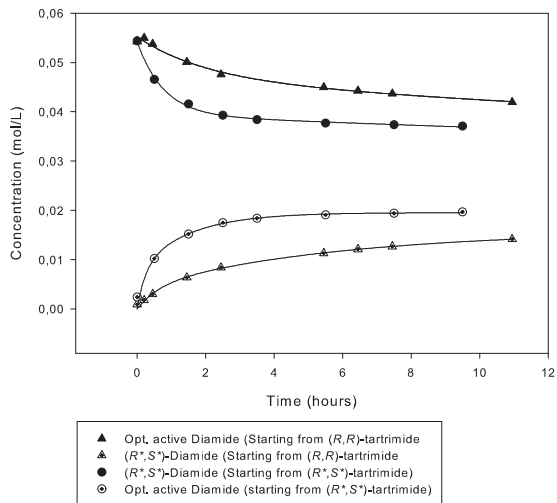


Figure 5.12 Isomerization of the formed diamides **27** is different depending on the stereochemistry of the starting tartramide **1**.

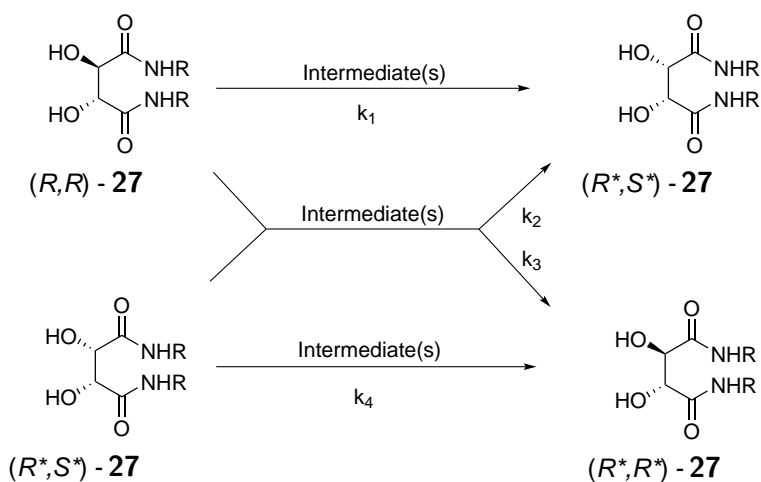


Figure 5.13 Possible explanations for the observed trends: 1) Different intermediates where $k_4 > k_1$ 2) Same intermediate with higher prevalence for one stereochemistry; $k_3 > k_2$.

5.4 Suggested isomerization mechanisms

In the theory chapter of this thesis, two mechanisms for isomerization of the stereocenters in the tartaric acid moiety were introduced; ketene intermediates and isomerization through ion-pair formation at a saturated carbon.

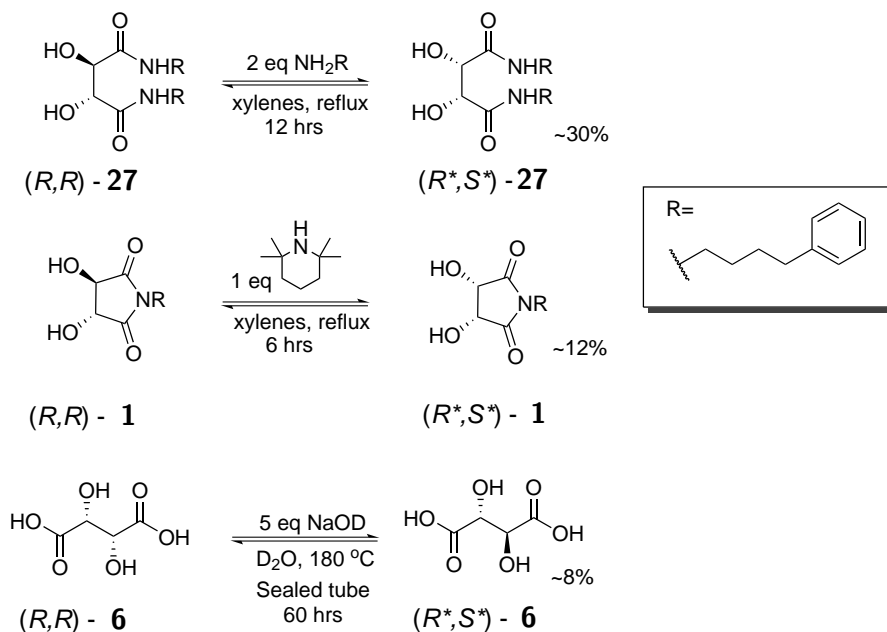


Figure 5.14 Grade of isomerization in different substrates under different reaction conditions.

As seen from Figure 5.14, the highest observed degree of isomerization was for the diamides in this chapter. This points towards a mechanism that is affected by the nature of the substituent attached to the carbonyl group, which may be both leaving group stability (for ketene intermediates) and ability to temporarily stabilize a negative charge (ion-pair mechanism). Steric effects of the substituent might also come into play, in addition to optimal structures in the given reaction environments.

Both isomerization mechanisms may be applied to explain most of the observed phenomena in this chapter. The slower isomerization for the chiral diamides may, as an example, be explained by one side of the intermediate being less sterically hindered than the other. Hence, one stereochemistry will have prevalence over the other (Figure 5.15), as discussed in 3.1.

The only observation which cannot be explained by both mechanisms, is the rate of isomerization being almost the same for the reactions with one

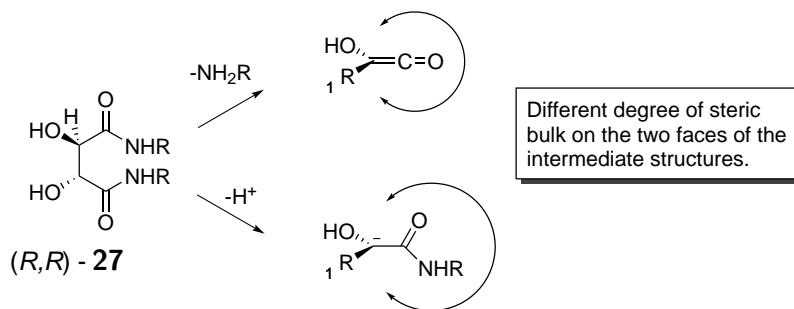


Figure 5.15 Possible explanation for isomerization from optically active diamides to *meso*-diamide being slower than the opposite reaction.

and two equivalents amine added to the reaction mixture. The amine concentration is less important above a certain concentration, as there was no inversion of stereocenters at low concentrations of added amine (0.1 equivalents). The ion-pair mechanism would be expected to undergo faster at higher amine concentrations as the rate determining step probably is the removal of the proton, creating the ion-pair. While a ketene mechanism might have a unimolecular rate determining step, less dependent on the base concentration.

By looking back to the phenomenon shown in Figure 5.11, there is a possibility that the cyclic tartrimide **1** is an intermediate in the isomerization reaction. Furthermore, the structure of the cyclic imides may also be favorable for coordination of the free amine in a nucleophilic Bürgi-Dunitz trajectory. A suggested coordination on cyclic imide shows hydrogenbonding with the amine in a 6-ring fashion, which are sometimes found to be favorable coordinations.⁵⁸ This coordination specie would favor a ketene intermediate, as a simple proton transfer would create a favorable leaving group and create the ketene Figure 5.16. The coordination looks reasonable when considering the reported form of cyclic imides by Polonski *et al.*⁵⁹ The stereochemistry of molecules in this mechanism would be dictated by step 3, and to some degree step 2. From which side of the plane the nucleophile enters to attack the LUMO might have influence on stereochemistry, as the initial form of the zwitterionic intermediate after nucleophilic addition will be dictated by this. However, it is the interaction between the leaving proton from the nitrogen specie and HOMO in the sp² enolate-like intermediate (step 3) which is expected to have greatest influence on stereochemistry in this mechanism.

Earlier in this chapter, the relative steric stability of the cyclic imides **1**

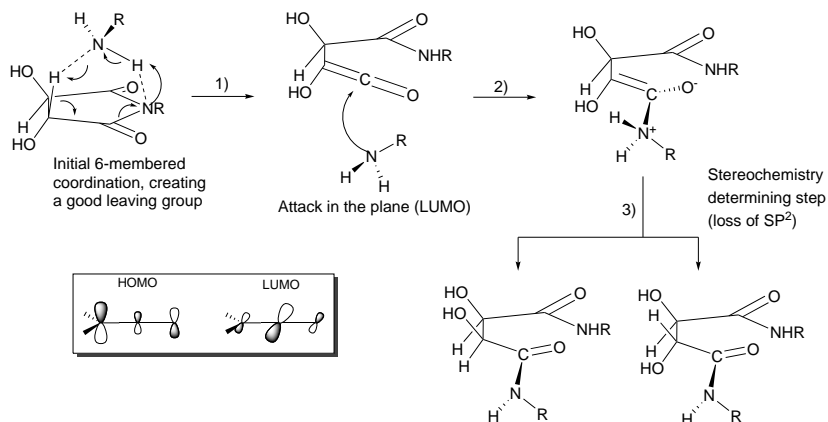


Figure 5.16 Suggested isomerization mechanism with the cyclic imide **1** as an intermediate, followed by 6-membered hydrogen bonding coordination and formation of the ketene.

with different stereochemistry was discussed. It was found that (R^*,S^*) -**1** is less energetically favorable than the corresponding chiral (R^*,R^*) -**1** (Figure 5.6). This can be seen as a contradiction to the mechanism suggested in this section. However, the rate determining step in this mechanism is expected to be formation of the ketene intermediate, hence the steric energy of the cyclic imides will have little influence on the observed rate of isomerization. Higher strain on the ring structure might even increase the rate, as that would result in a smaller ΔG^\ddagger due to relief of strain in the rate determining opening to form the ketene.

Based on the preliminary data, a ketene mechanism possibly through a six-ring coordination of the nucleophile to the cyclic imides seems to be the more probable mechanism. This would explain the apparent isomerization taking place in the imide-diamide equilibrium. Having a good leaving group, as proposed in the mechanism, would lower the energy of the isomerization, which would explain the observed different behaviour for (R,R) and (R^*,S^*) . Stereochemistry was found to dictate stereochemistry to a higher degree than expected, this might point towards lowering of ΔG^\ddagger for the isomerization. However, as none of the results are sufficient for exclusion of either of the proposed mechanisms, both mechanisms are still considered viable. Even though the ketene isomerization mechanism is the current best fit to the data obtained.

6. Reactions of the monoacid (*R,R*)-**3** with free amine

The effect of free amine on the monoamido tartaric acid (*R,R*)-**3** was investigated. The diamide byproduct in Figure 6.1 may also arise from direct amide formation with the monoacid as from the cyclic imide described in the previous chapter.

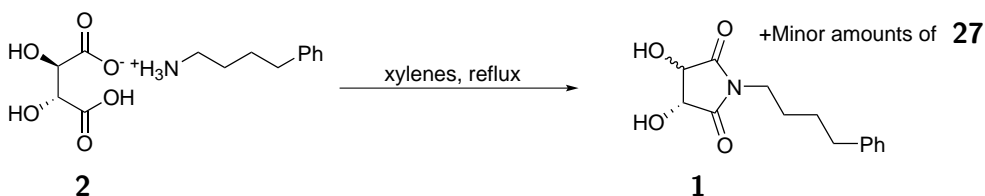


Figure 6.1 Formation of partially isomerized cyclic tartramide from ammonium tartrate monosalt.

In an attempt to provide more data to elucidate the isomerization mechanism, several experiments were conducted with the thermolytic reaction of **3** with varying amounts of 4-phenylbutyl amine (**28**) (Figure 6.2). Detailed experimental descriptions can be found in Section 11.7.3. Spectra and chromatograms can be found in Appendix N.

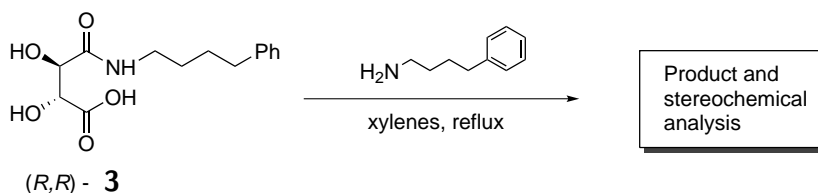


Figure 6.2 Thermolytic reaction of (*R,R*)-**3** with varying amounts of 4-phenylbutylamine in refluxing xylenes.

6.1 Isomerization of the formed cyclic imides **1**

As one of the main objectives in this project was to look into the partial isomerization occurring in the formed cyclic tartramide, this was investigated before the stereochemical composition of the formed diamides. The diamides formed in these reactions are addressed in the next section. The experiments in this section was performed according to the conditions specified in Table 6.1. The reaction conducted with two equivalents of amine added is excluded from this section, due to no cyclic imide observed in the reaction mixture throughout the experiment.

Table 6.1 Different amounts of amine added to (*R,R*)-**3** ($56.9 \cdot 10^{-3}$ mol/L) in refluxing xylenes (12.5 mL).

Ex. No.	Amine added (eq)	(hours)	(<i>R*,S*</i>)- 1 ^a	chiral 1 ^a
1	0.1	9	est. <2%	(<i>R,R</i>)
2	1.0	9	est. <2%	(<i>R*,R*</i>)
3	1.1	11	est. <2%	(<i>R*,R*</i>)

^aLast sample

Experiment 1 in Table 6.1 showed as expected a slight formation of the non-isomerized (*R,R*)-**27** in addition to the major product (*R,R*)-**1**. However, towards the end of the experiment a slight asymmetry was observed for the α -proton peak for (*R,R*)-**1**. As the respective ¹H NMR peaks for (*R,R*)-**1** and (*R*,S**)-**1** is only separated by 0.2-0.3 ppm, this asymmetry might indicate slight formation of (*R*,S**)-**1** (Figure N.1). HPLC analysis was performed in order to verify, but due to solubility issues, the sample had to be diluted to such a degree that quantification was difficult.

The partial isomerization of (*R,R*)-**1** to (*R*,S**)-**1** was more evident from the experiments when more amine was added to the reaction mixture (experiment 2 and 3 in Table 6.1). ¹H NMR spectroscopy indicated formation of a minor amount of (*R*,S**)-**1**, but HPLC analysis showed a completely different picture. The chromatogram from HPLC analysis of the fraction taken out after 9 hours for experiment 2 in Table 6.1, shows the presence of the doubly inverted (*S,S*)-**1** in higher concentrations than the singly inverted (*R*,S**)-**1**. The same trend was also observed for experiment 3 (Table 6.1).

These results coincide with the results observed in Section 5.2, where (*R*,S**)-**1** was found to be energetically less favored (1.5 kcal/mol) than the corresponding chiral (*R*,R**)-**1** (seen from observed data and MM2

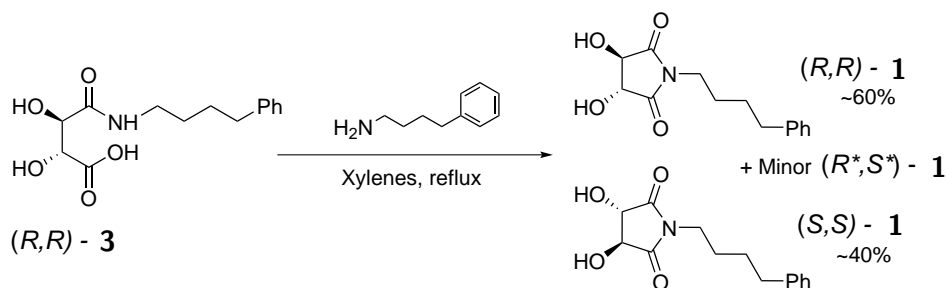


Figure 6.3 The observed composition of **1** (from HPLC) after 9 hours of refluxing time with 1 equivalent of amine added. Composition and amounts of formed **27** is not shown in this figure.

minimization). Figure 6.4 presents a possible explanation for the observed trends for cyclic imides **1** formed in these reactions, along with the data obtained in Section 5.2.

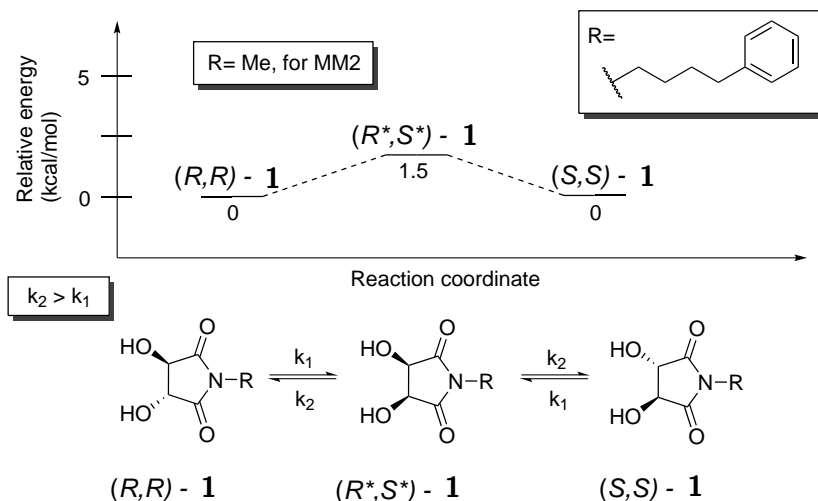


Figure 6.4 Suggested explanation to the observed doubly inverted (S,S) -**1** late in the experiment. Free amine is not shown here, but is evidently needed to induce the isomerization.

Looking back to at experiments conducted, the cyclization performed with conditions lacking free amine showed no isomerization throughout the reaction. This clearly indicates, along with data obtained from other sections in this thesis, that free amine is vital for the different compounds to undergo isomerization.

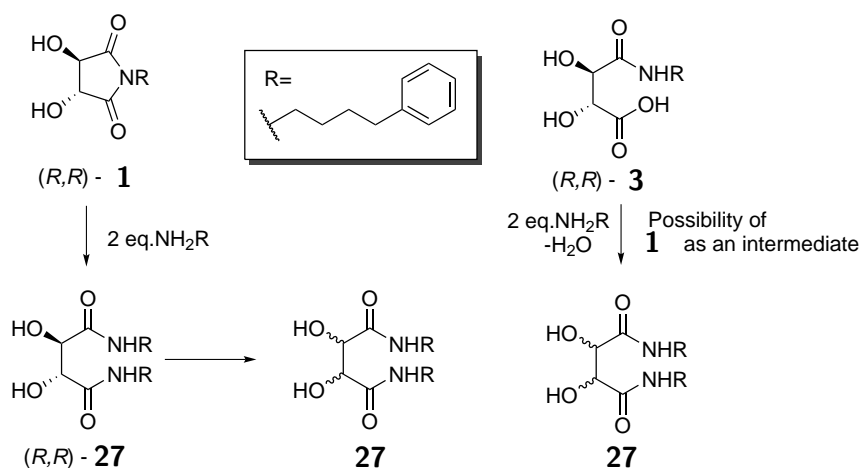
6.2 Isomerization of diamides **27**

Figure 6.5 Formation and stereochemical isomerization of **27** either from (*R,R*)-**1** or (*R,R*)-**3** in presence of 2 equivalents of 4-phenylbutylamine.

Isomerization tendencies for **27** in these experiments were higher than in the experiments conducted for addition of free amine to **1** (Section 5.3). As seen from Figure 6.6, equilibrium conditions for the different stereoisomers of **27** is obtained faster when adding excess amine to **3** compared to when doing the same to **1**.

The difference in rate of isomerization can be calculated from the plots showing formation of (*R*,S**)-**27**, as they both start at 0 mol/L for t_0 in both experiments. The rate of isomerization was determined at the 3 hour mark, which shows the most distinguishable difference in rates for the two scenarios (Table 6.2).

Table 6.2 Observed difference in rate of isomerization for **27** at the 3 hour mark for the substrates (56.9×10^{-3} mol/L) added 2 equivalents of 4-phenylbutylamine.

Substrate	Rate (M*hour ⁻¹)
(<i>R,R</i>)- 1	0.0013
(<i>R,R</i>)- 3	0.0027

The isomerization rate was found to be around twice as fast for the

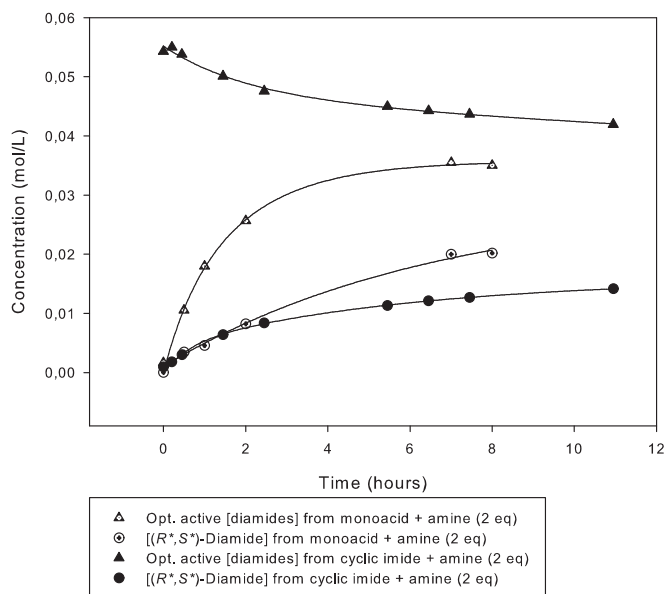


Figure 6.6 Reaching a stereoisomeric equilibrium between the different forms of **27** was observed to be faster from **3** + 2 eq. amine than for **1** + 2 eq. amine.

experiment where 2 eq. of amine was added to (*R,R*)-**3** compared to the experiment starting with (*R,R*)-**1** (Section 5.3).

6.3 Possible explanations for the observed changes in stereochemistry

If the inversion of **27** takes place during the formation of **27** from **3**, the increased isomerization rate may be explained in accordance to the mechanism outlined for cyclization of **3** in Section 4.3. This mechanism is supported by data reported in the literature,^{18,19} showing initial activation through a carboxylic dimer in order to induce the direct amide formation (Figure 6.7). The mechanism for the isomerization may also involve the same carboxylic activation, making it faster than isomerization of the already formed diamide. Another possible explanation combines the lack of (*R*^{*},*S*^{*})-**1** and formation of the doubly inverted (*S,S*)-**1** for experiment 2 in Table 6.1 with the observed formation of (*R*^{*},*S*^{*})-**27** for the experiment with **3** in Table 6.2. The faster formation of (*R*^{*},*S*^{*})-**27** may be explained due to the rapid opening of (*R*^{*},*S*^{*})-**1** formed throughout the reaction.

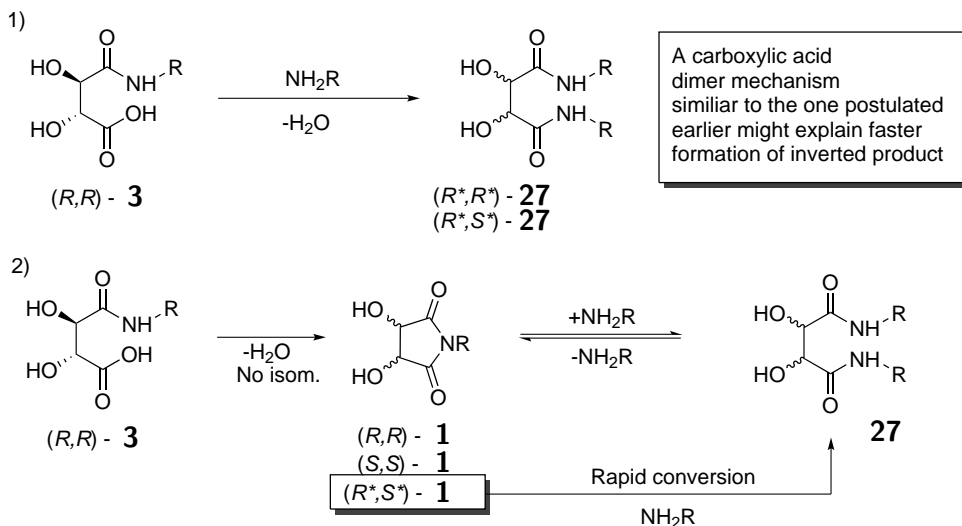


Figure 6.7 1) Direct diamide formation with isomerization through an carboxylic acid dimer assisted mechanism (4.3). 2) Initial cyclization condensation followed by imide-diamide equilibrium and rapid ringopening of formed (*R*,S**)-**1** due to higher steric energy.

The isomerization mechanism for pathway 1 would be assumed to be like the isomerization mechanism for the observed partial inversion for **1** when starting from the ammonium tartrate salt (Figure 3.5 in Section 3.2), as it would be a direct amide formation with partial isomerization from free amine. The changes in stereochemistry in pathway 2 can be explained with the mechanism proposed in the previous chapter (Figure 5.16 in Section 5.4), where the isomerization happens through initial 6-ring coordination to the cyclic imide followed by formation of a ketene intermediate. However, the pathways presented in Figure 6.7 are not backed up by computational studies. Furthermore, there is little literature to be found regarding similar concepts. Future experimental and computational data may provide evidence for either of the two suggestions, or discredit them both. In the current frame of knowledge however, both mechanisms seems to be reasonable explanations for the observed stereochemical changes.

7. Studying the initial amide formation from **2**

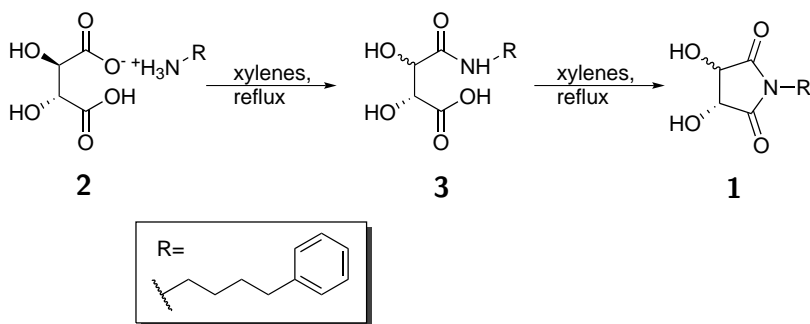


Figure 7.1 Formation of partially isomerized **1** from **2**, with **3** as a stable intermediate.

As data pointed more and more towards partial isomerization happening during the initial formation of **3** from **2**, a strategy was laid out to study this step separately. In order to do a kinetic assessment of this part of the reaction system, the starting compound had to be modified. If not, the formed monoacid from the initial amide formation would rapidly cyclize and form the cyclic tartramide. This was unfavorable, not just because of constant changes to the monoacid concentration, but also because of overlapping signals in analysis (around 4.4 ppm in ^1H NMR, as seen from spectra in Appendix K). As discussed thoroughly in Section 10.3, the reactions involving the monoacid was analyzed mostly with ^1H NMR spectroscopy with occasional supporting HPLC experiments. The characteristic peak used for determining the concentration of **2** was overlapped by chemical shifts from **1** (4.4 ppm). All detailed experimental data for this section can be found in Sections 11.5.13 and 11.7.4.

The plan was to block one of the acid groups with a thermally stable

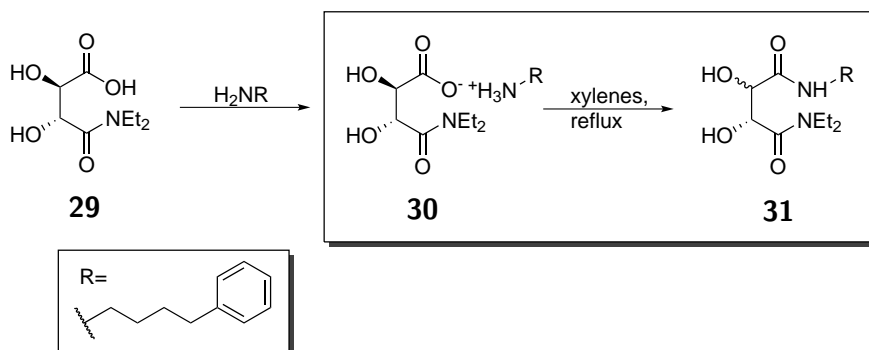


Figure 7.2 Strategy laid out in order to separately study the initial amide formation of the ammonium tartrate salt into the monoamido tartrate.

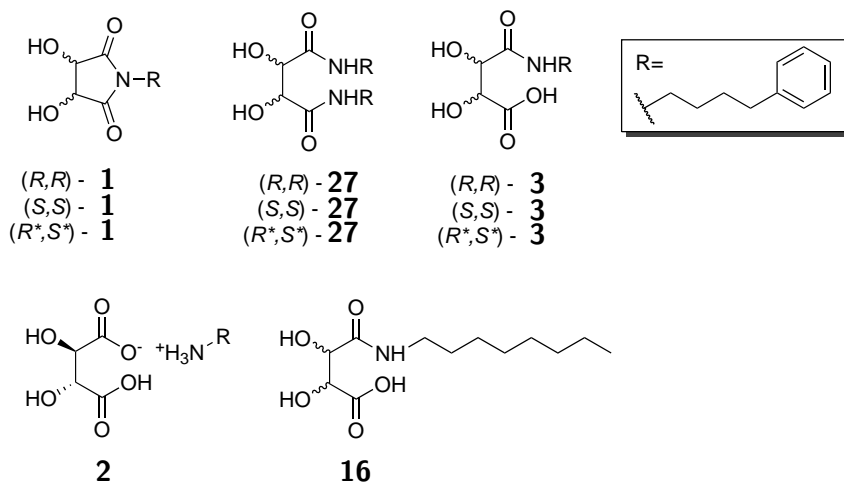
non-reactive substituent in order to stop the reaction after the initial amide formation. The diethyl amino moiety was chosen on background of accessibility and expected behaviour. In addition, there already existed a synthetic pathway for preparing the monoamido functionalized tartaric acids from their correspondent diacetyl tartaric acid anhydrides (Section 9.5). However, due to problems with the workup of the product **29**, as addressed in Section 9.9, obtaining the pure compound proved to be difficult. The purest obtained compound still contained residual acetic acid and probably minor amounts of NaCl.

After obtaining the semi-pure compound **29**, formation of the ammonium salt was attempted. The salt did not precipitate out as for **2**, so the solvent was removed *in vacuo*. Instead of obtaining a white powder as for **2**, there was observed a yellow oil with residual solvent in addition to the already accumulated pollutants. However, a test reaction was conducted in order to see if the amide **31** formed as planned. Due to high degree of impurities present in the reaction mixture and lack of reference compounds, the experiments did not yield any usable data.

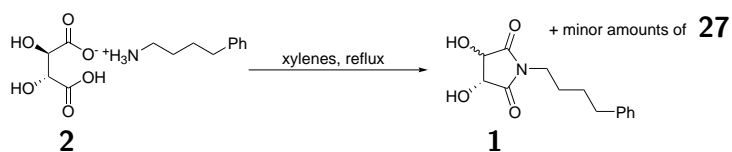
Due to the project deadline approaching, there was not put more time into purifying the starting material **29** and synthesizing the proper reference materials. However, this reaction might yield useful information of the partial isomerization taking place and enable for HPLC analysis of the products due to removal of the carboxylic acid moiety.

8. Conclusion and further work

A number of optically pure starting materials/reference compounds were successfully synthesized by using known methods, or extrapolations of known methods.



Furthermore, analytical methods for study of the different reactions and compounds were outlined, stereoselective HPLC separation and ^1H NMR spectroscopy methods were developed and applied in order to properly study the chosen reactions. Several pre-column derivatization techniques for HPLC was also looked into, especially for the monoacid compounds (**3** and **16**).



The above mentioned compounds and methods were used to study different reaction steps observed during the preparation of **1** from **2** with partial isomerization.

By studying the cyclization condensation reaction of **3** with kinetics and molecular modelling, a reaction mechanism was outlined for the intramolecular cyclization reaction in nonpolar solvents (Figure 8.1). The mechanism involves initial activation through carboxylic acid dimers followed by intermolecular proton transfer and a intramolecular nucleophilic attack by a sterically constricted nitrogen-specie. This mechanism proceeds without isomerization. The two step pathway is assumed to be more probable due to the long distance between the proton transfer species in the one step intermediate **25**.

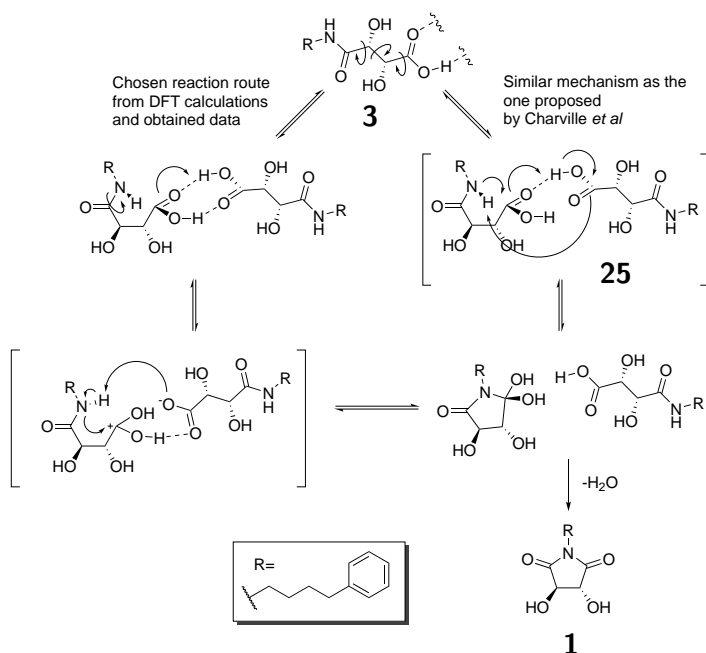


Figure 8.1 Proposed mechanisms for cyclic imide formation.

Presence of free amine in the reaction mixture were found to be of pivotal importance in order for both partial isomerization and initial amide formation to take place. Initial direct amide formation was thought to go through a carboxylic dimer mechanism presented by Charville *et al.*^{18,19} Results found for isomerization during initial direct amide formation leans more towards a ketene isomerization mechanism, than isomerization through ion pairs. However, as none of the experiments enabled for direct distinguishing between the two, both are still considered valid mechanisms. The isomerization of diamides **27** and cyclic imides **1** were suggested to go through ketene intermediates, were the imides **1** were also suggested as intermediates for diamide isomerization (Figure 8.2).

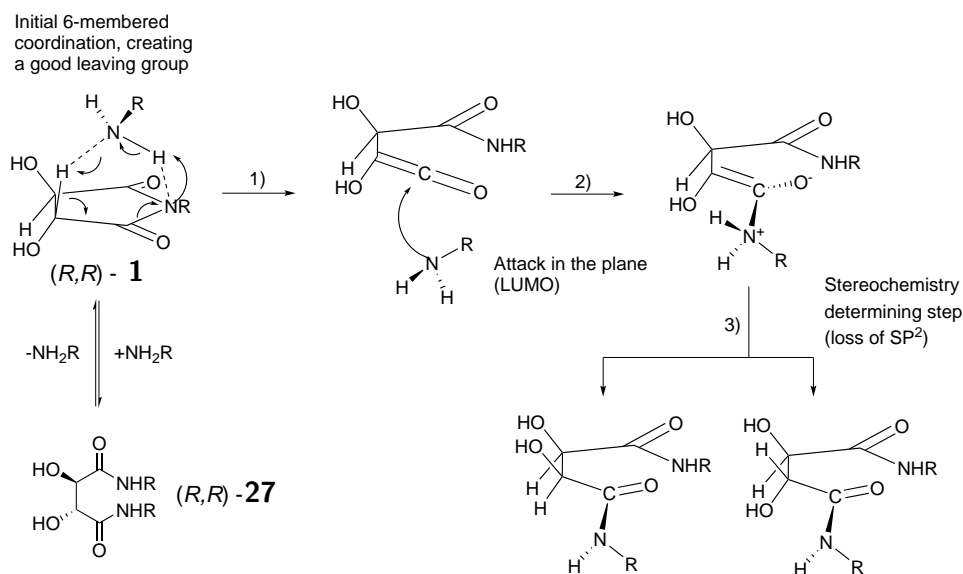


Figure 8.2 Suggested isomerization mechanism for **1** and **27**.

Furthermore, it was found that stereochemistry dictates chemical behaviour to a higher degree than first expected. This can be seen from the experiments conducted in Chapter 5, where the initial reaction of **1** with amine was different for the (R^*,S^*)-form than for the optically active (R,R)-form.

8.1 Further work

A rather large part of the time invested in this project was used to prepare starting materials and looking into different analysis methods. As most of the synthesis routes, derivatization techniques and analysis methods now have been established, further work should be mainly directed at further studies on the reactions for creating a broader scientific platform for the working hypotheses. Further studies on the reactions should include more analysis by chiral HPLC methods with a proper IS, as following the mass balance of the reactions is of interest.

8.1.1 Synthesis of deuterated tartaric acid (**32**)

Further work with this part of the project should include experiments with compounds containing a thermally stable substituent on one side of tartaric acid. Subjecting these compounds to the same reaction conditions as tartaric acid will hopefully provide indications to which degree the dicarboxylic acid structure of tartaric acid influences the susceptibility for it to undergo hydrogen-deuterium exchange, as mentioned in Section 9.1.1. Further work should also mainly revolve around microwave irradiation, considering that microwave chemistry was the only method that afforded any degree of hydrogen-deuterium exchange.

8.1.2 Deuterium experiments

If synthesis of **32** should prove to be successful, attempts at quantifying kinetic isotope effects would be of particular interest, as they might provide important information of the transition states in the isomerization mechanisms.

Furthermore, one particular experiment that should be of priority, is the reaction shown in Figure 8.3. This reaction might yield data that enables for distinguishing between the two postulated isomerization mechanisms. By looking at the isotope ratios for the intermediate products throughout the reaction.

8.1.3 Initial amide formation

More work should be put into making a mono-"protected" tartaric acid for studies on the initial amide formation, as was attempted in chapter 7. As it was found that the isomerization for the partially isomerized cyclic imide **1** most likely takes place in this step.

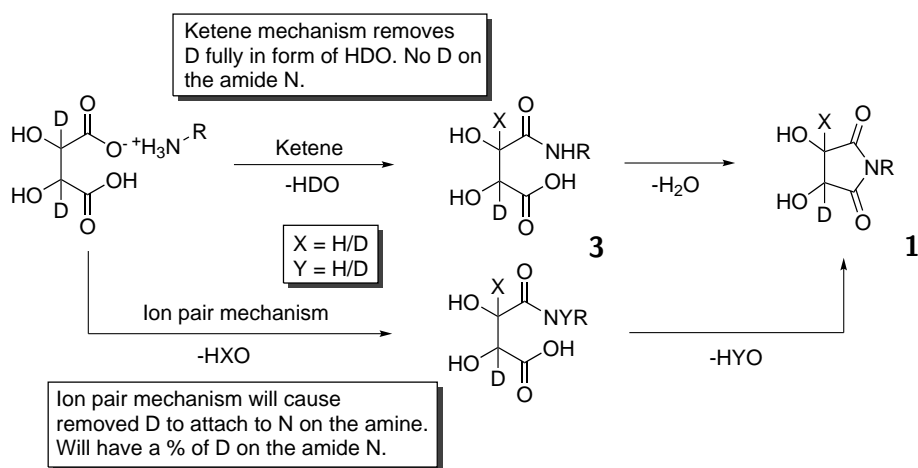


Figure 8.3 Suggested deuterium experiment for further studies. There is expected to be a difference in isotopic ratios for **3** and **1** for the ion pair mechanism, due to exchange of deuterium through this mechanism causes the amine to be partially deuterium enriched. If the ratios for the two are the same, a ketene mechanism would be the most likely cause for isomerization.

9. Synthesis results

9.1 Synthesis of 2d,3d-(*DL*)-tartaric acid (**13**)

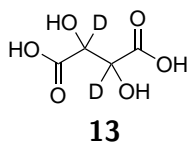


Figure 9.1 2d,3d-tartaric acid

One of the initial goals of this study was to use 2d,3d-(*DL*)-tartaric acid (**13**) in order to study the deuterium kinetic isotope effect⁶⁰ on the partial isomerization reaction. The compound was also to be used for quantifying the isomerization and exchange with mass spectrometry and NMR.⁶¹ However, the price of this compound is relatively high and with a limited number of suppliers. In addition, the reported synthesis for (2d,3d)-tartaric acid (**13**)⁴³ is a rather elaborate procedure containing a number of complex reaction steps, and with the time on hand this idea was also discarded right away. The strategy laid out was to develop an inexpensive one step method to obtain the wanted compound.

9.1.1 α -H activation in tartaric acid with ionic barium in basic media

Ruthenium and rhodium metal catalysts have been used for hydrogen-deuterium isotope exchange,⁶² but these catalysts often require special experimental conditions. In addition these compounds are often relatively expensive. The idea with this line of experiments revolved around creating a simple and inexpensive method for deuterium labeling of α -hydroxy acids.

Literature⁶³⁻⁶⁵ shows usage of ionic barium derivatives in order to increase the electrophilicity of carbonyl groups. The increase in reactivity

arises from the transfer of electron density from the carbonyl to the extramolecular space between the barium ion and the oxygen atom. This will render the sp^2 -carbon more susceptible for nucleophilic attack. The Lewis acid properties exhibited in ionic barium are also shown by the crystal structure of barium(II) L-tartrate.⁶⁶ As seen from Figure 9.2; barium(II) will coordinate to one of the carboxyl oxygens on C1 and the hydroxy oxygen on C3. This coordination will, as explained above, siphon electron density from the tartrate moiety and render it more electron deficient.

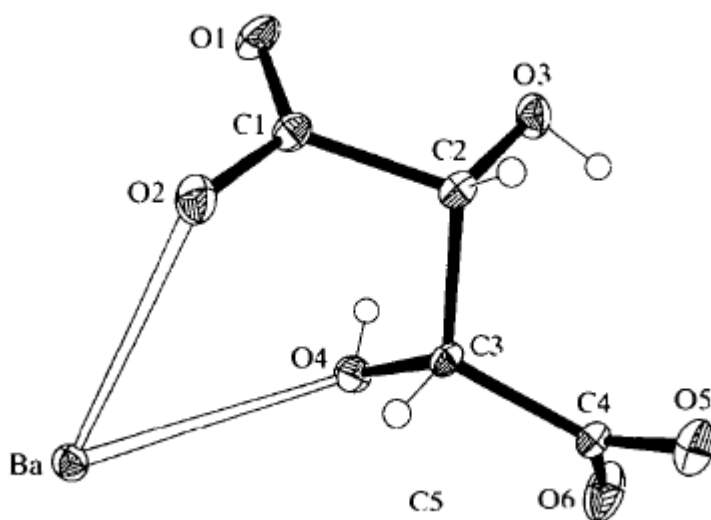


Figure 9.2 Barium *L*-tartrate crystal structure.⁶⁶

As the structure of tartaric acid indicates, ionic barium will not be sufficient in order to induce exchange of the protons attached to the α -carbons. The first reported synthesis of *DL*-tartaric acid involved reflux with a large excess of sodium hydroxide.⁶⁷ The racemization of tartaric acid in the presence of hydroxyl ions indicate that there might be an exchange of the protons on the α -carbons. Thus, the strategy laid out from this point was to use a strongly basic environment with the presence of barium(II) in order to achieve the wanted result. The reasoning behind the usage of a basic barium compound instead of sodium hydroxide as reported in the racemization reaction of tartaric acid⁶⁷ arises from hard-soft interaction considerations. The hard-soft-acid-base (HSAB) theory introduced by Pearson,²⁹ states that hard-hard and soft-soft interactions are energetically preferred compared to hard-soft reaction partners, as discussed in Section 2.4.1. Barium has a

higher degree of nuclear screening than sodium and is thus considered to be softer. The thought was that barium will create a more favorable less hard-soft interaction with the relatively soft oxygen moieties in tartaric acid making it a better lewis acid than sodium.

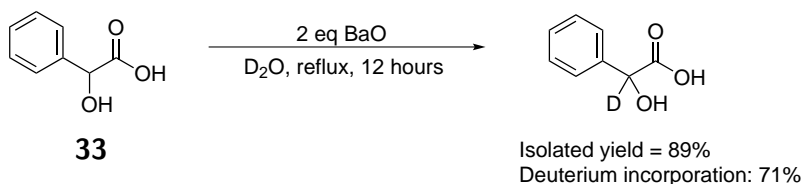


Figure 9.3 Deuterium incorporation in mandelic acid with barium(II)oxide and heavy water (determined by ^1H NMR spectroscopy).^{68,69}

Barium oxide (BaO) was the choice of compound capable of creating the wanted environment, considering that it will convert into $\text{Ba}(\text{OH})_2$ in aqueous media affording a basic environment and providing the system with barium ions for coordination in addition to being readily available in the laboratory. Literature⁶⁸ showed that BaO was able to induce exchange at the α -proton site in the simpler L-mandelic acid (**33**) with good yields. These results were also successfully reproduced in a previous project.⁶⁹

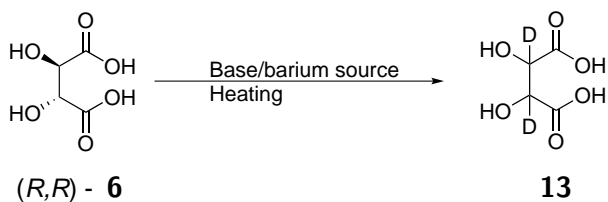


Figure 9.4 Synthesis of **13** with Ba(II) in basic media.

Several attempts were made in order to make the target 2d,3d-tartaric acid (**13**), however neither of the methods employed in Table 9.1 yielded the target compound to any measurable degree by ^1H NMR. Experimental details are found in Section 11.2. The first attempts (Table 9.1 entries 1 and 3) used the same conditions as those yielding good incorporation to mandelic acid,⁶⁸ when this did not yield any incorporation of deuterium to tartaric acid more rigorous conditions were employed (Table 9.1 entries 2 and 4), however neither yielded any incorporation. It was quite clear that different conditions were required when the sealed tube reaction at 180°C for 4 days did not yield any product.

The first potential source of error explored was the accessibility of barium ions, since there was white unidentified precipitate present in the reaction flask (assumed to be $\text{Ba}(\text{OH})_2$). This was not observed with the usage of a different barium salt; Barium(II) chloride. However, neither of the attempts made with the usage of BaCl_2 yielded any of the wanted product. Reaction conditions are seen in Table 9.1 (entries 5 and 6) and experimental details are found in Section 11.2.

As previously mentioned, the procedure for racemization of optically active tartaric acid⁶⁷ utilized sodium hydroxide in refluxing water. More recent studies conducted by Yang and Evilia shows the racemization and hydrogen-deuterium exchange in amino acids with sodium deuterioxide in supercritical deuterium oxide.⁷⁰ Therefore, a couple of attempts were made to achieve the wanted compound **13** using sealed tubes and high concentrations of sodium deuterioxide. As can be seen from entries 7 and 8 in Table 9.1 neither afforded any hydrogen-deuterium exchange.

Table 9.1 Yields and conditions for attempts to synthesize **13** from (*R,R*)-**6**, where deuteration with BaO , BaCl and NaOD was attempted.

$(R,R)\text{-6}$ $\xrightarrow[\text{Heating}]{\text{Base/barium source}}$ **13**

Attempt	Ba(II)/base source	Eq	T °C	Time hours	D ^a (%)
1 ^b	BaO	1	reflux	6	0
2	BaO	1	130 ^c	27	0
3 ^b	BaO	3	reflux	6	0
4	BaO	3	180 ^c	96	0
5	BaCl_2 (no base)	1	reflux	16	0
6	BaCl_2 (no base)	1	reflux	16	0
7	NaOD	5	180 ^c	12	0
8	NaOD	5	180 ^c	67	0

^aDetermined by ¹H NMR

^bN₂

^cSealed tube

A possible explanation for the lack of deuterium incorporation might arise from the fact that tartaric acid is a dicarboxylic acid. When added to a basic environment tartaric acid will form the dianionic tartrate moiety which contains two delocalized negative charges (as the tartrate moiety depicted in Figure 9.2). The tartrate will be present in solution with cations, in this case barium(II) and sodium(I). Though, if the cation coordination does not provide sufficient neutralization, there might be excess electron density present in the tartrate moiety. This will then lower the acidity of the protons attached to the α -carbon, rendering them incapable of exchange under the present conditions.

However, considering the HSAB principles, the reactions with barium(II)-ions present should be more susceptible for exchange. This was experienced during analysis of some reaction mixtures containing residual barium(II). The samples dissolved in d_4 -MeOH showed an increased rate of esterification compared to a reference sample (Figure 9.5). Spectroscopic data for this observation can be found in Appendix H. This indicates that ionic barium do have Lewis acid properties in the chosen reaction system, but not sufficient to, along with the basic media, induce exchange under the given conditions.

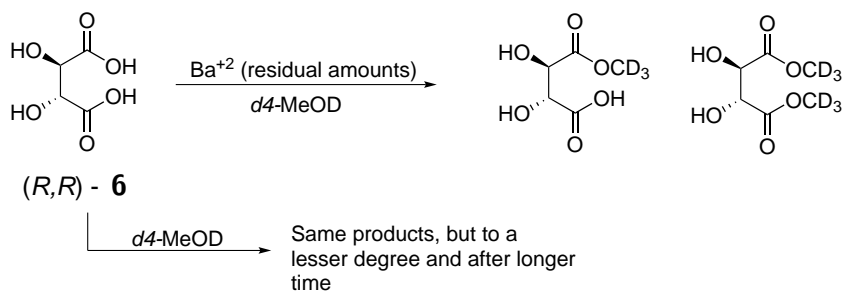


Figure 9.5 Formation of monomethyl- and dimethyltartrate with deuterated methanol in the NMR tube. Esterification was a lot higher for sample containing residual barium(II).

9.1.2 Acid induced α -H activation in tartaric acid

Due to the experiments utilizing a basic media did not yield incorporation of deuterium, a different approach was tried in order to obtain the wanted compound **13**. One of the concerns regarding the reactions in basic media was the possible deactivation of tartrate due to insufficient charge neutralization. This could be avoided by treating tartaric acid with a strong acid, and this way induce hydrogen-deuterium exchange through enolization (Figure 9.6).

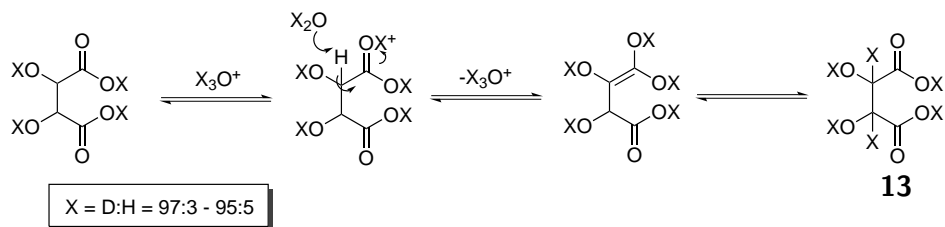


Figure 9.6 Possible enolformation of tartaric acid in acidic environment.

There are no literature reports on this type of transition states for tartaric acid. However, there are conducted studies on the thermodynamic properties of a similar transition state in acetic acid.⁷¹ There is also a study done by Yang and Evilia on the deuteration of the alpha carbon in amino acids with strong acids in supercritical water.⁷²

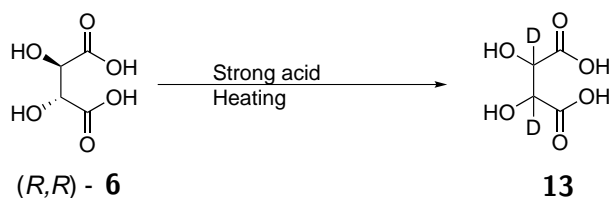
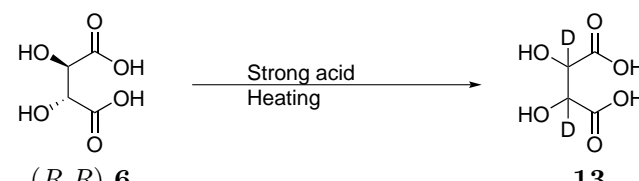


Figure 9.7 Synthesis of **13** from *R,R*-**6** with strong acids.

Several attempts with differing reaction conditions were tried in order to obtain the wanted compound **13**, but none yielded any measurable deuterium content (Table 9.2). Detailed experimental description can be found in Section 11.2. The initial experiments were done under relatively mild conditions, followed by gradually harsher conditions throughout the series. The sealed tube reactions at 180 °C was the toughest conditions employed, with equipment readily available in the lab. This is still far from the conditions used by Yang and Evilia in their study with supercritical water.⁷²

Considering the fact that decarboxylation of the amino acids was a problem for Yang and Evilia indicates that the hydrogen-deuterium exchange in tartaric acid only takes place under really hard conditions with the current reagents.⁷² The exchange happens on the borderline of decomposition and this set of reactions were far from reaching those conditions.

Table 9.2 Yields and conditions for attempts to synthesize **13** from (*R,R*)-**6** with strong acids.


Attempt	Acid	Eq	T °C	Time hours	D ^a (%)
1	H ₂ SO ₄	cat.	rt	16	0
2 ^b	HCl	cat.	rt	16	0
3	H ₂ SO ₄	1	180 ^c	47	0

^aDetermined by ¹H NMR^b+BaCl₂ (1eq)^cSealed tube

9.1.3 α-H activation in tartaric acid using microwave radiation

Considering the more efficient energy transfer and higher local energies for dipolar and ionic species, a strategy towards microwave assisted synthesis of deuterated tartaric acid (**13**) was laid out. As the previous attempts of reaching this compound with the use of conventional heating and sealed tubes proved fruitless and the fact that Yang and Evilia^{70,72} reported the use of extreme conditions in order to obtain deuteration in similar electronic environments, microwave irradiation was considered to be a probable way to obtain the wanted reaction conditions.

The experimental conditions were extrapolated from the method reported by Yang and Evilia, as to the chemical conditions were duplicated and exposed to microwave radiation instead of supercritical aqueous media.^{70,72} Yang and Evilia reported the usage of both acidic and basic media for obtaining the wanted compound, basic media was chosen for the microwave experiments due to sodium deuterioxide being fairly easy to prepare and was already available in the lab.

Several attempts of synthesizing compound **13** from (*R,R*)-**6** were made, and only one experiment showed some degree of incorporation. However, reproducing this one experiment under the seemingly same reaction conditions

failed. Detailed experimental description can be found in Section 11.2.4.

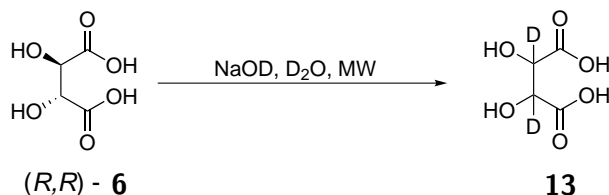


Figure 9.8 Synthesis of **13**.

The bottleneck of this line of experiments were the upper temperature and pressure limits for the microwave reaction vessels, they could not take temperatures and pressures above 190 °C and 20 bar (security valve opening pressure at 70 bar). The settings were set as to operate in the upper level of what the vessels were able to withstand without posing a threat to the reactor or operating personell.

Table 9.3 Yields and conditions for attempts to synthesize **13** from (R,R) -**6** with assisted microwave irradiation in various environments.

(R,R) -**6** $\xrightarrow{\text{NaOD, D}_2\text{O, MW}}$ **13**

Attempt	Reagent	Eq	T ^a °C	Time hours	D (%)
1	NaOD	5	120	2	78.3 ^{bc}
2	NaOD	5	105	2	0 ^d
3	NaOD	5	105	1	0 ^d
4	NaOD	5	105-140	4	0 ^d
5	NaOD	5	190	0.5	0 ^d
6	BaO	2	110	1.5	0 ^d
7	Nothing	-	110	1	0 ^d

^aReference probe

^bDetermined by MS

^c62.6% di-D, 31.3% mono-D and 6.1% non-D

^dDetermined by ¹H NMR

One of the big uncertainties of these reactions were the measurement of

actual temperature, because an internal temperature sensor to the actual reaction flask was not present. This because sodium deuterioxide would corrode and possibly destroy the fairly expensive glass temperature probe which was to be used as an internal pressure and temperature sensor. To get an indication of the actual conditions inside the vessel, a reference vessel containing sodium chloride at the same concentration as sodium deuterioxide in the reaction vessel was prepared. However, no control experiments were conducted as to verify the credibility of the extrapolation, other than looking at the difference in temperature for the two vessels with the internal IR sensor in the reactor. Deviations in temperature between the reference vessel and the reaction vessel is what might have caused the single experiment that successfully incorporated deuterium to the alpha position in tartaric acid. Immediately after opening the vessel after letting it cool down, it was clear that a lot higher temperatures were obtained in this experiment than the other experiments. This was evident from black and brown residue from decomposed starting material. However, as stated above, reproduction of this experiment proved fruitless.

9.2 Introduction to synthesis of stereochemically pure compounds

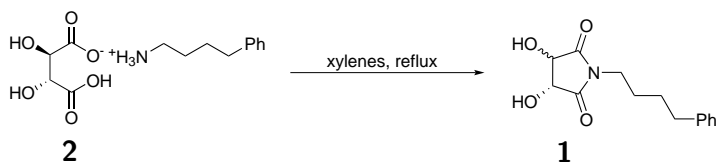


Figure 9.9 Partial isomerization when starting from **2** to make **1**.

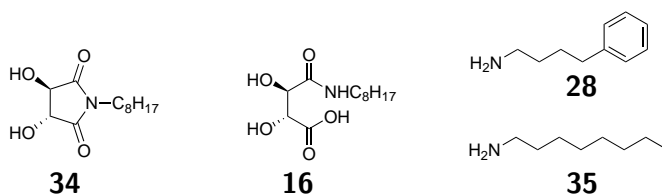


Figure 9.10 Extrapolation of the reaction system.

Synthesis of the compounds in this part of the study were carried out in order to create a better platform of evidence for the formation of the various byproducts in the reaction system. They also worked as starting materials for various reactions that were carried out throughout the project.

The partial isomerization reaction was first encountered in synthesis of the cyclic imide **34** with an octyl chain. The synthesis of the open mono-acid **16** was then considered as a reasonable starting point. However, it turned out that the compounds containing an octyl tail were hard to work with, as further elaborated in Section 10.3. After the discovery of this, in order to simplify the work, octylamine (**35**) was swapped for 4-phenylbutylamine (**28**). The phenyl group was assumed to increase UV-detectability during analysis and lower surfactant properties. This was still considered to be a reasonable extrapolation from the current system, as the change lies more than three carbons away from the functionality of interest.

9.3 Synthesis of **36**, a starting block for **3**

Synthesis of **36** is a simple one-step procedure reported in the literature.^{73–75} The experimental description is given in Section 11.3. Spectra is shown in Appendix F. This anhydride scaffold is a lot more prone to react with nucleophiles and thus require milder conditions. It has also been shown that

introducing a steric bulk to the α -hydroxyl groups, in this case acyl groups, lowers the susceptibility towards isomerization.¹⁵ This together with the mild reaction conditions avoids partial isomerization.

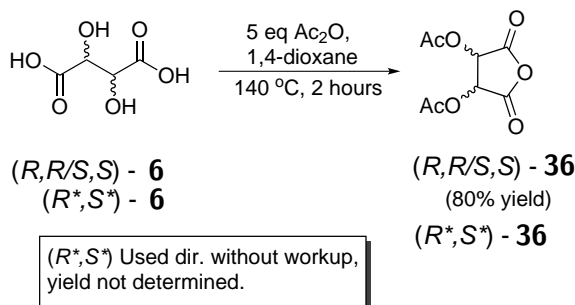


Figure 9.11 Synthesis of **36**.

9.4 Synthesis of octyl monoamido (*R,R*)-tartaric acid **16**

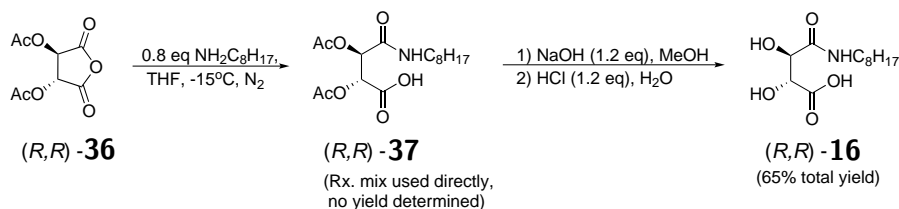


Figure 9.12 Synthesis of **16**.

The optically pure octylamino tartaric acid **16** was synthesized by nucleophilic ring opening with octylamine followed by deacetylation with NaOH in methanol.^{2,73,76} The experimental description is given in Section 11.4.1. ¹H NMR spectra are shown in Appendix G

This synthesis is relatively simple and gives good yields. This synthesis were originally worked up through recrystallization, but in this study a couple of other methods were explored in order to find a simpler route. It was found that by utilizing the acid-base properties of **16** one could purify the compound through filtering and pH-switching. By working up the product with this method the yield is lowered, but since synthesis optimization was not one of the main goals of this study it was considered acceptable.

A different method for deacetylation of the intermediate product to form **16** was also explored. Literature reported deacetylation with catalytic amounts of acyl chloride in methanol.⁷⁷

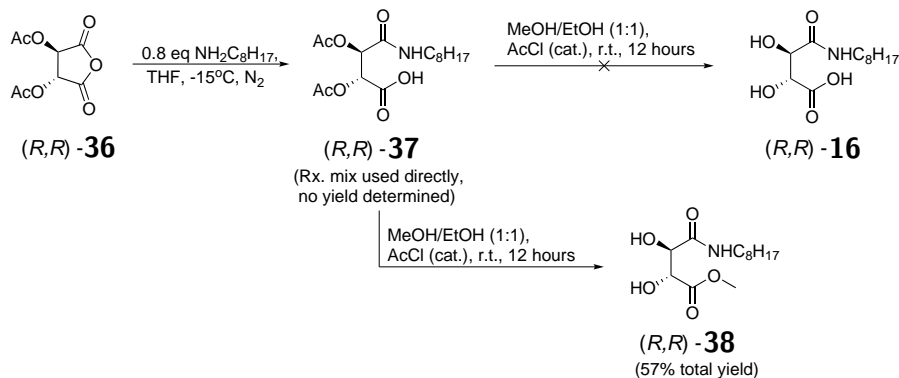
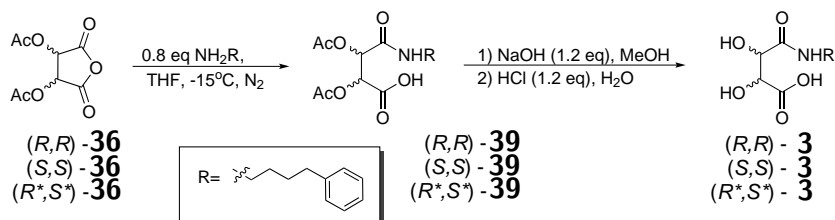


Figure 9.13 Observed product **38** with AcCl as deacetylation reagent.

This deacetylation technique was discarded for this synthesis as it turns out that it created the methyl ester of the wanted compound. Further workup from this point to regain the wanted product only caused an increase of unidentified byproducts. Deacetylation with acyl chloride was tried before treatment with NaOH, because there existed a bit of uncertainty regarding potential isomerization of the stereochemistry with usage of NaOH. Treatment with catalytic acyl chloride was considered to be a milder method and was employed and discarded as stated above, before basic treatment with aqueous NaOH in MeOH was chosen as the preferred deacetylation route.

9.5 Synthesis of 4-phenylbutyl monoamido tartaric acids **3**Figure 9.14 Synthesis of **3**.

All the three different isomers of **3** were prepared through the same procedure as used for synthesis of **16** in Figure 9.12. Experimental description can be found in Sections 11.5.1, 11.5.2 and 11.5.3. Full characterization of **3** can be found in Appendix A. The synthesis of these compounds came along simpler due to an already established procedure from the work on the octyl amino system. However, as can be seen from Figure 9.12 the yields for these compounds are lower than for **16** (65%). The mono-acid (R^*,S^*)-**3** was expected to have a lower yield due to its increased solubility in polar solvents compared to the optically active mono-acids (R,R)-**3** and (S,S)-**3**.⁷⁸ However, as stated above, also the optically active species suffered from increased solubility in water. This might indicate that the new non-polar part of the molecule have less influence of the total polarity of the molecule than the octyl chain. Which makes the compounds more soluble in water, causing a lowering of the total yield compared to **16** (Table 9.4).

Table 9.4 Yields for the synthesis of **3** from **36**.

Compound	Yield ^a (%)
(R,R) - 3	38
(S,S) - 3	41
(R^*,S^*) - 3	18

^aIsolated yields

9.6 Synthesis of 4-phenylbutyl tartrimidates **1**

All three isomers of **1** were prepared through a thermal condensation reaction of **3** with azeotropic removal of water (Figure 9.15).^{2,49}

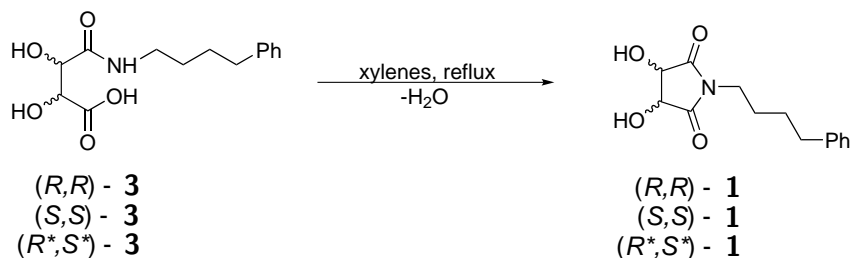


Figure 9.15 Synthesis of **1**.

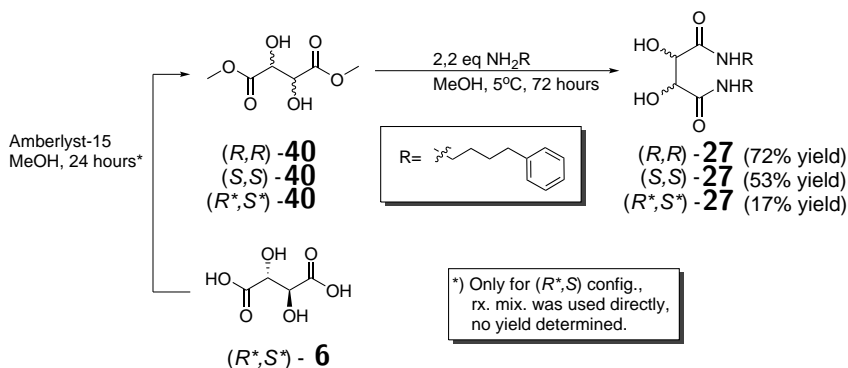
A detailed experimental procedure can be found in Sections 11.5.8, 11.5.9 and 11.5.10. Full characterization of **1** can be found in Appendix C. To ensure full conversion to cyclic tartrimide, a Dean-Stark condenser was used along with long reaction times. The low yields in these reactions, as seen from Table 9.5, arise from the sub-optimal solvent composition used for recrystallization. Throughout the reaction an unidentified byproduct is causing the reaction mixture and the crude product to take on a scarlet color. This byproduct was removed through recrystallization. However, due to the main focus on making pure reference materials quickly, the solvent composition was extrapolated from the methods regarding the system created with octylamine.² NMR of the crude product showed the wanted product as the main compound, with only small amounts of byproduct. This indicates that the main source for the low yield is the recrystallization step. The reactions yielded enough pure reference material for the reactions in mind, so no further optimization was done.

Table 9.5 Yields for the synthesis of **1** from **3**.

Compound	Reaction time (hrs)	Yield ^a (%)
(<i>R,R</i>)- 1	20	36
(<i>S,S</i>)- 1	24	9
(<i>R*,S*</i>)- 1	24	42

^aIsolated yields

9.7 Synthesis of 4-phenylbutyl tartradiamides 27

Figure 9.16 Synthesis of **27**.

All three isomers of **27** were prepared by reacting the appropriate dimethyl tartrate (**40**) with 4-phenylbutyl amine (**28**) in methanol at 5°C for 2-3 days (Figure 9.16).^{16,79-81} Detailed experimental description can be found in sections 11.5.5, 11.5.6 and 11.5.7. Full characterization of **27** can be found in Appendix B. The optically active species (R,R) -**27** and (S,S) -**27** were readily prepared with acceptable yields. (R^*,S^*) -**27**, on the other hand proved to be more difficult. Firstly, the appropriate *meso*-dimethyl tartrate had to be synthesized from *meso*-tartaric acid monohydrate. This was done with Amberlyst-15 in methanol at room temperature.⁸² Working up the reaction mixture from this step in order to obtain pure *meso*-dimethyl tartrate failed. Several options were explored before a working method was found. The reaction mixture from the esterification with Amberlyst-15 was filtered followed by partial evaporation of the solvent *in vacuo*. The amine was then added to this partially evaporated solution and put in cold storage. After 3 days the wanted product precipitated out as white crystals, these were filtered off and washed, yielding the wanted (R^*,S^*) -**27**. The downside of this procedure was a rather low yield compared to the optically active products (Figure 9.16).

9.8 Synthesis of 4-phenylbutyl ammonium (*R,R*)-tartrate **2**

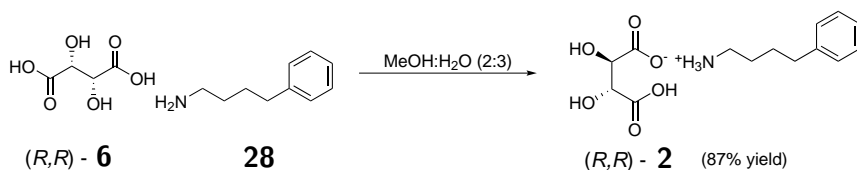


Figure 9.17 Synthesis of **2**.

The salt (*R,R*)-**2** was prepared through mixing (*R,R*)-**6** and 4-phenylbutyl amine in a solvent where they were both soluble and the salt was not (Figure 9.17).² The salt precipitated out with good yields. Detailed experimental description can be found in Section 11.5.11. Full characterization of **2** can be found in Appendix E.

9.9 Synthesis of diethyl monoamido (*R,R*)-tartaric acid **29**

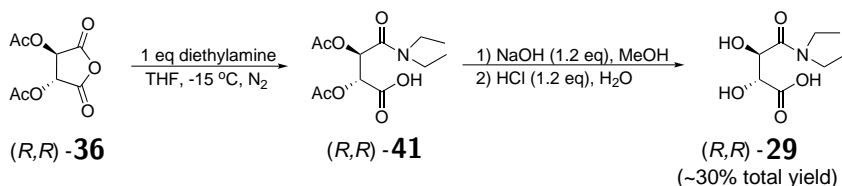


Figure 9.18 Synthesis of **29**.

The compound (*R,R*)-**29** was synthesized using the same method as described for preparation of **16** and **3** in Sections 9.4 and 9.5. Due to the highly aqueous affinity of the product, some other methods had to be applied. Detailed experimental description can be found in Section 11.5.13. ¹H NMR spectra of the impure **29** can be found in Appendix I.

The synthesis of compound **29** was the same as for the previous monoamide tartrates, but the workup proved to be fairly more challenging. Due to the above mentioned tendencies, removal of byproducts and excess reagents proved difficult. The major pollutants in the reaction mixture were excess hydrochloric acid, NaCl and acetic acid. All of these compounds are readily soluble in water along with the wanted product. In order to remove sodium

chloride from the mixture, the reaction mixture was added to THF and stirred for a couple of minutes in order to dissolve all wanted product and were then filtered to remove sodium chloride. After drying of the product, the sticky/oily substance was added to diethylether and filtered in order to remove acetic acid. As the wanted product seemingly was not soluble in ether, and acetic acid is known to be partially soluble. After filtration the product was dried on a high vacuum line for several days in order to remove the remaining acetic acid. The product was considered sufficiently pure for testing, even if there still were residual acetic acid present (assumed to be around 5%).

10. Compound analysis

10.1 Spectroscopy of new compounds

10.1.1 4-Phenylbutyl monoamido tartaric acids **3**

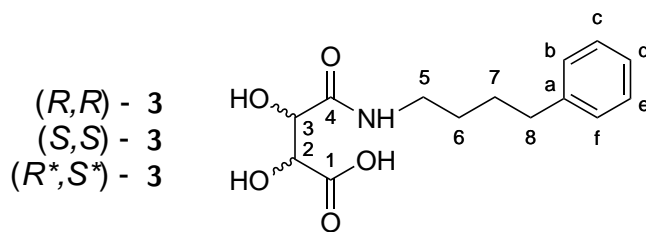


Figure 10.1 Numbering of carbon atoms in **3**.

Mass spectrometry

Table 10.1 Mass spectrometry (ESI) of **3** with molecular formula: $C_{14}H_{19}NO_5$.

Compound	Calcd. $[M+H]^+$ (m/z)	$[M+H]^+$ (m/z)	std. (ppm)
(R,R) - 3	282.1336	282.1331	1.74
(S,S) - 3	282.1336	282.1331	1.74
(R^*,S^*) - 3	282.1336	282.1332	1.53

Infrared spectroscopy

As can be seen from table Table 10.2, there is a distinct difference in the peak pattern of the *meso* compound ((R^*,S^*) -**3**) and the optically active compounds ((R,R) -**3** and (S,S) -**3**) in the area between 1600 and 1700 cm^{-1} . The IR spectra for the three monoacids **3** can be found in Appendix A.

Table 10.2 Infrared spectroscopy of **3** for the C=O stretching frequencies.

	cm^{-1}	Intensity
(R,R) - 3	1645	s
	1681	w
	1734	m
(S,S) - 3	1646	s
	1681	w
	1734	m
(R^*,S^*) - 3	1632	s
	1753	s

Optical rotation

Table 10.3 Optical rotation of **3** in methanol.

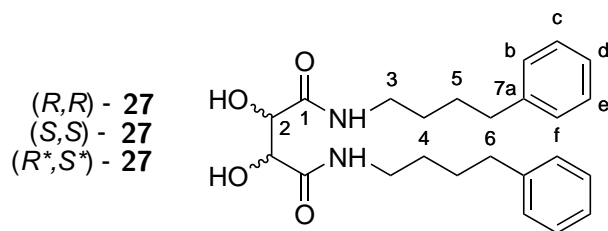
Compound	$[\alpha]_D^{20}$	c
(R,R) - 3	+55.8	1.01
(S,S) - 3	-57.4	1.06
(R^*,S^*) - 3	-0.5	0.96

NMR spectroscopy

Chemical shifts for (*R,R*)-**3**, (*S,S*)-**3** and (*R*,S**)-**3** was assigned according to table Table 10.4. Shifts and multiplicities are derived from 1D and 2D (HSQC) ¹H NMR and ¹³C NMR experiments, spectra can be found in Appendix A. The chemical shifts exhibited by the compounds were as expected from looking at data of similar compounds with an octyl chain. Shifts of the similar compounds were found in the doctoral thesis written by Gonzalez.²

Table 10.4 Assigned shifts for **3**.

Carbon no.	δH (ppm)	M	J (Hz)	δC (ppm)
Compound (<i>R,R</i>)- 3 and (<i>S,S</i>)- 3				
1	-	-	-	175.4
2	4.60	d	1.8	73.0
3	4.48	d	1.8	74.2
4	-	-	-	174.0
5	3.30-3.24	m	-	39.9
6	1.72-1.51	m	-	29.9
7	1.72-1.51	m	-	29.7
8	2.65	t	7.5	36.4
9a	7.28-7.10	m	-	143.4
9b-f	7.28-7.10	m	-	129.3-126.6
Compound (<i>R*,S*</i>)- 3				
1	-	-	-	174.4
2	4.49	d	2.6	75.6
3	4.35	d	2.6	74.3
4	-	-	-	173.5
5	3.29-3.19	m	-	40.0
6	1.74-1.47	m	-	30.2
7	1.74-1.47	m	-	30.0
8	2.69-2.57	m	-	36.6
9a	7.29-7.07	m	-	143.7
9b-f	7.29-7.07	m	-	129.6-126.8

10.1.2 4-Phenylbutyl tartaric diamides **27**Figure 10.2 Numbering of carbon atoms in **27**.

Mass spectrometry

Table 10.5 Mass spectrometry (ESI) of **27** with molecular formula: $C_{24}H_{32}O_4N_2$.

Compound	Calcd. $[M]^{*+}$ (<i>m/z</i>)	$[M]^{*+}$ (<i>m/z</i>)	std. (ppm)
(<i>R,R</i>)- 27	412.2357	412.2357	0.10
(<i>S,S</i>)- 27	412.2357	412.2355	0.39
(<i>R*,S*</i>)- 27	412.2357	412.2352	1.11

Optical rotation

Table 10.6 Optical rotation of **27** in DMF.

Compound	$[\alpha]_D^{20}$	<i>c</i>
(<i>R,R</i>)- 27	+52.6	1.01
(<i>S,S</i>)- 27	-55.2	0.98
(<i>R*,S*</i>)- 27	-0.2	0.81

NMR spectroscopy

Chemical shifts for (*R,R*)-**27**, (*S,S*)-**27** and (*R*,S**)-**27** was assigned according to table Table 10.7. Shifts and multiplicities are derived from 1D and 2D (HSQC) ¹H NMR and ¹³C NMR experiments, spectra can be found in Appendix B. Shifts exhibited by the diamides **27** is similar to shifts presented for compounds with an octyl chain by Gonzalez and Carlsen.²⁰

Table 10.7 Assigned shifts for **27**.

Carbon no.	δH (ppm)	M	J (Hz)	δC (ppm)
Compound (<i>R,R</i>)- 27 and (<i>S,S</i>)- 27				
1	-	-	-	172.3
2	4.20	d	6	73.0
3	3.15-3.09	m	-	38.6
4	1.60-1.38	m	-	29.3
5	1.60-1.38	m	-	28.7
6	2.61-2.53	m	-	35.3
7a	7.28-7.09	m	-	142.6
7b-f	7.28-7.09	m	-	128.8-126.1
Compound (<i>R*,S*</i>)- 27				
1	-	-	-	171.1
2	4.09	d	5.08	74.2
3	3.15-2.99	m	-	38.4
4	1.61-1.34	m	-	29.3
5	1.61-1.34	m	-	28.8
6	2.59-2.52	m	-	35.3
7a	7.28-7.09	m	-	142.7
7b-f	7.28-7.09	m	-	128.8

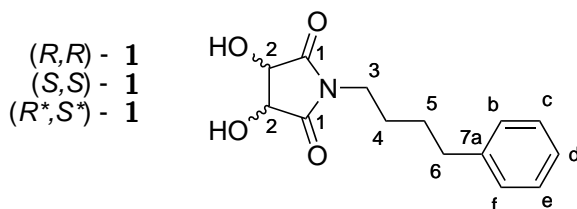
10.1.3 4-Phenylbutyl tartrimides **1**

Figure 10.3 Numbering of carbon atoms in **1**.

Mass spectrometry

Table 10.8 Mass spectrometry (ESI) of **1** with molecular formula: $C_{14}H_{17}O_4N$.

Compound	Calcd. $[M]^{*+}$ (<i>m/z</i>)	$[M]^{*+}$ (<i>m/z</i>)	std. (ppm)
(<i>R,R</i>)- 3	263.1152	263.1147	1.94
(<i>S,S</i>)- 3	263.1152	263.1155	1.10
(<i>R*,S*</i>)- 3	263.1152	263.1152	0.04

Infrared spectroscopy

The observed carbonyl stretching frequency is observed to be slightly lower for (*R*,S**)-**1** than for the chiral imides (Table 10.9). IR spectra of all the cyclic imides **1** can be found in Appendix C.

Table 10.9 Infrared spectroscopy of **1** for the C=O stretching frequencies.

	cm^{-1}	Intensity
(<i>R,R</i>)- 1	1701	s
(<i>S,S</i>)- 1	1701	s
(<i>R*,S*</i>)- 1	1685	s

Optical rotation

There was observed a rather big difference in specific rotation between (*R,R*)-**1** and (*S,S*)-**1** (Table 10.10). However, as also can be seen from Table 10.10, the concentration of (*S,S*)-**1** was low, which makes bigger room for measuring errors. The reason for the low concentration is that the sample was prepared from the remaining amount of (*S,S*)-**1**.

Table 10.10 Optical rotation of **1** in DMF.

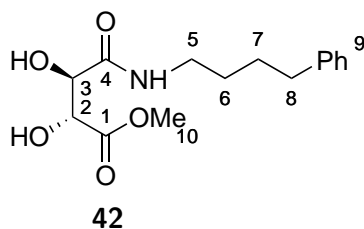
Compound	$[\alpha]_D^{20}$	<i>c</i>
(<i>R,R</i>)- 3	+72.9	1.06
(<i>S,S</i>)- 3	-97.3	0.15
(<i>R*,S*</i>)- 3	0	0.50

NMR spectroscopy

Chemical shifts for (*R,R*)-**1**, (*S,S*)-**1** and (*R*,S**)-**1** was assigned according to table Table 10.11. Shifts and multiplicities are derived from 1D and 2D (HSQC) ¹H NMR and ¹³C NMR experiments, spectra can be found in Appendix C. Shifts exhibited by the compounds **1** are similar to the shifts found by Gonzalez for the similar imides with an octyl chain.²

Table 10.11 Assigned shifts for **1**.

Carbon no.	δH (ppm)	M	J (Hz)	δC (ppm)
Compound (<i>R,R</i>)- 1 and (<i>S,S</i>)- 1				
1	-	-	-	175.2
2	4.30	s	-	74.8
3	3.64-3.46	m	-	37.9
4	1.57-1.40	m	-	28.6
5	1.57-1.40	m	-	27.2
6	2.60-2.53	m	-	35.0
7a	7.31-7.10	m	-	142.3
7b-f	7.31-7.10	m	-	128.8-126.1
Compound (<i>R*,S*</i>)- 1				
1	-	-	-	176.9
2	4.33	s	-	68.3
3	3.43-3.34	m	-	37.7
4	1.62-1.40	m	-	28.5
5	1.62-1.40	m	-	27.2
6	2.60-2.53	m	-	35.1
7a	7.29-7.11	m	-	142.3
7b-f	7.29-7.11	m	-	128.8-126.2

10.1.4 4-Phenylbutyl monoamido methyl (*R,R*)-tartrate **42**Figure 10.4 Numbering of carbon atoms in **42**.

Mass spectrometry

Table 10.12 Mass spectrometry (ESI) of **42** with molecular formula: $C_{15}H_{21}O_5N$.

Compound	Calcd. $[M]^{*+}$ (<i>m/z</i>)	$[M]^{*+}$ (<i>m/z</i>)	std. (ppm)
43	295.1414	295.1415	0.10

Optical rotation

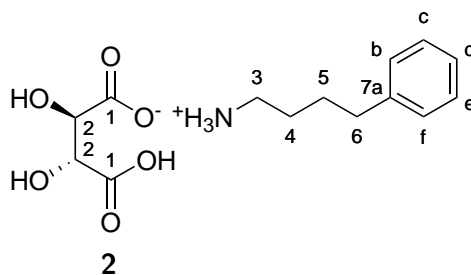
Optical rotation for **42** was found to be $[\alpha]_D^{20} = +31.1$ ($c = 0.55$, MeOH).

NMR spectroscopy

Chemical shifts for **42** was assigned according to table Table 10.13. Shifts and multiplicities are derived from 1D and 2D (HSQC) ^1H NMR and ^{13}C NMR experiments, spectra can be found in Appendix D.

Table 10.13 Assigned shifts for **43**.

Carbon no.	δH (ppm)	M	J (Hz)	δC (ppm)
1	3.76	s	-	52.8
2	-	-	-	174.3
3	4.56	d	2.1	73.6
4	4.38	d	2.1	74.4
5	-	-	-	173.9
6	3.29-3.19	m	-	40.1
7	1.74-1.50	m	-	30.2
8	1.74-1.50	m	-	29.9
9	2.62	t	7.2	36.6
10a	7.28-7.09	m	-	143.7
10b-f	7.28-7.09	m	-	129.5-126.8

10.1.5 4-Phenylbutyl ammonium (*R,R*)-tartrate **2**Figure 10.5 Numbering of carbon atoms in **2**

Optical rotation

Optical rotation of **2** was found to be $[\alpha]_D^{20} = +14.4$ ($c = 0.55$, H_2O).

NMR spectroscopy

Chemical shifts for **2** was assigned according to table Table 10.14. Shifts and multiplicities are derived from 1D and 2D (HSQC) ^1H NMR and ^{13}C NMR experiments, spectra can be found in Appendix E. **2** were found to be exhibiting the same chemical shift as a similar salt synthesized by Gonzalez,² the compound synthesized by Gonzalez had an octyl chain instead of a 4-phenylbutyl substituent.

Table 10.14 Assigned shifts for **2**.

Carbon no.	δH (ppm)	M	J (Hz)	δC (ppm)
1	-	-	-	176.9
2	4.39	s	-	74.2
3	2.92	t	7.1	40.8
4	1.79-1.64	m	-	29.5
5	1.79-1.64	m	-	28.3
6	2.67	t	7.1	36.3
7a	7.33-7.17	m	-	143.0
7b-f	7.33-7.17	m	-	129.59-127.1

10.2 Quantification of deuterium in tartaric acid

In order to quantify the deuterium content of tartaric acid, several different methods were employed. A study conducted by Kotanigawa *et al.*, showed usage of spin-gated decoupling ^{13}C NMR to quantify hydrogen-deuterium ratios.⁶¹ In order to obtain quantitative data from this method, the nuclear Overhauser enhancement (NOE) must be fully quenched for the ^{13}C nuclei, as NOE distorts the integrals observed in the obtained spectra. This method was discarded as it required a high spin-lattice relaxation time (T_1) and a high number of scans.

Instead of using quantitative ^{13}C NMR, regular ^1H NMR with a high number of scans and an internal standard (mandelic acid) were used as it was a faster method. However, this method did not provide sufficiently accurate data of the deuterium content in tartaric acid. The method was then used as a quick way to scope for possible incorporation of deuterium. If the ^1H NMR spectra showed deuterium content, samples were analyzed with mass spectrometry.

10.2.1 Quantification of deuterium in tartaric acid with positive EI

The possibly deuterated tartaric acids were subjected to positive mode electron ionization mass spectrometry.

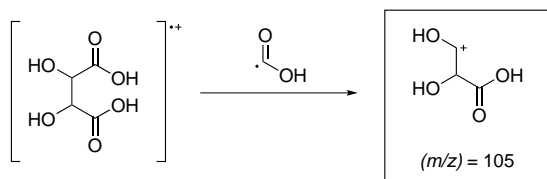


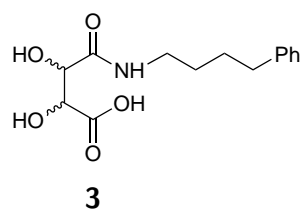
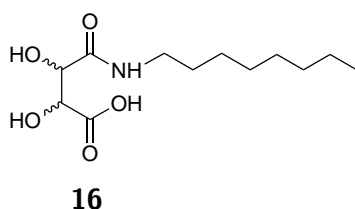
Figure 10.6 Main fragment elucidated for quantification of deuterium in tartaric acid.

The main fragment used for quantification of deuterium content in tartaric acid is shown in Figure 10.6. The positively charged decarboxylated fragment still contains both the alpha hydrogen atoms and was found to have a satisfactory signal intensity. Quantification of deuterium was done by looking at the signal intensities for the peaks in the 105-107 m/z interval, as non-deuterated will be 105, mono-deuterated 106 and di-deuterated 107 m/z . The peak intensities for 106 and 107 were subtracted the calculated natural abundance of isotopes before the ratios between the peaks were de-

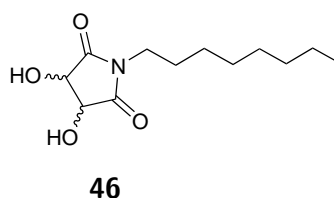
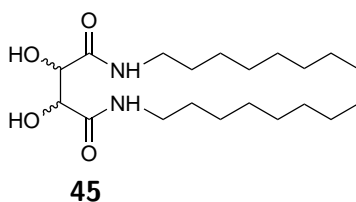
terminated. Mass spectra of the successful incorporation experiment is shown in Figure H.1 in Appendix H.

10.3 Chromatography

10.3.1 Detection and quantification of the monoamido tartaric acids **16** and **44**



As mentioned previously in this thesis, the detection of the monoacids **16** and **3** by HPLC proved to be more difficult than expected. The plan was to quantify the isomeric ratios from the kinetic experiments and confirm the optical purity of the starting materials utilizing a chiral normal phase column from Chiralcel. The Chiralcel OD-H column had already been successfully used for quantifying reaction samples consisting of stereochemical mixtures of octylamino tartaric diamides **45** and the octylamino cyclic imides **46** with a mixture of 95:5 n-hexane:isopropanol as the mobile phase.²



Several attempts were made to detect **16** with the current system, which consisted of 95:5 n-hexane:isopropanol as the eluent, 1 mL/min flow and the diode array detector set to 210 nm. The detection wavelength was set to 210 nm due to this being the absorption area of the carbonyl groups in the polar head area of the molecules (π -n transition). However, none of the attempts afforded any indication of detectability of the monoacid. Chiral separation of compounds containing carboxyl groups often require addition of an acidic additive, usually a 0.1-0.3% addition of acetic acid or TFA. This because of the tight binding between carboxylic acid groups and

the most activated seats on the column, which will cause the compound to elute out as a broad peak, sometimes so broad that it will not be detectable. One other option for achieving detection of the monoamido tartaric acid was to increase the polarity of the mobile phase, in order to reduce the elution time. As can be seen from table Table 10.15, several different systems were tried without success. One of the major issues encountered while finding a suitable elution system for compound **16** was the fact that the column needed to run over night in order to stabilize a proper baseline with a acceptable signal to noise ratio.

Table 10.15 Different elution systems and conditions tried for quantification of **16** and **3** with HPLC.

	column	n-Hexane %	IPA %	EtOH %	AcOH %	flow mL/min	det. 16 or 3
1	OD-H	95	5	-	-	1	no
2	OD-H	95	5	-	0.1	1	no
3	OD-H	90	10	-	-	1	no
4	OD-H	50	50	-	-	0.5	no
5	OD-H	50	-	50	-	0.5	no
6	OD-H	50	-	50	0.1	0.5	no
7	OD-H	50	-	50	0.3	0.5	no
8	LUX	95	5	-	-	2	no
9	LUX	95	5	-	0.1	2	no
10	LUX	95	-	5	0.1	2	no
11	LUX	90	10	-	-	2	no
12	LUX	50	50	-	-	2	no
13	LUX	50	-	50	-	2	no
14	LUX	50	-	50	0.1	2	yes ^a
15	LUX	50	-	50	0.3	2	no

^a Asymmetric low intensity peak.

After failing to detect the compound using these eluent systems, the octyl chain in the monoacid was substituted for a 4-phenyl butyl chain in order to lower surfactant behaviour and increase UV absorption. A new chiral HPLC column was also acquired in order to simplify analysis. The new Phenomenex LUX column utilized the same chiral packing material, but could handle more rigorous conditions. This column also needed less time to obtain a sufficient signal to noise ratio. The Phenomenex LUX was tested with the same approach as the Chiralcel OD-H, the only differ-

ence was the increased flow rate as the LUX column was able to withstand higher backpressures. However, only one of these elution systems worked. Condition number 14 in Table 10.15 gave a reproducible signal for **3**. This attempt was done as a last resort as the polarity is high and the pressure is approaching the upper limit of what the column can take. In addition, the conditions employed in 14 will probably not yield separation between the different enantiomers.

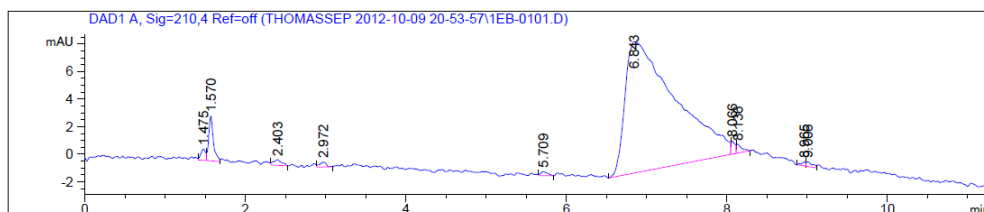


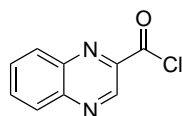
Figure 10.7 Chromatogram of compound (*R,R*)-**3** (asymmetric peak at 6.8 minutes) with a Phenomenex LUX column, n-hexane:EtOH:AcOH (50:50:0.1), 2 ml/min flow and the diode array detector set at 210 nm.

As can be seen from figure Figure 10.7; the signal strength is low, the peak is broad and there is a lot of asymmetry present. Substituting the octyl chain for a 4-phenyl butyl chain was done in part, as mentioned above, to increase the UV absorption. Introducing a phenyl ring to the compound should make it absorb well in the range around 254 nm, this however, was not the case. The 4-phenylbutyl monoamido tartaric acid absorbed some at 254 nm, but this absorption was around 15 times lower than the absorption at 210 nm (seen from different wavelenghts on the DAD, this was also confirmed by regular UV-VIS). When attempt 14 did not afford integrable and quantifiable results, it was clear that a different approach was needed in order to properly quantify the monoamido tartaric acids.

Precolumn derivatization of monoamido tartaric acids

In order to provide information regarding mass balance and enantiomeric ratios for the reaction mixture samples containing 4-phenylbutyl monoamido tartaric acid (**3**), several derivatization techniques was looked into.

A study conducted by Brightwell *et al.* suggests 2-quinoxaloyl chloride (**47**) as a suitable precolumn derivatization agent for hydroxy carboxylic acids.⁸³ This technique should increase ultraviolet absorption in addition to make the carboxylic acid group more sterically hindered by binding to the



47

Figure 10.8 2-Quinoxaloyl chloride for alpha hydroxy derivatization.

alpha hydroxy group (most nucleophilic), and thus lower the susceptibility towards tight binding to the most activated sites in the column. However, due to the monoacids containing two α -hydroxyl groups, there was a possibility that derivatization would cause arisal of three products; **48**, **49** and **50**. Hence, the derivatization method was discarded.

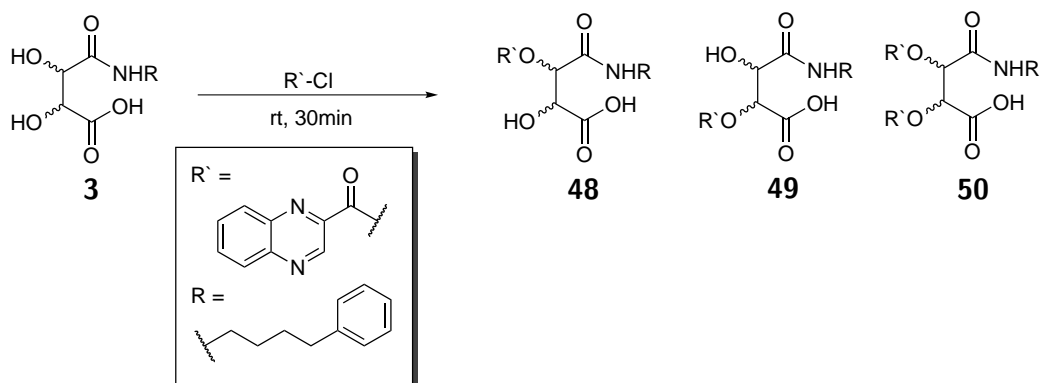


Figure 10.9 Possible products from 2-quinoxaloyl derivatization, there might also be possibility of forming the anhydride product.

The brunt of the problem seemed to revolve around the carboxylic acid group of the compound, thus a form for derivatization that eliminates the carboxyl group properties of the compound was explored. Earlier in the study, the octyl monoamido tartaric methylester **38** was prepared by mistake when trying to obtain the monoacid **16**. This procedure was then repeated according to experimental description found in Section 11.5.4 for obtaining the 4-phenylbutyl monoamido tartaric methylester **42**. The ester **42** was then eluted with the conditions in entry 8 in Table 10.15. **42** eluted with good detection and peak symmetry, thus the next step was to find a method to derivatize the samples from the mechanistic experiments without disturbing the product ratios.

One way to obtain the methyl ester was through stirring overnight in MeOH over Amberlyst-15,⁸² however, this method leaves residues from the Amberlyst-

15 in the product mixture after filtration. These residues might not be healthy for the column.

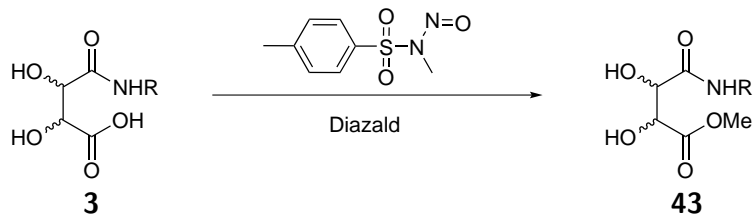
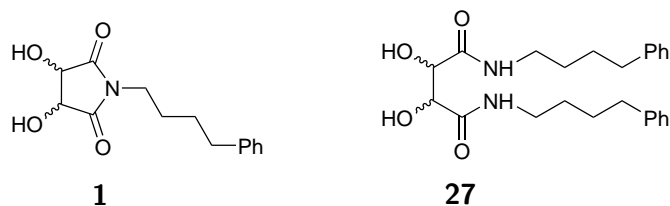


Figure 10.10 Derivatization with diazomethane (precursor is shown).

Preparing the methyl ester with diazomethane, is a fast and mild esterification method.⁸⁴ The major issue is the toxic, carcinogenic and explosive properties of the both the precursor Diazaldtm and the formed diazomethane. A small reactor was acquired from Sigma-Aldrich and a test reaction was done with success (refer to Section 11.10), but due to the time and safety measures that needs to be considered the method was not applied to the reaction mixture samples. It was decided that from a both safety and timeframe point of view that the ratios of the monoamido tartaric acids should be determined from NMR analysis alone.

10.3.2 Quantification of compounds **1** and **27**



All the isomers of **1** and **27** were eluted with conditions 10 in table Table 10.15 in the previous section. This system was chosen due to giving complete separation of all the compounds in a short timeframe with good peak shapes. The 0.1% of AcOH added was to help eluting monoacids present in some of the samples.

One of the major issues of being able to determine the product ratios of these compounds with certainty was the influence of the monoamido tartaric acids on the system. Even though the monoacids were not detectable in the system, they were still present in the reaction mixture samples that were

analyzed. When running standard samples of the compounds **1** and **27** the retention times were the same each run, with minor deviations. However, when monoacids **3** or **16** were introduced on the column through either the same sample or the previous, the retention times increased (Figure 10.11). The usual effect observed when substances get stuck in an HPLC column is decreased retention times as there are less adsorption sites available for the compounds passing through. In this case the observed trend was the opposite. One possible explanation for the observed effect might be the surfactant-like properties of the monoamido tartaric acids. The polar head group which contains the carboxylic acid which, as mentioned above, will bind tightly to the most activated sites on the column. If this tight binding happens at the head group, the tail of the molecule might be pointing outwards and in this way create a non-polar like zone on the column. This will then increase the retention times for compounds **1** and **27**. This effect was also experienced in a previous study where there were n-octylmonoamido tartaric acid (**51**) present in the sample injected on the column.

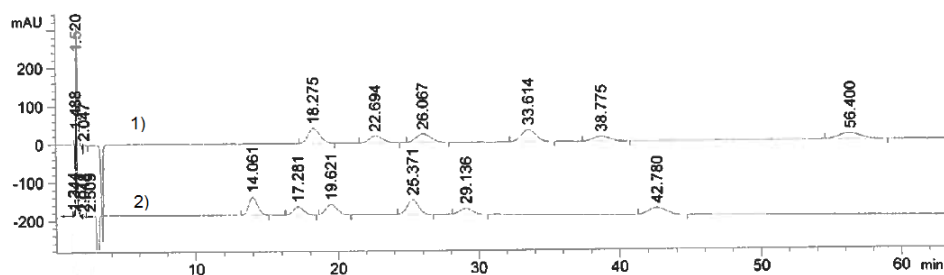


Figure 10.11 Reference mixture of all **27** and **1**. 1) With and, 2) without addition of **3**. Elution order (chronological): (*R,R*)-**27**, (*S,S*)-**27**, (*R*,S**)-**27**, (*R,R*)-**1**, (*S,S*)-**1** and (*R*,S**)-**1**. Conditions: n-hexane:EtOH:AcOH (95:5:0.1), 2 mL/min, Phenomenex LUX and 210 nm.

After the discovery of changing retention times was made, all the calibration samples and some reaction mixture fractions were co-eluted with already prepared standards in order to with certainty assign the correct signal to the correct compound. Even though the retention times seemed to differ, the order of which the compounds eluted was consistent, the order can be seen from table Table 10.16 along with shortest and longest observed elution time for each compound.

Table 10.16 Elution order and retention time extremas for **1** and **27** due to varying presence of **3** in the system during analysis. Elution conditions: n-hexane:EtOH:AcOH (95:5:0.1), 2 mL/min, Phenomenex LUX and 210 nm.

Compound	Elution order	Shortest elution (min)	Longest elution (min)
<i>(R,R)</i> - 27	1	14	23
<i>(S,S)</i> - 27	2	17	26
<i>(R*,S*)</i> - 27	3	19	28
<i>(R,R)</i> - 1	4	25	41
<i>(S,S)</i> - 1	5	29	40
<i>(R*,S*)</i> - 1	6	43	66

11. Experimental section

11.1 General methods

11.1.1 Chemicals and solvents

Chemicals and solvents were supplied by Sigma-Aldrich, Merck, VWR, Fluka Chemica and Fisher Scientific. All chemicals and solvents applied were of PA quality unless otherwise stated and used as received without further purification.

2d,3d-Tartaric acid was prepared by Rajesh Raju from a literature procedure.⁴³

Dry xylenes were dried by reflux over sodium followed by distillation and storage under N₂.

Sodium deuterioxide was prepared from mixing sodium hydride and heavy water under N₂.

11.1.2 Spectroscopic analyses

NMR spectra were recorded on Bruker Advance DPX300 or DPX400 instruments. TMS was used as an internal standards for samples dissolved in CDCl₃. The spectroscopic data was analyzed with Bruker Topspin 3.1 and shifts were assigned according to the following techniques:

1D-NMR: ¹H, ¹³C

2D-NMR: HSQC

IR spectra were obtained with a Thermo Nicolet Nexus FT-IR Spectrometer, recorded using a Smart Endurance reflection cell.

Mass spectra were obtained on a Thermo Quest MAT95X double focusing high resolution instrument using electron impact ionization (EI) at 70eV or electrospray (ESI), or on an Agilent 6520 QTOF MS instrument with an ESI source (SINTEF, Biotechnology).

Optical rotations were measured on a Perkin-Elmer Model 341 Polarimeter.

Ultraviolet absorption was measured on a single beam Cary 50 scan (Varian), with Cary Win UV (Version 02.00(25)) as data processing software.

11.1.3 Chromatography

Chiral HPLC analyses were performed on either an Agilent 1290 chromatograph or an Agilent 1100 chromatograph. Both were equipped with quaternary pumps, a chiral 5 μm Phenomenex LUX column or a Chiralcel OD-H column and a diode array detector set at 210 nm and 245 nm. A mixture of n-hexane and ethanol, both of chromatographic quality, was used at a 95:5 ratio with a 2 mL/min flow rate. In addition to ethanol and n-hexane, acetic acid was used as a acidic modifier at a 0,1% concentration.

Retention times reported in this experimental chapter are obtained from the following conditions: Phenomenex LUX 5 μm , 95:5:0.1 EtOH:n-hexane:AcOH, 2 mL/min and detection at 210nm.

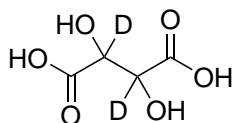
Samples were prepared in 1:4 EtOH:n-hexane.

Samples containing 4-phenylbutylamine were centrifuged with pentane in order to remove amine, as it would precipitate on the column under the above given conditions. The pentane wash was done before sample was dissolved in EtOH:n-hexane.

11.1.4 Other equipment

Microwave experiments were conducted with a Anton-Paar 3000 multiwave reactor equipped with an internal pressure and temperature sensor.

11.2 Preparation of α -deutero tartaric acid (13)



11.2.1 α -Deuteration with Barium compounds

1. *L*-Tartaric acid (0.503 g, 3.35 mmol) and dry BaO (0.511 g, 3.35 mmol, 1 eq) were added to D₂O (10 mL) before the mixture was refluxed under N₂ atmosphere for 6 hours. NaSO₄ (1 eq) and aqueous HCl (excess, 37%) was added to the reaction mixture before it was centrifuged and decanted in order to remove insoluble BaSO₄, followed by freeze drying. No deuterium incorporation was observed from ¹H NMR analysis with mandelic acid as an internal standard.
2. *L*-Tartaric acid (0.503 g, 3.35 mmol) and dry BaO (1.530 g, 10 mmol, 3 eq) were added to D₂O (14 mL) before the mixture was refluxed under N₂ atmosphere for 6 hours. H₂SO₄ (1.02 g, 10 mmol, concentrated) was added to the reaction mixture before it was centrifuged and decanted in order to remove insoluble BaSO₄, followed by freeze drying. No deuterium incorporation was observed from ¹H NMR analysis with mandelic acid as an internal standard.
3. *L*-Tartaric acid (0.500 g, 3.33 mmol) and dry BaO (0.513 g, 3.35 mmol, 1 eq) were added to D₂O (10 mL) before the mixture was heated in a sealed tube to 130 °C for 27 hours. NaSO₄ (0.473 g, 1 eq) and aqueous HCl (excess, 37%) was added to the reaction mixture before it was centrifuged and decanted in order to remove insoluble BaSO₄ followed by freeze drying. No deuterium incorporation was observed from ¹H NMR analysis with mandelic acid as an internal standard.
4. *L*-Tartaric acid (0.500 g, 3.33 mmol) and BaCl₂ (0.693 g, 3.33 mmol, 1 eq) were dissolved in D₂O (10 mL). The reaction mixture was refluxed for 16 hours before the heavy water was removed using a lyophilizer. The solid reaction mixture was then added to THF (40 mL) and filtered in order to remove excess BaCl₂. THF was removed *in vacuo* yielding a white powder. No deuterium incorporation was observed from ¹H NMR analysis with mandelic acid as an internal standard.

5. *L*-Tartaric acid (0.250 g, 1.66 mmol) and dry BaO (0.763 g, 4.98 mmol, 3 eq) were added to D₂O (5 mL) and heated to 180 °C in a sealed glass tube for 4 days. Aqueous HCl (0.922 g, 6 eq, 37%) was added to the reaction mixture before heavy water was removed using a lyophilizer. Followed by dissolving the solid in dry THF (20 mL), filtrating off BaCl₂ and removing THF *in vacuo* yielding a brown powder. No deuterium incorporation was observed from ¹H NMR analysis with mandelic acid as an internal standard.
6. *L*-Tartaric acid (0.500 g, 3.33 mmol) and BaCl₂ (0.693 g, 3.33 mmol, 1 eq) were dissolved in D₂O (10 mL). The reaction mixture was refluxed for 16 hours before heavy water was removed using a lyophilizer. The solid reaction mixture was then added to THF (40 mL) and filtered in order to remove excess BaCl₂. THF was removed *in vacuo* yielding a white powder. No deuterium incorporation was observed from ¹H NMR analysis with mandelic acid as an internal standard.

11.2.2 α-Deuteration with acid catalysis

1. *L*-Tartaric acid (0.101 g, 0.67 mmol) were dissolved in D₂O (5 mL) containing a catalytic amount of sulfuric acid (approx. 0.05 mL). The reaction mixture was stirred at rt for 16 hours before BaCl₂ (excess) was added to the solution followed by centrifugation and decanting in order to remove insoluble BaSO₄. Water was removed from the reaction mixture using a lyophilizer. The solid reaction mixture was then added to THF (10 mL) and filtered in order to remove excess BaCl₂. THF was removed *in vacuo* yielding a brown powder. No deuterium incorporation was observed from ¹H NMR analysis with mandelic acid as an internal standard.
2. *L*-Tartaric acid (0.101 g, 0.67 mmol) and BaCl₂ (0.143 g, 0.68 mmol, 1 eq) were dissolved in D₂O (4 mL) containing catalytic amounts of aqueous hydrochloric acid (approx. 0.05 mL). The reaction mixture was stirred for 16 hours before the heavy water was removed using a lyophilizer. The solid reaction mixture was then added to THF (10 mL) and filtered in order to remove excess BaCl₂. THF was removed *in vacuo* yielding a slightly purple powder. No deuterium incorporation was observed from ¹H NMR analysis with mandelic acid as an internal standard.
3. *L*-Tartaric acid (0.250 g, 1.66 mmol) and H₂SO₄ (0.15 g, 1.47 mmol, 0.9 eq) were added to D₂O (6 mL) and heated to 180 °C in a sealed

glass tube for 47 hours. BaCl_2 (0.611 g, 2.93 mmol) was added to the reaction mixture before it was centrifuged and decanted in order to remove insoluble BaSO_4 . Heavy water was removed from the mixture using a lyophilizer before it was dissolved in THF (20 mL) followed by filtration in order to remove BaCl_2 . Removal of THF *in vacuo* yielded an off-white powder. No deuterium incorporation was observed from ^1H NMR analysis with mandelic acid as an internal standard.

11.2.3 α -Deuteration in a basic environment

L-Tartaric acid (0.100 g, 0.67 mmol) and NaOD (0.358 g, 3.33 mmol, 40% in D_2O , 5 eq) were added to D_2O (2 mL) and heated to 180 °C in a sealed glass tube for 12 hours, followed by addition of aqueous HCl (0.343 g, 3.33 mmol, 37%). Heavy water was removed from the mixture using a lyophilizer before the solid mixture was added to THF (20 mL) and filtrated in order to remove NaCl. Removal of THF *in vacuo* yielded a thick, off-white substance. No deuterium incorporation was observed from ^1H NMR analysis with mandelic acid as an internal standard.

11.2.4 α -Deuteration using microwave irradiation

General procedure, see Table 11.1 for detailed reaction conditions employed. *L*-Tartaric acid and NaOD (5 eq, 40% in D_2O)/BaO (2 eq) was dissolved in D_2O and irradiated at a set temperature (see Table 11.1) in an Anton-Paar multiwave 3000 reactor (temperature probe was in a reference vessel containing NaCl solution, due to the glass corrosive properties of NaOD). Aqueous HCl (5eq, 37%) was added to the reaction mixture before it was freeze dried and added to THF. The solution was then filtered and the THF removed *in vacuo* yielding a thick, brown substance.

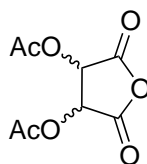
Table 11.1 Incorporation of deuterium and conditions for experiments with assisted microwave irradiation in basic environment.

Ex. No.	<i>L</i> -Tartaric acid	Reagent	D ₂ O (mL)	T ^a °C	Time hours	D ^b (%)
1	0.2	NaOD	4	120	2	78.3 ^c
2	0.2	NaOD	5	105	2	0
3	0.2	NaOD	5	105	1	0
4	1	NaOD	25	105-140	4	0
5	0.25	NaOD	5	190	0.5	0
6	0.2	BaO	4	110	1.5	0

^aReference probe^bDeuterium incorporation determined by MS^c62.6% di-D, 31.3% mono-D and 6.1% non-D

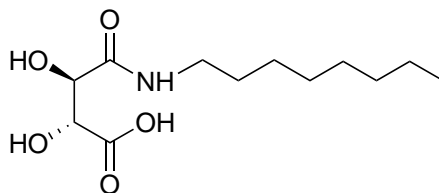
11.3 Diacetyltartaric anhydrides (**36**)^{73–75}

The appropriate tartaric acid (*L*, *D* or *meso*) (3.00 g, 20 mmol) was added to 1,4-dioxane (14 mL) and refluxed with Ac₂O (10 mL, 5 eq) at 140 °C for two hours. Furthermore, approximately 60% of the solvent was evaporated off *in vacuo* before it was put in cold storage for crystallization. The precipitated crystals were washed twice with Et₂O over suction and white crystals were obtained (3.45 g, 16 mmol, 80%), except for the *meso*-anhydride where the yellow oily reaction mixture was used directly after solvent evaporation due to the increased solubility of the compound. When the compounds were not directly used in further synthesis they were either stored in cold storage or in an exicator over CaCl₂. Data for (*R,R*)-diacetyltartaric acid anhydride: ¹H NMR (400 MHz, CDCl₃): δ = 5.70 (s, 2H, 2xCH), 2.25 (s, 6H, 2xCH₃) ppm.

**36**

11.4 Octylammonium tartaric acid system

11.4.1 (2*R*,3*R*)-2,3-Dihydroxy-4-(octylamino)-4-oxobutanoic acid (**16**)^{2,73,76}

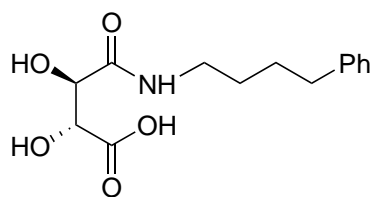
**16**

1. *L*-Diacetyltartaric anhydride [(*R,R*)-**36**] (3.45 g, 15.97 mmol) was dissolved in THF (20 mL) and cooled down to -15°C and put under N_2 atmosphere. Octylamine (1.65 g, 12.77 mmol, 0.8 eq) was dissolved in THF (5 mL) and added dropwise to the reaction mixture over five minutes. The reaction mixture was stirred at -15°C for one hour and allowed to reach room temperature before the solvent was evaporated off *in vacuo*. The solid reaction mixture was dissolved in MeOH (20 mL) and EtOH (20 mL) before acyl chloride (3 mL) was added slowly at 0°C . The solution was furthermore stirred for 12 hours before the solvent was evaporated *in vacuo* and the solid mixture was dissolved in aqueous HCl (70 mL, 1 M) and left for stirring over night. Precipitate was filtered off the reaction mixture using a glass sinter before it was dried on a high vacuum line yielding white crystals (3 g, 10.89 mmol, 68%) consisting of the methylated mono-amide ((2*R*,3*R*)-methyl 2,3-dihydroxy-4-(octylamino)-4-oxobutanoate, similar to **42** in Section 11.5.4) instead of the wanted product. Spectroscopic data of the similar **42** (with a 4-phenylbutyl chain instead of octyl) are also to be found in Section 11.5.4. Further attempts at obtaining the wanted product from this point only caused accumulation of more impurities.
2. *L*-Diacetyltartaric anhydride [(*R,R*)-**36**] (3.4 g, 15.74 mmol) was dissolved in THF (20 mL) and cooled down to -15°C and put under N_2 atmosphere. Octylamine (1.62 g, 12.53 mmol, 0.8 eq) was dissolved in THF (5 mL) and added dropwise to the reaction mixture over five minutes. The reaction mixture was stirred at -15°C for one hour and allowed to reach room temperature before the solvent was evaporated off *in vacuo*. The crude reaction mixture was then dissolved in MeOH (20 mL) before $\text{NaOH}_{(aq)}$ (1.2 eq, 10 mL, 2 M) was added dropwise to the

solution and let it stir at room temperature over night. The (2*R*,3*R*)-2,3-dihydroxy-4-(octylamino)-4-oxobutanoate sodium salt was filtered off the solution with a glass sinter. The precipitate was stirred in water (20 mL) and added HCl_(aq) (1.2 eq, 20 mL, 1 M) before it again was filtrated with a glass sinter. The precipitate was dried on a high vacuum line affording **16** as a white powder (2.69 g, 10.30 mmol, 65%). ¹H NMR (400 MHz, CD₃OD): δ = 4.55 (d, *J*=1.89 Hz, 1H, HO-CH-CO-OH), 4.44 (d, *J* = 1.89 Hz, 1H, HO-CH-CO-NH), 3.30-3.21 (m, 2H, -NH-CH₂-), 1.60-1.49 (m, 2H, NH-CH₂-CH₂-), 1.42-1.24 (m, 10H, aliphatic), 0.91 (t, *J* = 6.7 Hz, 3H, CH₃) ppm.

11.5 4-Phenyl butyl ammonium tartaric acid system

11.5.1 (2*R*,3*R*)-2,3-Dihydroxy-4-oxo-4-((4-phenylbutyl)amino) butanoic acid [(*R,R*)-**3**]^{2,73,76}

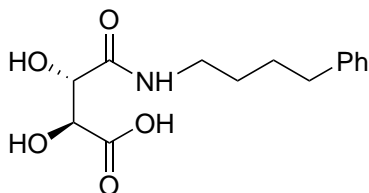


(*R,R*) - **3**

L-Diacetyltartaric anhydride [(*R,R*)-**36**] (2.6 g, 12.03 mmol) was dissolved in THF (20 mL) and cooled down to -10°C and put under N₂ atmosphere. 4-Phenylbutylamine (1.43 g, 9.60 mmol, 0.8 eq) was dissolved in THF (5 mL) and added dropwise to the reaction mixture over five minutes. The reaction mixture was stirred at -10°C for one hour and allowed to reach room temperature before the solvent was evaporated off *in vacuo*. The crude reaction mixture was then dissolved in MeOH (20 mL) before NaOH_(aq) (1.2 eq, 2 M) was added dropwise to the solution and let it stir at room temperature over night. The (2*R*,3*R*)-2,3-dihydroxy-4-oxo-4-((4-phenylbutyl)amino)butanoate sodium salt was filtered off the solution through a glass sinter. The precipitate was stirred in water (10 mL) and added HCl_(aq) (1.2 eq, 14.5 mL, 1 M) before it again was filtrated through a glass sinter. The precipitate was dried on a high vacuum line affording (*R,R*)-**3** as a white powder (1.30 g, 4.62 mmol, 38%). Mp: 136-137 °C. $[\alpha]_D^{20} = +55.5$ (*c* = 1.01, MeOH). ¹H NMR (400 MHz,

CD₃OD): δ = 7.28-7.10 (m, 5H, **Ph**), 4.60 (d, J = 1.8 Hz, 1H, HO-**CH**-CO-OH), 4.48 (d, J = 1.8 Hz, 1H, HO-**CH**-CO-NH), 3.30-3.24 (m, 2H, -NH-**CH**₂), 2.65 (t, J = 7.5 Hz, 2H, -**CH**₂-Ph), 1.72-1.51 (m, 4H, -NH-**CH**₂-**CH**₂-**CH**₂) ppm. ¹³C NMR (100 MHz, CD₃OD): δ = 175.4 (C1), 174.0 (C4), 143.4 (C9a), 129.3 (C9b-f), 129.2 (C9b-f), 126.6 (C9b-f), 74.2 (C3), 73.0 (C2), 39.9 (C5), 36.4 (C8), 29.9 (C6), 29.7 (C7) ppm. IR: 3497 (w), 3399 (w), 3298 (m), 3061 (w), 3028 (w), 2925 (w), 1734 (m), 1646 (s), 1535 (s), 1472 (w), 1453 (w), 1304 (w), 1263 (w), 1241 (s), 1198 (m), 1122 (s), 1070 (s), 923 (m), 870 (m), 831 (m), 739 (m), 694 (m), 669 (s), 585 (s) cm⁻¹. HRMS (+ESI) m/z : Calcd. for C₁₄H₂₀NO₅ [M+H]⁺ 282.1336, Found 282.1331.

11.5.2 (2*S*,3*S*)-2,3-Dihydroxy-4-oxo-4-((4-phenylbutyl)amino) butanoic acid [(*S,S*)-**3**]^{2,73,76}



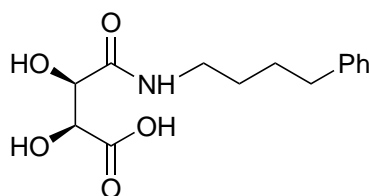
(*S,S*) - **3**

D-diacetyltartaric anhydride [(*S,S*)-**36**] (1.29 g, 5.83 mmol) was dissolved in THF (10 mL) and cooled down to -16°C and put under N₂ atmosphere. 4-Phenylbutylamine (0.69 g, 4.62 mmol, 0.8 eq) was dissolved in THF (5 mL) and added dropwise to the reaction mixture over five minutes. The reaction mixture was stirred at -16°C for one hour and allowed to reach room temperature before the solvent was evaporated off *in vacuo*. The crude reaction mixture was then dissolved in MeOH (20 mL) before NaOH_(aq) (1.2 eq, 3.5 mL, 2 M) was added dropwise to the solution and let it stir at room temperature over night. The (2*S*,3*S*)-2,3-dihydroxy-4-oxo-4-((4-phenylbutyl)amino)butanoate sodium salt was filtered off the solution through a glass sinter. The precipitate was stirred in water (10 mL) and added HCl_(aq) (1.2 eq, 7 mL, 1 M) before it again was filtrated through a glass sinter. The precipitate was dried on a high vacuum line affording (*S,S*)-**3** as a white powder (0.67 g, 2.38 mmol, 41%).

Mp: 137°C . $[\alpha]_D^{20} = -54.5$ ($c = 1.06$, MeOH). ¹H NMR (400 MHz, CD₃OD): δ = 7.28-7.10 (m, 5H, **Ph**), 4.60 (d, 1H, $J = 1.7$ Hz, HO-**CH**-CO-OH), 4.48 (d, 1H, $J = 1.7$ Hz, HO-**CH**-CO-NH), 3.30-3.24 (m, 2H, NH-**CH**₂), 2.65 (t,

2H, $J = 7.5$ Hz, $-\text{CH}_2\text{-Ph}$), 1.72-1.51 (m, 4H, $-\text{NH-CH}_2\text{-CH}_2\text{-CH}_2$) ppm. ^{13}C NMR (100 MHz, CD_3OD): $\delta = 175.4$ (C1), 174.0 (C4), 143.4 (C9a), 129.3 (C9b-f), 129.2 (C9b-f), 126.6 (C9b-f), 74.2 (C3), 73.0 (C2), 39.9 (C5), 36.4 (C8), 29.9 (C6), 29.7 (C7) ppm. IR: 3498 (w), 3391 (w), 3298 (m), 3062 (w), 3029 (w), 2926 (w), 1734 (m), 1646 (s), 1535 (s), 1495 (w), 1472 (w), 1453 (w), 1304 (w), 1263 (w), 1241 (s), 1198 (m), 1122 (s), 1098 (w), 1071 (s), 1030 (w), 923 (m), 870 (m), 831 (m), 775 (w), 739 (m), 718 (m), 694 (m), 669 (s), 585 (s) cm^{-1} . HRMS (+ESI) m/z : Calcd. for $\text{C}_{14}\text{H}_{20}\text{NO}_5$ $[\text{M}+\text{H}]^+$ 282.1336, Found 282.1332.

11.5.3 (2*R**,3*S**)-2,3-Dihydroxy-4-oxo-4-((4-phenylbutyl)amino) butanoic acid [(*R**,*S**)-3]^{2,73,76}



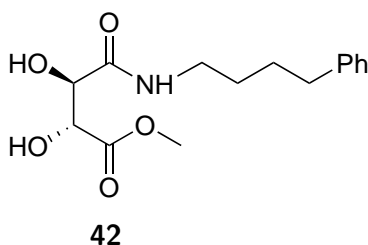
(*R**,*S**) - 3

The crude yellow oily *meso*-diacetyltartaric anhydride [(*R**,*S**)-36] (from 5 mmol *meso* tartaric acid) was dissolved in THF (5 mL) and cooled down to -10°C and put under N_2 atmosphere. 4-Phenylbutylamine (0.60 g, 4 mmol, 0.8 eq) was dissolved in THF (5 mL) and added dropwise to the anhydride solution over 5 minutes. The reaction was then stirred at -10°C for one hour and allowed to reach room temperature before the solvent was evaporated off *in vacuo*. The crude reaction mixture was dissolved in MeOH (7 mL) before $\text{NaOH}_{(aq)}$ (1.2 eq, 3 mL, 2 M) was added dropwise to the solution and let it stir at room temperature over night. (2*R**,3*S**)-2,3-dihydroxy-4-oxo-4-((4-phenylbutyl)amino)butanoate sodium salt was filtered off the solution through a glass sinter. The sodium salt was dissolved in water before $\text{HCl}_{(aq)}$ (1.2 eq, 6 mL, 1 M) was added to the solution and the precipitate filtered off through a glass sinter. The precipitate was dried on a high vacuum line affording (*R**,*S**)-3 as a white powder (0.25 g, 0.89 mmol, 18%).

Mp: 131°C . $[\alpha]_D^{20} = -0.5$ ($c = 0.96$, MeOH). ^1H NMR (400 MHz, CD_3OD): $\delta = 7.29\text{-}7.07$ (m, 5H, Ph), 4.49 (d, $J = 2.6$ Hz, 1H, HO-CH-CO-OH), 4.35 (d, $J = 2.6$ Hz, 1H, HO-CH-CO-NH), 3.29-3.19 (m, 2H, $-\text{NH-CH}_2$), 2.69-2.57 (m, 2H, $-\text{CH}_2\text{-Ph}$), 1.74-1.47 (m, 4H, $-\text{NH-CH}_2\text{-CH}_2\text{-CH}_2$) ppm. ^{13}C

NMR (100 MHz, CD₃OD): δ = 174.4 (C1), 173.5 (C4), 143.7 (C9a), 129.6 (C9b-f), 129.4 (C9b-f), 126.8 (C9b-f), 75.6 (C3), 74.3 (C2), 40.0 (C5), 36.6 (C8), 30.2 (C6), 30.0 (C7) ppm. IR: 3531 (w), 3435 (m), 3312 (w), 2933 (w), 2565 (w), 1754 (s), 1633 (s), 1540 (s), 1496 (w), 1477 (w), 1453 (w), 1301 (s), 1228 (s), 1199 (w), 1114 (s), 1094 (s), 998 (w), 876 (m), 817 (w), 786 (w), 765 (w), 744 (m), 696 (s), 614 (s), 589 (w), 555 (m) cm⁻¹. HRMS (+ESI) m/z : Calcd. for C₁₄H₂₀NO₅ [M+H]⁺ 282.1336, Found 282.1332.

11.5.4 Methyl (2*R*,3*R*)-2,3-Dihydroxy-4-oxo-4-((4-phenylbutyl)amino) butanoate (**42**)

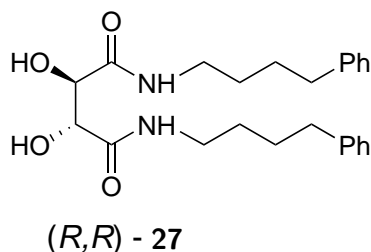


L-Diacetyltartaric anhydride, **36**, (1.0 g, 4.63 mmol) was dissolved in THF (10 mL) and cooled down to -15°C and put over N₂ atmosphere. 4-Phenylbutylamine (0.55 g, 3.69 mmol, 0.8 eq) was dissolved in THF (5 mL) and added dropwise to the reaction mixture over five minutes. The reaction mixture was stirred at -15°C for one hour and allowed to reach room temperature before the solvent was evaporated off *in vacuo*. The crude reaction mixture was dissolved in MeOH (20 mL) before AcCl (2 mL, 28.03 mmol) was added slowly at 0°C and the solution was stirred over night at room temperature. The solvent was removed *in vacuo* and the reaction mixture was added to HCl_(aq) (10 mL, 1 M) and stirred for 40 minutes. The precipitate was filtered off the solution through a glass sinter, and dried on a high vacuum line affording **42** as white crystals (0.25 g, 0.84 mmol, 18%).

Mp: 100°C . $[\alpha]_D^{20} = +31.1$ ($c = 0.55$, MeOH). ¹H NMR (400 MHz, CD₃OD): δ = 7.28-7.09 (m, 5H, **Ph**), 4.56 (d, $J = 2.1$ Hz, 1H, HO-**CH**-CO-**CH**₃), 4.38 (d, $J = 2.1$ Hz, 1H, HO-**CH**-CO-NH), 3.76 (s, 3H, -O-**CH**₃), 3.29-3.19 (m, 2H, -NH-**CH**₂), 2.62 (t, 2H, $J=7.2$ Hz, -**CH**₂-Ph), 1.74-1.50 (m, 4H, -NH-**CH**₂-**CH**₂-**CH**₂) ppm. ¹³C NMR (100 MHz, CD₃OD): δ = 174.3 (C2), 173.9 (C5), 143.7 (C10a), 129.5 (C10b-f), 129.4 (C10b-f), 126.8 (C10b-f), 74.4 (C4), 73.6 (C3), 52.8 (C1), 40.1 (C6), 36.6 (C9), 30.2 (C7), 29.9 (C8) ppm. IR: 3463 (w), 3364 (w), 3335 (w), 3127 (w), 2933 (w), 1751 (s), 1713 (s), 1644 (s), 1534 (s), 1495 (w), 1476 (w), 1449 (m), 1436 (m),

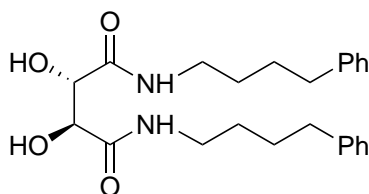
1375 (w), 1311 (w), 1275 (s), 1215 (s), 1121 (s), 1075 (s), 1022 (s), 995 (w), 959 (w), 941 (w), 871 (w), 845 (w), 816 (w), 783 (w), 763 (w), 739 (s), 707 (w), 698 (s), 601 (s), 581 (m) cm^{-1} . HRMS (+ESI) m/z : Calcd. for $\text{C}_{15}\text{H}_{21}\text{O}_5\text{N}$ $[\text{M}]^{*+}$ 295.1414, Found 295.1415.

11.5.5 (2*R*,3*R*)-2,3-Dihydroxy-*N*1,*N*4-bis(4-phenylbutyl) succinamide [(*R,R*)-**27**]^{16,79–81}



L-Dimethyltartrate (0.25 g, 1.40 mmol) was dissolved in MeOH (3 mL) before 4-phenylbutylamine (0.48 mL, 3.08 mmol, 2.2 eq) was added and the solution stored at 4 °C with occasional stirring for 3 days. The precipitated diamide was filtered off over suction and washed with small amounts of cold MeOH affording (*R,R*)-**27** as white crystals (0.42 g, 1.01 mmol, 72%).

Mp: 170-171 °C. $[\alpha]_D^{20} = +52.6$ ($c = 1.01$, DMF). ^1H NMR (400 MHz, d_6 -DMSO): $\delta = 7.63$ (2H, t, $J=5.6$, NH/OH), 7.28-7.09 (10H, m, Ph), 5.47 (s, $J = 7$ Hz, 2H, NH/OH), 4.20 (d, $J = 7$ Hz, 2H, HO-CH-CO-NH), 3.15-3.09 (m, 4H, -NH-CH₂), 2.61-2.53 (m, 4H, -CH₂-Ph), 1.60-1.38 (m, 8H, -NH-CH₂-CH₂-CH₂) ppm. ^{13}C NMR (100 MHz, d_6 -DMSO): $\delta = 172.3$ (C1), 142.6 (C7a), 128.8 (C7b-f), 128.7 (C7b-f), 126.1 (C7b-f), 73.0 (C2), 38.6 (C3), 35.3 (C6), 29.3 (C4), 28.7 (C5) ppm. IR: 3354 (m), 3213 (w), 3183 (w), 3166 (w), 2931 (w), 2873 (w), 2854 (w), 1640 (s), 1540 (s), 1494 (m), 1476 (w), 1450 (w), 1429 (w), 1376 (w), 1312 (w), 1292 (w), 1259 (w), 1221 (w), 1176 (w), 1129 (s), 1092 (m), 1084 (m), 1066 (m), 1059 (m), 1029 (w), 826 (m), 782 (w), 762 (w), 738 (s), 709 (m), 697 (s), 604 (s), 590 (m), 584 (w), 573 (w), 556 (w) cm^{-1} . HRMS (ESI) m/z : Calcd. for $\text{C}_{24}\text{H}_{32}\text{O}_4\text{N}_2$ $[\text{M}]^{*+}$ 412.2357, Found 412.2357. Chiral HPLC (r_t , conditions in 11.1.3): 17.1 minutes.

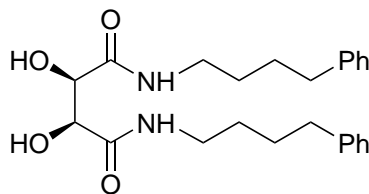
**(*S,S*) - 27**

11.5.6 (*2S,3S*)-2,3-Dihydroxy-*N1,N4*- bis(4-phenylbutyl) succinamide [(*S,S*)-27]^{16,79–81}

D-Dimethyltartrate (0.25 g, 1.40 mmol) was dissolved in MeOH (3 mL) before 4-phenylbutylamine (0.48 mL, 3.08 mmol, 2.2 eq) was added and the solution stored at 4 °C with occasional stirring for 3 days. The precipitated diamide was filtered off over suction and washed with small amounts of cold MeOH affording (*S,S*)-27 as white crystals (0.31 g, 0.75 mmol, 53%).

Mp: 170-171 °C. $[\alpha]_D^{20} = -55.2$ ($c = 0.98$, DMF). ¹H NMR (400 MHz, d₆-DMSO): $\delta = 7.63$ (2H, t, $J = 5.6$, NH/OH), 7.28-7.09 (10H, m, Ph), 5.47 (s, $J = 7$ Hz, 2H, NH/OH), 4.20 (d, $J = 7$ Hz, 2H, HO-CH-CO-NH), 3.15-3.09 (m, 4H, -NH-CH₂), 2.61-2.53 (m, 4H, -CH₂-Ph), 1.60-1.38 (m, 8H, -NH-CH₂-CH₂-CH₂) ppm. ¹³C NMR (100 MHz, d₆-DMSO): $\delta = 172.3$ (C1), 142.6 (C7a), 128.8 (C7b-f), 128.7 (C7b-f), 126.1 (C7b-f), 73.0 (C2), 38.6 (C3), 35.3 (C6), 29.3 (C4), 28.7 (C5) ppm. IR: 3354 (m), 3191 (w), 2930 (w), 2854 (w), 1640 (s), 1532 (s), 1494 (m), 1476 (w), 1450 (m), 1429 (w), 1376 (w), 1312 (w), 1292 (w), 1259 (w), 1233 (w), 1176 (w), 1130 (s), 1092 (m), 1084 (m), 1059 (s), 1029 (m), 827 (w), 783 (w), 761 (w), 738 (s), 709 (s), 697 (s), 651 (w), 631 (w), 604 (s), 590 (m), 584 (m), 571 (w), 559 (w) cm⁻¹. HRMS (ESI) m/z : Calcd. for C₂₄H₃₂O₄N₂ [M]⁺⁺ 412.2357, Found 412.2355. Chiral HPLC (r_t , conditions in 11.1.3): 21.0 minutes.

11.5.7 (*2R*,3S**)-2,3-Dihydroxy-*N1,N4*- bis(4-phenylbutyl) succinamide [(*R*,S**)-27]^{16,79–81}

**(*R*,S**) - 27**

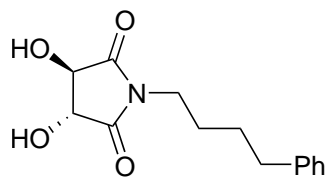
1. *meso*-Tartaric acid monohydrate (0.15 g, 0.90 mmol) was dissolved in MeOH (2.5 mL) before Amberlyst-15 (2.2 g) was added and the solution was stirred over night at room temperature. The Amberlyst-15 was filtered off the solution before 4-phenylbutylamine (0.29 g, 1.94 mmol, 2.2 eq) was added and the mixture stored at 4 °C with occasional stirring for 4 days. Removal of the solvent *in vacuo* yielded a brown sticky solid, further attempts at purification failed.
2. *meso*-Tartaric acid monohydrate (0.17 g, 1.01 mmol) was dissolved in MeOH (7.5 mL) before Amberlyst-15 (2.2 g) was added and the solution was stirred over night at room temperature. The Amberlyst-15 was then filtered off and some of the MeOH was removed *in vacuo* before 4-phenylbutylamine (0.33 g, 2.21 mmol, 2.2 eq) was added and the mixture was stored at 4 °C with occasional stirring for 3 days. The precipitated diamide was filtered off over suction and washed with small amounts of cold MeOH affording (*R**,*S**)-**27** as off-white crystals (0.07 g, 0.17 mmol, 17%).

Mp: 155-156 °C. $[\alpha]_D^{20} = -0.2$ ($c = 0.81$, DMF). ¹H NMR (400 MHz, d₆-DMSO): $\delta = 7.50$ (2H, t, $J = 5.8$ Hz, NH/OH), 7.30-7.11 (10H, m, Ph), 5.55 (d, $J = 5.3$ Hz, 2H, NH/OH), 4.09 (d, $J = 5.3$ Hz, 2H, HO-CH-CO-NH), 3.15-2.99 (m, 4H, -NH-CH₂), 2.59-2.52 (m, 4H, -CH₂-Ph), 1.61-1.34 (m, 8H, NH-CH₂-CH₂-CH₂) ppm. ¹³C NMR (100 MHz, d₆-DMSO): $\delta = 171.1$ (C1), 142.7 (C7a), 128.8 (C7b-f), 128.7 (C7b-f), 126.1 (C7b-f), 74.2 (C2), 38.4 (C3), 35.3 (C6), 29.3 (C4), 28.8 (C5) ppm. IR: 3334 (w), 3236 (m), 2938 (w), 2914 (w), 2858 (w), 1639 (s), 1602 (w), 1567 (s), 1492 (w), 1451 (s), 1440 (s), 1374 (w), 1351 (m), 1258 (m), 1194 (m), 1175 (w), 1097 (s), 1063 (w), 1051 (m), 1026 (w), 959 (w), 901 (w), 885 (w), 818 (w), 797 (w), 735 (s), 697 (s), 572 (s) cm⁻¹. HRMS (ESI) m/z : Calcd. for C₂₄H₃₂O₄N₂ [M]⁺ 412.2357, Found 412.2352. Chiral HPLC (*r_t*, conditions in 11.1.3): 24.0 minutes.

11.5.8 (2*R*,3*R*)-3,4-Dihydroxy-1-(4-phenylbutyl) pyrrolidine-2,5-dione [(*R*,*R*)-1]^{2,49}

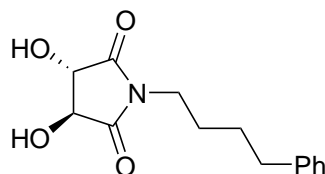
The monoacid (*R*,*R*)-**3** (0.5 g, 1.8 mmol) was added to xylenes (25 mL) and refluxed at 160 °C with a Dean-Stark apparatus for 24 hours. The mixture was cooled to 0 °C and filtered over suction affording a brown powder which then was recrystallized in a 1:1 solution of acetonitrile and toluene affording (*R*,*R*)-**1** as a white powder (0.17 g, 0.65 mmol, 36%)

Mp: 166 °C. $[\alpha]_D^{20} = +72.9$ ($c = 1.06$, DMF). ¹H NMR (400 MHz, d₆-

**(*R,R*) - 1**

DMSO): $\delta = 7.31-7.10$ (m, 5H, **Ph**), 6.23 (d, 2H, $J = 5.2$ Hz, **NH/OH**), 4.30 (d, 2H, $J = 4.4$ Hz, **HO-CH-CO-NH**), 3.64-3.46 (m, 2H, **-N-CH₂**), 2.60-2.53 (m, 2H, **-CH₂-Ph**), 1.57-1.40 (m, 4H, **-N-CH₂-CH₂-CH₂**) ppm. ¹³C NMR (100 MHz, d₆-DMSO): $\delta = 175.2$ (C1), 142.3 (C7a), 128.8 (C7b-f), 128.69 (C7b-f), 128.65 (C7b-f), 126.1 (C7b-f), 74.8 (C2), 37.9 (C3), 35.0 (C6), 28.6 (C4), 27.2 (C5) ppm. IR: 3364 (w), 3249 (w), 2946 (w), 1701(s), 1465 (w), 1453 (w), 1437 (w), 1403 (w), 1369 (w), 1346 (m), 1272 (w), 1217 (w), 1158 (m), 1147 (m), 1101 (m), 1077 (s), 1048 (s), 1032 (w), 980 (m), 899 (w), 858 (w), 812 (m), 751 (s), 733 (w), 696 (s), 657 (w), 643 (w), 609 (w), 583 (w), 572 (w), 551 (w) cm⁻¹. HRMS (ESI) m/z : Calcd. for C₁₄H₁₇O₄N [M]⁺ 263.1152, Found 263.1147. Chiral HPLC (r_t , conditions in 11.1.3): 31.0 minutes.

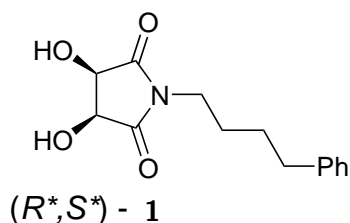
11.5.9 (2*S*,3*S*)-3,4-Dihydroxy-1-(4-phenylbutyl) pyrrolidine-2,5-dione [(*S,S*)-1]^{2,49}

**(*S,S*) - 1**

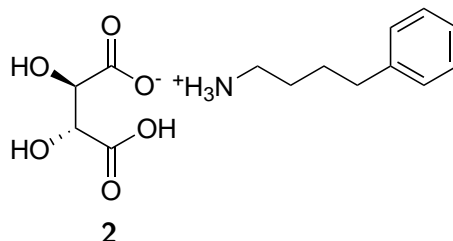
The monoacid (*S,S*)-**3** (0.4 g, 1.44 mmol) was added to xylenes (25 mL) and refluxed at 160 °C with a Dean-Stark apparatus for 24 hours. The mixture was cooled to 0 °C and filtered over suction affording a brown powder which then was recrystallized in a 1:1 solution of acetonitrile and toluene affording (*S,S*)-**1** as a white powder (0.017 g, 0.065 mmol, 9%) Mp: 166 °C. $[\alpha]_D^{20} = -97.3$ ($c = 0.15$, DMF). ¹H NMR (400 MHz, d₆-DMSO): $\delta = 7.31-7.10$ (m, 5H, **Ph**), 6.23 (d, 2H, $J = 5.2$ Hz, **NH/OH**), 4.30 (d, 2H, $J = 5.4$ Hz, **HO-CH-CO-NH**), 3.64-3.46 (m, 2H, **-N-CH₂**), 2.60-2.53 (m, 2H, **-CH₂-Ph**), 1.57-1.40 (m, 4H, **-N-CH₂-CH₂-CH₂**) ppm. ¹³C NMR

(100 MHz, d₆-DMSO): δ = 175.2 (C1), 142.3 (C7a), 128.8 (C7b-f), 128.69 (C7b-f), 128.65 (C7b-f), 126.1 (C7b-f), 74.8 (C2), 37.9 (C3), 35.0 (C6), 28.6 (C4), 27.2 (C5) ppm. IR: 3375 (w), 2945 (w), 1701 (s), 1462 (w), 1453 (w), 1437 (w), 1402 (w), 1368 (w), 1346 (s), 1272 (w), 1217 (m), 1157 (m), 1147 (m), 1101 (s), 1077 (s), 1048 (s), 1032 (w), 980 (m), 858 (w), 812 (m), 751 (s), 733 (w), 696 (s), 657 (w), 643 (w), 609 (w), 594 (w), 583 (w), 571 (w), 553 (w) cm⁻¹. HRMS (ESI) m/z : Calcd. for C₁₄H₁₇O₄N [M]⁺ 263.1152, Found 263.1155. Chiral HPLC (r_t , conditions in 11.1.3): 35.3 minutes.

11.5.10 (2*R**,3*S**)-3,4-Dihydroxy-1-(4-phenylbutyl) pyrrolidine-2,5-dione [(*R**,*S**)-1]^{2,49}

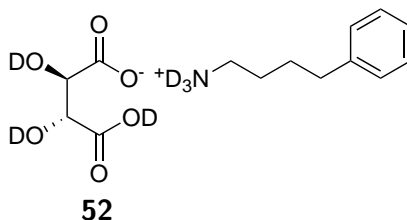


The (*R**,*S**)-monoacid (*R**,*S**)-**3** (2.0 g, 7.1 mmol) was added to xylenes (50 mL) and refluxed at 160 °C with a Dean-Stark apparatus for 24 hours. The mixture was cooled to 0 °C and filtered over suction affording a brown powder which then was recrystallized in a 1:1 solution of acetonitrile and toluene affording (*R**,*S**)-**1** as a off white powder (0.8 g, 3.0 mmol, 42%) Mp: 142-143 °C. $[\alpha]_D^{20}$ = 0.0 (c = 0.5, DMF). ¹H-NMR (400MHz, d₆-DMSO): δ = 7.29-7.11 (m, 5H, **Ph**), 5.91 (s, 2H, **NH/OH**), 4.33 (s, 2H, **HO-CH-CO-NH**), 3.43-3.34 (m, 2H, **-N-CH₂**), 2.60-2.53 (m, 2H, **-CH₂-Ph**), 1.62-1.40 (m, 4H, **-N-CH₂-CH₂-CH₂**) ppm. ¹³C NMR (100 MHz, d₆-DMSO): δ = 176.9 (C1), 142.3 (C7a), 128.8 (C7b-f), 128.7 (C7b-f), 128.6 (C7b-f), 126.2 (C7b-f), 68.3 (C2), 37.7 (C3), 35.1 (C6), 28.5 (C4), 27.2 (C5) ppm. IR: 3387 (s), 3027 (w), 2944 (w), 2923 (w), 2853 (w), 1784 (w), 1706 (w), 1685 (s), 1603 (w), 1494 (w), 1463 (w), 1453 (w), 1437 (m), 1414 (m), 1376 (w), 1351 (m), 1317 (w), 1298 (w), 1276 (w), 1254 (w), 1221 (m), 1166 (m), 1141 (s), 1112 (w), 1100 (w), 1083 (m), 1074 (w), 1049 (w), 1026 (w), 993 (w), 934 (m), 909 (w), 886 (s), 837 (m), 800 (m), 743 (m), 710 (w), 696 (s), 667 (w), 617 (w), 609 (w), 592 (w), 571 (m) cm⁻¹. HRMS (ESI) m/z : Calcd. for C₁₄H₁₇O₄N [M]⁺ 263.1152, Found 263.1152. Chiral HPLC (r_t , conditions in 11.1.3): 51.6 minutes.

11.5.11 4-Phenylbutan-1-aminium (*2R,3R*)-3-carboxy- 2,3-dihydroxypropanoate (**2**)²

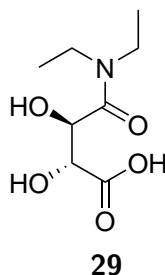
L-tartaric acid (1.50 g, 10 mmol) was dissolved in H₂O (3 mL) and 4-phenylbutylamine (1.58 mL, 10 mmol) was dissolved in MeOH (2 mL) before the two solutions were mixed in a cold water bath. The precipitated salt was filtered off over suction and washed with diethyl ether affording **2** as white crystals (2.61 g, 8.70 mmol, 87%).

$[\alpha]_D^{20} = +14.4$ ($c = 0.55$, MeOH). ¹H NMR (400 MHz, CD₃OD): $\delta = 7.33$ - 7.17 (m, 5H, **Ph**), 4.39 (s, 2H, HO-**CH**-CO), 2.92 (t, 2H, $J = 7.1$ Hz, NH₃⁺-**CH**₂), 2.67 (t, 2H, $J = 7.1$ Hz, -**CH**₂-Ph), 1.79-1.64 (m, 4H, CO-NH-**CH**₂-**CH**₂-**CH**₂) ppm. ¹³C NMR (100 MHz, CD₃OD): $\delta = 176.9$ (C1), 143.0 (C7a), 129.59 (C7b-f), 129.57 (C7b-f), 127.1 (C7b-f), 74.2 (C2), 40.8 (C3), 36.3 (C6), 29.5 (C4), 28.3 (C5) ppm. IR: 3466 (w), 3359 (w), 3128 (w), 2907 (w), 1698 (w), 1629 (w), 1581 (m), 1514 (w), 1496 (w), 1456 (w), 1393 (w), 1236 (m), 1126 (s), 1069 (s), 1032 (w), 1014 (w), 981 (w), 886 (s), 832 (m), 740 (s), 719 (m), 693 (s), 669 (w), 613 (s), 586 (m) cm⁻¹.

11.5.12 d₆-4-Phenylbutan-1-aminium (*2R,3R*)-3-carboxy-2,3-dihydroxypropanoate

The ammonium tartrate salt **2** (0.100 g, 0.33 mmol) was stirred in D₂O (6 mL) and stirred for 8 hours before it was freeze dried and the process repeated. The white powder obtained after second freeze drying was kept under nitrogen in cold storage.

11.5.13 Attempted synthesis of (2*R*,3*R*)-4-(Diethylamino)-2,3-dihydroxy-4-oxobutanoic acid (**29**)^{2,73,76}



L-Diacetyltartaric anhydride [(*R,R*)-**36**] (5 g, 23.14 mmol) was dissolved in THF (40 mL) and cooled down to -15°C and put under N_2 atmosphere. Diethylamine (2.39 mL, 18.50 mmol, 0.8 eq) was dissolved in THF (10 mL) and added dropwise to the reaction mixture over five minutes. The reaction mixture was stirred at -15°C for one hour and allowed to reach room temperature before the solvent was evaporated off *in vacuo*. The crude reaction mixture was dissolved in MeOH (40 mL) before the solution was adjusted to pH 13 with dropwise addition of $\text{NaOH}_{(aq)}$ (approx. 5 mL, 6 M) at 0°C , followed by overnight stirring. The solution was made acidic with $\text{HCl}_{(aq)}$ (approx. 20 mL, 2 M) before solvent was removed *in vacuo*. The crude product was dissolved in THF and filtered in order to remove NaCl before it was added to Et_2O and filtered in order to remove acetic acid from the solid product. Drying on a high vacuum line afforded **29** as white crystals (1.47 g, 7.30 mmol, approx. 30%) with 2.5% AcOH (deduced from ^1H NMR).

^1H NMR (400 MHz, CDCl_3): $\delta = 4.86$ (s, 1H, HO-CH-CO-NEt₂), 4.31 (s, 1H, HO-CH-CO-OH), 3.53-3.22 (m, 4H, -CH₂), 1.15 (2x3, 6H, -CH₃) ppm.

11.6 Molecular modelling parameters and data

11.6.1 DFT^{85,86}

All initial structures were truncated with a methyl substituent on nitrogen and subjected to a MM2 force field minimization before the resulting structure were subjected to DFT modelling as described below.

The DFT geometry optimizations were performed with the B3LYP hybrid density functional and the 6-31G(2d) basis set. The B3LYP functional is a

hybrid of Becke's three-parameter hybrid exchange functional(B3)⁸⁵ combined with the Lee, Yang and Parr correlation functional (LYP).⁸⁶ The calculations were performed on a AMD Phenom x4 quad core computer with the GAMESS software through the ChemBio3D interface. Zero point vibrational energies were obtained by performing calculations on the optimized intermediate structures with the B3LYP hybrid density functional and 6-311G(2df), and the potential energy surface was found by adding the energy found in the optimization together with the calculated zero point vibrational energies.

11.6.2 Force field optimizations (MM2)²⁸

All force field minimizations were conducted utilizing the ChemBio3D interface. The MM2 force field is a second generation force field developed by Norman Allinger and is parametrized for a broad range of molecules.²⁸ MM2 is an improved successor of the MM1 force field, where the dihedral terms and bending terms were extended along with exclusion of cross terms between stretches and bends.

List of experiments where molecular mechanics were utilized

- Determining qualitative energy difference between **3** and **1**.
- Determining relative energy between initial and reorganized **3** dimers.
- Determining relative energy between cyclic tartramide (**1**) and diamide (**27**) with different stereochemistry ((R,R) vs (R^*,S^*)).

11.7 Kinetic experiments

11.7.1 Cyclization of **3** to form **1**

The monoacid **3** (in one experiment **16**) was added to a given amount of xylenes in a three necked roundbulb, before 2-methoxynaphthalene (**IS**) was added. The reaction mixture was equipped with a reflux condenser, internal and external thermometer and heated in an oil bath. The oil bath was set to 160 °C to ensure reflux conditions at all times. Samples were taken with a standard syringe at given times and temperatures during the course of the reaction. Detailed amounts of compounds used is depicted in Table 4.1 in Section 4.1.1 and Table 4.2 in Section 4.1.3. Spectra can be found in Appendix L.

Special conditions employed in addition to the above mentioned procedure:

- Experiment where active water removal with a Dean-Stark condenser was used.

11.7.2 Ringopening of **1** with an amine

The tartramide **1** was added to a given amount of xylenes in a three necked roundbulb, before 2-methoxynaphthalene (IS) was added. The reaction mixture was equipped with a reflux condenser, internal and external thermometer and heated in an oil bath. The oil bath was set to 160 °C to ensure reflux conditions at all times. The mixture was heated to reflux before an appropriate amount of 4-phenylbutylamine was added. Samples were taken with a standard syringe at given times and temperatures during the course of the reaction. Detailed amounts of compounds used is depicted in Figure 5.2 in Section 5.1 and Figure 5.5 in Section 5.2. Spectra and chromatograms can be found in Appendix C.

11.7.3 Refluxing **3** with an amine

The monoacid **3** was added to a given amount of xylenes in a three necked roundbulb, before 2-methoxynaphthalene (IS) was added. The reaction mixture was equipped with a reflux condenser, internal and external thermometer and heated in an oil bath. The oil bath was set to 160 °C to ensure reflux conditions at all times. The mixture was heated to reflux before an appropriate amount of 4-phenylbutylamine was added. Samples were taken with a standard syringe at given times and temperatures during the course of the reaction. Detailed amounts of compounds used is depicted in Table 6.1 in Section 6.1. Spectra and chromatograms can be found in Appendix N.

11.7.4 Attempted monitoring of the monoacid formation, starting from **29**

The monoacid **29** (0.115 g, 0.63 mmol) was added to xylenes (12.5 mL) in a three necked roundbulb, before 2-methoxynaphthalene (IS, 12.5 mg) was added. The reaction mixture was equipped with a reflux condenser, internal and external thermometer and heated in an oil bath. The oil bath was set to 160 °C to ensure reflux conditions at all times. The mixture was heated to reflux before 4-phenylbutylamine (0.094 g, 0.63 mmol, 1 eq.) was added. Samples were taken with a standard syringe at given times and

temperatures during the course of the reaction. Spectra can be found in Appendix O.

11.7.5 Monitoring of the entire reaction, starting from the ammonium tartrate salt **2**

The tartramide **2** (0.200 g, 0.71 mmol) was added to xylenes (12.5 mL) in a three necked roundbulb, before 2-methoxynaphthalene (IS, 12.5mg) was added. The reaction mixture was equipped with a reflux condenser, internal and external thermometer and heated in an oil bath. The oil bath was set to 160 °C to ensure reflux conditions at all times. Samples were taken with a standard syringe at given times and temperatures during the course of the reaction. Spectra and chromatograms can be found in Appendix K.

11.8 Various mechanistic experiments

11.8.1 Cyclization of 2d,3d-tartaric acid with an amine

2d,3d-Tartaric acid (0.025 g, 0.16 mmol) was mixed with 4-phenylbutylamine (0.025 mL, 0.96 eq) and added to xylenes (4 mL). The mixture was then refluxed for 20 hours. A reference reaction with non-deuterated *L*-tartaric acid was subjected to the same treatment. Samples taken out after 20 hours were analyzed with HPLC, MS and ¹H NMR.

11.8.2 Cyclization of **52**

Dry xylenes controllably contaminated with heavy water was prepared from bubbling nitrogen through heavy water and into the reaction vessel containing xylenes.

The heteroatom deuterated salt **52** (0.1 g, 0,33 mmol) was added to the xylenes (8mL) above and refluxed under nitrogen flow for 20 hours. Samples taken out after 20 hours were analyzed with HPLC, MS and ¹H NMR.

11.8.3 Test for possible ringopening of (*R,R*)-**1** to form (*R,R*)-**3** with aqueous reflux

(*R,R*)-**1** (0.100 g, 0.38 mmol) was added to H₂O (4 mL, 0.22 mol) and refluxed for 4 hours before samples were taken out, freeze dried and analyzed with ¹H NMR.

11.8.4 Test for isomerization of (*R,R*)-1 with a sterically hindered base

The cyclic tartramide (*R,R*)-1 (0.05 g, 0.19 mmol) was added to xylenes (4 mL) before 2,2,6,6-tetramethylpiperidine (0.19 mmol, 1 eq.) was added and the mixture refluxed for 5 hours. Samples were then taken for analysis with ^1H NMR and HPLC.

11.8.5 Isomerization of dimethyltartrate with NaOH

L-Dimethyltartrate (0.118 g, 0.66 mmol) and NaOH (0.33 mL, 6 M, 3 eq) was added to xylenes (10 mL) before it was refluxed for 4.5 hours. A reference experiment with *L*-tartaric acid was subjected to the same treatment. Samples taken after 4.5 hours were analyzed with ^1H NMR.

11.9 Test of possible internal standards for NMR and HPLC purposes

1. 2-Methoxynaphthalene (0.250 g, 1.58 mmol) was added to 4-phenylbutylamine (0.24 g, 1.61 mmol) and xylenes (10 mL) before to 160 °C for 24 hours. ^1H NMR of the mixtures showed the 2-methoxynaphthalene to not interact with amine under these reaction conditions.
2. Phthalimide (0.100 g, 0.68 mmol) was added to 4-phenylbutylamine (0.20 g, 1.34 mmol) and xylenes (10 mL) before heated to 160 °C for 24 hours. ^1H NMR of the mixtures showed side reactions that might have risen from the addition of phthalimide to the reaction system.

11.10 Derivatization of **53** with diazomethane⁸⁷

The monoacid **53** (0.08 g, 0.30 mmol) and Et_2O (3 mL) was added to the outer tube of the diazald apparatus before Diazald (0.3 g, 1.40 mmol, 4.7 eq) was added to the inner tube and dissolved in carbinol (1 mL). The entire apparatus was immersed in a ice bath before $\text{KOH}_{(aq)}$ (1.5 mL, 37%) was added dropwise to the inner tube through the septum. After addition of base the entire vessel was gently shaken before left immersed in ice for one hour, followed by addition of silicic acid (0.15 g) to the inner tube. Solvent and excess CH_2N_2 were removed with a gentle stream of nitrogen yielding **42** as an off-white powder (quantitative yield, 98% conversion).

The product from this derivatization exhibited the same spectroscopic properties as **42** in Section 11.5.4.

Bibliography

- (1) Tadros, T., *Applied surfactants*; Wiley-VCH: 2005.
- (2) Gonzalez, S. V. Optically active surfactants from the tartaric acids. Synthesis and properties., Ph.D. Thesis, NTNU, 2009.
- (3) [Http://bcgc.berkeley.edu/marine-oil-spill](http://bcgc.berkeley.edu/marine-oil-spill) response.
- (4) Lang, S.; Wullbrandt, D. *Appl. Microbiol. Biotechnol.* **1999**, *51*, 22–32.
- (5) Fuhrhop, J. H.; Helfrich, W. *Chem. Rev.* **1993**, *93*, 1565–82.
- (6) Allen, T. M.; Cullis, P. R. *Science* **2004**, *303*, 1818–1822.
- (7) Langer, R. *Science* **2001**, *293*, 58–59.
- (8) Discher, D. E.; Eisenberg, A. *Science* **2002**, *297*, 967–973.
- (9) Mazzeo, J. R.; Grover, E. R.; Swartz, M. E.; Petersen, J. S. *J. Chromatogr., A* **1994**, *680*, 125–35.
- (10) Wheatley, M. A.; Singhal, S. *React. Polym.* **1995**, *25*, 157–66.
- (11) Wang, W.; Moser, C. C.; Wheatley, M. A. *J. Phys. Chem.* **1996**, *100*, 13815–13821.
- (12) Li, J.; Tang, Y.; Wang, Q.; Li, X.; Cun, L.; Zhang, X.; Zhu, J.; Li, L.; Deng, J. *J. Am. Chem. Soc.* **2012**, *134*, 18522–18525.
- (13) Carey, F. A., *Organic chemistry*, 7.; McGraw-Hill: 2008.
- (14) Patterson, T. S. *Ann. Sci.* **1938**, *3*, 431–4.
- (15) Zheng, J.-L.; Liu, H.; Zhang, Y.-F.; Zhao, W.; Tong, J.-S.; Ruan, Y.-P.; Huang, P.-Q. *Tetrahedron: Asymmetry* **2011**, *22*, 257–263.
- (16) Gonzalez, S. V.; Carlsen, P. *Tetrahedron Lett.* **2008**, *49*, 3925–3926.
- (17) Carey F. A.; Sundberg, R. J., *Advanced organic chemistry part A: Structure and mechanisms*; Springer: 2007, pp 14–15, 272–275, 332–335.

- (18) Charville, H.; Jackson, D. A.; Hodges, G.; Whiting, A.; Wilson, M. R. *Eur. J. Org. Chem.* **2011**, *2011*, 5981–5990.
- (19) Charville, H. Direct Amide Formation Between Carboxylic Acids and Amines: Mechanism and Development of Novel Catalytic Solutions., Ph.D. Thesis, Durham University, 2012.
- (20) Gonzalez S. V.; Carlsen, P. Synthesis of Tartaric acid diamides by thermolysis of tartaric acid with alkylamines.
- (21) Raju, R.; Carlsen, P.; Gonzalez, S. V. In writing.
- (22) Chorkendorff I.; Niemantsverdriet, J., *Concepts of modern catalysis*; Wiley-VCH: 2010, pp 23–45.
- (23) Kappe O. K.; Dallinger, D. M. S. S., *Practical Microwave Synthesis for Organic Chemists*, 7.; Wiley-VCH: 2009.
- (24) Haugland, M. M. Synthesis of a Novel Tocopherol/Caratenoid Derivative., diploma thesis, NTNU, 2012.
- (25) Gedye, R.; Smith, F.; Westaway, K.; Ali, H.; Baldisera, L.; Laberge, L.; Rousell, J. *Tetrahedron Lett.* **1986**, *27*, 279–82.
- (26) Giguere, R. J.; Bray, T. L.; Duncan, S. M.; Majetich, G. *Tetrahedron Lett.* **1986**, *27*, 4945–8.
- (27) Leach, A. R., *Molecular modelling: Principles and application*, 2.; Pearson Education Limited: 2001, pp 272–275.
- (28) Allinger, N. L. *J. Am. Chem. Soc.* **1977**, *99*, 8127–34.
- (29) Pearson, R. G.; Songstad, J. *J. Am. Chem. Soc.* **1967**, *89*, 1827–36.
- (30) Bürgi, H. B.; Dunitz, J. D.; Shefter, E. *J. Am. Chem. Soc.* **1973**, *95*, 5065–5067.
- (31) Bürgi, H. B.; Dunitz, J. D.; Lehn, J. M.; Wipff, G. *Tetrahedron* **1974**, *30*, 1563–1572.
- (32) Boehme, H.; Lerche, G. *Justus Liebigs Ann. Chem.* **1967**, *705*, 154–63.
- (33) Klages, F.; Zange, E. *Justus Liebigs Ann. Chem.* **1957**, *607*, 35–45.
- (34) Truce, W. E.; Bailey Philip S., J. *J. Org. Chem.* **1969**, *34*, 1341–5.
- (35) Tidwell, T. T. *Acc. Chem. Res.* **1990**, *23*, 273–9.
- (36) Allen, A. D.; Andraos, J.; Kresge, A. J.; McAllister, M. A.; Tidwell, T. T. *J. Am. Chem. Soc.* **1992**, *114*, 1878–9.
- (37) Maas, G.; Brueckmann, R. *J. Org. Chem.* **1985**, *50*, 2801–2.

- (38) Concannon, P. W.; Ciabattini, J. *J. Am. Chem. Soc.* **1973**, *95*, 3284–9.
- (39) Allen, A. D.; Stevenson, A.; Tidwell, T. T. *J. Org. Chem.* **1989**, *54*, 2843–8.
- (40) Shelkov, R.; Nahmany, M.; Melman, A. *J. Org. Chem.* **2002**, *67*, 8975–8982.
- (41) Cram, D. J.; Gosser, L. *J. Am. Chem. Soc.* **1964**, *86*, 5457–65.
- (42) Cram, D. J.; Rickborn, B.; Kingsbury, C. A.; Haberfield, P. *J. Am. Chem. Soc.* **1961**, *83*, 3678–87.
- (43) Lobell, M.; Grout, D. H. G. *J. Chem. Soc., Perkin Trans. 1* **1996**, 1577–1581.
- (44) Lien, V. Unpublished DFT modelling., Not published, 2011.
- (45) Raju, R. In writing., Ph.D. Thesis, NTNU, 2014.
- (46) Cossy, J.; Pale-Grosdemange, C. *Tetrahedron Letters* **1989**, *30*, 2771–2774.
- (47) Goossen, L. J.; Ohlmann, D. M.; Lange, P. P. *Synthesis* **2009**, 160–164.
- (48) Al-Zoubi, R. M.; Marion, O.; Hall, D. G. *Angew. Chem. Int. Ed.* **2008**, *47*, 2876–2879.
- (49) Giroux, S.; Rubini, P.; Gerardin, C.; Selve, C.; Henry, B. *New J. Chem.* **2000**, *24*, 173–178.
- (50) Chocholousova, J.; Vacek, J.; Hobza, P. *J. Phys. Chem. A* **2003**, *107*, 3086–3092.
- (51) Balabin, R. M. *J. Phys. Chem. A* **2009**, *113*, 4910–4918.
- (52) Gora, R. W.; Grabowski, S. J.; Leszczynski, J. *J. Phys. Chem. A* **2005**, *109*, 6397–6405.
- (53) Huggins, M. L. *J. Org. Chem.* **1936**, *1*, 407–56.
- (54) Pasalic, H.; Aquino, A. J. A.; Tunega, D.; Haberhauer, G.; Gerzabek, M. H.; Georg, H. C.; Moraes, T. F.; Coutinho, K.; Canuto, S.; Lischka, H. *J Comput Chem* **2010**, *31*, 2046–55.
- (55) Semmler, J.; Irish, D. E. *J. Solution Chem.* **1988**, *17*, 805–24.
- (56) Wu, Z.; Ban, F.; Boyd, R. J. *J. Am. Chem. Soc.* **2003**, *125*, 3642–3648.
- (57) Hermans, P. H.; Streef, J. W. *Makromol. Chem.* **1964**, *74*, 133–44.

- (58) Zimmerman, H. E.; Traxler, M. D. *J. Am. Chem. Soc.* **1957**, *79*, 1920–1923.
- (59) Polonski, T. *J. Chem. Soc., Perkin Trans. 1* **1988**, *0*, 629–637.
- (60) Wiberg, K. B. *Chem. Rev.* **1955**, *55*, 713–743.
- (61) Kotanigawa, T.; Shimokawa, K.; Yoshida, T.; Yamamoto, M. *J. Phys. Chem.* **1979**, *83*, 3020–3.
- (62) Lockley, W. J. S.; Hesk, D. *J. Labelled Comp. Radiopharm.* **2010**, *53*, 704–715.
- (63) Khodabakhshi, S. *Organic Chemistry International* **2012**, *2012*, 5.
- (64) Yamada, Y. M. A.; Shibasaki, M. *Tetrahedron Lett.* **1998**, *39*, 5561–5564.
- (65) Santos, A. M. B.; Martínez, M.; Mira, J. A. *Chem. Eng. Technol.* **1996**, *19*, 538–542.
- (66) Gonzalez-Silgo, C.; Gonzalez-Platas, J.; Ruiz-Perez, C.; Lopez, T.; Torres, M. *Acta Crystallogr., Sect. C: Cryst. Struct. Commun.* **1999**, *C55*, 740–742.
- (67) Holleman, A. F. *Organic Syntheses* **1926**, 82.
- (68) Eliason, R.; Platz, J.; Carlsen, P. H. J. *Acta Chem. Scand.* **1991**, *45*, 491–3.
- (69) Bakka, T. Synthesis of alpha-deuterated alpha-hydroxy carboxylic acids., Project at NTNU, 2011.
- (70) Yang, Y.; Evilia, R. F. *J. Supercrit. Fluids* **1996**, *9*, 113–117.
- (71) Guthrie, J. P. *Can. J. Chem.* **1993**, *71*, 2123–2128.
- (72) Yang, Y.; Evilia, R. F. *J. Supercrit. Fluids* **1996**, *9*, 161–166.
- (73) Liesen, G. P.; Sukenik, C. N. *J. Org. Chem.* **1987**, *52*, 455–457.
- (74) Lucas, H. J.; Baumgarten, W. *J. Am. Chem. Soc.* **1941**, *63*, 1653–7.
- (75) Roberts, J. C. *J. Chem. Soc.* **1952**, 3315–16.
- (76) Serrano, P.; Casas, J.; Llebaria, A.; Zucco, M.; Emeric, G.; Delgado, A. *J. Comb. Chem.* **2007**, *9*, 635–643.
- (77) Yeom, C.-E.; Lee, S. Y.; Kim, Y. J.; Kim, B. M. *ChemInform* **2005**, *36*.
- (78) Apelblat, A.; Manzurola, E. *J. Chem. Thermodyn.* **1987**, *19*, 317–20.
- (79) Dobashi, A.; Hamada, M. *J. Chromatogr.* **1997**, *780*, 179–189.

-
- (80) Meier, I. K.; Lassila, K. R.; Slone, C. S. Low foaming N,N'-dialkyl tartaramide wetting agents and their preparation US6399543B1., 2002.
- (81) Viswanathan, A.; Kiely, D. E. *J. Carbohydr. Chem.* **2003**, *22*, 903–918.
- (82) Anand, R. C.; Vimal *Synth. Commun.* **1998**, *28*, 1963–1965.
- (83) Brightwell, M.; Pawlowska, M.; Zukowski, J. *J. Liq. Chromatogr.* **1995**, *18*, 2765–81.
- (84) Black, T. H. *Aldrichimica Acta* **1983**, *16*, 3–10.
- (85) Becke, A. D. *J. Chem. Phys.* **1993**, *98*, 5648–52.
- (86) Lee, C.; Yang, W.; Parr, R. G. *Phys. Rev. B: Condens. Matter* **1988**, *37*, 785–9.
- (87) Aldrich, S., online, <http://www.sigmaaldrich.com/catalog/product/aldrich/z411736?lang=en®ion=NO>.

Appendixes

A. Spectroscopic data for **3**

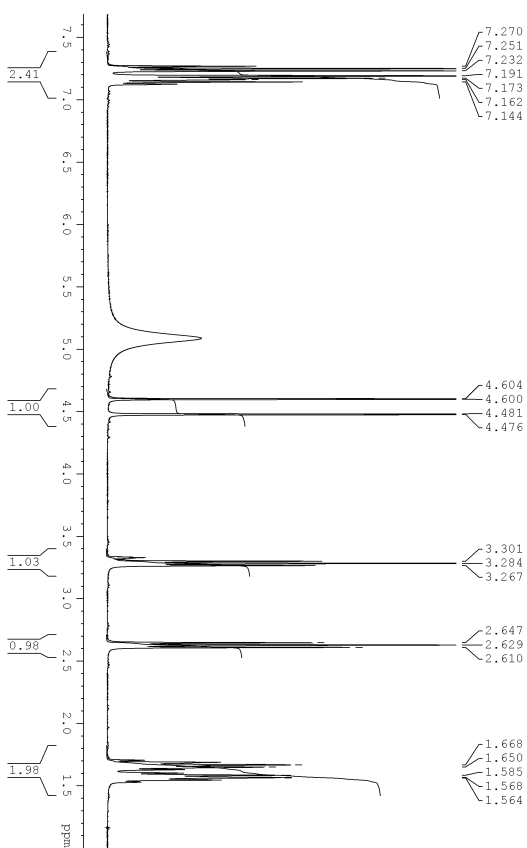


Figure A.1 ^1H NMR spectra of (R,R) -**3**.

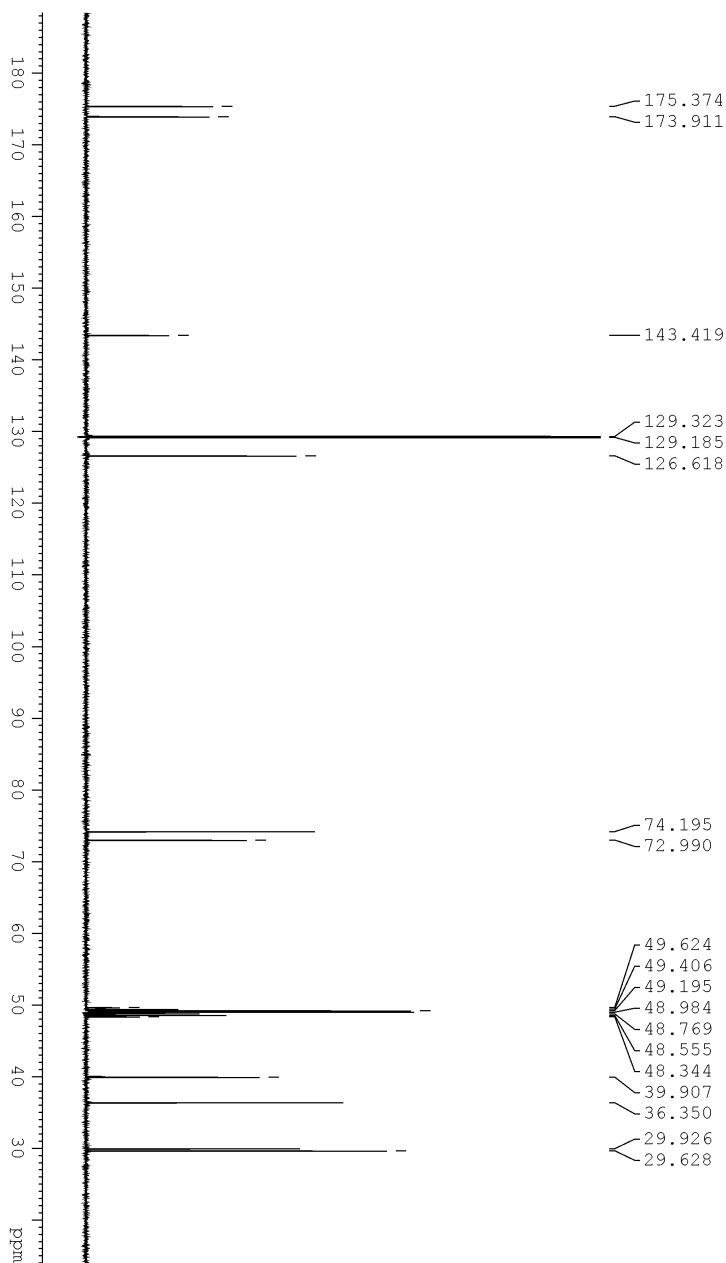


Figure A.2 ^{13}C NMR spectra of (*R,R*)-**3**.

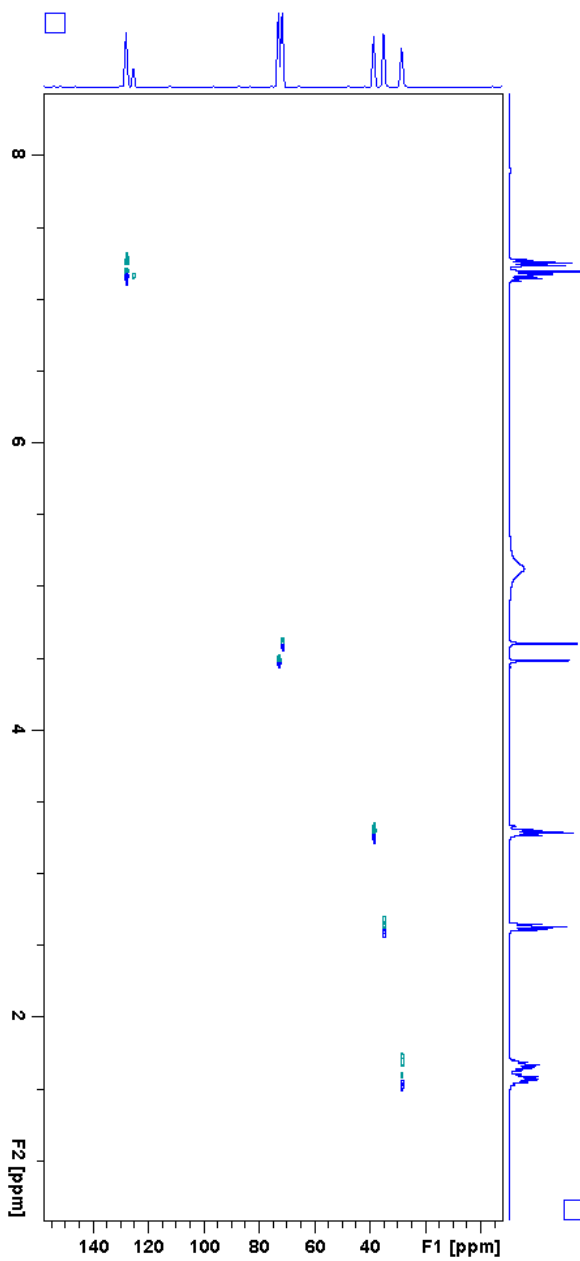


Figure A.3 HSQC spectra of (R,R) -3.

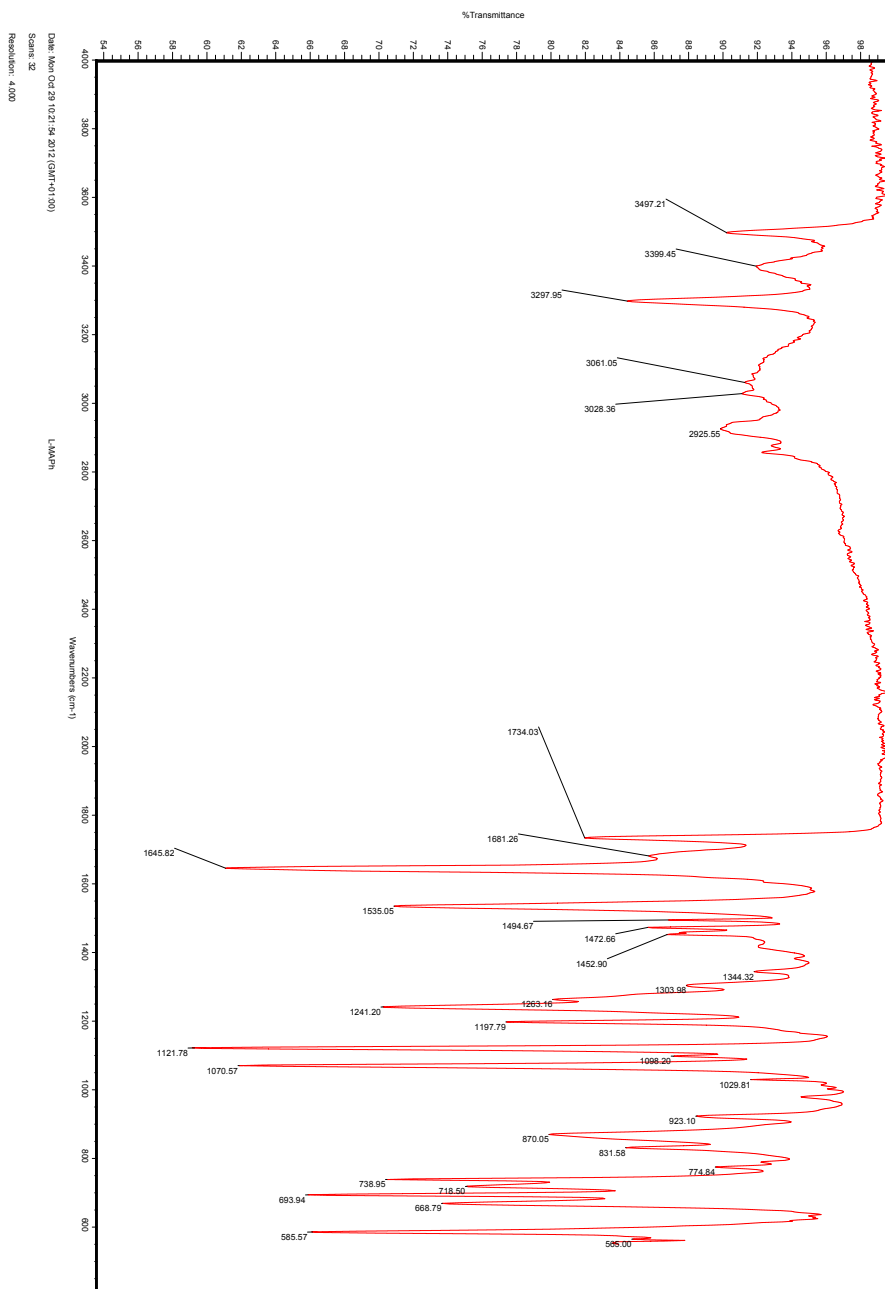


Figure A.4 IR spectra of (*R,R*)-3.

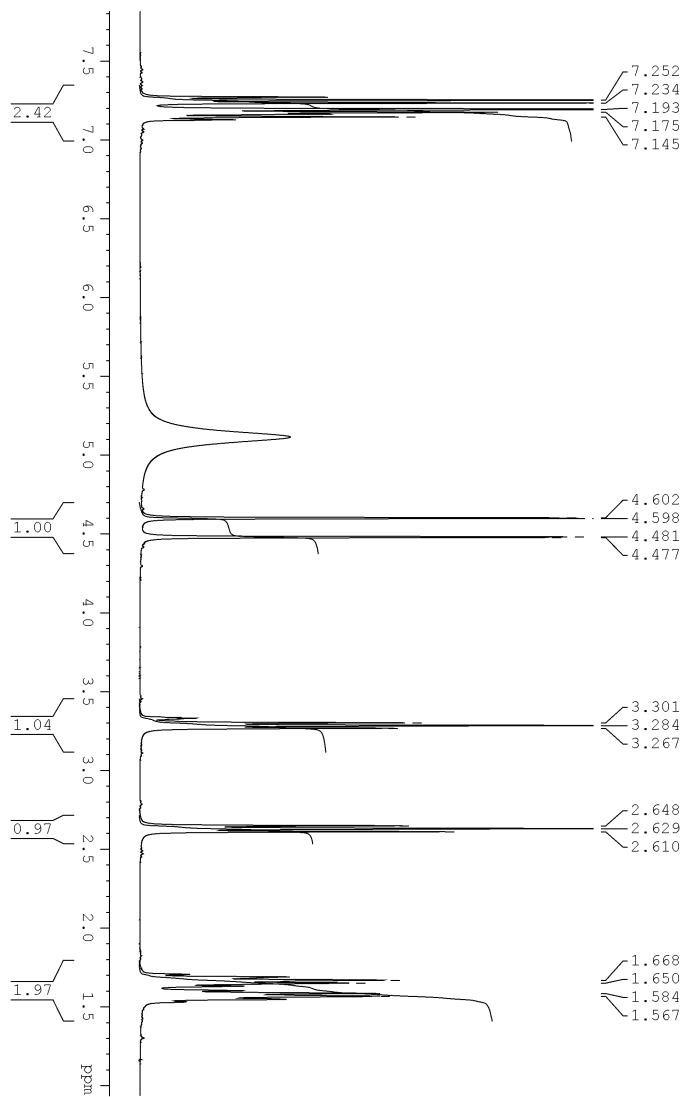


Figure A.5 ^1H NMR spectra of (S,S) -3.

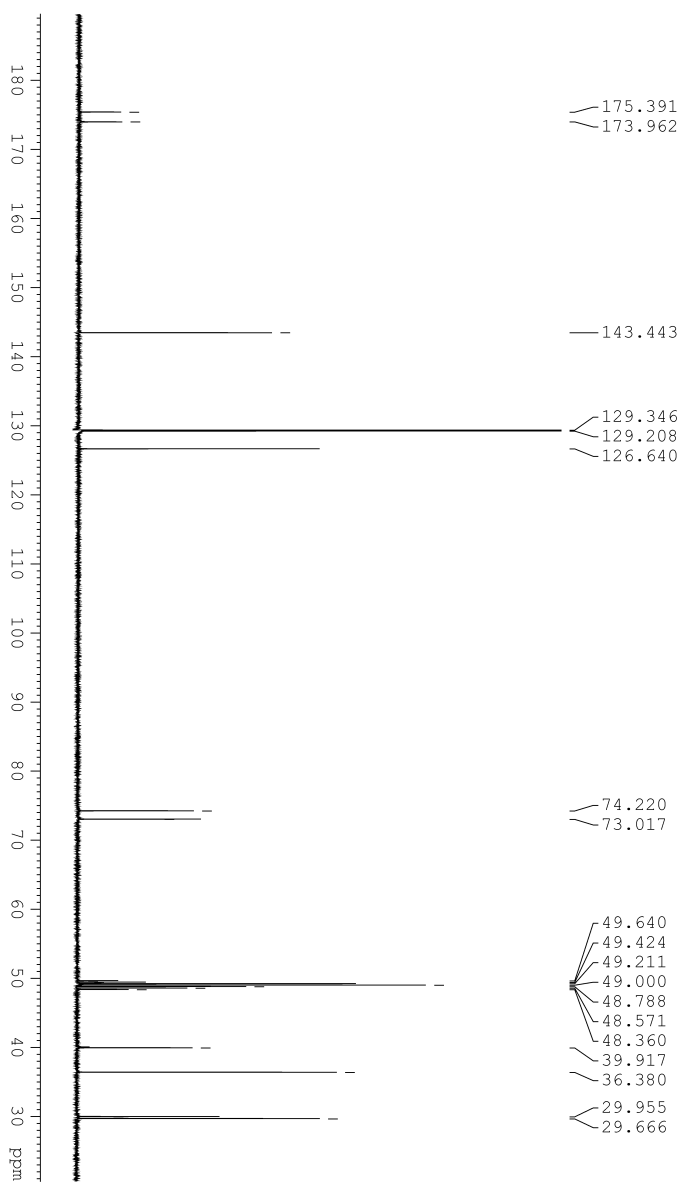


Figure A.6 ^{13}C NMR spectra of (*S,S*)-**3**.

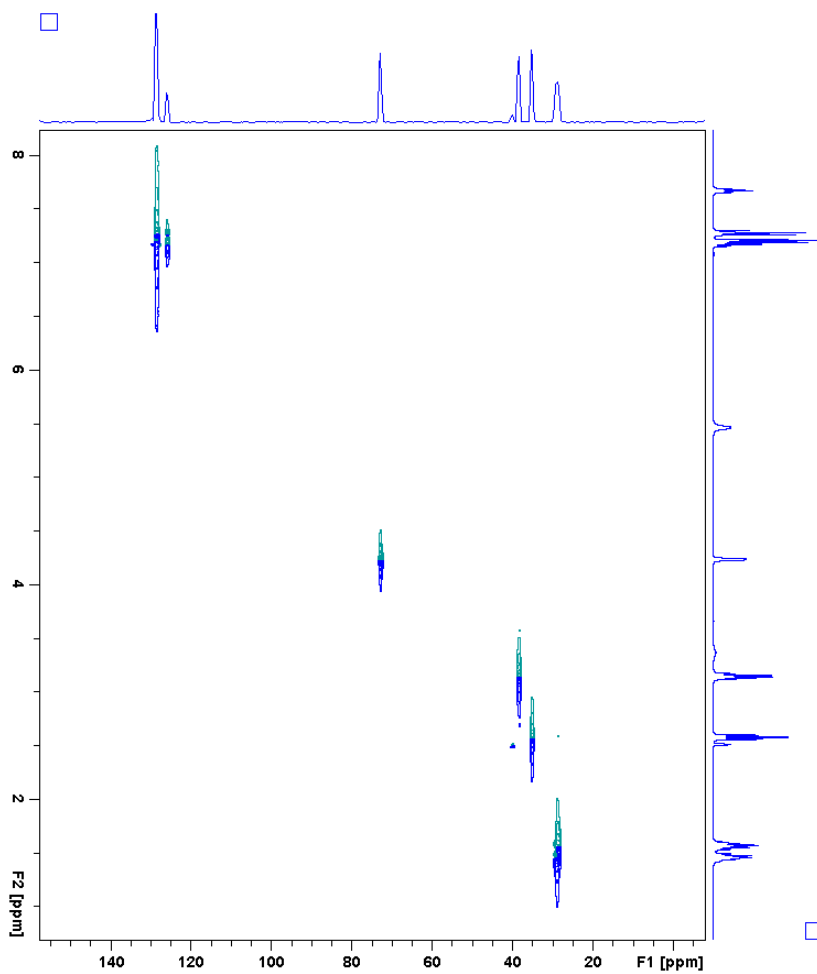


Figure A.7 HSQC spectra of (S,S)-3.

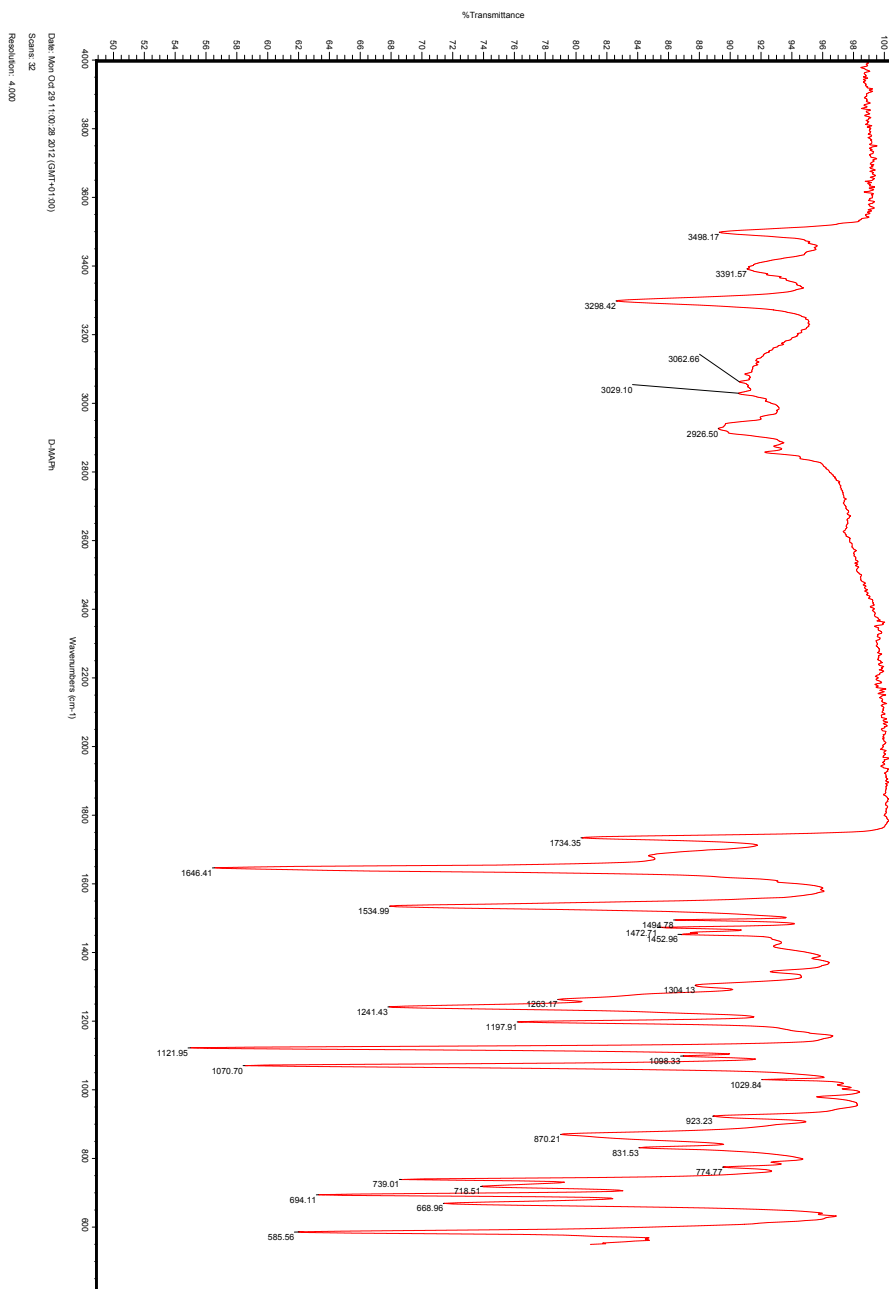


Figure A.8 IR spectra of (S,S)-3.

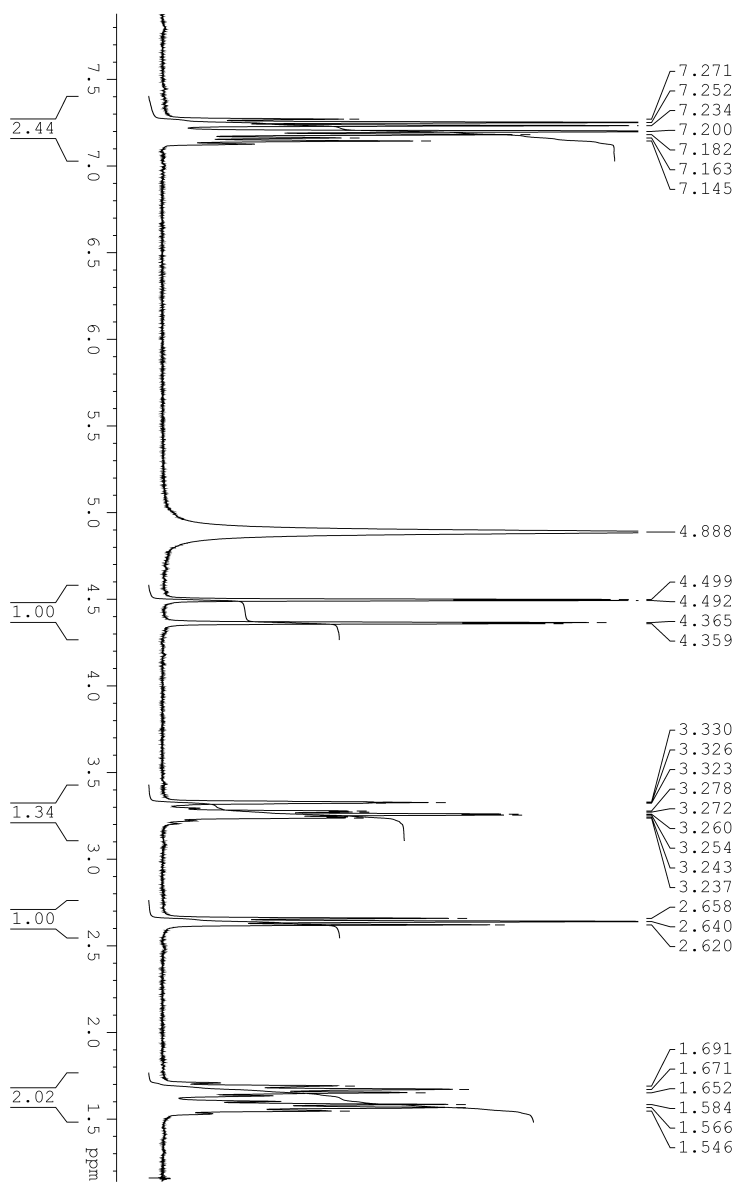


Figure A.9 ^1H NMR spectra of (R^*,S^*) -3.

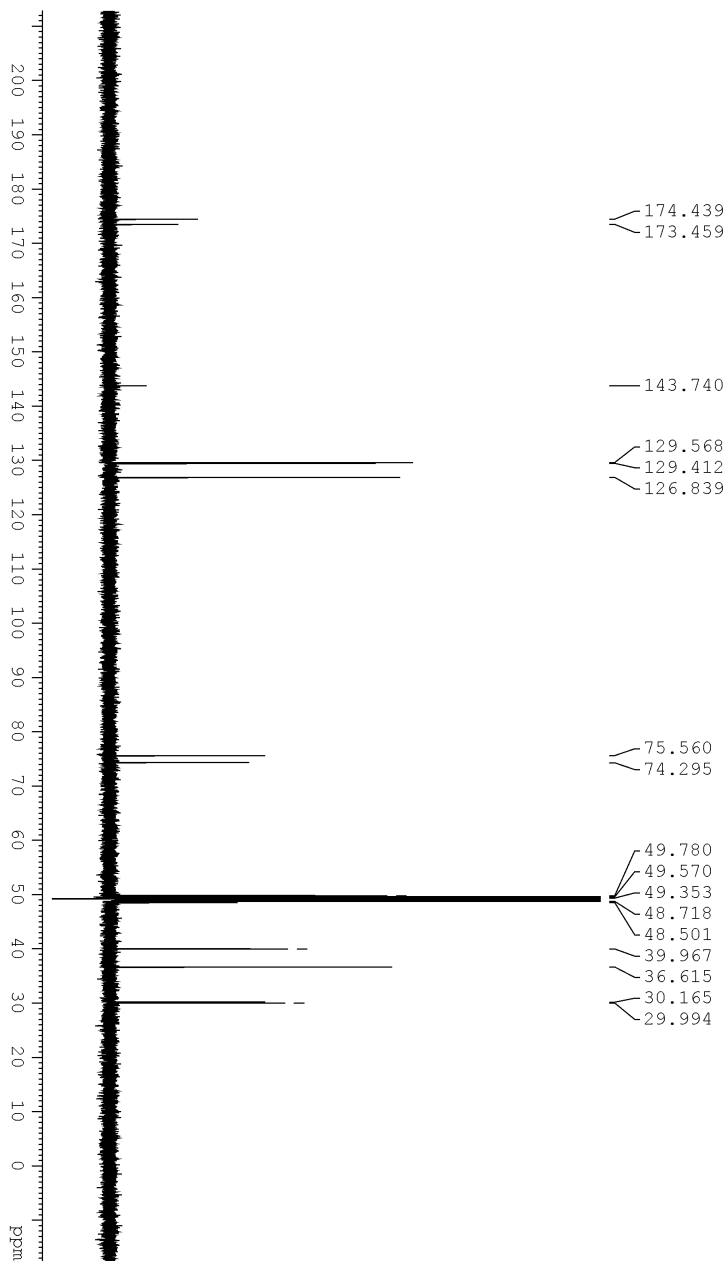


Figure A.10 ^{13}C NMR spectra of $(R^*,S^*)\text{-3}$.

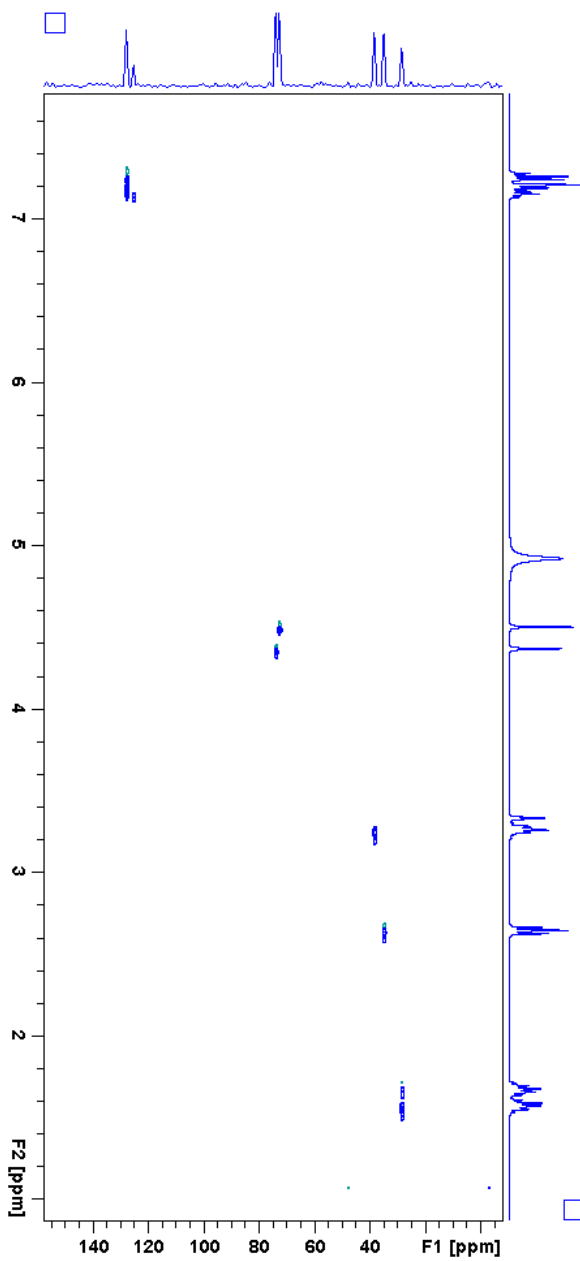


Figure A.11 HSQC spectra of (R^*,S^*) -3.

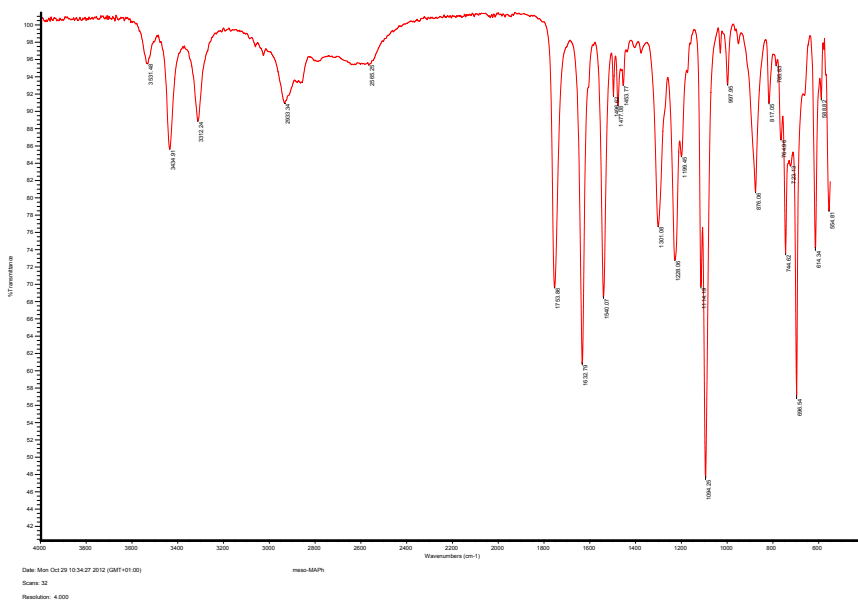


Figure A.12 IR spectra of (R*,S*)-3.

B. Spectroscopic data for 27

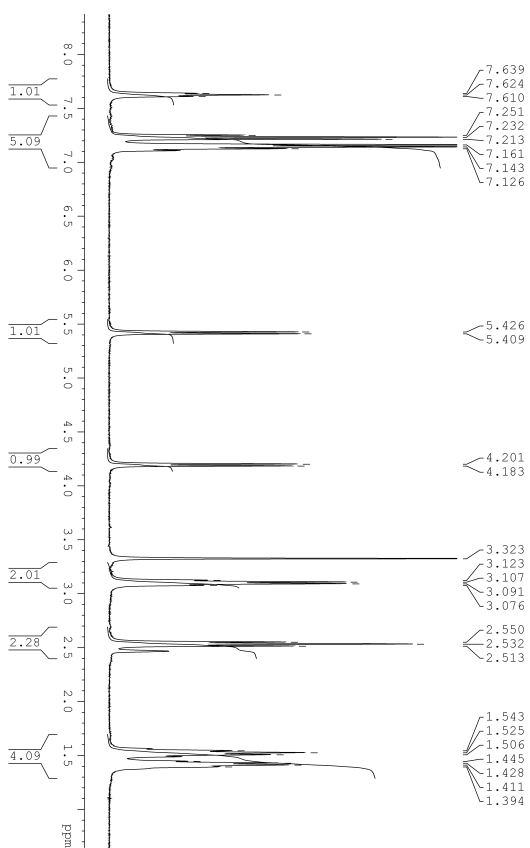


Figure B.1 ^1H NMR spectra of (R,R) -27.

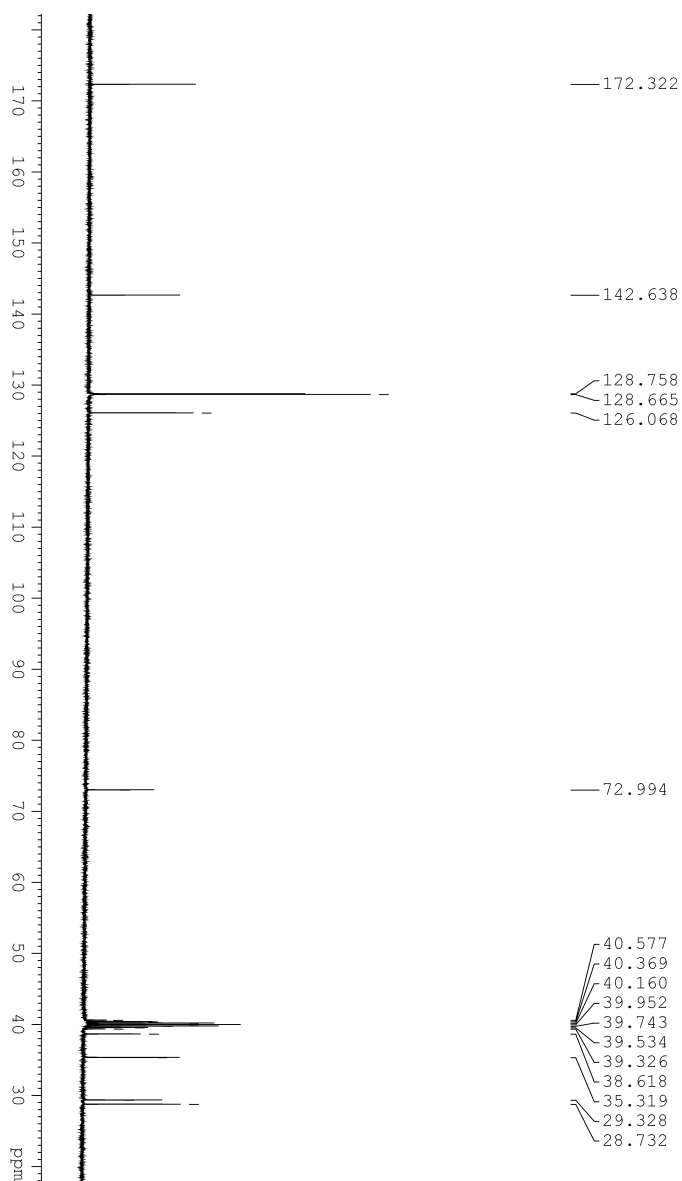


Figure B.2 ^{13}C NMR spectra of (R,R) -27.

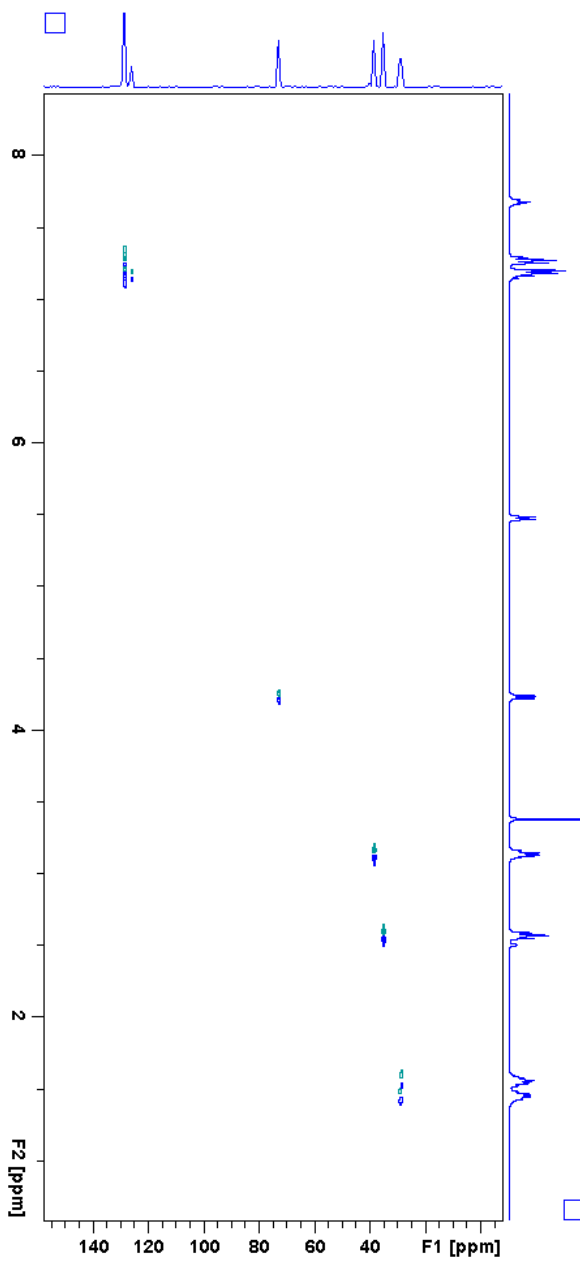


Figure B.3 HSQC spectra of (*R,R*)-27.

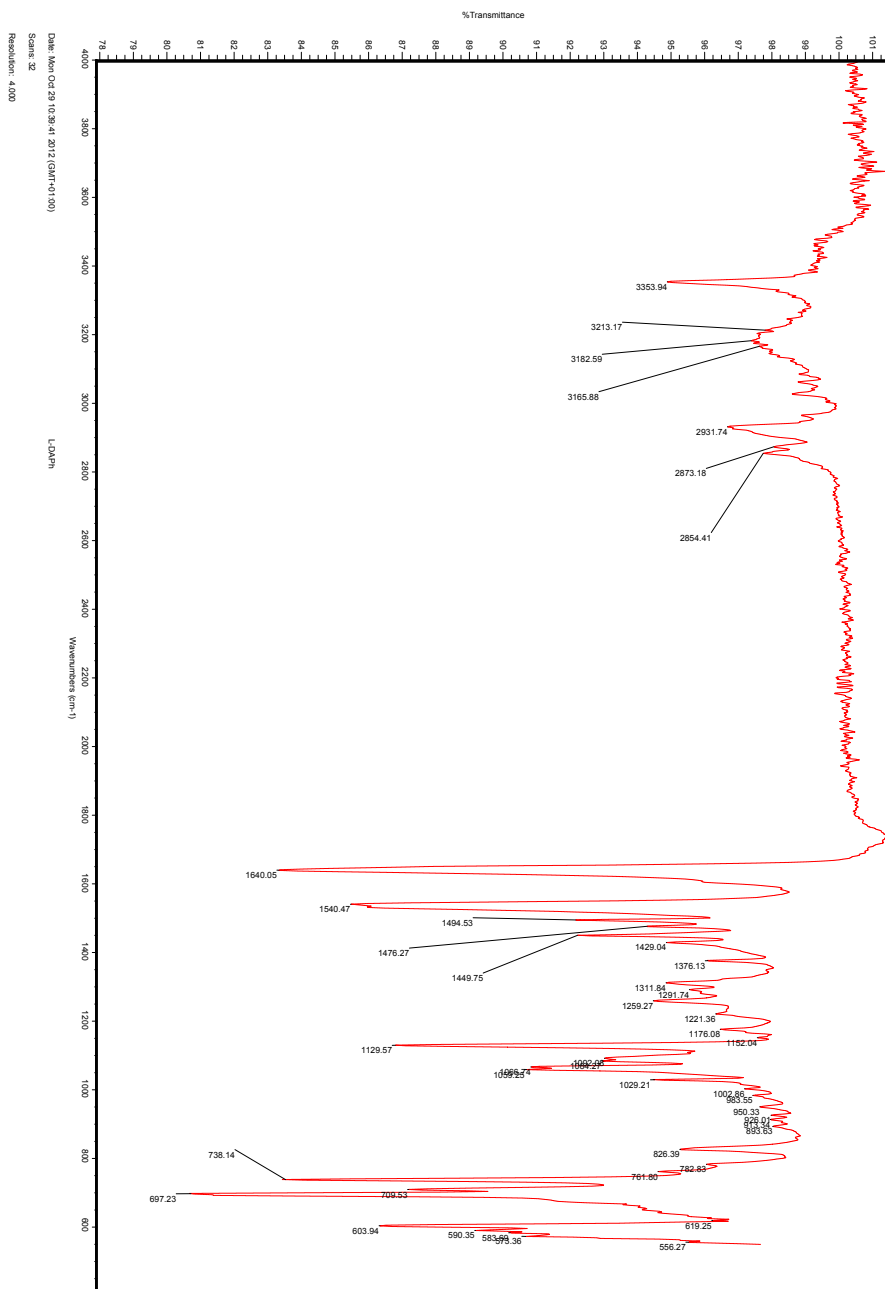


Figure B.4 IR spectra of (R,R)-27.

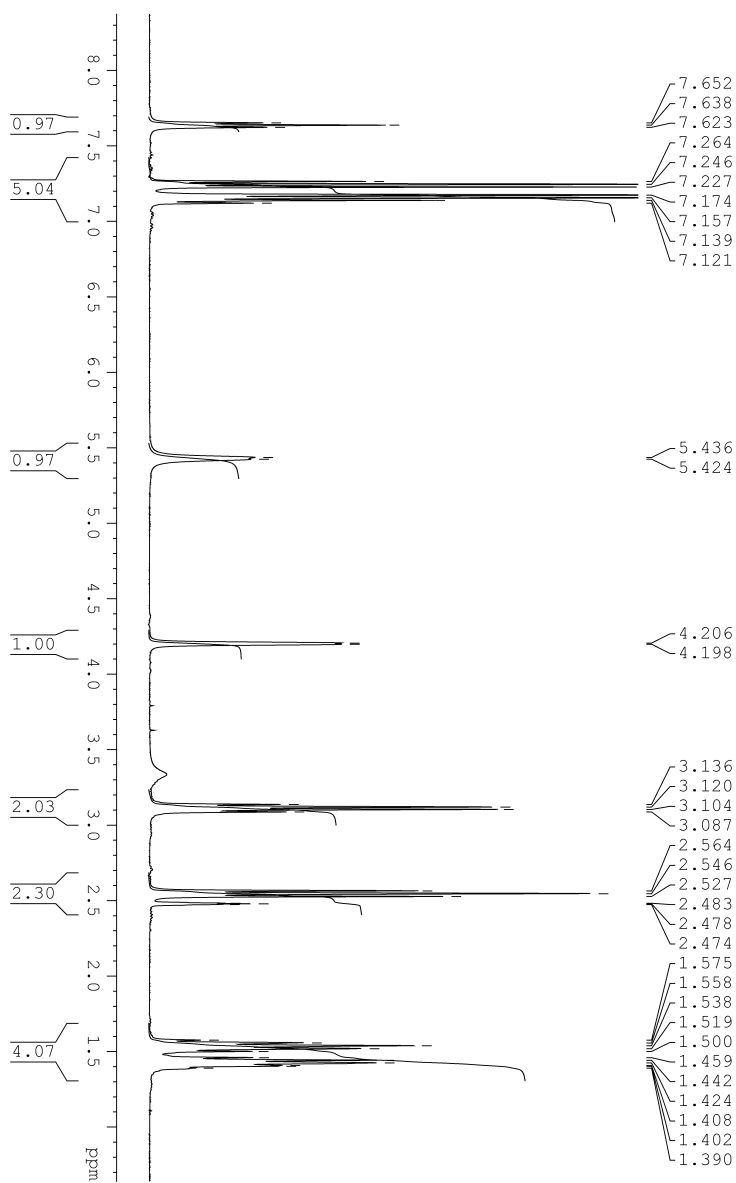


Figure B.5 ^1H NMR spectra of (S,S) -27.

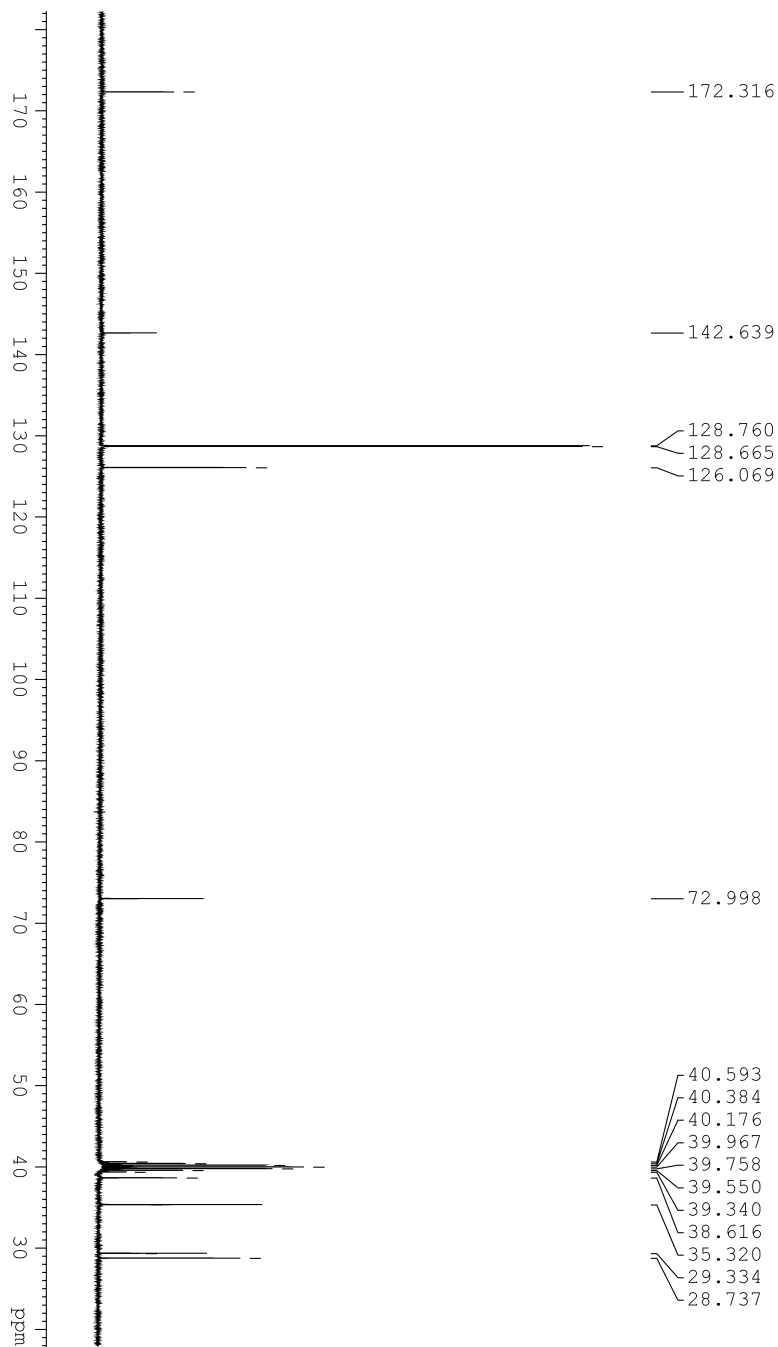


Figure B.6 ^{13}C NMR spectra of (*S,S*)-27.

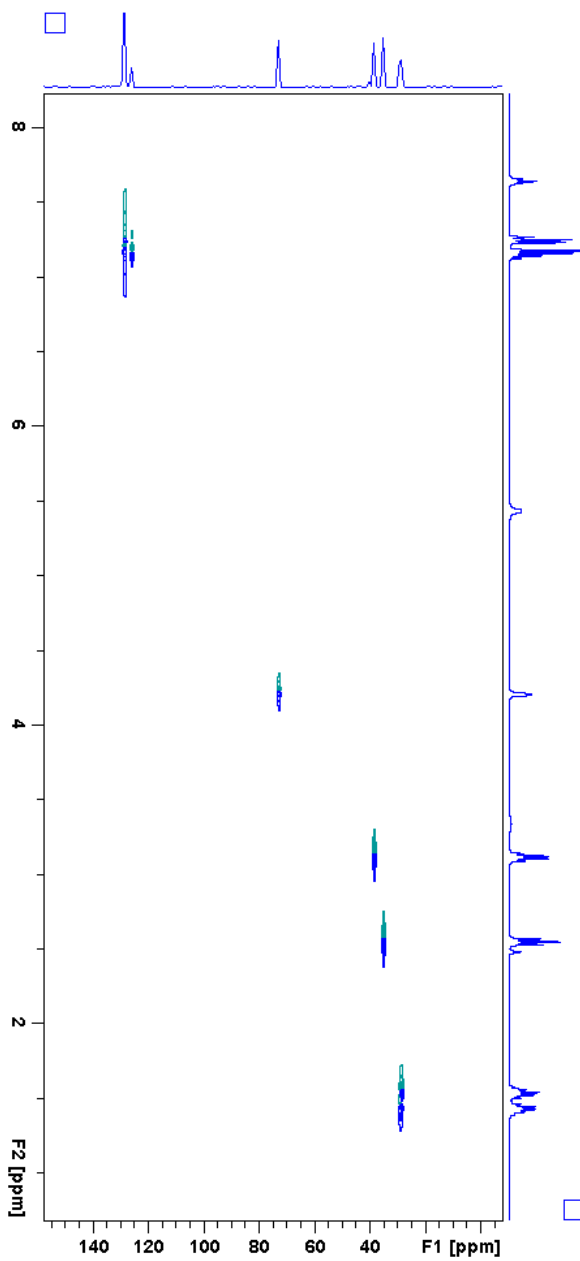


Figure B.7 HSQC spectra of (*S,S*)-27.

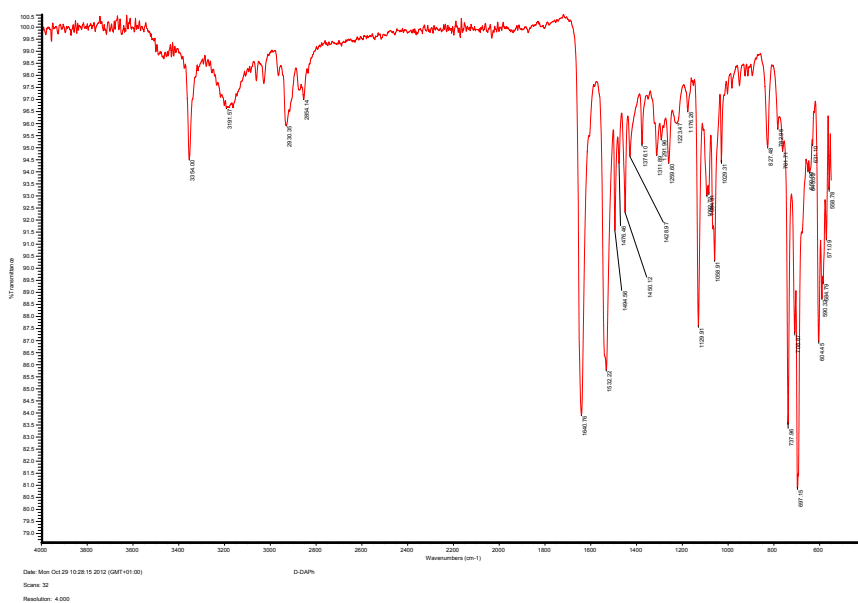


Figure B.8 IR spectra of (S,S)-27.

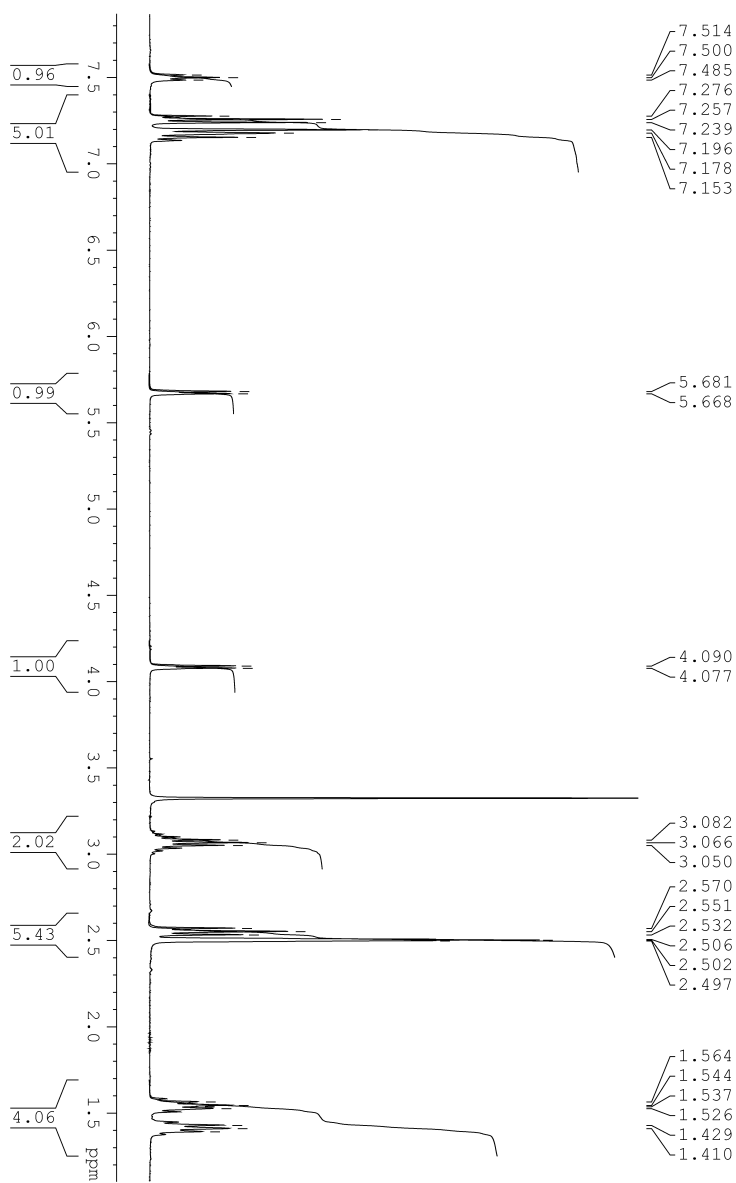


Figure B.9 ¹H NMR spectra of (*R*^{*},*S*^{*})-**27**.

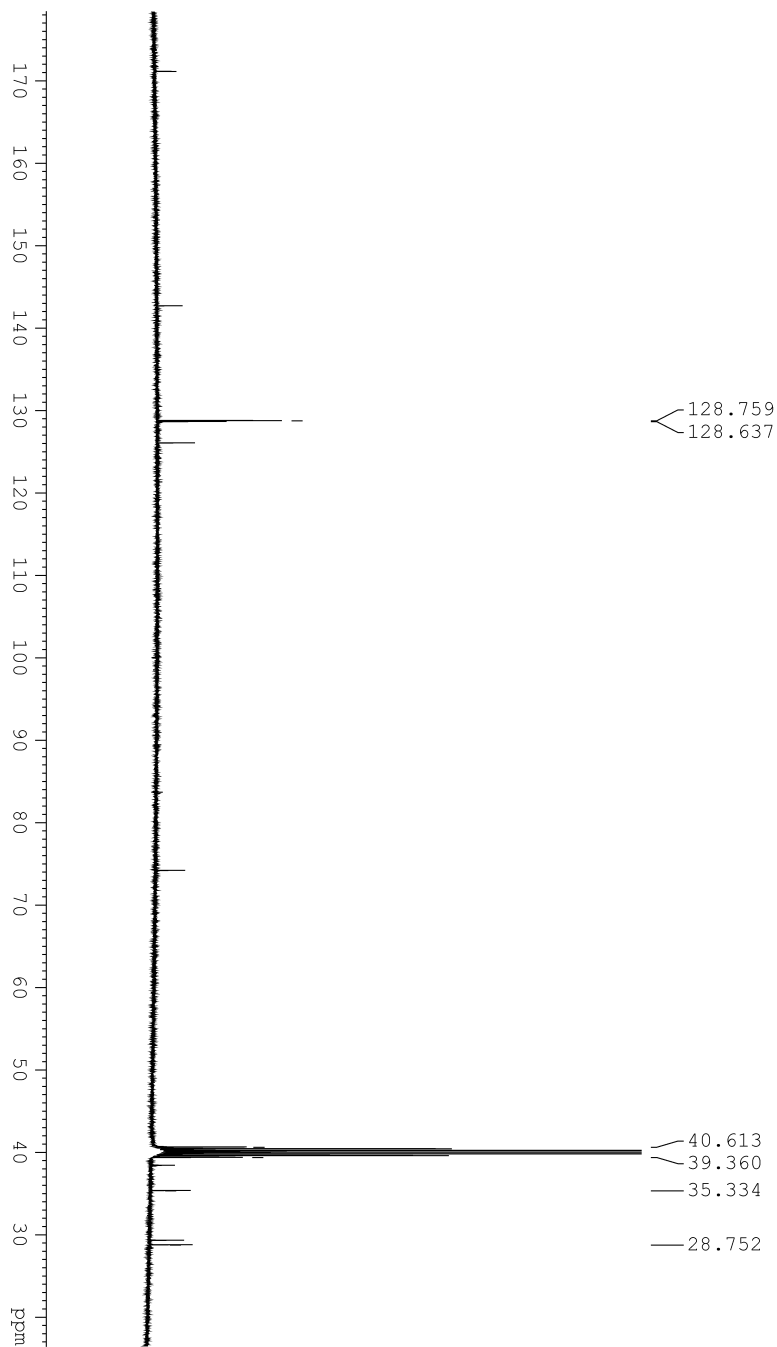


Figure B.10 ^{13}C NMR spectra of (R^*,S^*) -27.

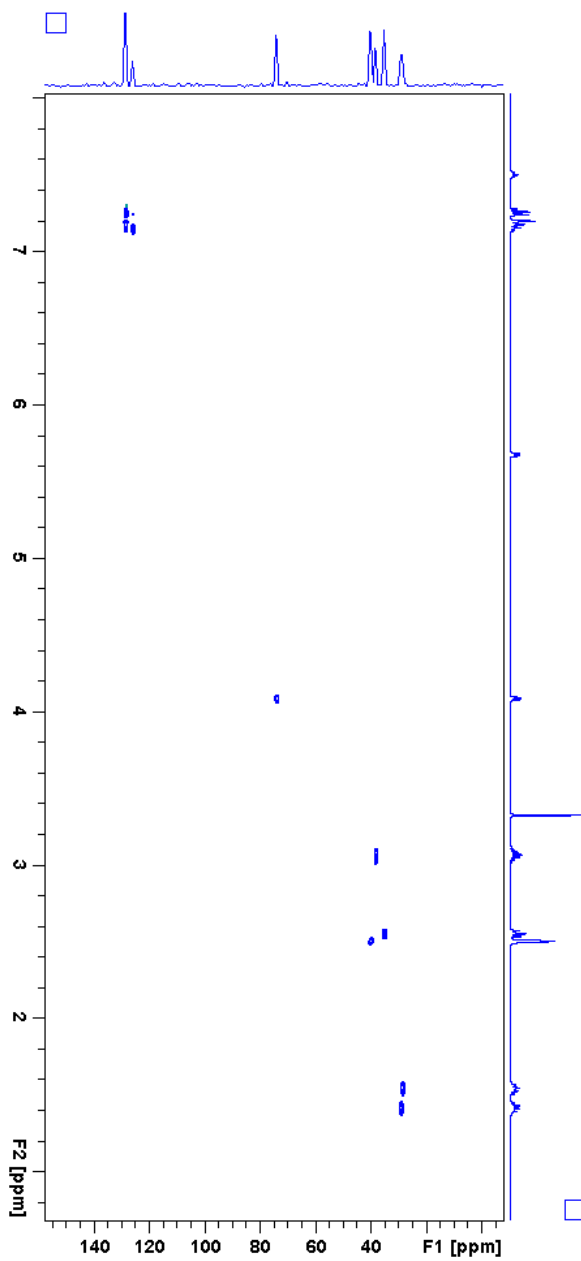


Figure B.11 HSQC spectra of (R^*,S^*) -27.

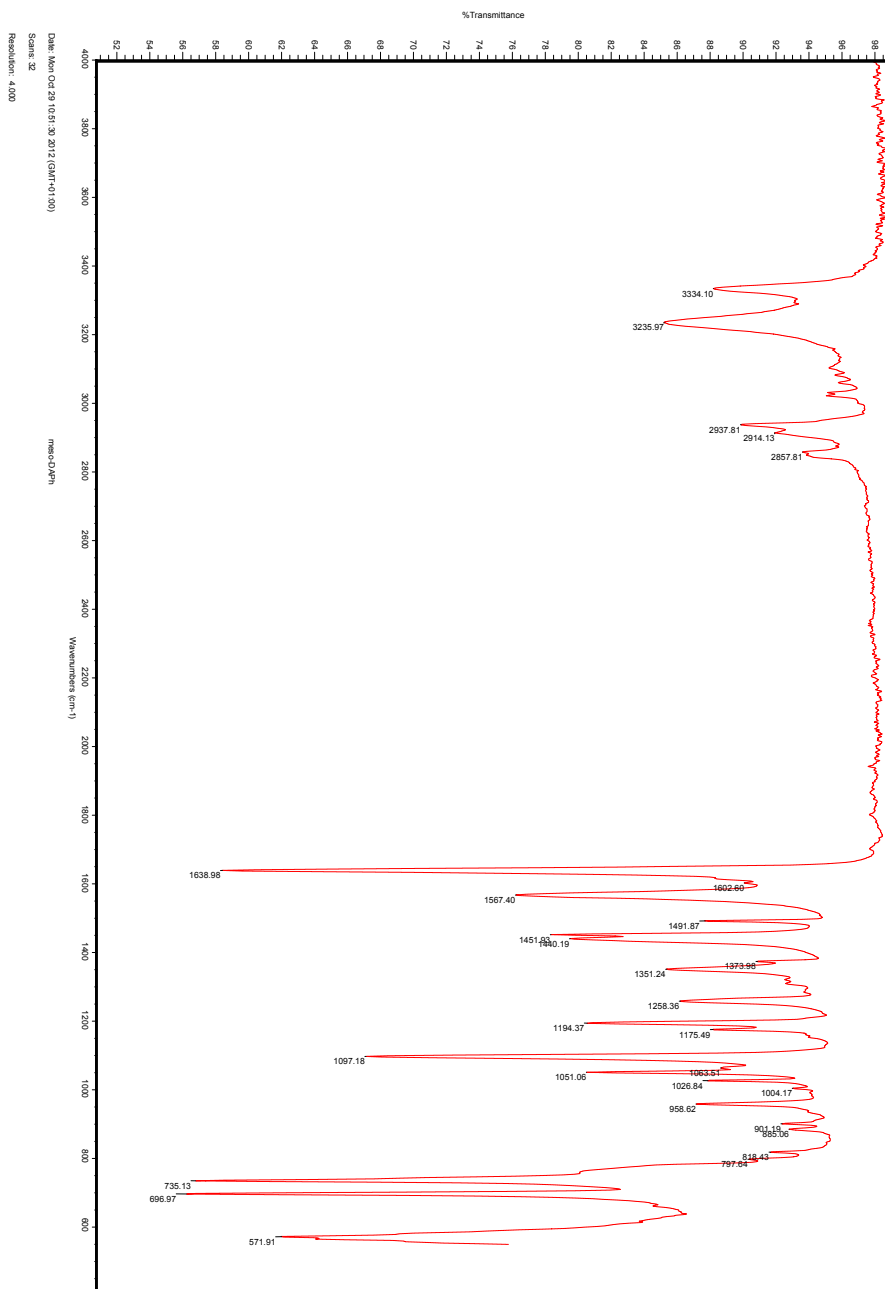


Figure B.12 IR spectra of (R^*,S^*) -27.

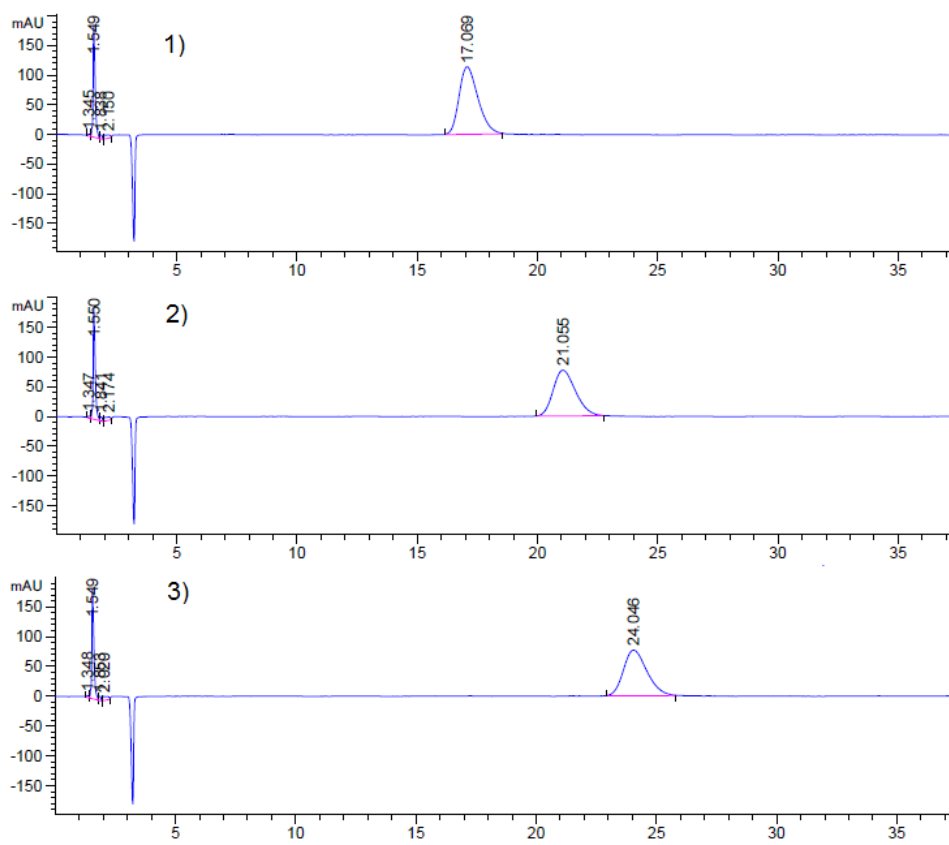


Figure B.13 HPLC chromatogram of the three diamides **27**. 1) (*R,R*) 2) (*S,S*) 3) (*R*,S**).

C. Spectroscopic data for 1

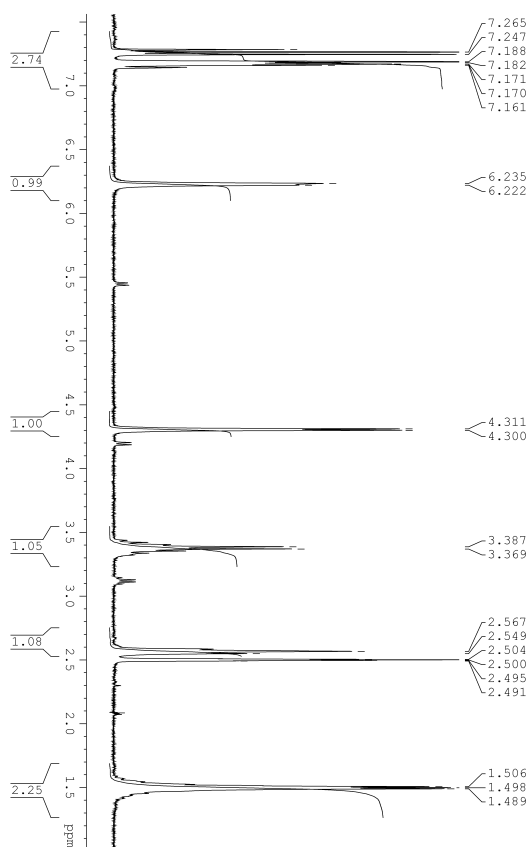


Figure C.1 ^1H NMR spectra of (R,R) -1.

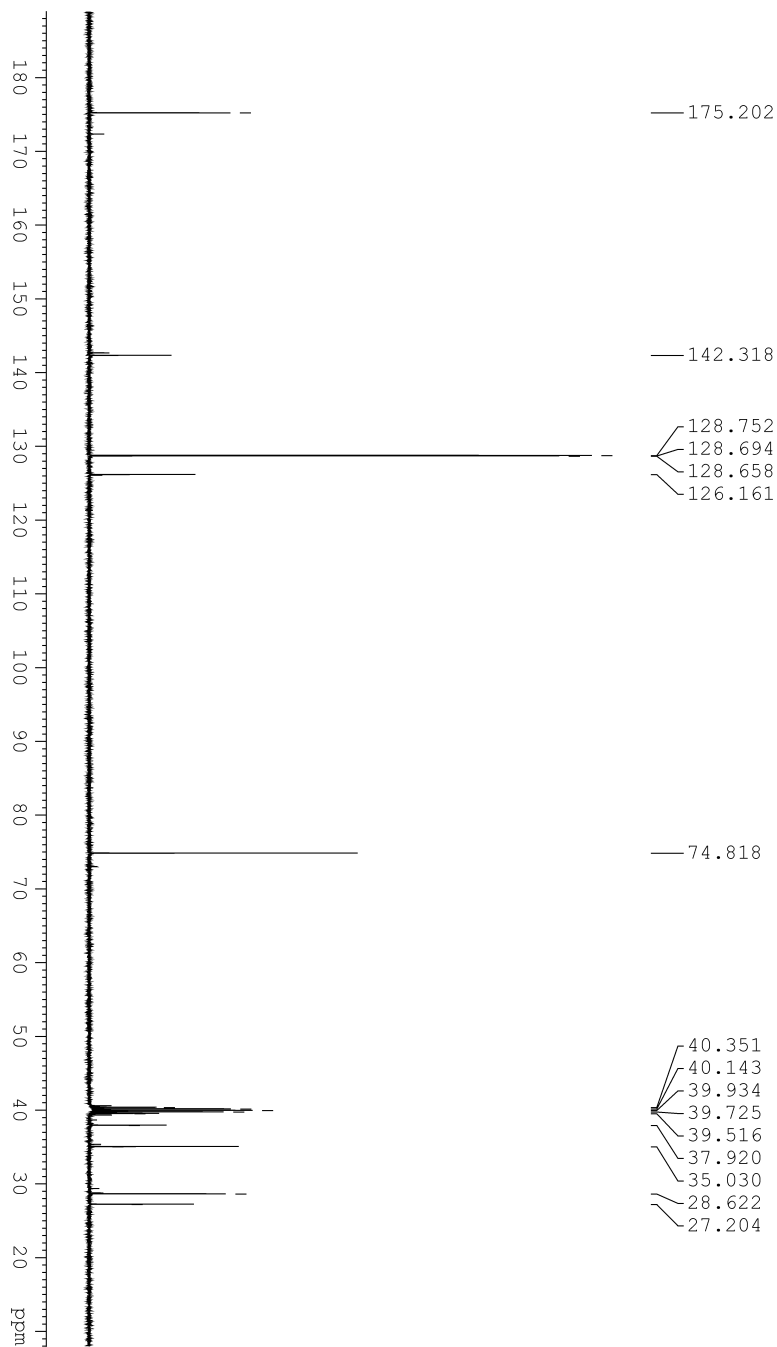


Figure C.2 ^{13}C NMR spectra of (*R,R*)-1.

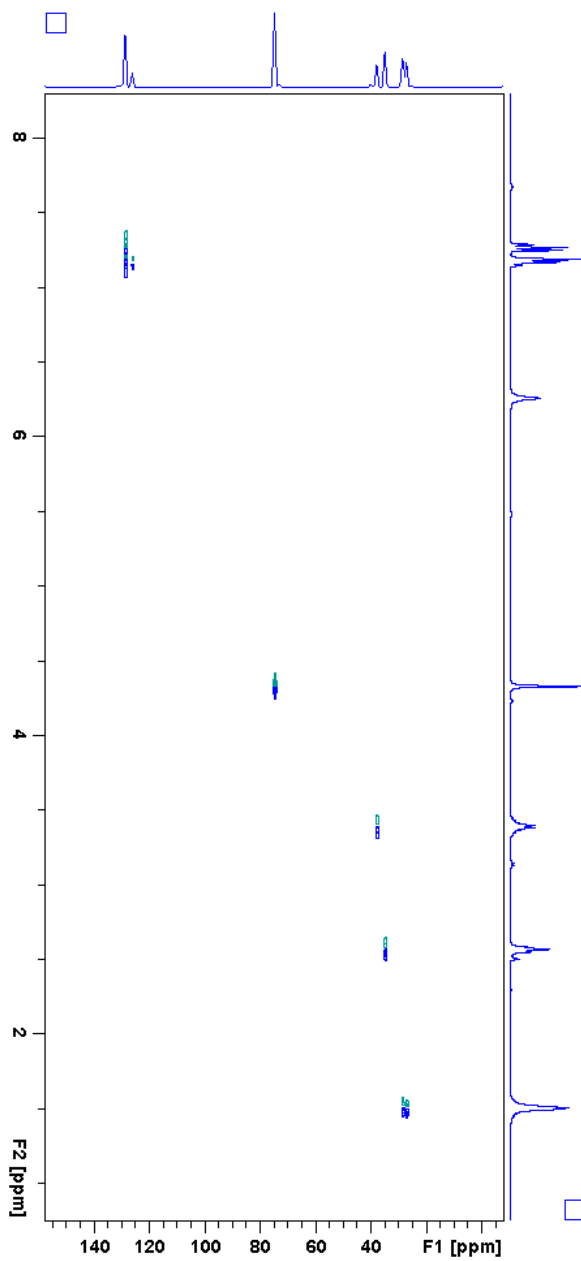


Figure C.3 HSQC spectra of (R,R) -1.

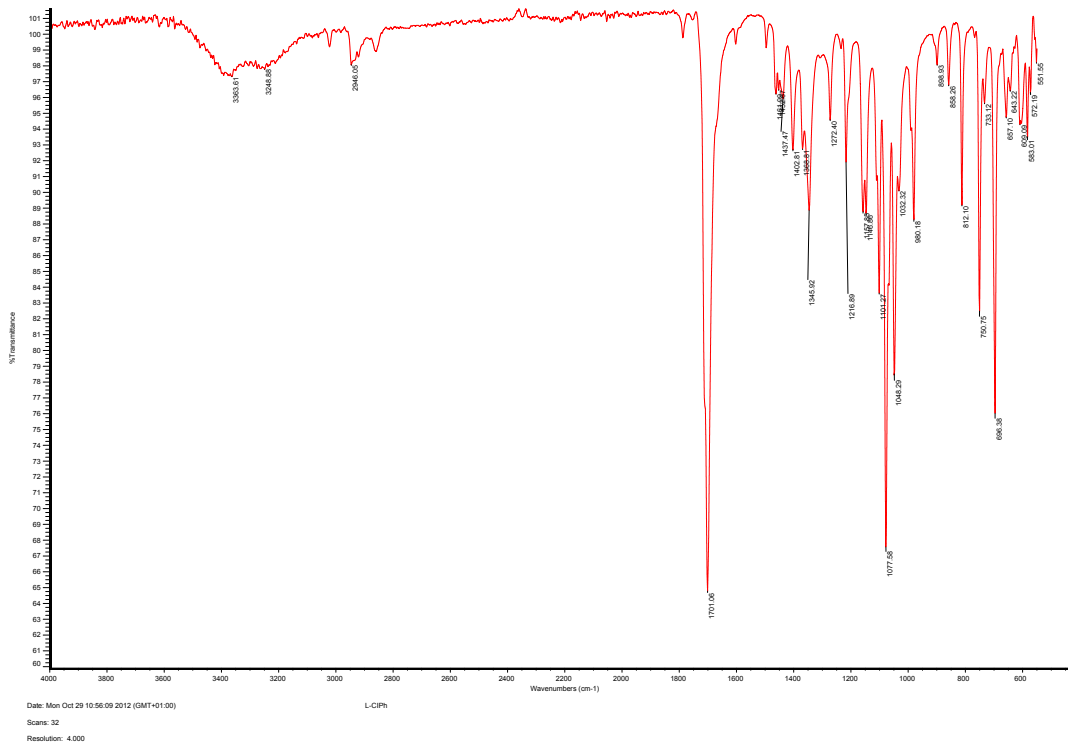


Figure C.4 IR spectra of (*R,R*)-1.

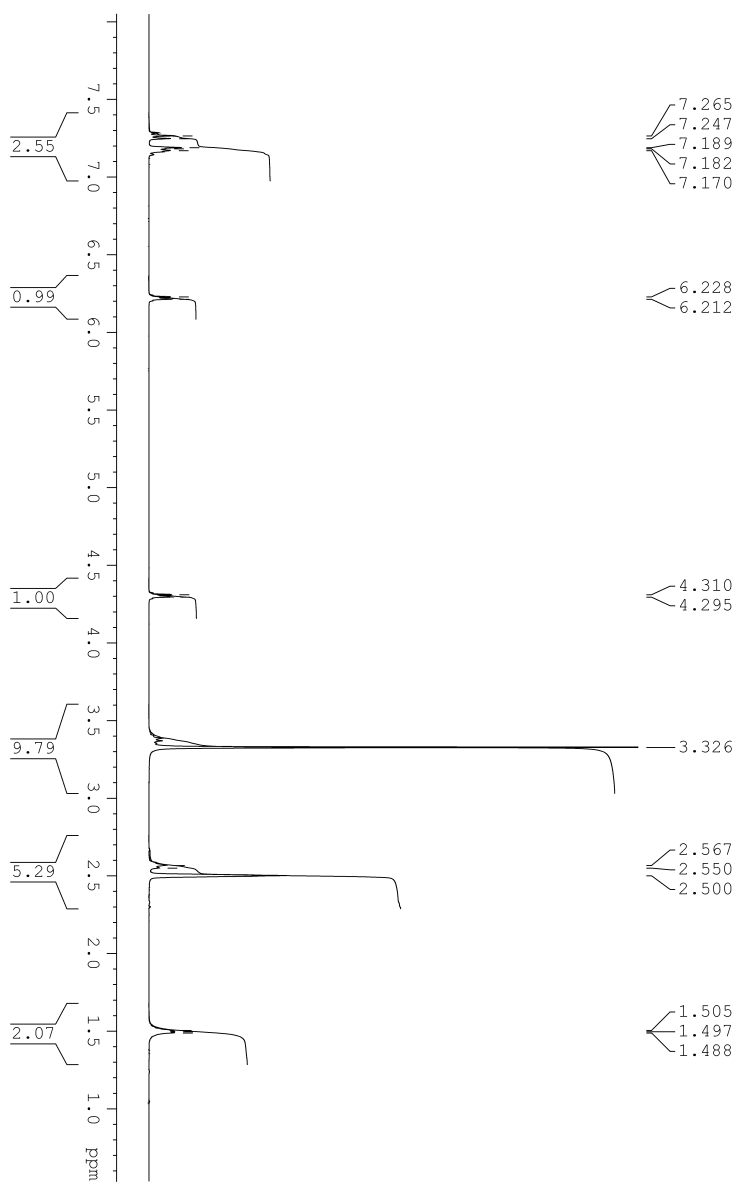


Figure C.5 ^1H NMR spectra of (S,S) -1.

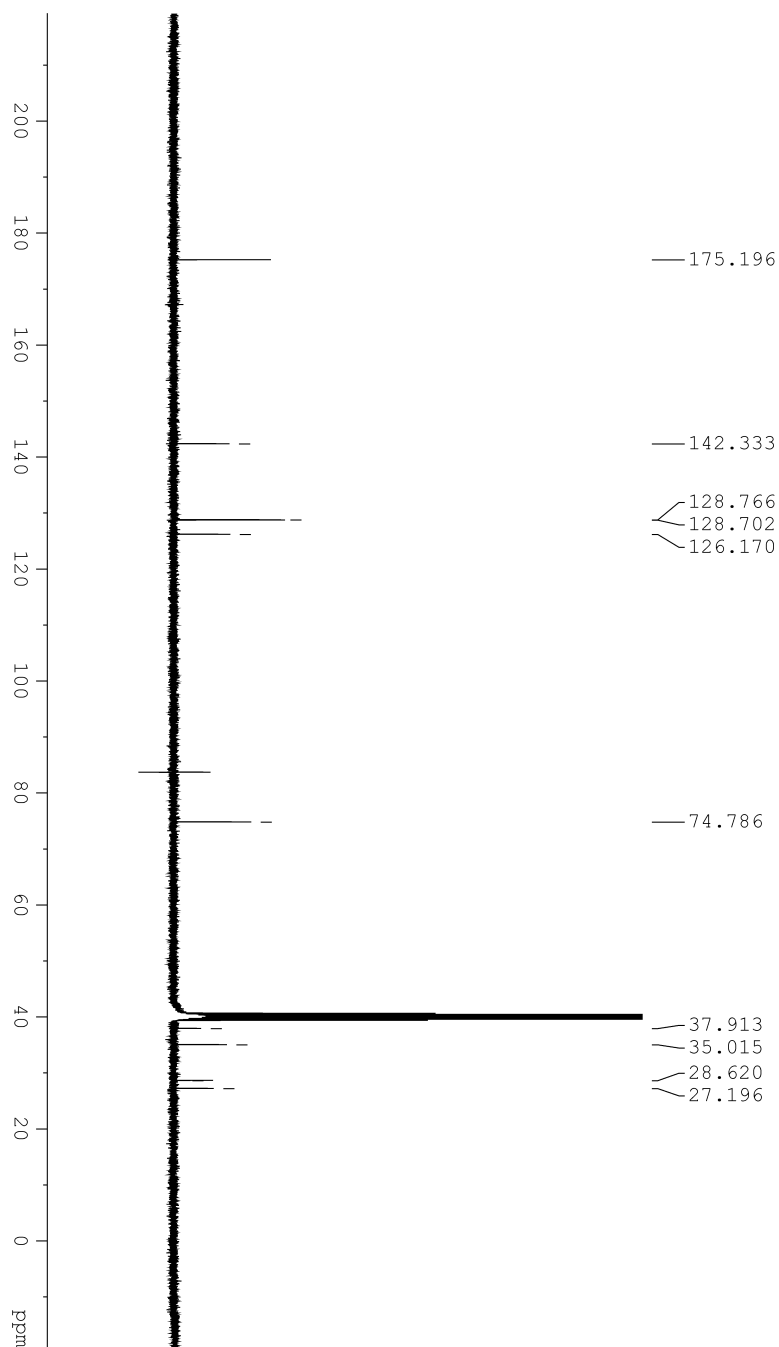


Figure C.6 ^{13}C NMR spectra of (*S,S*)-1.

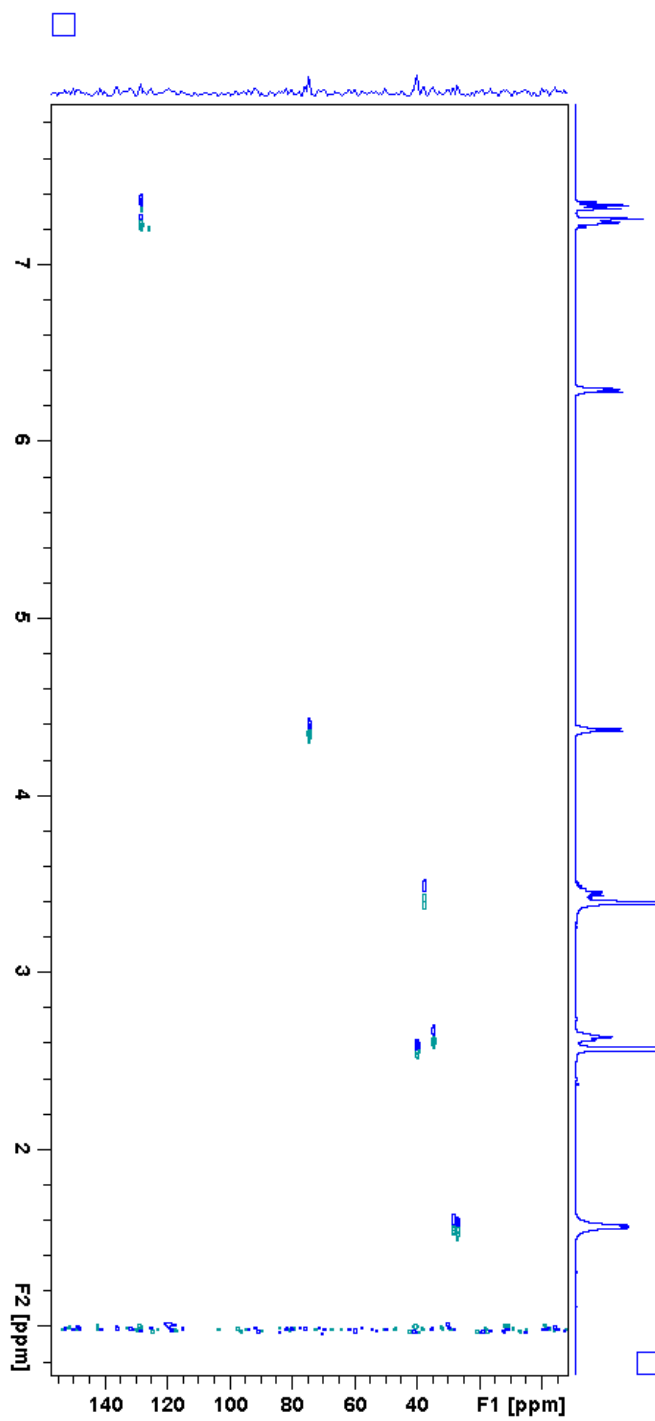


Figure C.7 HSQC spectra of (S,S)-1.

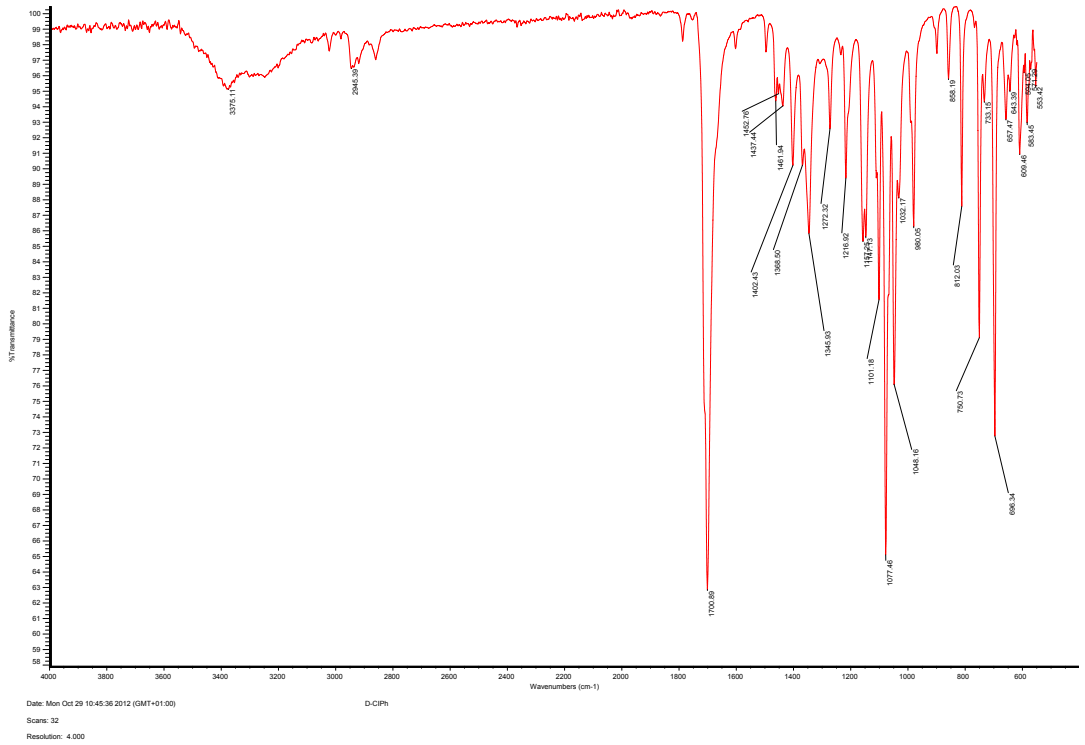


Figure C.8 IR spectra of (*S,S*)-1.

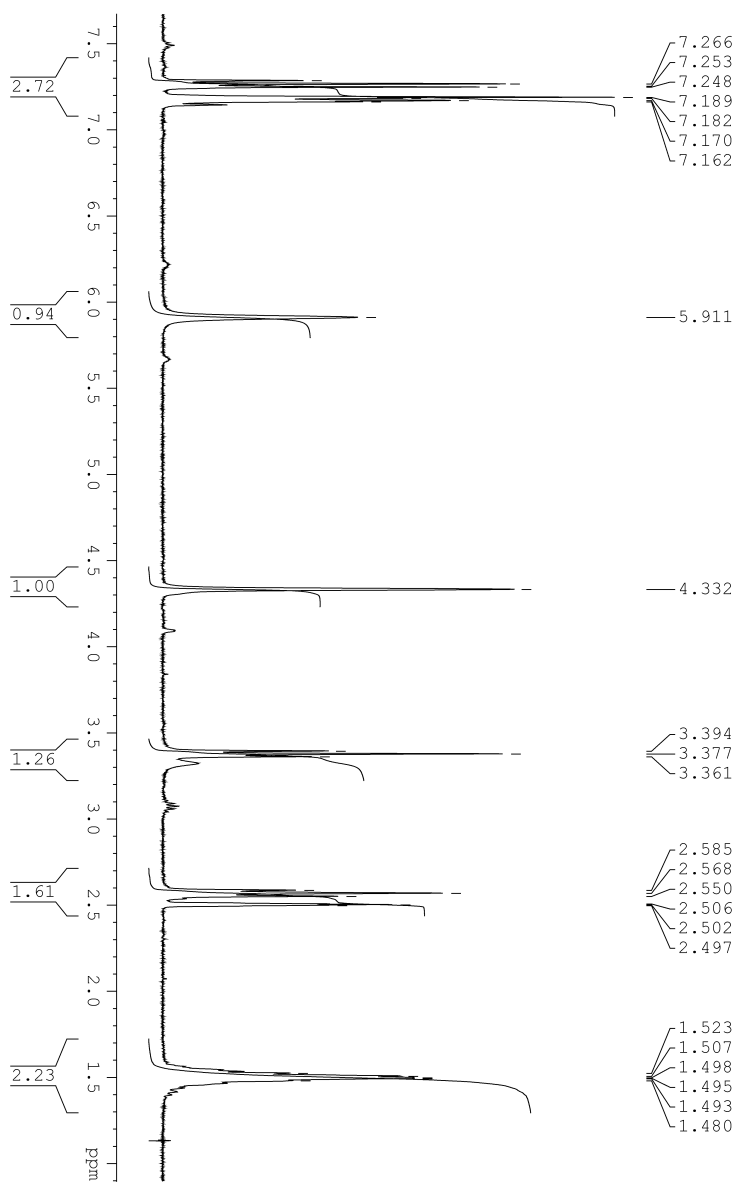


Figure C.9 ^1H NMR spectra of (R^*,S^*) -1.

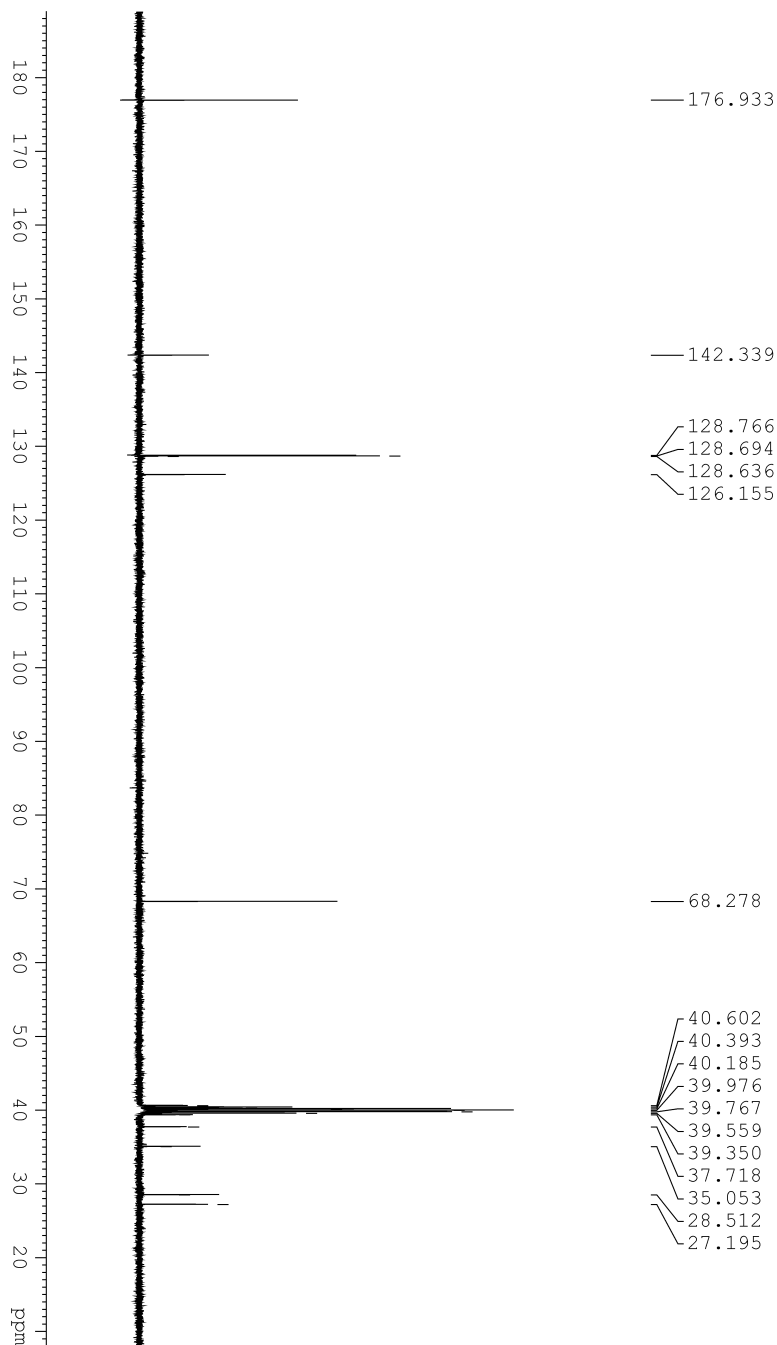


Figure C.10 ^{13}C NMR spectra of (R^*,S^*) -1.

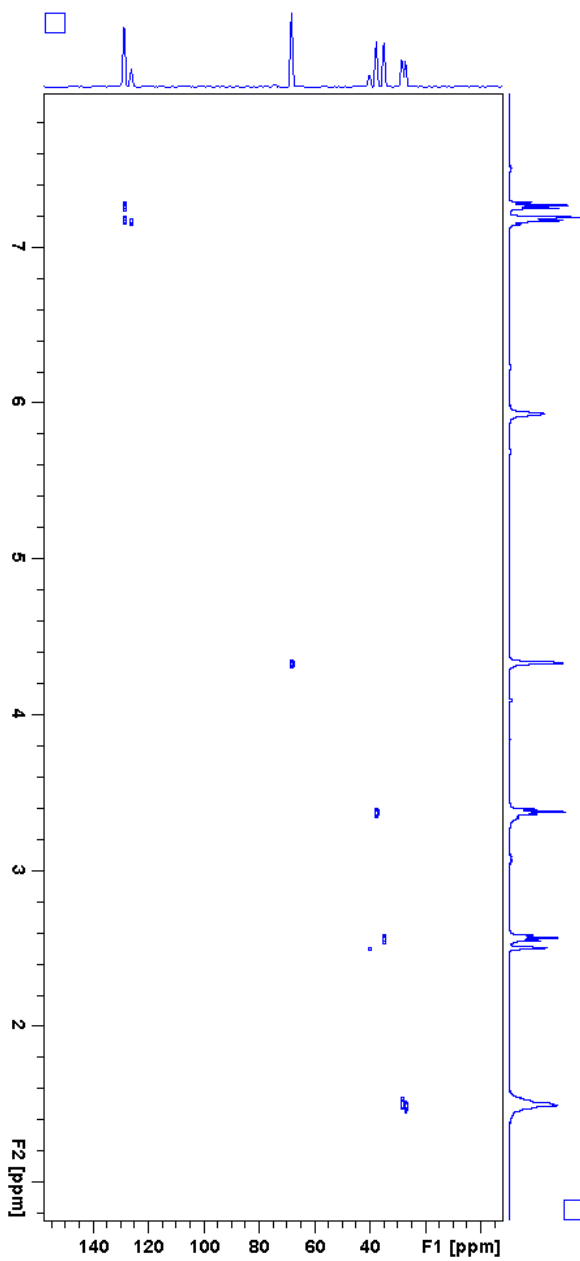


Figure C.11 HSQC spectra of (R^*,S^*) -1.

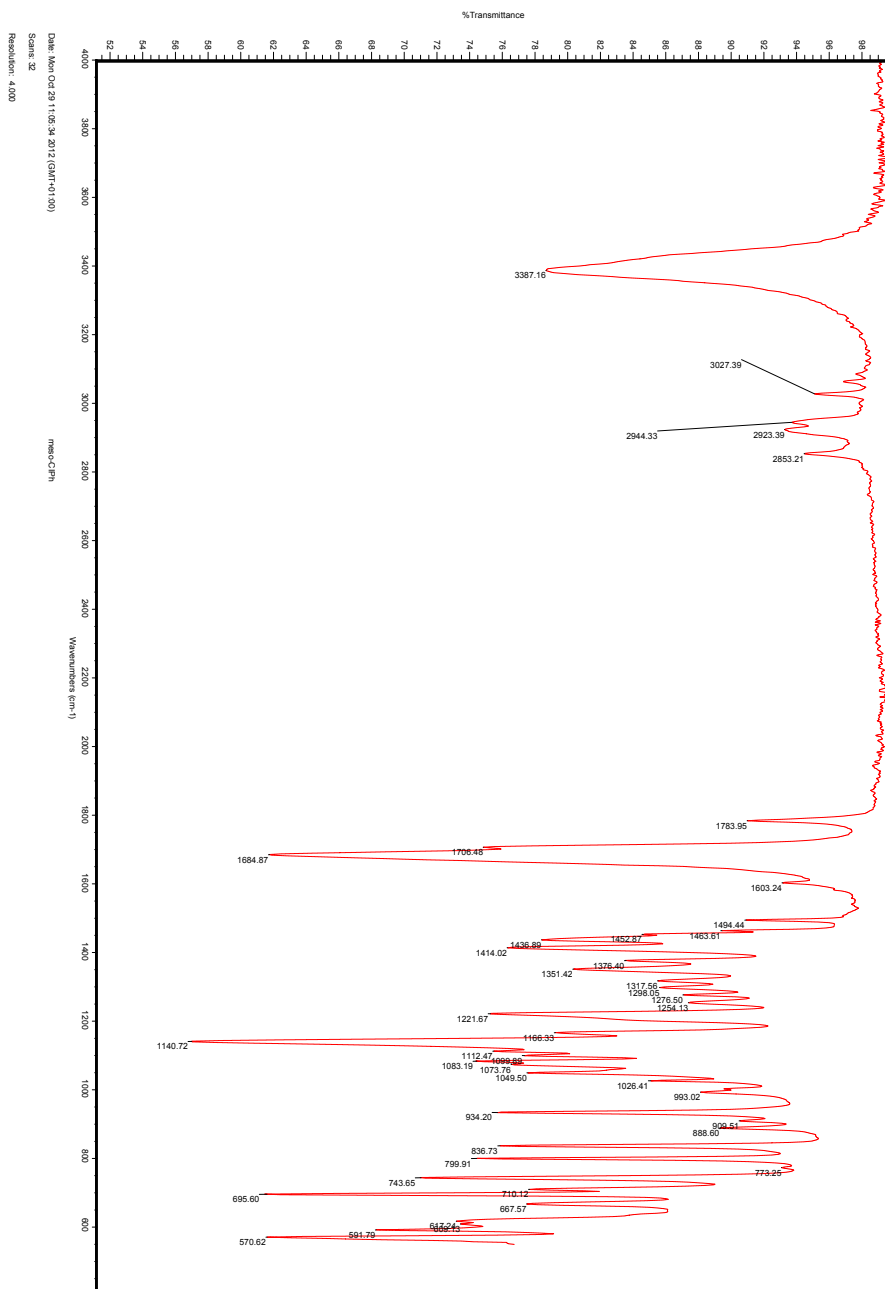


Figure C.12 IR spectra of (R^*,S^*) -1.

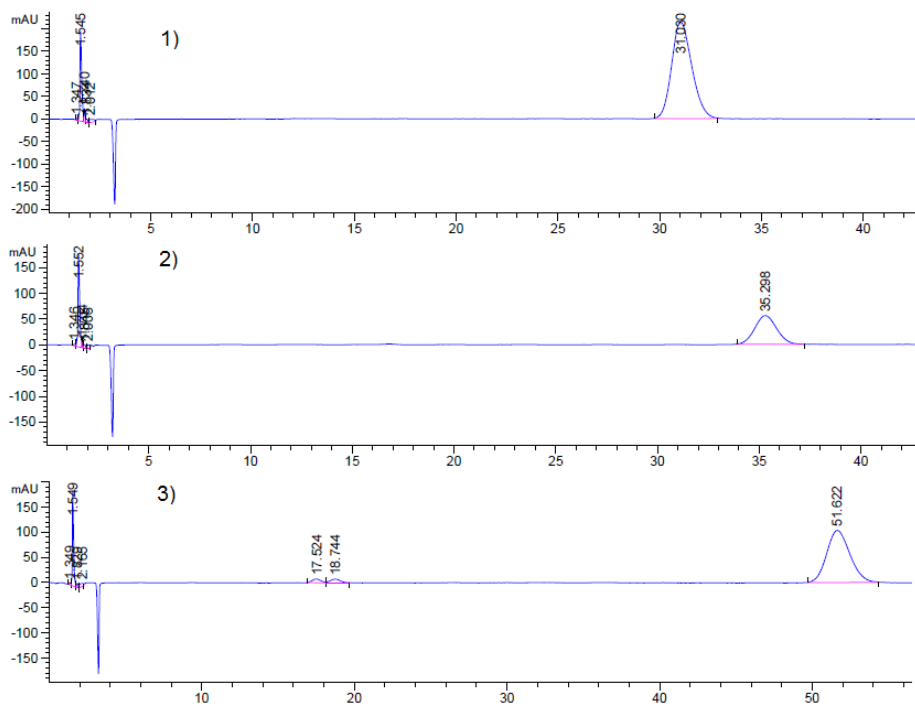


Figure C.13 HPLC chromatogram of the three imides 1. 1) (*R,R*) 2) (*S,S*) 3) (*R*,S**).

D. Spectroscopic data for 42

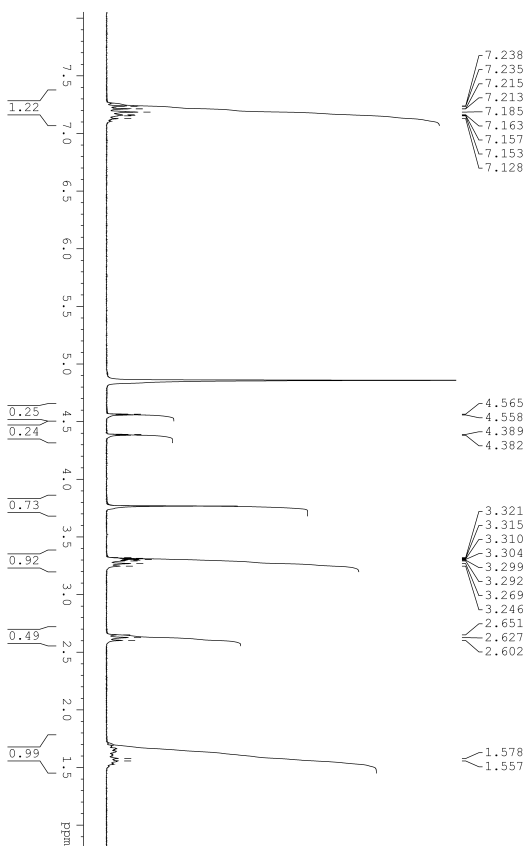


Figure D.1 ^1H NMR spectra of 42.

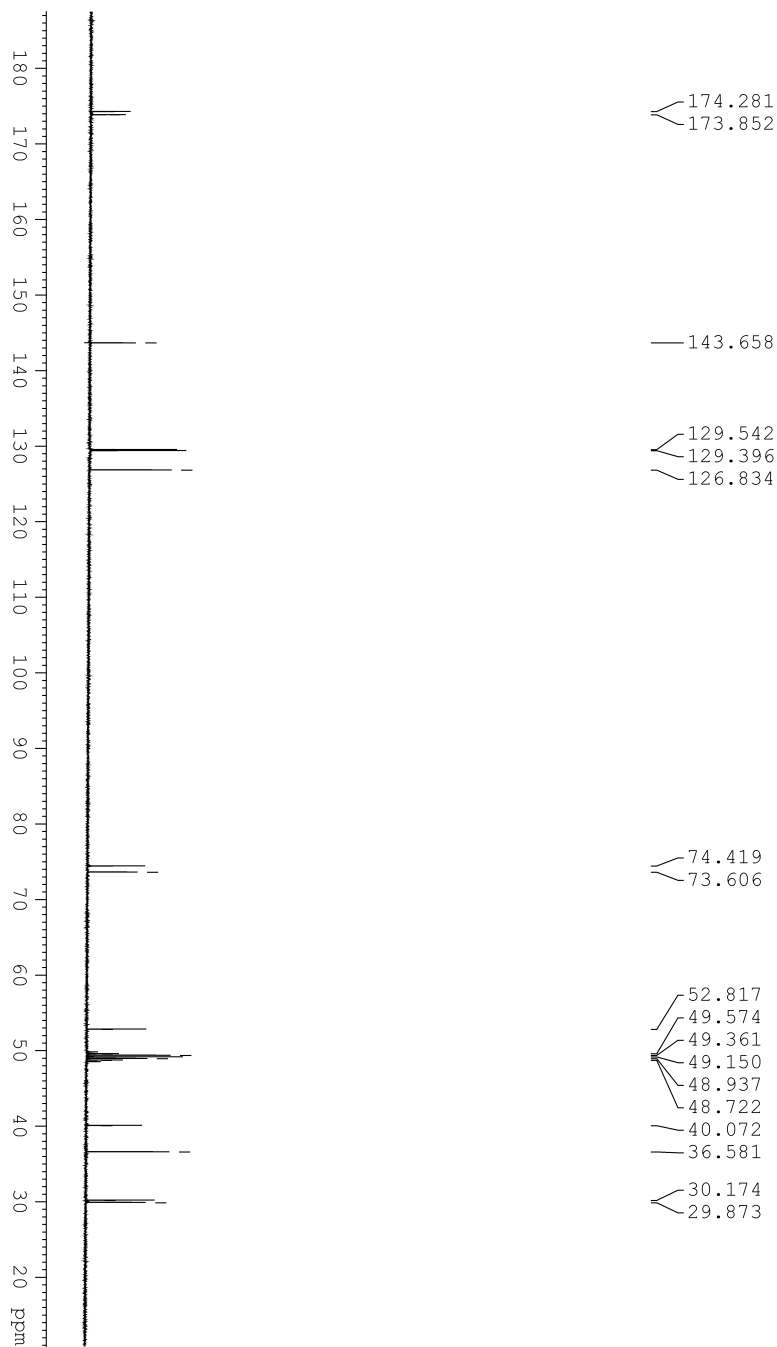


Figure D.2 ^{13}C NMR spectra of 42.

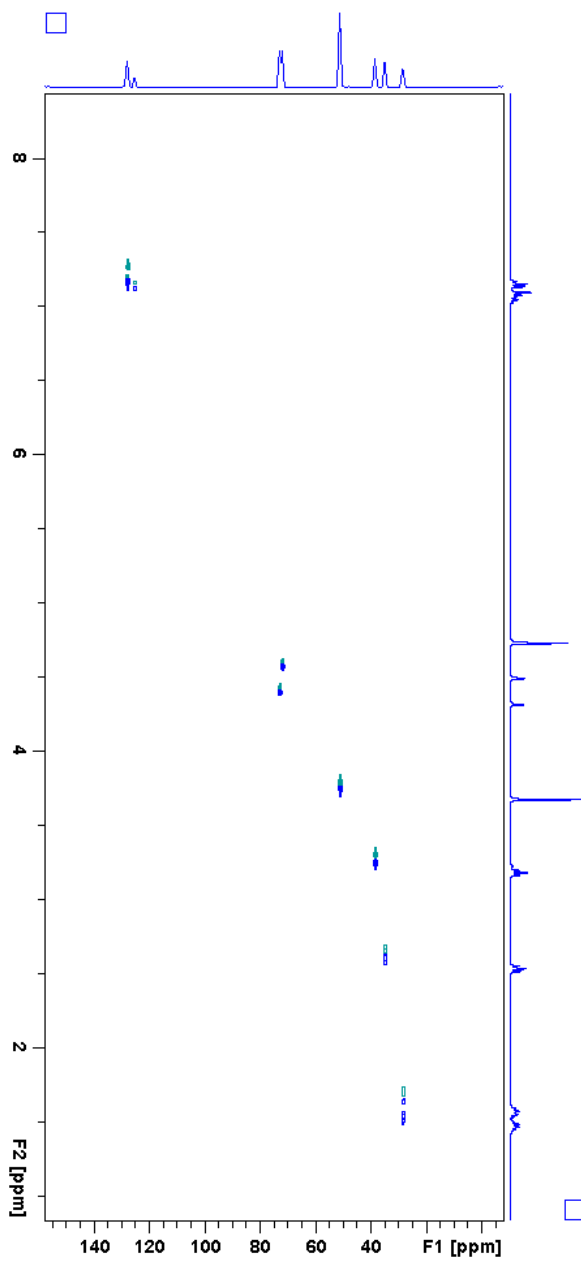


Figure D.3 HSQC spectra of 42.

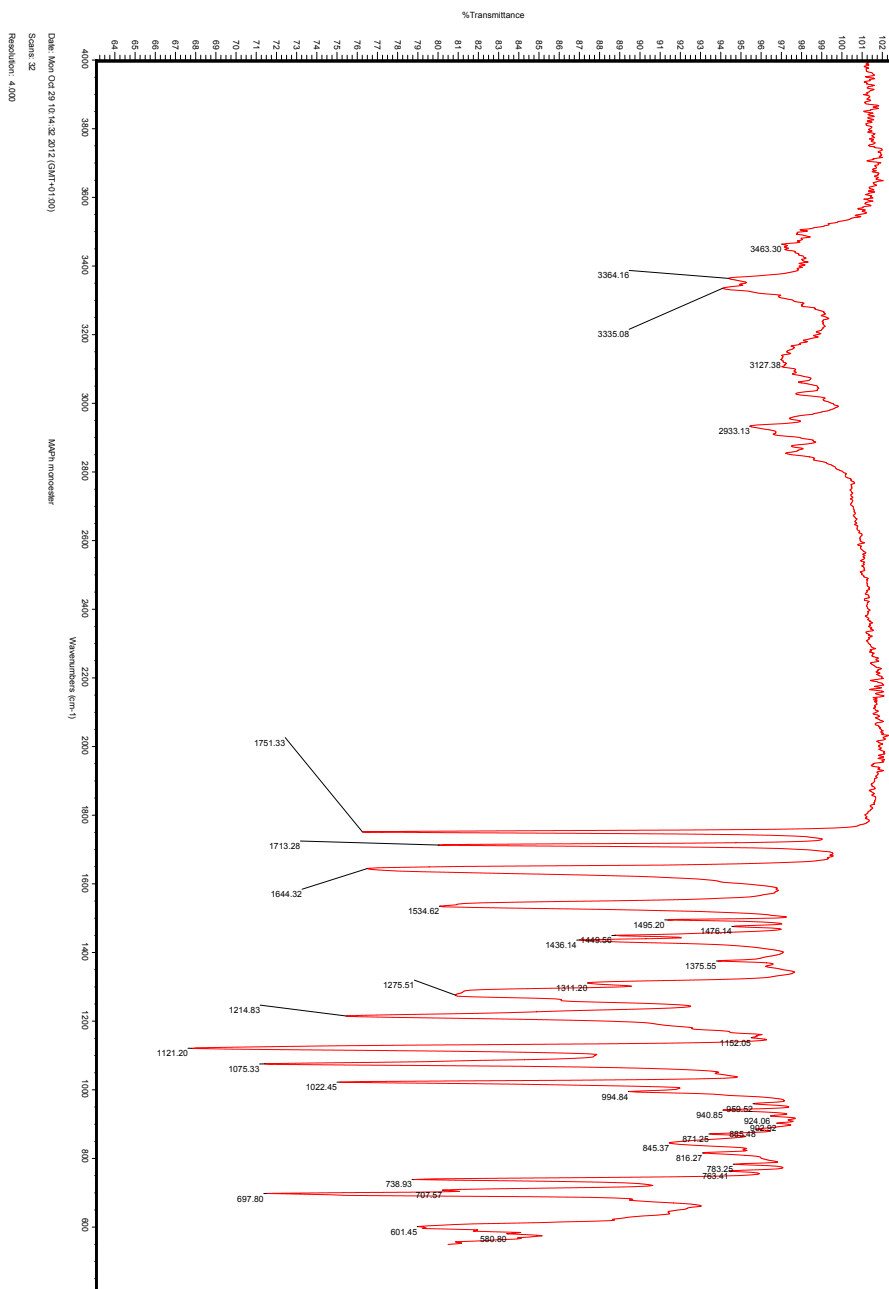


Figure D.4 IR spectra of 42.

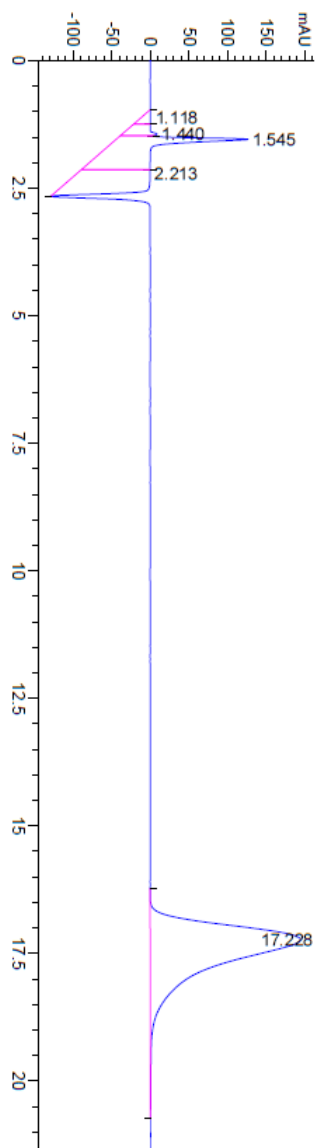


Figure D.5 HPLC chromatogram of **42**.

E. Spectroscopic data for **2**

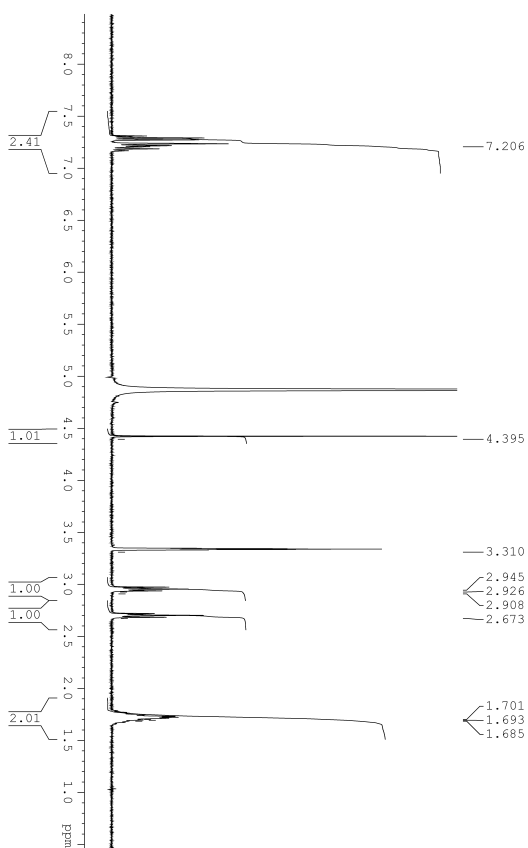


Figure E.1 ^1H NMR spectra of **2**.

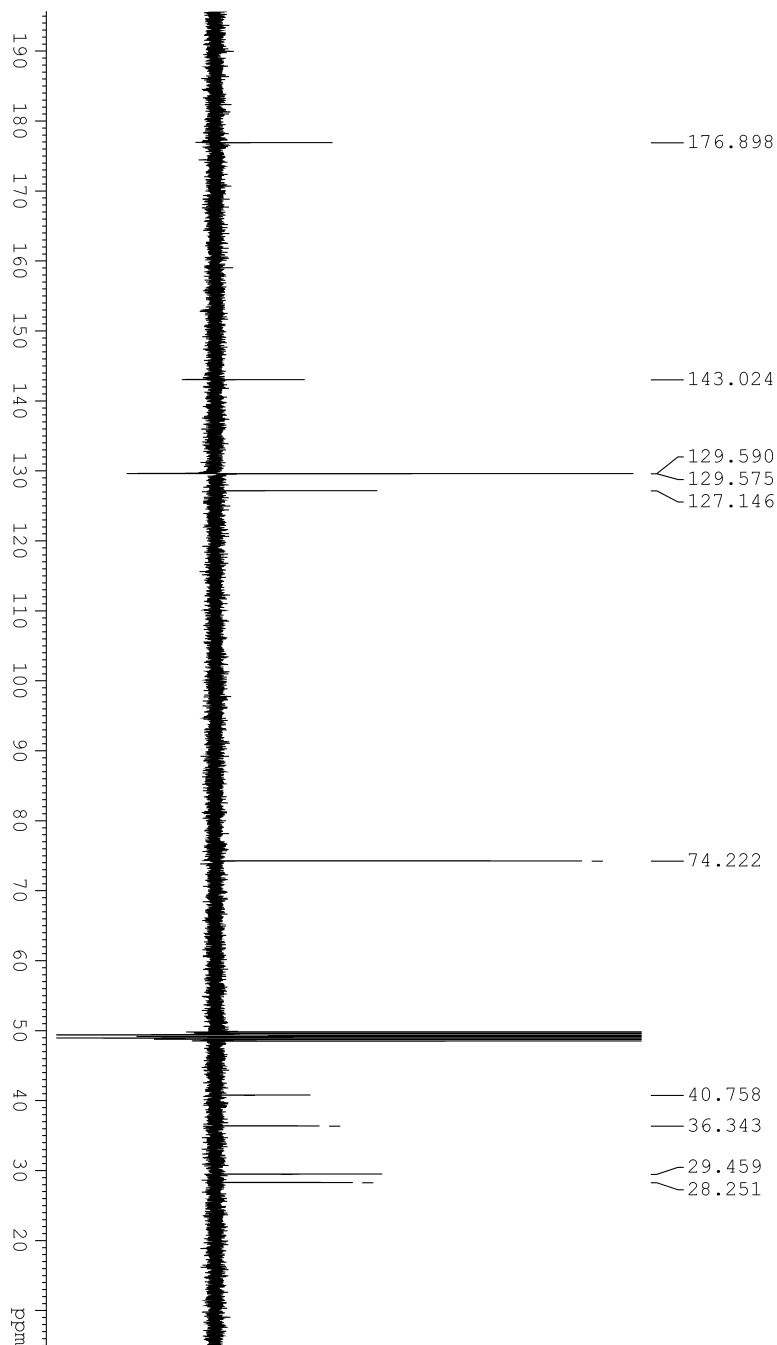


Figure E.2 ^{13}C NMR spectra of 2.

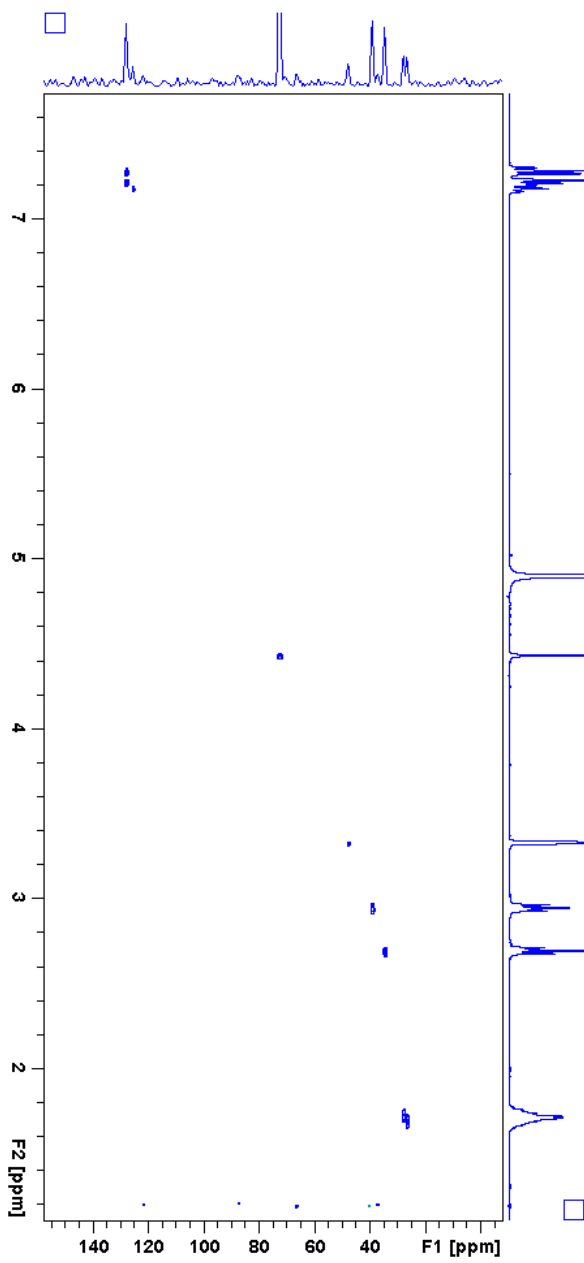


Figure E.3 HSQC spectra of 2.

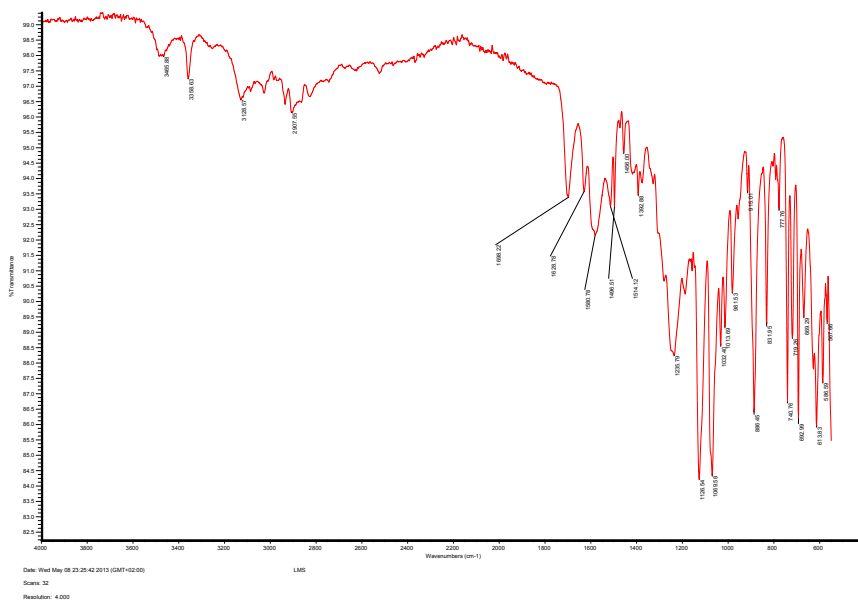


Figure E.4 IR spectra of 2.

F. Spectroscopic data for **36**

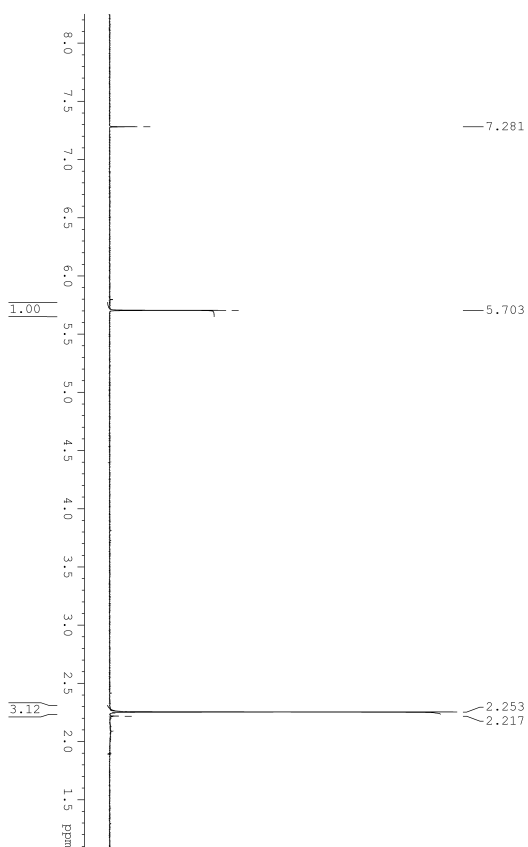


Figure F.1 ^1H NMR spectra of **36**.

G. Spectroscopic data for 16

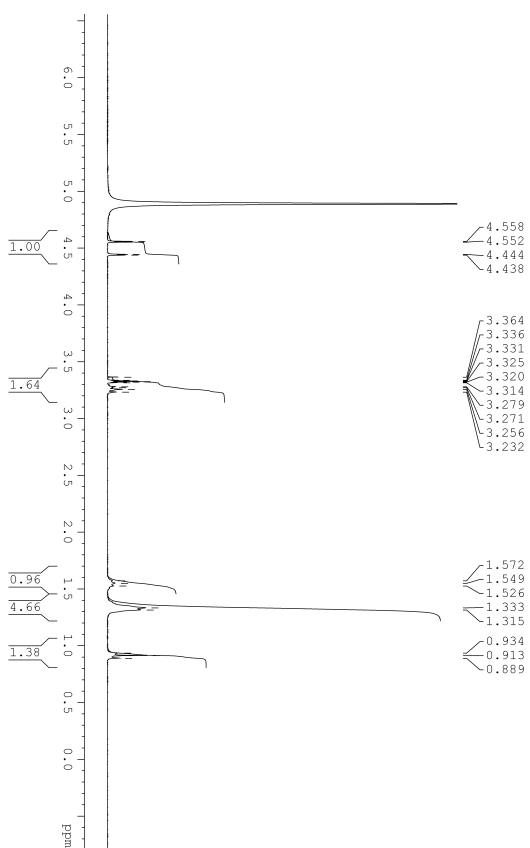


Figure G.1 ^1H NMR spectra of 16.

H. Spectroscopic data from 2d,3d-tartaric acid synthesis

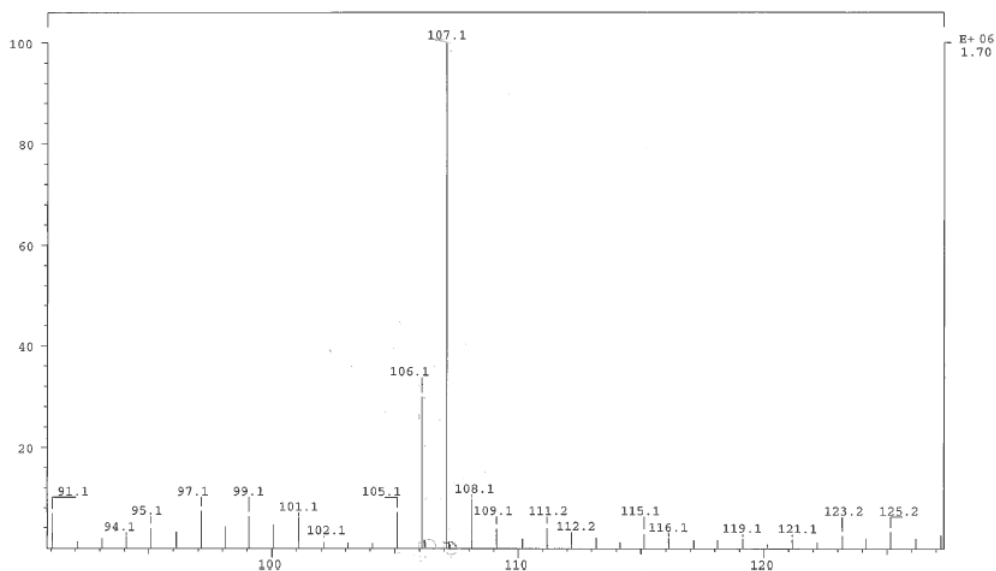


Figure H.1 Mass spectra of 13.

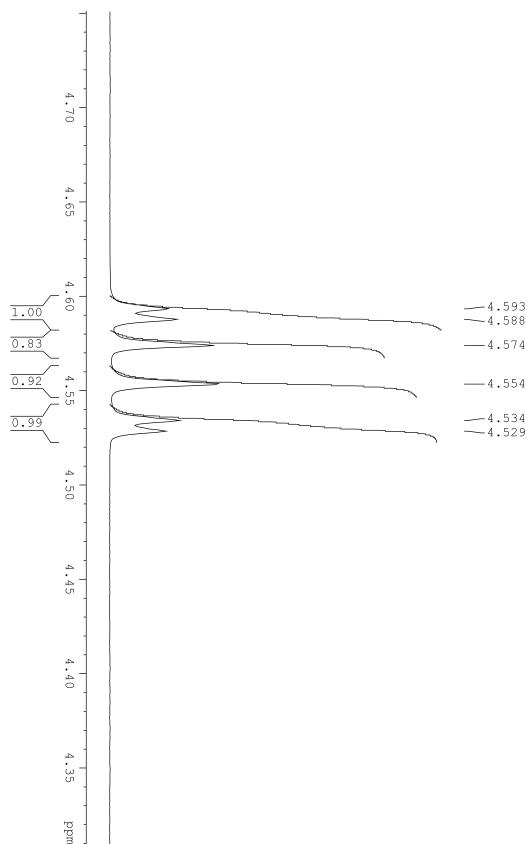


Figure H.2 ^1H NMR spectra of esterification in NMR tube.

I. Spectroscopic data from attempted synthesis of **29**

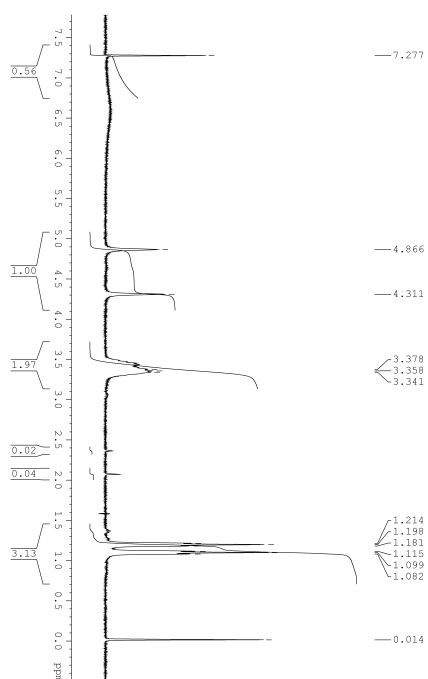


Figure I.1 ^1H NMR spectra of impure **29**.

J. General procedure for kinetic experiments

Samples were taken out at given times, dissolved in an NMR solvent and analyzed with ^1H NMR. The spectra below (Figure J.1) shows a typical result from a sample.

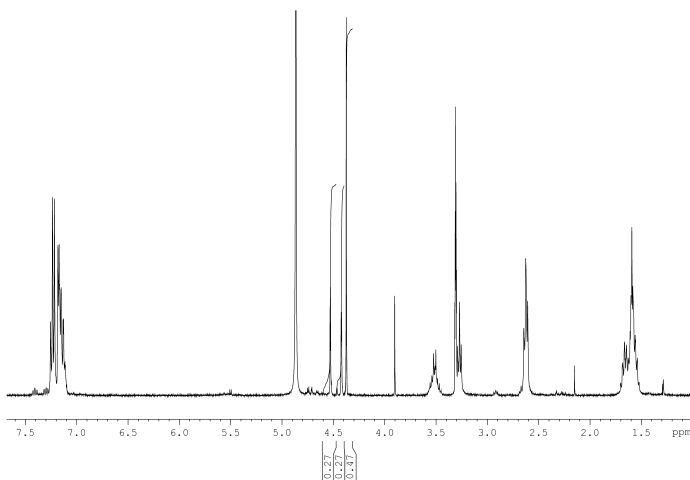


Figure J.1 Typical ^1H NMR spectra from the cyclization of **3**.

The part of the spectra used for quantification of compound ratios in the mixture were the region for the alpha protons in the area around 4-4.5 ppm. This part was used because of acceptable separation of the different compound peaks and little noise. A zoomed in version of Figure J.1 can be seen in Figure J.2. All subsequent spectra are shown for the alpha proton regions.

Obtaining the product ratios from the same spectra multiple times in-

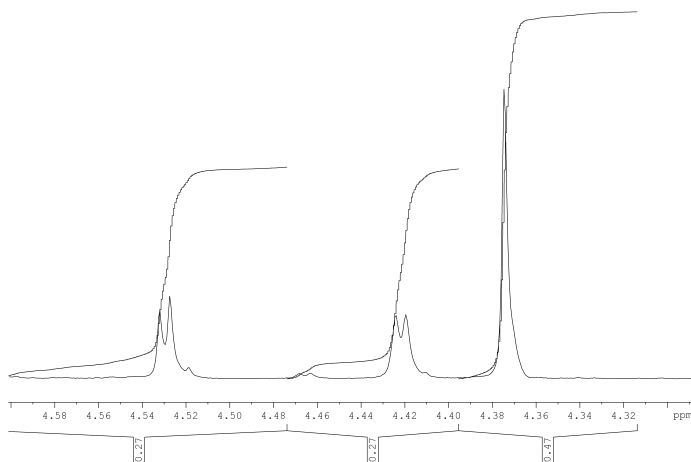


Figure J.2 α -H region of the spectra shown in Figure J.1.

indicated a $\pm 0.5\%$ uncertainty for integration from the raw NMR spectra. This method was applied to the spectra of all the reaction mixture fractions obtained from an experiment (Figure J.3). Some experiments were supported by occasional HPLC analysis of some fractions in addition to the data obtained from ^1H NMR.

Product ratios deduced from ^1H NMR experiments were used to find the concentrations of the different compounds present at different times during the scope of the reaction. The now tabulated concentrations (Table J.1) were then plotted (Figure J.4) with respective 4 or 5 parameter exponential curves (decay or growth to maximum, seen in equations J.1 and J.2), as they were found to give the best curve fit to most of the data (R^2 closest to 1). The dynamic curve fitting algorithm in Sigmaplot v12.3 was used for fitting the exponential curves to the obtained data.

$$f(x) = y_0 + a(1 - e^{-bx}) + c(1 - e^{-dx}) \quad (\text{J.1})$$

$$f(x) = y_0 + a * e^{-bx} + c * e^{-dx} \quad (\text{J.2})$$

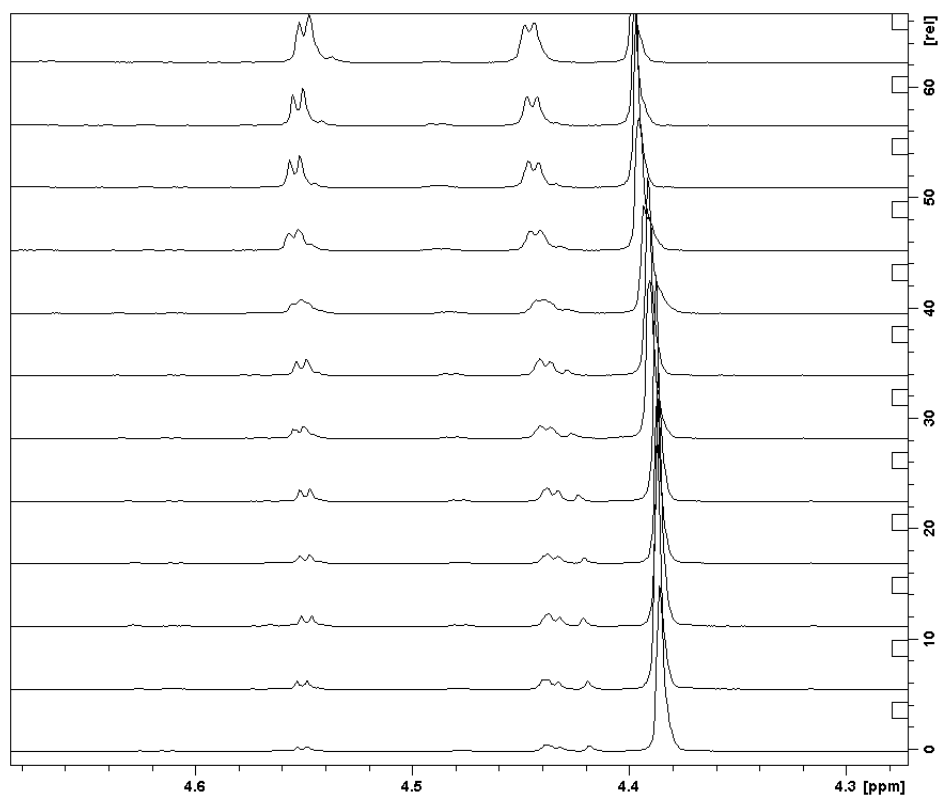
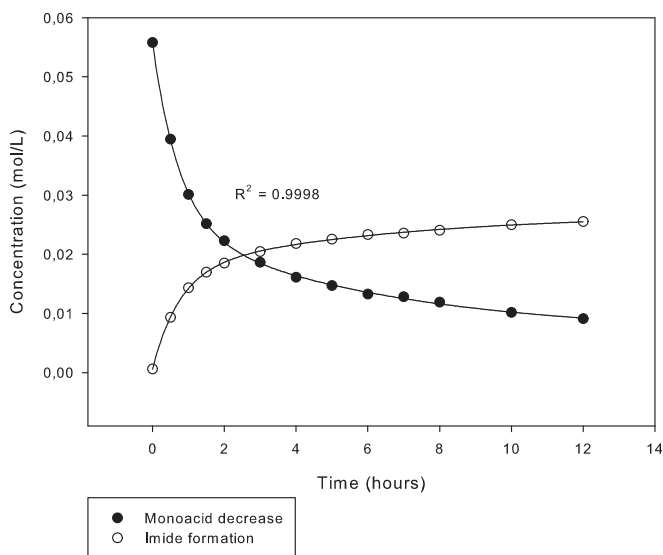


Figure J.3 α -H region of all the spectra in a typical experiment (cyclization of **3**).

Table J.1 Data deduced from ^1H NMR analysis of reaction mixtures for the cyclization of **3**

Frac.	Time (hours)	(<i>R,R</i>)- 3 (%)	(<i>R,R</i>)- 1 (%)	(<i>R,R</i>)- 3 (10^{-3}mol/L)	(<i>R,R</i>)- 1 (10^{-3}mol/L)
0	0	98.0	2.0	55.8	0.6
1	1	69.3	30.7	39.5	9.3
2	2	52.9	47.1	30.2	14.3
3	3	44.2	55.8	25.2	17.0
4	4	39.1	60.9	22.3	18.5
5	5	32.7	67.3	18.6	20.5
6	6	28.3	71.7	16.1	21.8
7	7	25.8	74.2	14.7	22.6
8	8	23.3	76.7	13.3	23.3
9	9	22.5	77.5	12.8	23.6
10	10	20.9	79.1	11.9	24.1
11	11	17.9	82.1	10.2	25.0
12	12	16.0	84.0	9.1	25.5

**Figure J.4** Plot of the results from Table J.1 with fitted curves.

K. Supplementary data for Chapter 3

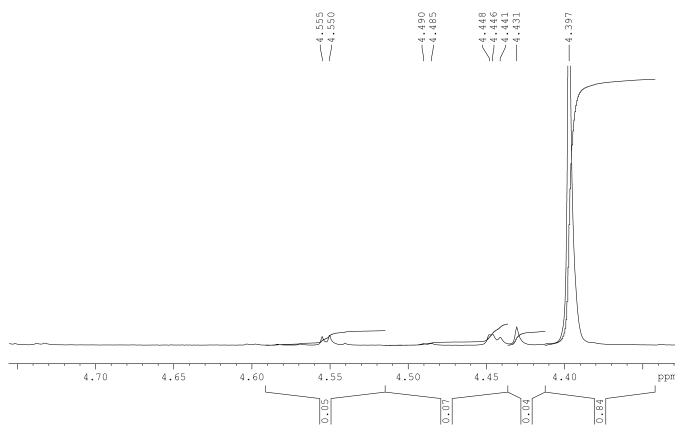


Figure K.1 ¹H NMR spectra from formation of **1** from **2**.

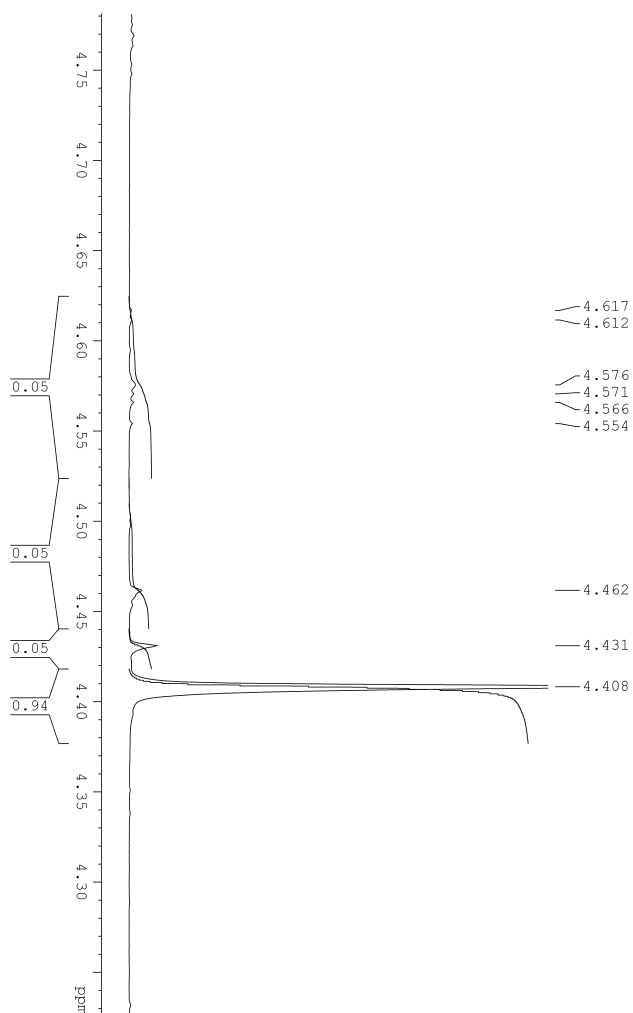


Figure K.2 ^1H NMR spectra from formation of **1** from **2**.

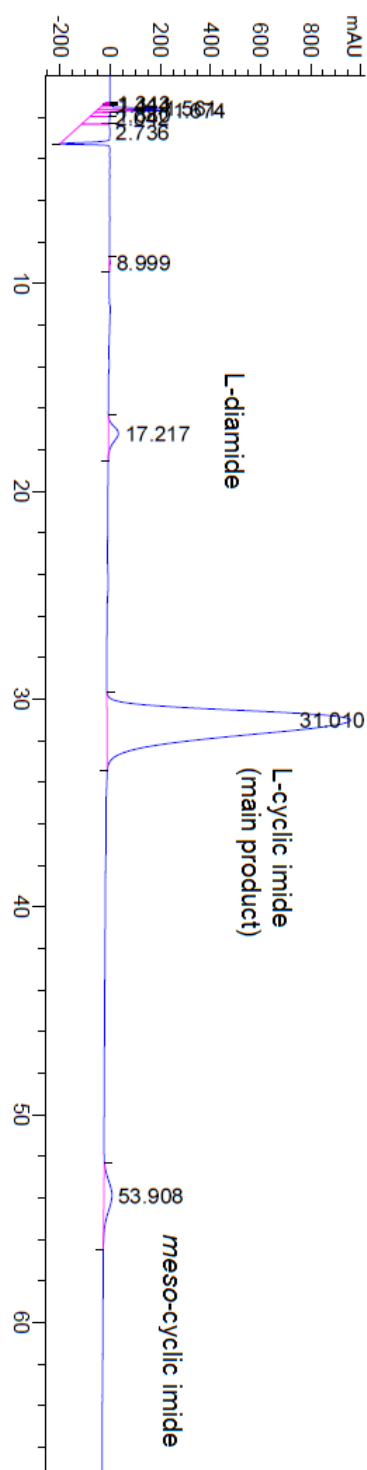


Figure K.3 HPLC chromatogram from formation of **1** from **2**.

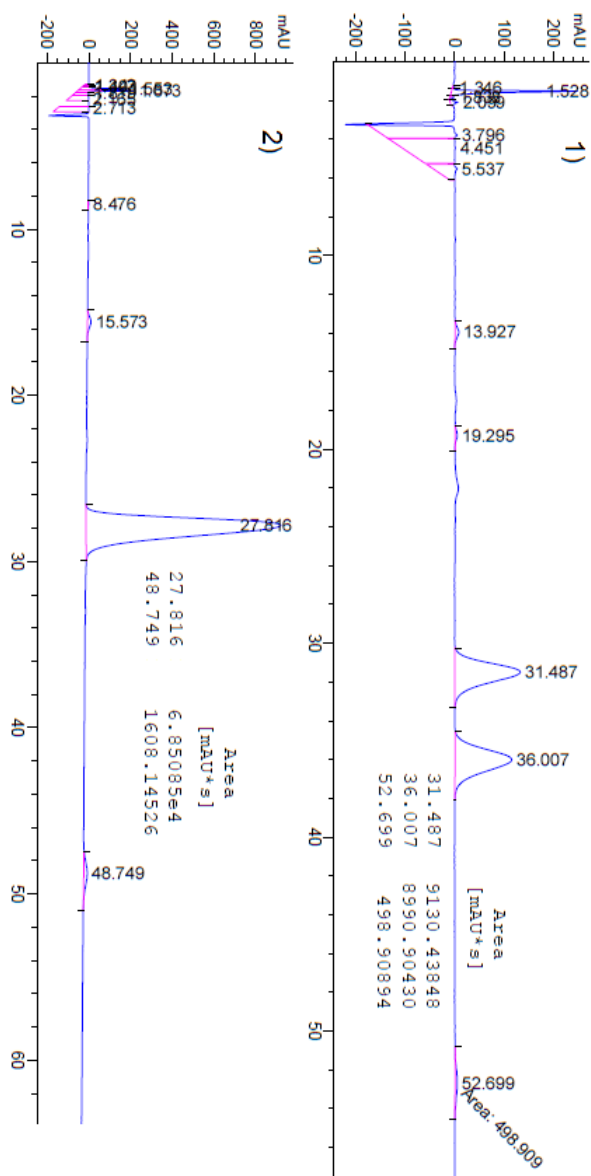


Figure K.4 HPLC chromatogram from: 1) Experiment conducted with **13**. 2) Experiment conducted with **15**.

L. Supplementary data for Chapter 4

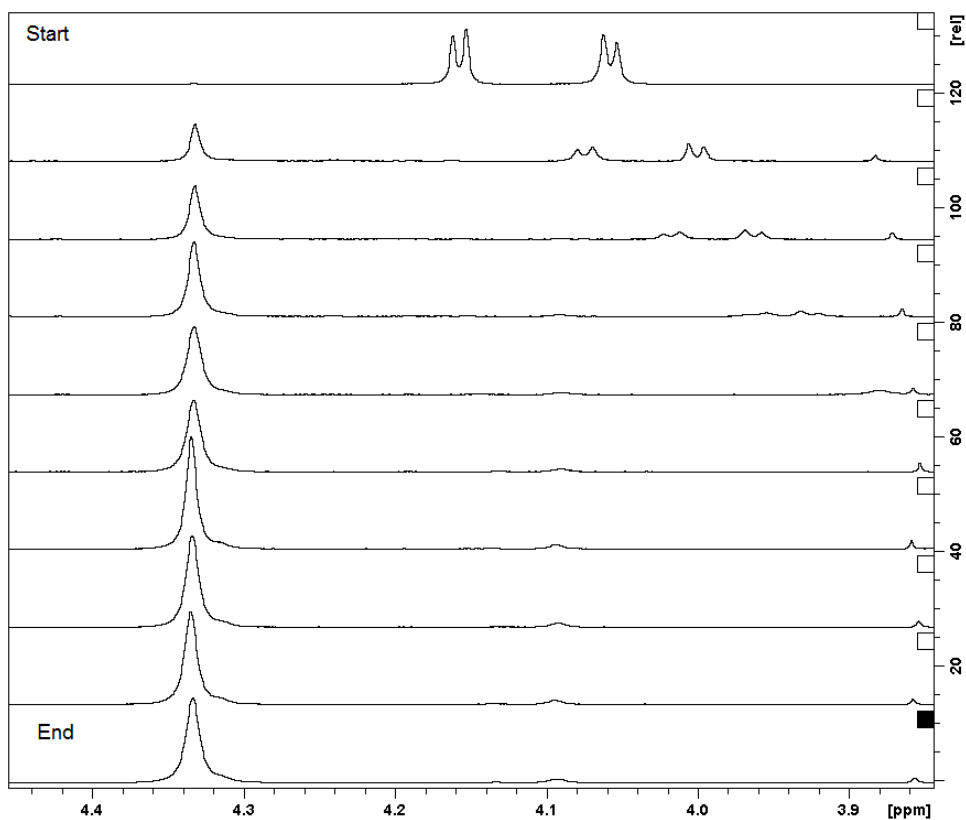


Figure L.1 ^1H NMR spectra from formation of **1** from **3** with a Dean-Stark apparatus.

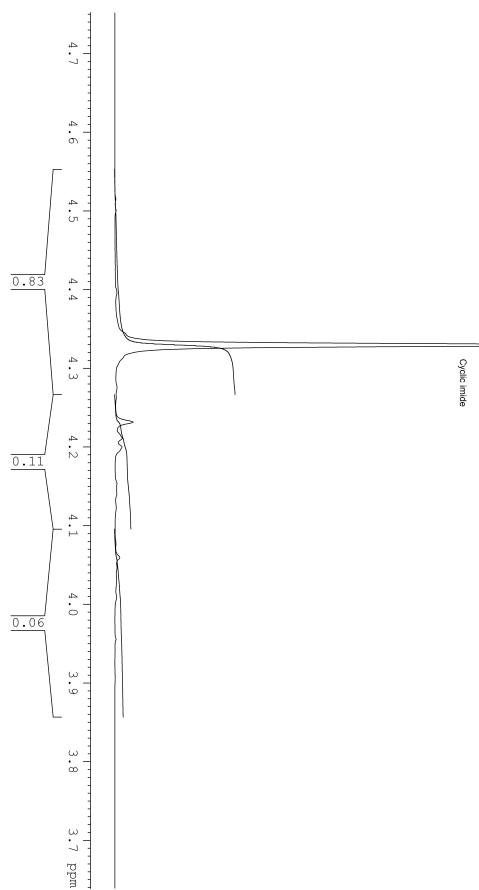


Figure L.2 ^1H NMR spectra from aqueous reflux of **1**.

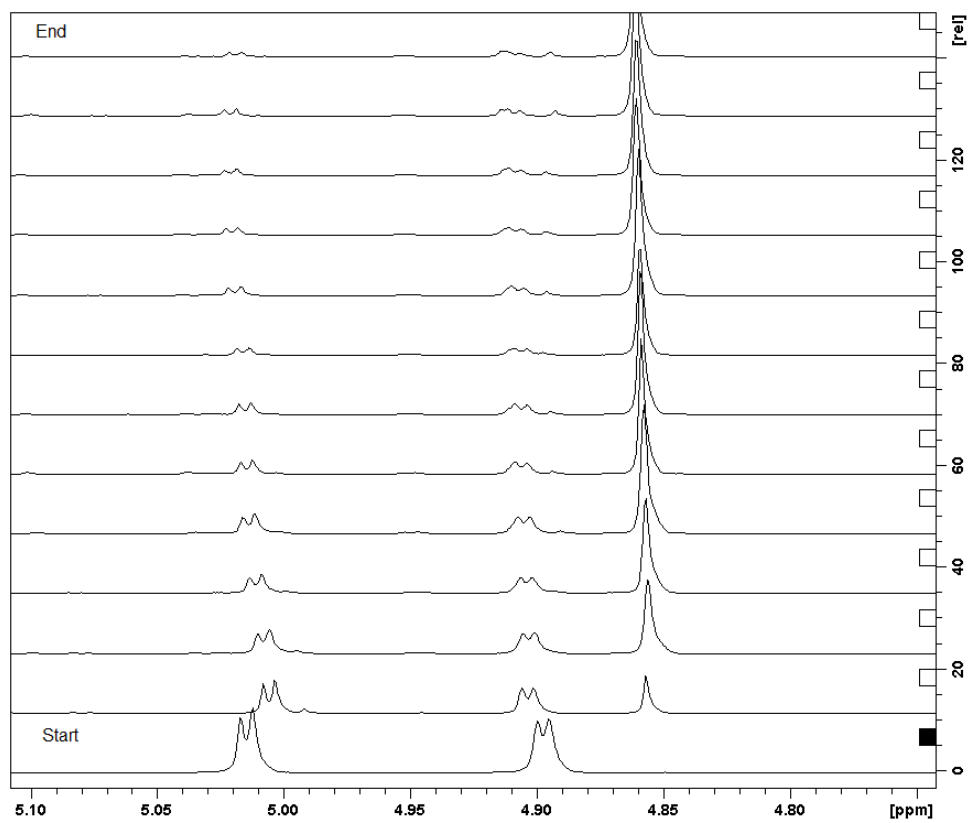


Figure L.3 ^1H NMR spectra from formation of **1** from **3**.

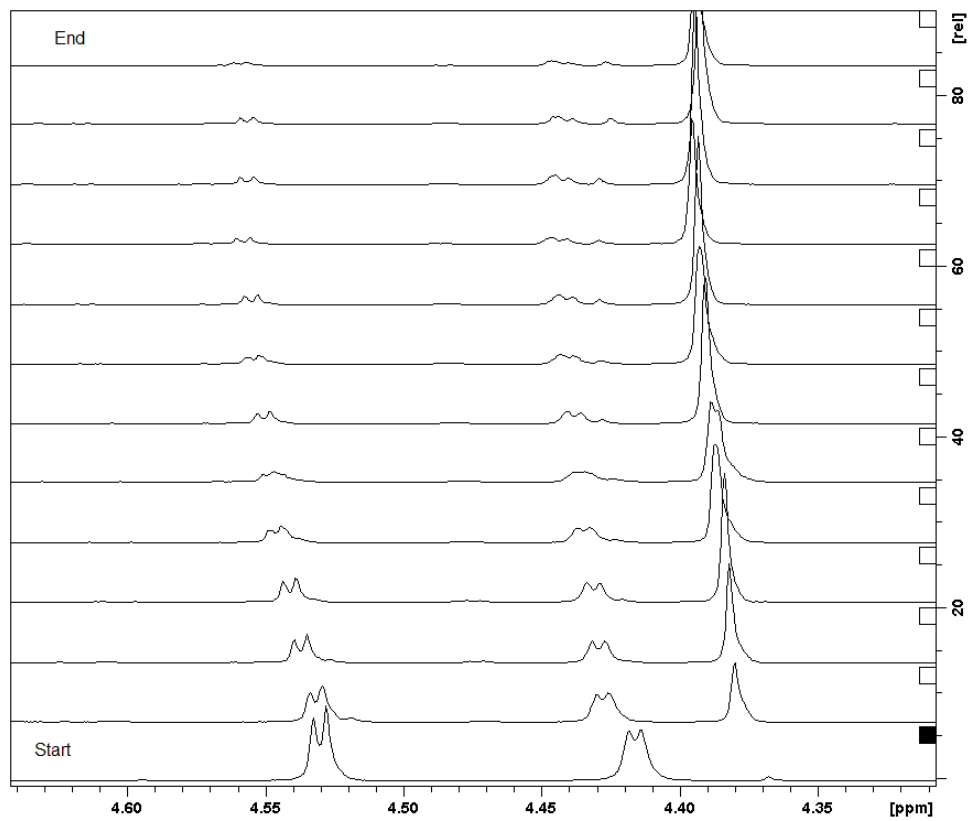


Figure L.4 ^1H NMR spectra from formation of **1** from **3**.

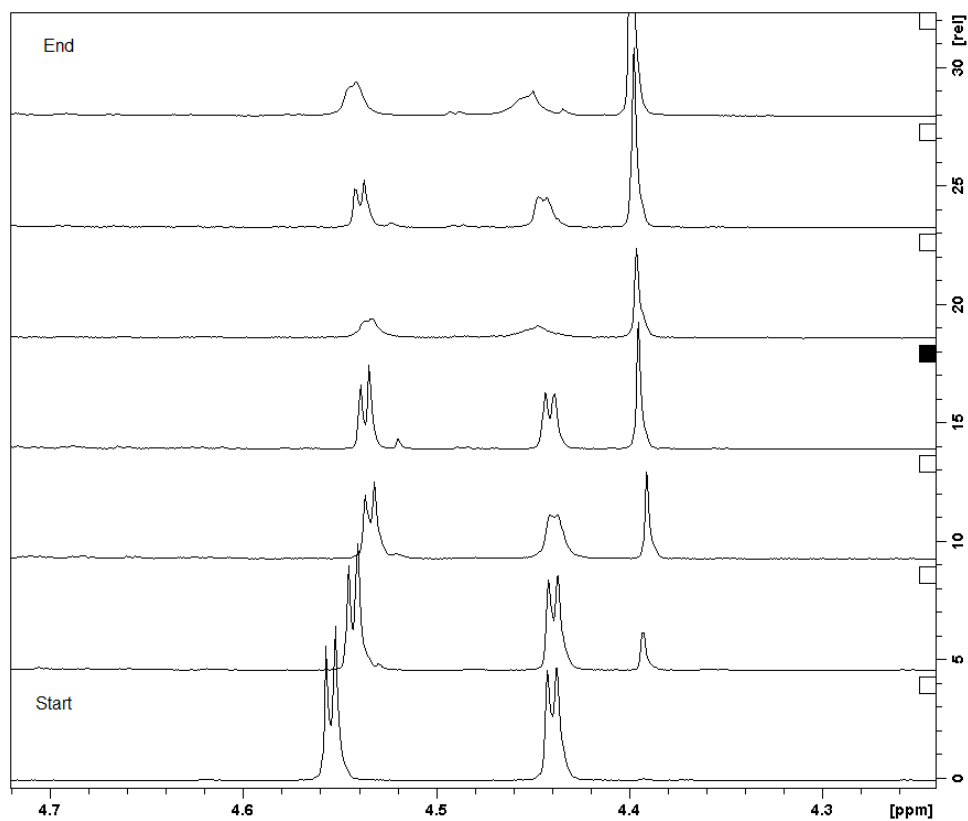


Figure L.5 ^1H NMR spectra from formation of **1** from **3**.

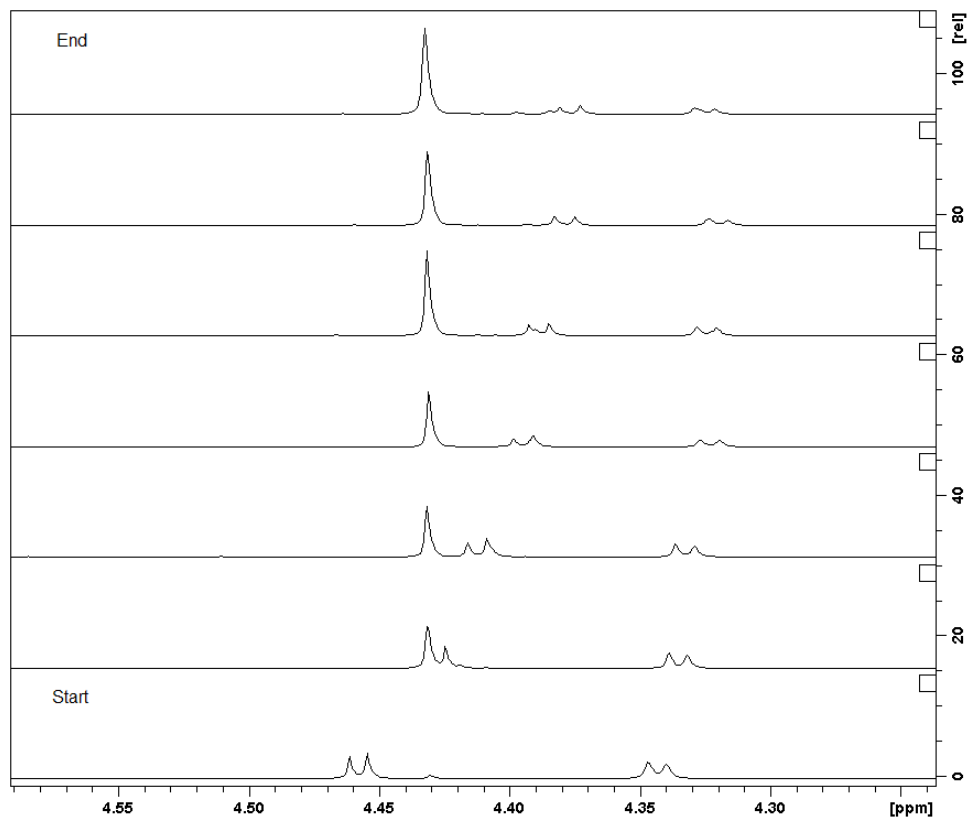


Figure L.6 ^1H NMR spectra from formation of **1** from **3**.

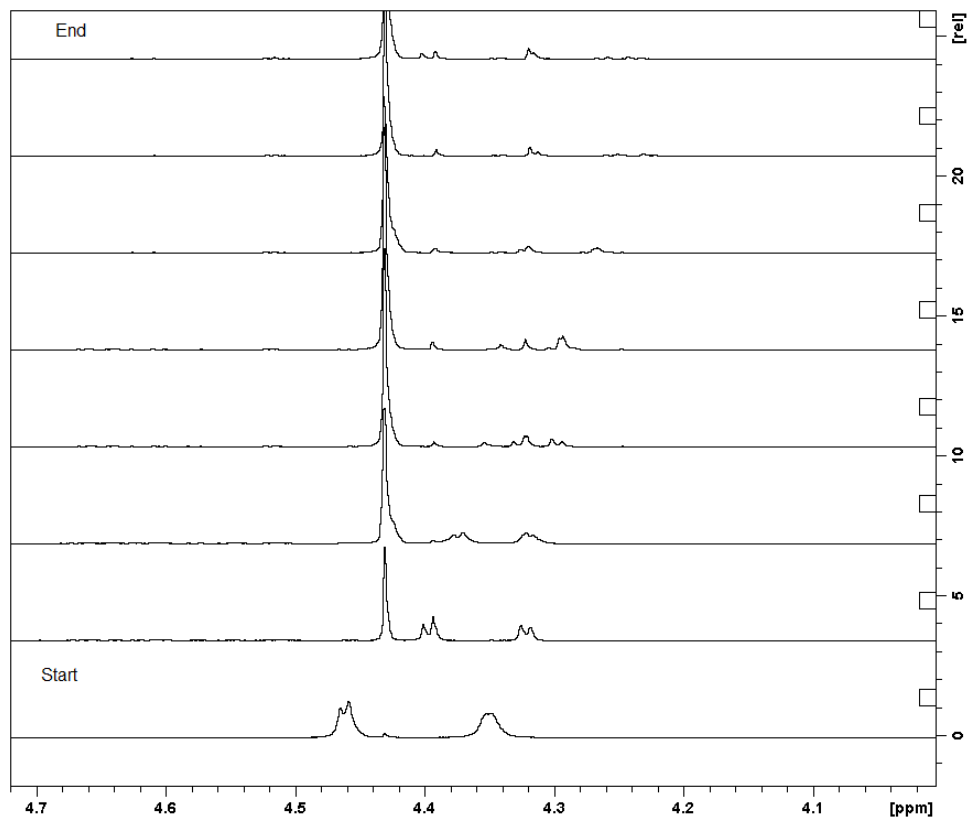


Figure L.7 ^1H NMR spectra from formation of **1** from **3**.

M. Supplementary data for Chapter 5

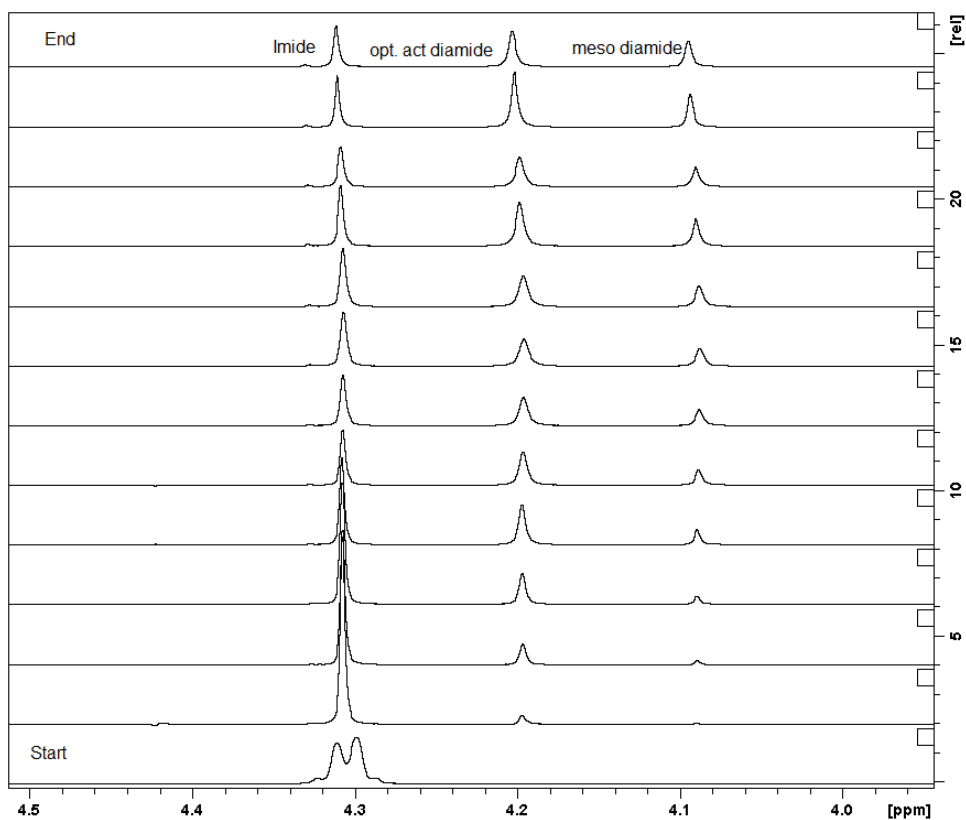


Figure M.1 ¹H NMR spectra from opening of (*R,R*)-**1** with 1 eq. 4-phenylbutylamine.

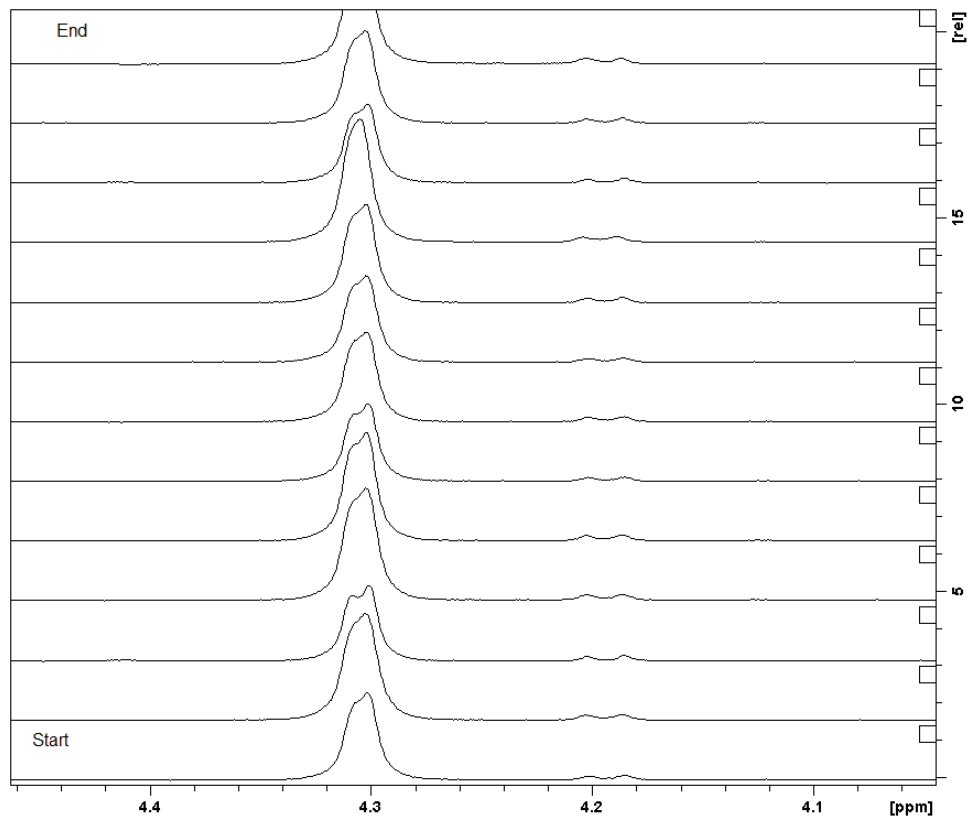


Figure M.2 ¹H NMR spectra from opening of (*R,R*)-**1** with 0.1 eq. 4-phenylbutylamine.

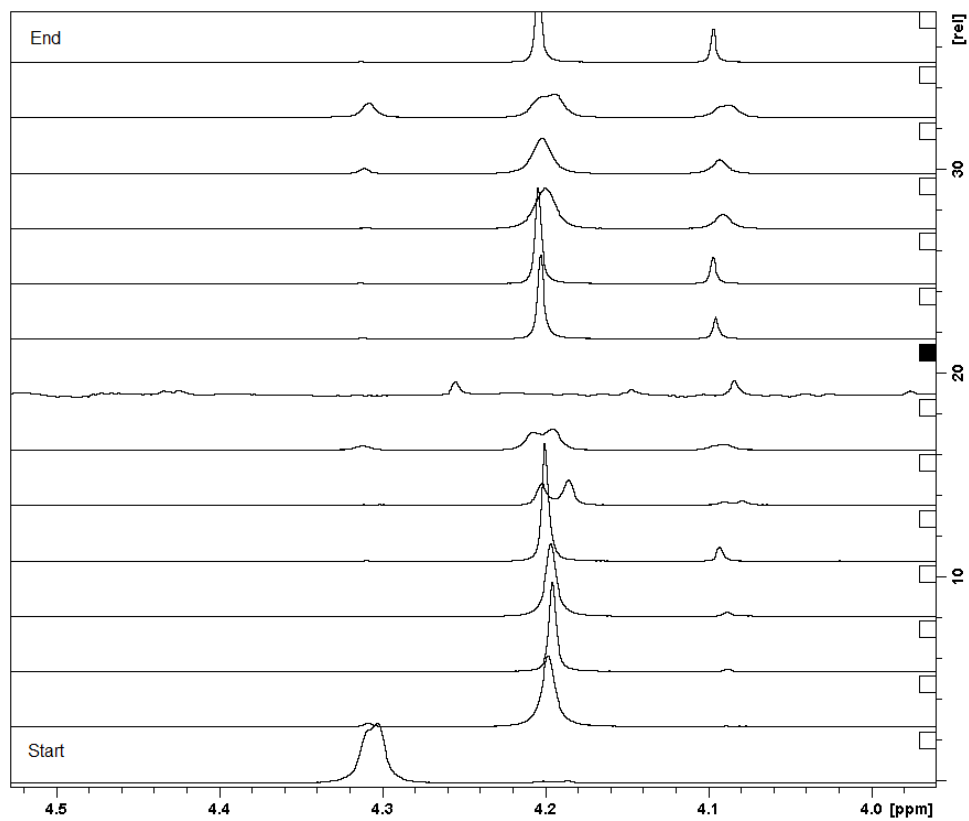


Figure M.3 ¹H NMR spectra from opening of (*R,R*)-**1** with 2 eq. 4-phenylbutylamine.

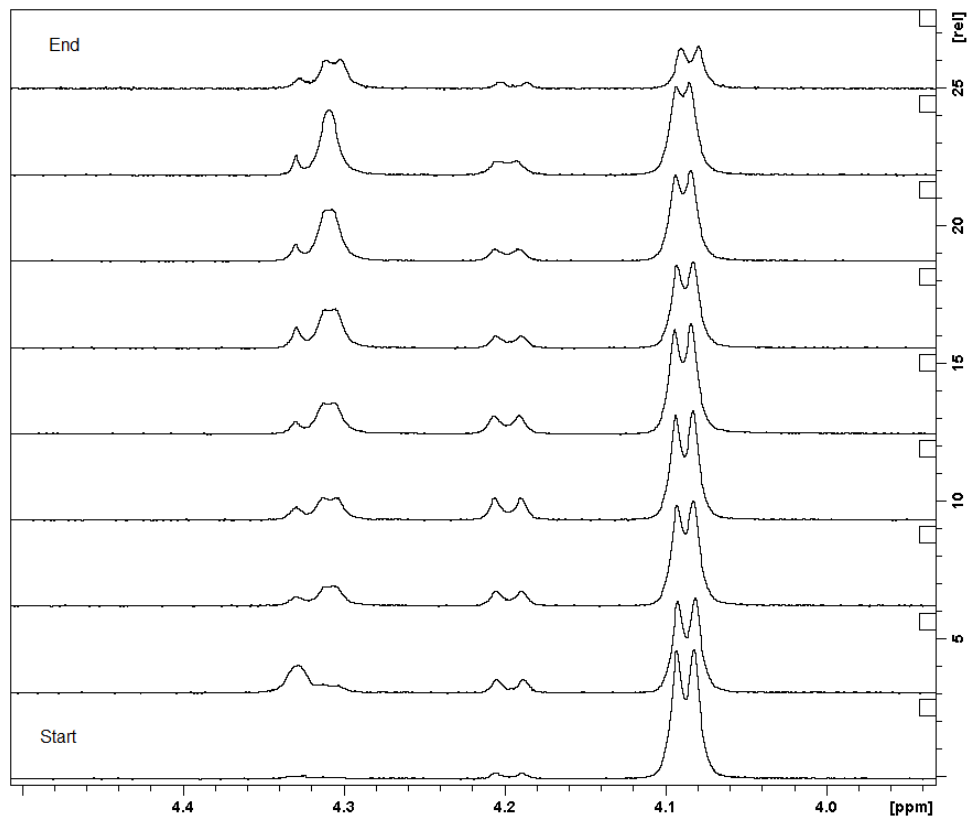


Figure M.4 ^1H NMR spectra from opening of (R^*,S^*) -1 with 1 eq. 4-phenylbutylamine.

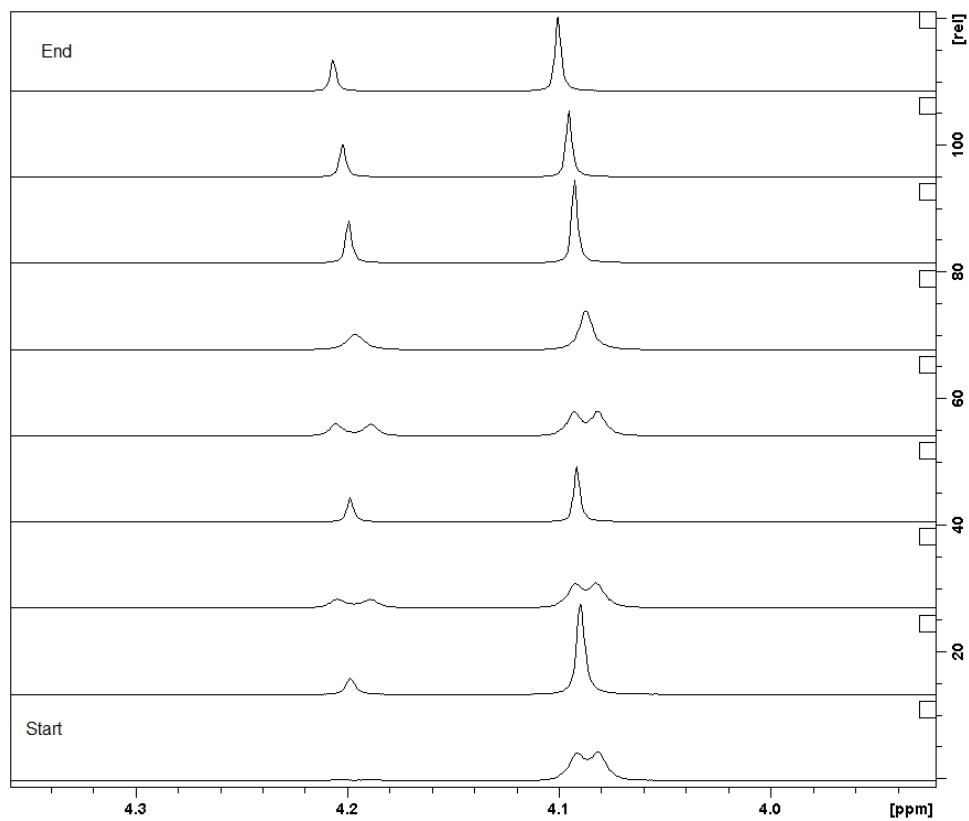


Figure M.5 ^1H NMR spectra from opening of (R^*,S^*)-1 with 2 eq. 4-phenylbutylamine.

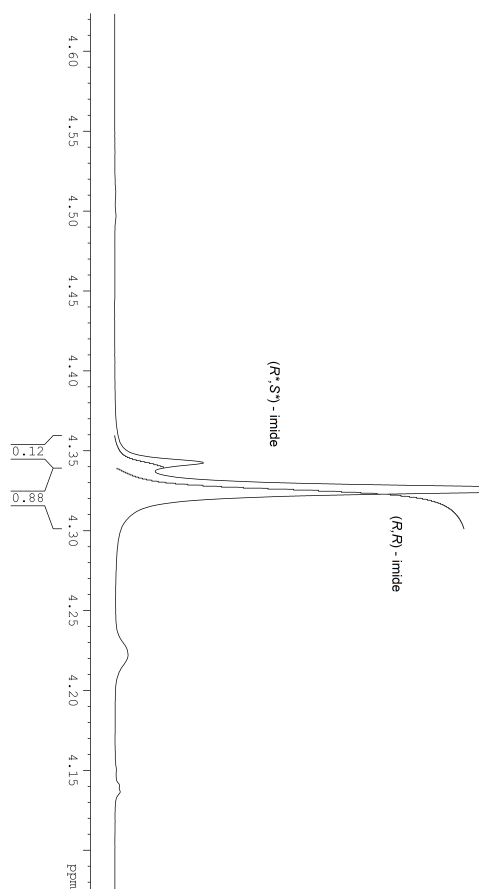


Figure M.6 ^1H NMR spectra from reflux of **1** and 2,2,6,6-tetramethylpiperidine in xylenes.

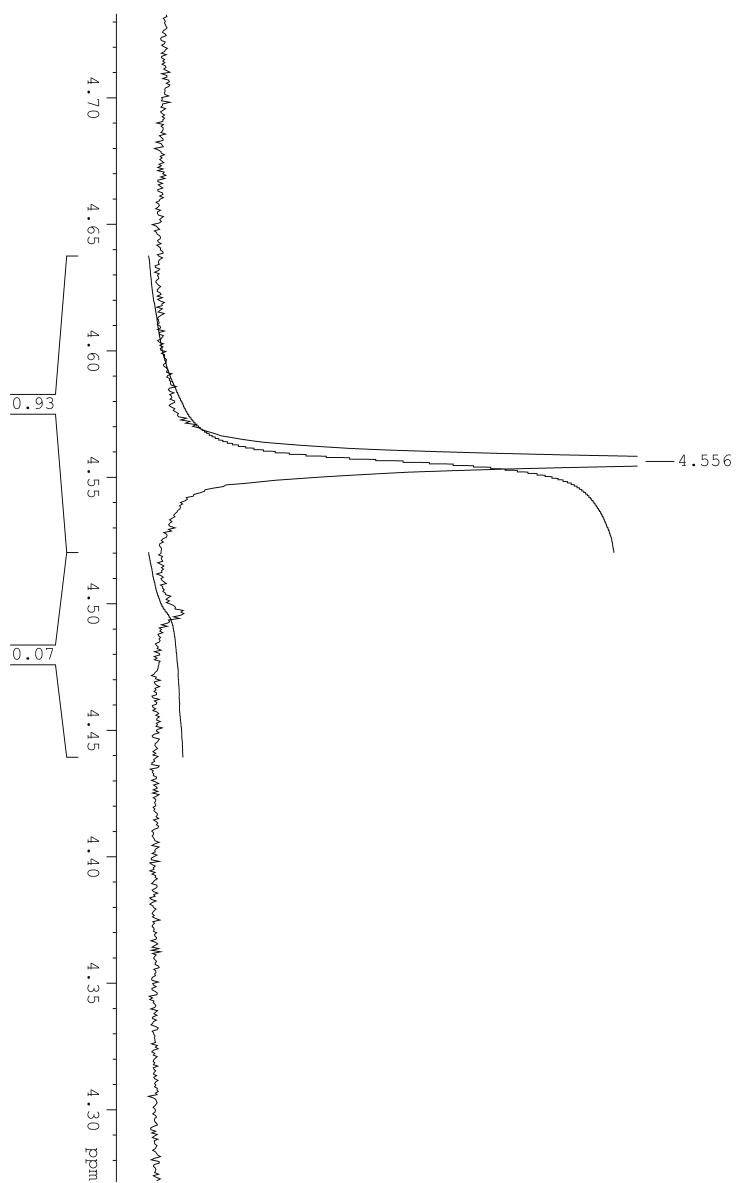


Figure M.7 ^1H NMR spectra from reflux of **54** and NaOD in xylenes.

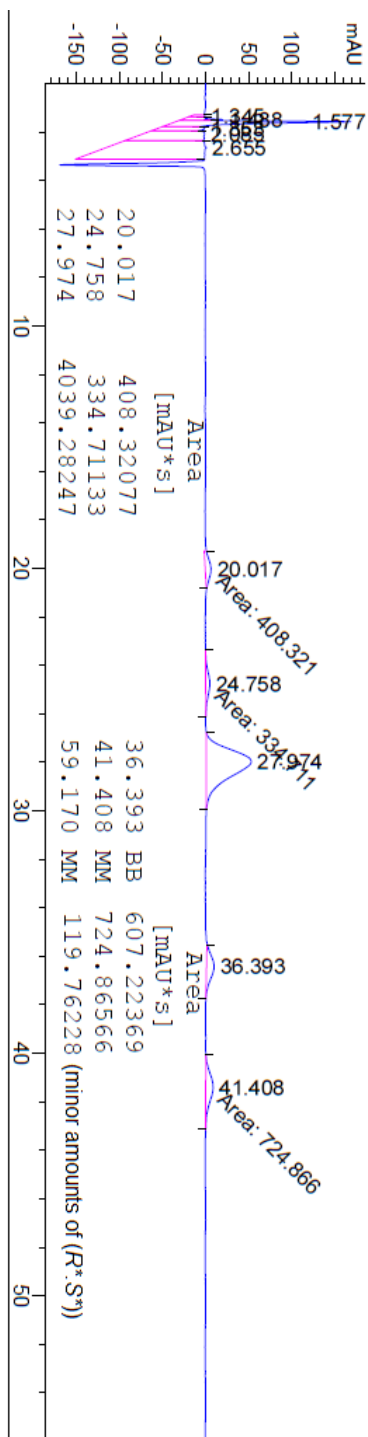


Figure M.8 HPLC chromatogram from formation opening of (R^*,S^*) -1 with 2 eq 4-phenylbutylamine.

N. Supplementary data for Chapter 6

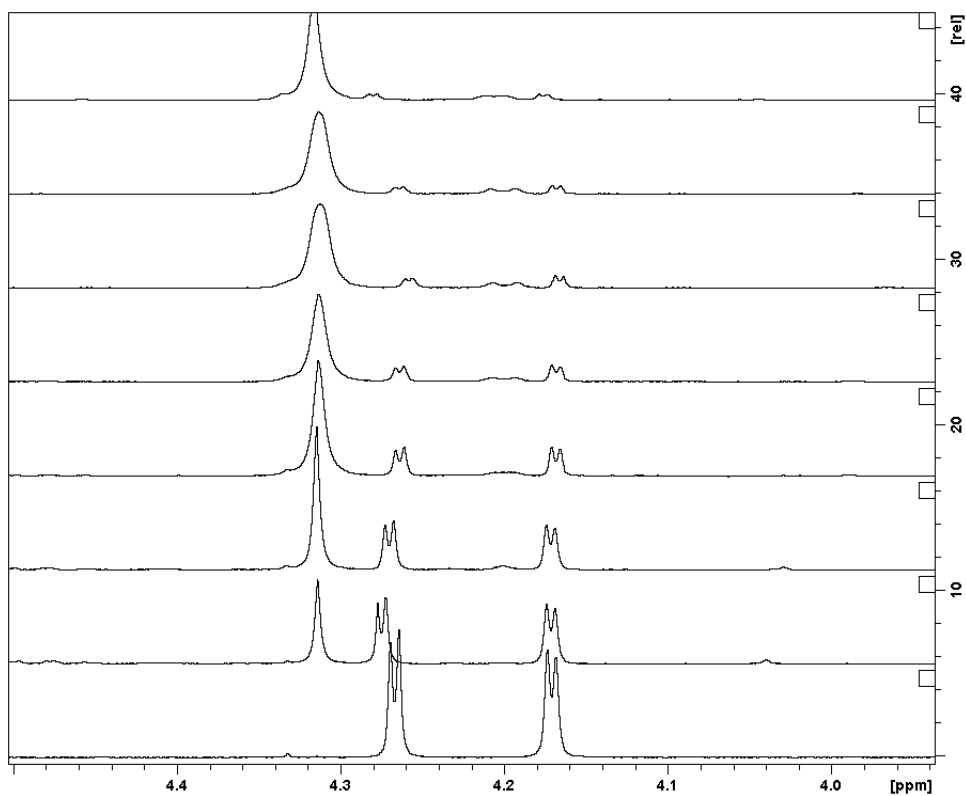


Figure N.1 ^1H NMR spectra from reaction of (*R,R*)-**3** with 0.1 eq. 4-phenylbutylamine.

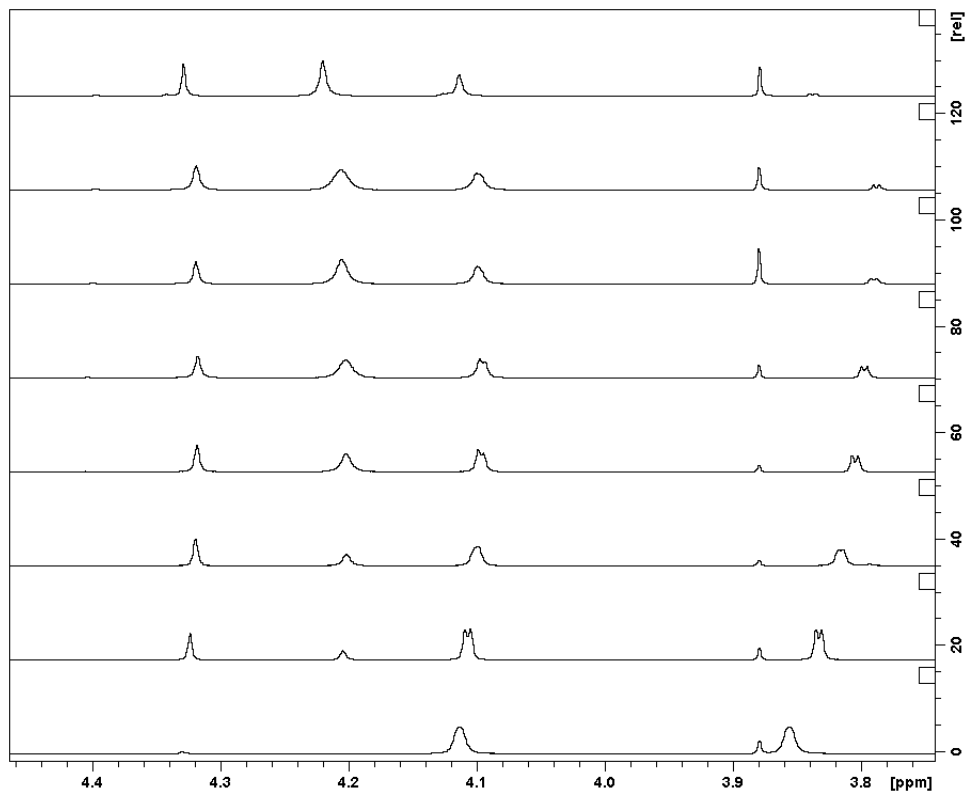


Figure N.2 ^1H NMR spectra from reaction of (R,R) -3 with 1.0 eq. 4-phenylbutylamine.

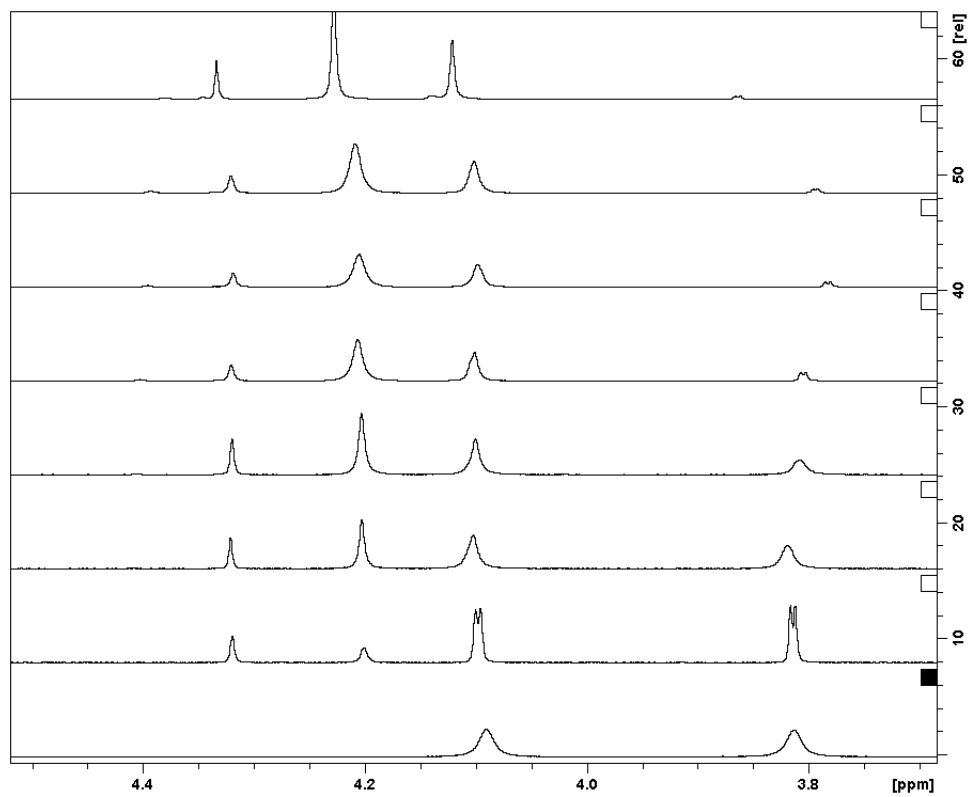


Figure N.3 ^1H NMR spectra from reaction of (*R,R*)-**3** with 1.1 eq. 4-phenylbutylamine.

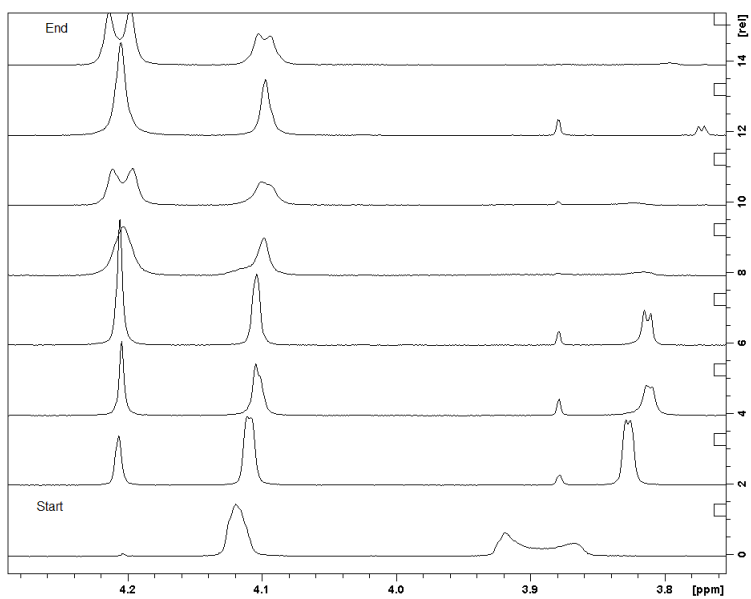


Figure N.4 ^1H NMR spectra from reaction of (R,R) -**3** with 2.0 eq. 4-phenylbutylamine.

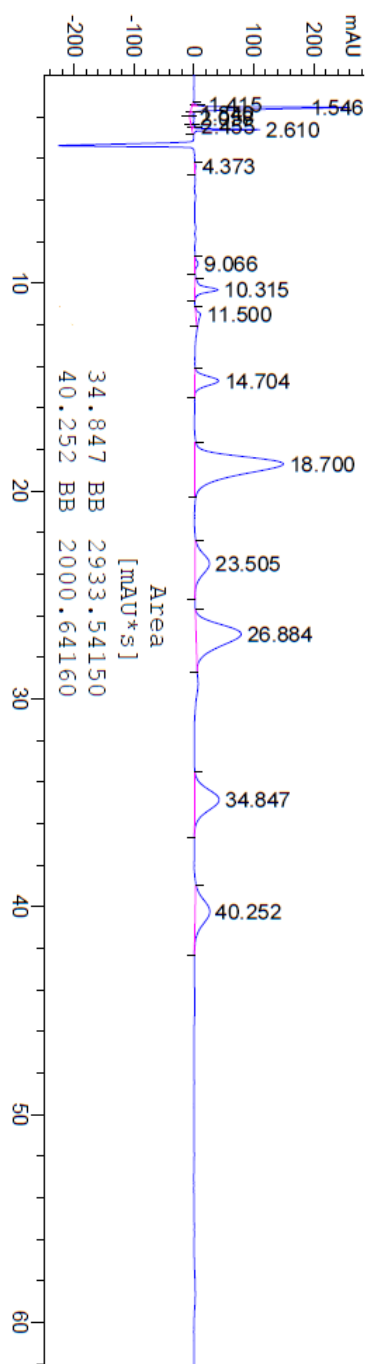


Figure N.5 HPLC chromatogram from reaction of (*R,R*)-**3** with 1.0 eq. 4-phenylbutylamine.

O. Supplementary data for Chapter 7

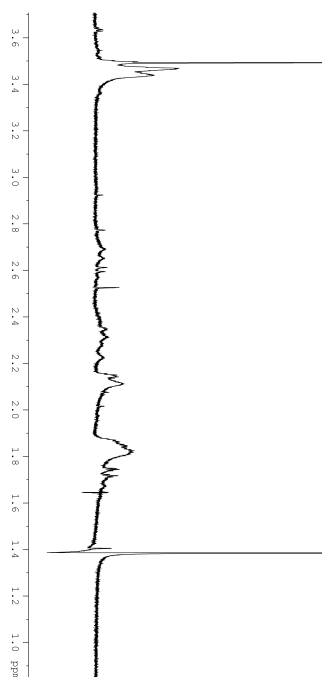


Figure O.1 ¹H NMR spectra from attempted amidation of **29** with 4-phenylbutylamine.